

**DYNAMICS AND CONTROL OF ORBITING DEPLOYABLE
MULTIMODULE MANIPULATORS**

Yang Cao

B.A.Sc., Shandong University, China, 1993

A THESIS SUBMITTED IN PARTIAL FULFILMENT OF
THE REQUIREMENT FOR THE DEGREE OF

Master of Applied Science

in

The Faculty of Graduate Studies
Department of Mechanical Engineering

We accept this thesis as conforming
to the required standard

The University of British Columbia

October 1999

© Yang Cao, 1999

In presenting this thesis in partial fulfilment of the requirements for an advanced degree at the University of British Columbia, I agree that the Library shall make it freely available for reference and study. I further agree that permission for extensive copying of this thesis for scholarly purposes may be granted by the head of my department or by his or her representatives. It is understood that copying or publication of this thesis for financial gain shall not be allowed without my written permission.

Department of Mechanical Engineering

The University of British Columbia
Vancouver, Canada

Date Oct. 14, 1999

ABSTRACT

This thesis focuses on the planar dynamics and control of a variable geometry manipulator which may be used in space- as well as ground-based operations. The system is composed of a flexible orbiting platform supporting two modules connected in a chain topology. Each module consists of two links: one free to slew while the other permitted to deploy. The model used and the governing order- N equations of motion, as developed by Caron, are explained. A detailed dynamical response study is undertaken which assesses the influence of initial conditions, system parameters, and manipulator maneuvers on the system response. Results suggest that under critical combinations of system parameters and disturbances the response may not conform to the acceptable limit. This points to a need for active control. Two different control methodologies are used: (i) the nonlinear Feedback Linearization Technique (FLT) applied to rigid degrees of freedom with flexible generalized coordinates indirectly regulated through coupling; (ii) a synthesis of the FLT and Linear Quadratic Regulator (LQR) to achieve active control of both rigid and flexible degrees of freedom. Furthermore, the FLT is used to track several prescribed trajectories with considerable accuracy. Finally, a two unit ground-based prototype manipulator, designed and constructed by Chu, is used to assess effectiveness of the Proportional-Integral-Derivative (PID) and FLT control procedures in performing several trajectory tracking maneuvers. The study lays a sound foundation for further exploration of this class of novel manipulators.

TABLE OF CONTENTS

ABSTRACT	ii
TABLE OF CONTENTS	iii
LIST OF SYMBOLS	vi
LIST OF FIGURES	xi
LIST OF TABLES	xvii
ACKNOWLEDGEMENT	xviii
1. INTRODUCTION	1
1.1 Preliminary Remarks	1
1.2 A Brief Review of the Relevant Literature	3
1.2.1 Characteristics of space-based manipulators	3
1.2.2 Dynamics and control of space-based manipulators	8
1.3 Scope of the Investigation	13
2. DYNAMICS OF SPACE BASED MULTI-MODULE MANIPULATORS	15
2.1 Background to Formulation	15
2.2 Simulation Methodology	17
2.3 Simulation Considerations	20
2.4 System Response	27
2.4.1 Effect of manipulator location and orientation	27
2.4.2 Response due to platform's tip excitation	38
2.4.3 Response to manipulator tip displacement	41

2.4.4	Response in presence of manipulator maneuvers	44
2.4.5	Effect of system parameters	47
3.	SYSTEM CONTROL	60
3.1	Control Methodologies	62
3.1.1	FLT control	64
3.1.2	FLT/LQR control	66
3.2	Simulation Results and Discussion: Commanded Maneuvers	70
3.2.1	FLT control	72
3.2.2	FLT/LQR control	76
3.3	Trajectory Tracking	91
4.	GROUND BASED EXPERIMENTS	106
4.1	System Description	106
4.1.1	Manipulator base	108
4.1.2	Manipulator module	108
4.1.3	Elbow joint	112
4.2	Hardware and Software Control Interface	112
4.3	Digital Control of the Ground-Based Manipulator	117
4.3.1	Discretization of inner nonlinear loop	119
4.3.2	Joint velocity estimates from position measurements	119
4.3.3	Discretization of outer PD/PID control loop	120
4.4	Controller Implementation	122
4.4.1	Dynamical equations for the ground-based Manipulator	122

4.4.2	Control system parameters	124
4.4.3	Controller design	126
4.5	Trajectory Tracking	127
4.5.1	Straight line trajectory.	128
4.5.2	Circular trajectory	135
5.	CONCLUDING REMARKS	142
5.1	Contributions	142
5.2	Conclusions	143
5.3	Recommendations for Future Work	144
	REFERENCES	146
	APPENDIX I: SPECTRAL DENSITY ANALYSIS OF DYNAMICAL		
	RESPONSE	151

LIST OF SYMBOLS

A, B	state-space representation of the flexible subsystem, Eq. (3.14)
C.M.	center of mass
d	position of the manipulator base from the center of the platform
e	orbital eccentricity
e_1, e_2	tip vibrations of modules one and two, respectively
e_p	platform tip vibration
EI_d, EI_s	Flexural rigidity of deployable and slewing links, respectively
EI_p	Flexural rigidity of the platform
F	vector containing the terms associated with the centrifugal, Coriolis, gravitational, elastic, and internal dissipative forces
F_1, F_2	deployment/retrieval forces at the prismatic joints one and two, respectively
I_{jz}	moment of inertia of the revolute joint
J	quadratic cost function which considers tracking errors and energy expenditure, Eq. (3.17)
K_i	spacecraft's inertia parameter, $(I_y - I_x)/I_z$, Eq. (2.5)
K_j	Stiffness of the revolute joint
K_{LQR}	optimal gain matrix, Eq. (3.18)
K_p, K_v	diagonal control matrices containing the proportional and derivative gains, respectively
l_d, l_s	length of deployable and slewing links, respectively
l_1, l_2	lengths of the manipulator modules one and two, respectively

l_p	length of the platform
L.H., L.V.	local horizontal and local vertical, respectively
m_d, m_s	mass of deployable and slewing links, respectively
m_j	mass of the revolute joint
m_p	mass of the platform
\mathbf{M}	system mass matrix
$\hat{\mathbf{M}}, \hat{\mathbf{F}}$	estimates of the discretized mass matrix and nonlinear terms \mathbf{M} and \mathbf{F} , respectively; Eq. (4.3)
$\tilde{\mathbf{M}}, \tilde{\mathbf{K}}$	mass and stiffness matrices for the linearized system, respectively; Eq. (3.11)
$\bar{\mathbf{M}}, \bar{\mathbf{K}}$	mass and stiffness matrices, respectively, corresponding to the elastic subsystem; Eq. (3.12)
$\mathbf{M}_{rr}, \mathbf{M}_{ff}$	rigid and flexible contributions to the system mass matrix \mathbf{M} , respectively
$\mathbf{M}_{rf}, \mathbf{M}_{fr}$	coupled contributions to the system mass matrix \mathbf{M}
N	number of bodies (i.e. platform and manipulator units) in the system
$O(N)$	order- N
\mathbf{P}_{LQR}	solution to the matrix Riccati equation, Eq. (3.19)
\mathbf{q}	set of generalized coordinates leading to the coupled mass matrix \mathbf{M}
\mathbf{q}_0	operation point used to linearize the governing nonlinear equation
\mathbf{q}_k	discretized generalized coordinates \mathbf{q}
$\mathbf{q}_r, \mathbf{q}_f$	rigid and flexible generalized coordinates, respectively
\mathbf{q}_s	specified or constrained coordinates
$\Delta\mathbf{q}_s$	desired variation of the specified or constrained coordinates

q_d	desired value of q
Q	generalized forces, including the control inputs
Q_{LQR}, R_{LQR}	symmetric weighting matrices which assign relative penalties to state errors and control effort, respectively; Eq. (3.17)
t	time
T	total kinetic energy of the system
T_{pr}, T_{pf}	torques provided by control momentum gyros for attitude control and vibration suppression, respectively
T_1, T_2	torques provided by actuators located at revolute joints one and two, respectively
u	vector containing the FLT control inputs, Eq. (3.5)
u_L	input determined from the Linear Quadratic Regulator, Eq. (3.16)
x, y, z	body coordinate system; in equilibrium x, y in the orbital plane with x along the local vertical, y along the local horizontal and z aligned with the orbit normal
x_d, y_d	desired trajectory for the manipulator tip
x_L	state vector for the flexible subsystem

Greek Symbols

α_1, α_2	rigid body rotations during slew maneuvers of modules one and two, respectively
β_1, β_2	contributions due to flexibility of revolute joints at modules one and two, respectively;

γ_i	rotation of the frame F_i , attached to the module i , with respect to the frame F_{i-1}
$\Delta\tau$	time required for maneuver, Eq. (2.4)
\mathbf{v}_k	digital joint velocity estimate, Eq. (4.6)
θ	true anomaly of the system
τ	time from start of maneuver
τ_k	digital control input for the robot arm, Eq. (4.4)
τ_p	librational period of the platform
ω_i	desired natural frequency associated with the error equation for rigid degrees of freedom, Eq. (3.9)
ω_ψ	frequency of platform librational motion
ω_p	platform's bending natural frequency
ω_{j1}	first revolute joint's torsional natural frequency
ω_{m1}	first module's bending natural frequency
ω_{j2}	second revolute joint's torsional natural frequency
ω_{m2}	second module's bending natural frequency
ξ_i	elastic deformation of the i^{th} -1 body in the transverse direction
ψ_p	platform's pitch angle

A dot above a character refers to differentiation with respect to time. A boldface italic character denotes a vector quantity. A boldface character denotes a matrix quantity.

Subscripts 'p' and 'd' correspond to the platform and deployable link, respectively. Subscript 's' refers to the slewing link or a specified coordinate.

LIST OF FIGURES

Figure 1-1	Artist view of the International Space Station with its Mobile Servicing System (MSS) as prepared by the Canadian Space Agency.	2
Figure 1-2	All the space-based manipulators have used, so far, revolute joints thus permitting only slewing motion of links.	4
Figure 1-3	Variable geometry manipulator showing: (a) single module with a pair of slewing and deployable links; (b) Several modules connected to form a snake-like geometry.	5
Figure 1-4	Variable geometry manipulator showing obstacle avoidance character.	6
Figure 1-5	Challenges faced by studies aimed at dynamics and control of large, space-based systems.	9
Figure 1-6	Schematic diagrams of space structure models: (a) Lips [33], rigid spacecraft with deployable beam-type members; (b) Ibrahim [34], rigid spacecraft with deployable beam- and plate-type members; (c) Shen [35], rigid spacecraft with slewing-deployable appendages; (d) Marom [36], flexible platform supporting one rigid slewing-deployable manipulator module and a rigid payload at the deployable link end. The revolute joint was flexible.	11
Figure 2-1	Schematic diagram of the mobile flexible variable geometry manipulator, based on an elastic space platform.	16
Figure 2-2	Coordinates describing flexibility of revolute joints.	18
Figure 2-3	Normalized time histories of the sinusoidal maneuvering profile showing displacement, velocity, and acceleration.	21
Figure 2-4	Schematic diagram of a two-module, flexible, variable geometry manipulator, based on an elastic space platform, considered for study.	23
Figure 2-5	Schematic diagram showing important parameters appearing in the response study.	26
Figure 2-6	Equilibrium of the system as affected by the manipulator's geometry and location on the platform. The diagram shows a case where the links are locked in position at $\alpha_1 = \alpha_2 = 90^\circ$ and $l_1 = l_2 = 7.5\text{m}$. The equilibrium configuration deviates from the local vertical by $\approx 0.13^\circ$.	29

Figure 2-7	Direction of rotation of the platform, initially in the local horizontal equilibrium position, due to a change in the manipulator orientation. It is governed by the location of the center of mass in different quadrants.	30
Figure 2-8	System response with a two-module manipulator located at different positions on the platform: (a) $d = 60$ m; (b) $d = 0$.	31
Figure 2-9	System response as affected by the initial orientation of the platform: (a) $\psi_p(0) = +10^\circ$;	33
	(b) $\psi_p(0) = -10^\circ$;	34
	(c) $\psi_p(0) = -80^\circ$.	35
Figure 2-10	System response with the manipulator when the platform is initially at: (a) $\psi_p(0) = -90^\circ$, i.e. aligned with the local vertical;	37
	(b) $\psi_p(0) = \psi_{p,e} = -90.13^\circ$; (c) $\psi_p(0) = -91^\circ$.	
Figure 2-11	Response of the system to an initial disturbance of 0.5m tip displacement of the platform:	
	(a) short duration behavior of rigid and flexible degrees of freedom;	39
	(b) long duration evolution of the platform's pitch libration.	40
Figure 2-12	System response to the manipulator's tip displacement of 0.2 m.	42
Figure 2-13	System response in presence of a manipulator maneuver with the platform initially aligned with the local vertical:	
	(a) long duration evolution of the platform pitch libration;	45
	(b) short duration behavior of rigid and flexible degrees of freedom.	46
Figure 2-14	System response in presence of a manipulator maneuver with the platform initially aligned with the local horizontal:	
	(a) long duration evolution of the platform pitch libration;	48
	(b) short duration behavior of rigid and flexible degrees of freedom.	49
Figure 2-15	System response as affected by payload with the manipulator completing simultaneous slew and deployment maneuvers in 0.03 orbit.	50
Figure 2-16	Influence of the speed of maneuver on the system response.	52
Figure 2-17	System response as affected by the joint stiffness which appears to be a rather critical parameter.	54
Figure 2-18	System response as affected by the number of modes used in flexibility discretization.	56

Figure 2-19	A likely procedure would involve slew and deployment separately instead of all four joints maneuvering at the same time.	57
Figure 2-20	System response, even under a set of conservative values for payload (2,000 kg), joint stiffness (5×10^4 Nm/rad) and maneuver speed (0.05 orbit), is unacceptable. This suggests a need for control.	58
Figure 3-1	A two-module manipulator system, showing frequently used symbols.	61
Figure 3-2	Schematic diagram of the manipulator system showing the location of the control actuators. The two torques $T_{pf}/2$, opposing each other, control the platform's vibration by regulating the local slope.	63
Figure 3-3	FLT-based control scheme showing inner and outer feedback loops.	67
Figure 3-4	Block diagram illustrating the combined FLT/LQR approach applied to the manipulator system.	71
Figure 3-5	Response of the system during a simultaneous 90° slew and 7.5m deployment maneuver of the two-unit manipulator with rigid degrees of freedom controlled by the FLT:	
	(a) rigid degrees of freedom and control inputs for module 1;	73
	(b) rigid degrees of freedom and control inputs for module 2;	74
	(c) flexible degrees of freedom.	75
Figure 3-6	FLT/LQR controlled response of the two-unit system during a simultaneous 90° slew and a 7.5 m deployment maneuver of the manipulator units:	
	(a) rigid degrees of freedom and control inputs for module 1;	77
	(c) rigid controlled degrees of freedom and control inputs for module 2.	78
	(c) flexible degrees of freedom.	79
Figure 3-7	FLT/LQR controlled response of the system during a simultaneous 90° slew and 7.5 m deployment maneuver of the two-unit manipulator with different payload ratios:	
	(a) rigid degrees of freedom and control inputs for module 1;	81
	(b) rigid degrees of freedom and control inputs for module 2;	82
	(c) flexible degrees of freedom.	83
Figure 3-8	Effect of the speed of maneuver on the FLT/LQR controlled response:	
	(a) platform and module 1;	85
	(b) module 2;	86
	(c) flexible degrees of freedom.	87

Figure 3-9	FLT/LQR controlled response as affected by the revolute joint stiffness during a manipulator maneuver:	
	(a) platform and module 1;	88
	(b) module 2;	89
	(c) flexible generalized coordinates.	90
Figure 3-10	Tracking of a straight line using the second module and the FLT:	
	(a) manipulator tip trajectory and errors;	93
	(b) response of the platform and rigid degrees of freedom with control inputs;	94
	(c) response of flexible degrees of freedom.	95
Figure 3-11	Tracking of a horizontal straight line with two revolute joints using the FLT:	
	(a) initial configuration and the trajectory error;	97
	(b) response of rigid degrees of freedom and control inputs;	98
	(c) response of flexible degrees of freedom.	99
Figure 3-12	Tracking of a circle using the two revolute joints and the FLT for control:	
	(a) manipulator tip trajectory and error during the period of 0-200 s;	101
	(b) manipulator tip trajectory and error during the period of 200-400s;	102
	(c) response of rigid degrees of freedom and control inputs;	103
	(d) response of flexible degrees of freedom.	104
Figure 4-1	The prototype manipulator system.	107
Figure 4-2	Main components of the two-module manipulator system.	109
Figure 4-3	Main components of the manipulator base assembly.	110
Figure 4-4	Prismatic joint mechanism which provides the deployment and retrieval capability.	112
Figure 4-5	Main components of the elbow joint assembly.	113
Figure 4-6	Open architecture of the manipulator control system for a single joint.	114
Figure 4-7	Digital robot control scheme.	118
Figure 4-8	Two-module ground based manipulator system.	123
Figure 4-9	Schematic diagram of the swing test to determine the moment of inertia of a manipulator link with different lengths.	125

Figure 4-10	Schematic diagrams for straight line tracking using: (a) one revolute joint and one prismatic joint; (b) two revolute joints.	129
Figure 4-11	Straight line tracking using one revolute and one prismatic joint under the PID control: (a) tip trajectory; (b) joint motion and the corresponding control signals.	130
Figure 4-12	Straight line tracking using two revolute joints under the PID control: (a) tip trajectories; (b) joint motion and corresponding control signals.	132
Figure 4-13	Straight line tracking using one revolute and one prismatic joint with the FLT: (a) tip trajectory; (b) joint motion and the corresponding control signals.	133
Figure 4-14	Straight line tracking using one revolute and one prismatic joint: comparison of the FLT and PID procedures.	134
Figure 4-15	Schematic diagram showing tracking of a circular trajectory using module 2.	136
Figure 4-16	Tracking of a circle, at a speed of 0.314 rad/s, using the PID control: (a) tip trajectories; (b) joint dynamics and control signals.	137
Figure 4-17	Tracking of a circle, at a speed of 0.628 rad/s, using the PID control: (a) tip trajectories; (b) joint motion and control signals.	138
Figure 4-18	Circle tracking behavior under the PID control at a speed of 0.209 rad/s: (a) tip trajectories; (b) joint dynamics and control effort.	139
Figure 4-19	Tracking of a circle, at a speed of 0.314 rad/s, with the FLT: (a) tip trajectories; (b) joint dynamics and control effort.	140
Figure I-1	Initial deflection of 5° applied to the revolute joint of module 1: (a) system response; (b) power spectral density distribution.	154 155
Figure I-2	Module 1 tip deflection of 0.2m: (a) system response; (b) power spectral density distribution.	156 157
Figure I-3	Module 2 tip deflection of 0.2m: (a) system response; (b) power spectral density distribution.	158 159

Figure I-4 Module two joint deflection of 5°:
 (a) system response;
 (b) power spectral density distribution.

160
161

LIST OF TABLES

Table 2-1	Important factors affecting the system performance.	22
Table 2-2	Fundamental natural frequencies of the components, forming the platform-based manipulator system, in absence of payload.	43
Table 4-1	Swing-test results for the ground-based robot.	125
Table 4-2	Controller gains for the prismatic joint of module 2.	127
Table 4-3	Controller gains for the revolute joint of module 2.	127
Table 4-4	Controller gains for the revolute joint of module 1.	128

ACKNOWLEDGEMENT

I wish to thank my supervisor Prof. Vinod J. Modi for his guidance, teaching and friendship throughout my graduate studies. His constant encouragement took me on an incredible journey of experience and learning throughout my graduate program.

I wish to thank my supervisor Prof. C. W. de Silva for his support and advice towards the completion of my research project.

Thanks are also due to my colleagues and friends. In the alphabetical order I wish to thank: Mr. Mathieu Caron, Mr. Jooyeol Choi, Mr. Mark Chu, Mr. Vijay Deshpande, Mr. Jean-François Goulet, Mr. Vincent Den Hertog, Dr. Sandeep Munshi, Mr. Behara Patnaik, Mr. Kenneth Wong, and Mr. Jian Zhang. They have shared their knowledge, experience, and culture with me and have thus broadened my horizons. They have made my stay in the University of British Columbia very enjoyable.

Funding for this research project has been provided through a Strategic Research Grant 5-82268 from the Natural Sciences and Engineering Research Council of Canada. It is jointly held by Dr. de Silva and Dr. Modi at the University of British Columbia, and Dr. A.K. Misra at McGill University.

1. INTRODUCTION

1.1 Preliminary Remarks

Robotic systems have been used in space as early as the 1960s [1]. In the late 60s, the unmanned Surveyor lunar mission used a rudimentary manipulator arm to dig and collect soil samples. The versatility of the space robots was demonstrated during the Surveyor 7 mission where the manipulator was employed to jab open an instrument that had failed to deploy automatically. In 1970, and again in 1973, the Soviet Lunakhod rovers surveyed large areas of the moon and used a deployable arm to lower an instrumentation package to the surface. The Viking landers, in 1976, used robotic manipulators to collect and process Martian soil samples.

The Canadian contribution to space robotics has been through the now famous Canadarm, introduced in 1981. It has played diverse, significant roles in almost all NASA's Space Shuttle missions: platform to support astronauts; position experiment modules; satellite launch and retrieval; loosen a jammed solar panel; even knocked-off a block of ice from a clogged waste water vent [2]. Perhaps its most dramatic success came in 1993 when it successfully retrieved the malfunctioning Hubble Space Telescope, placed it in the cargo bay for repair and relaunched it. In December 1998, it assisted in the integration of the U.S. 'Unity' module with the Russian control module called 'Zarya' (Sunrise), launched a few weeks earlier, thus initiating construction of the International Space Station.

For the Space Station, which is scheduled to be operational in year 2004, the Canadian contribution is through an extension of the Canadarm in the form of Mobile Servicing System (MSS, Figure 1-1). It consists of the Space Station Remote Manipulator System (SSRMS) and Special Purpose Dexterous Manipulator (SPDM). The MSS will play

an important role in the construction, operation, and maintenance of the space station [3-5]. It will also assist in the Space Shuttle docking maneuvers; handle cargo; as well as assemble, release, and retrieve satellites.

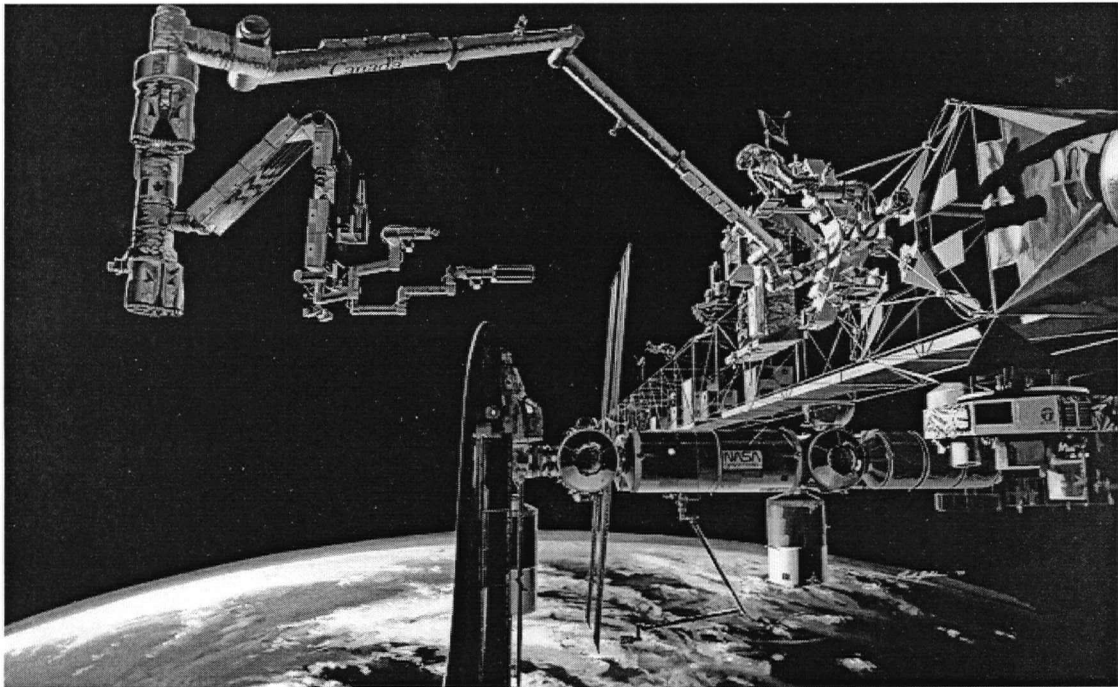


Figure 1-1 Artist view of the International Space Station with its Mobile Servicing System (MSS) as prepared by the Canadian Space Agency.

A number of other space robots have been proposed and some are under development. The American Extravehicular Activity Helper/Retriever (EVAHR) and Ranger Telerobotic Flight Experiment, as well as the Japanese ETS-VII, are examples of free-flying telerobotic systems which will be used for satellite inspection, servicing and retrieval [6,7]. Thus manipulators are serving as useful tools in the space exploration. All indications suggest the trend to accentuate with future missions becoming more dependent on robotic systems. As the Space Station will operate in the harsh environment at an altitude of 400 km, it is desirable to minimize extravehicular activity by astronauts. Robotics is identified as one

of the key technologies to reach that goal. It is important to point out that all the space-based robotic devices mentioned above use revolute joints, i.e. links are free to undergo slewing motion (Figure 1-2), as in the case of the Canadarm and MSS abode the International Space Station.

With this as background, the thesis undertakes a study aimed at a novel flexible multimodule manipulator capable of varying its geometry. Each module consists of two links (Figure 1-3a), one free to slew (revolute joint) while the other is permitted to deploy and retrieve (prismatic joint). A combination of such modules can lead to a snake-like variable geometry manipulator (Figure 1-3b) with several advantages [8]. It reduces coupling effects resulting in relatively simpler equations of motion and inverse kinematics, decreases the number of singularities, and facilitates obstacle avoidance for comparable degrees of freedom (Figure 1-4). Dynamics and control of such Multi-module Deployable Manipulator (MDM) system, free to traverse an orbiting elastic platform and carrying a payload, represent a challenging task.

1.2 A Brief Review of the Relevant Literature

As can be expected, the amount of literature available on the subject of robotics is literally enormous. The objective here is to touch upon contributions directly relevant to the study in hand.

1.2.1 Characteristics of space-based manipulators

There are several significant differences between the orbiting space platform supported manipulators and their ground-based counterparts:

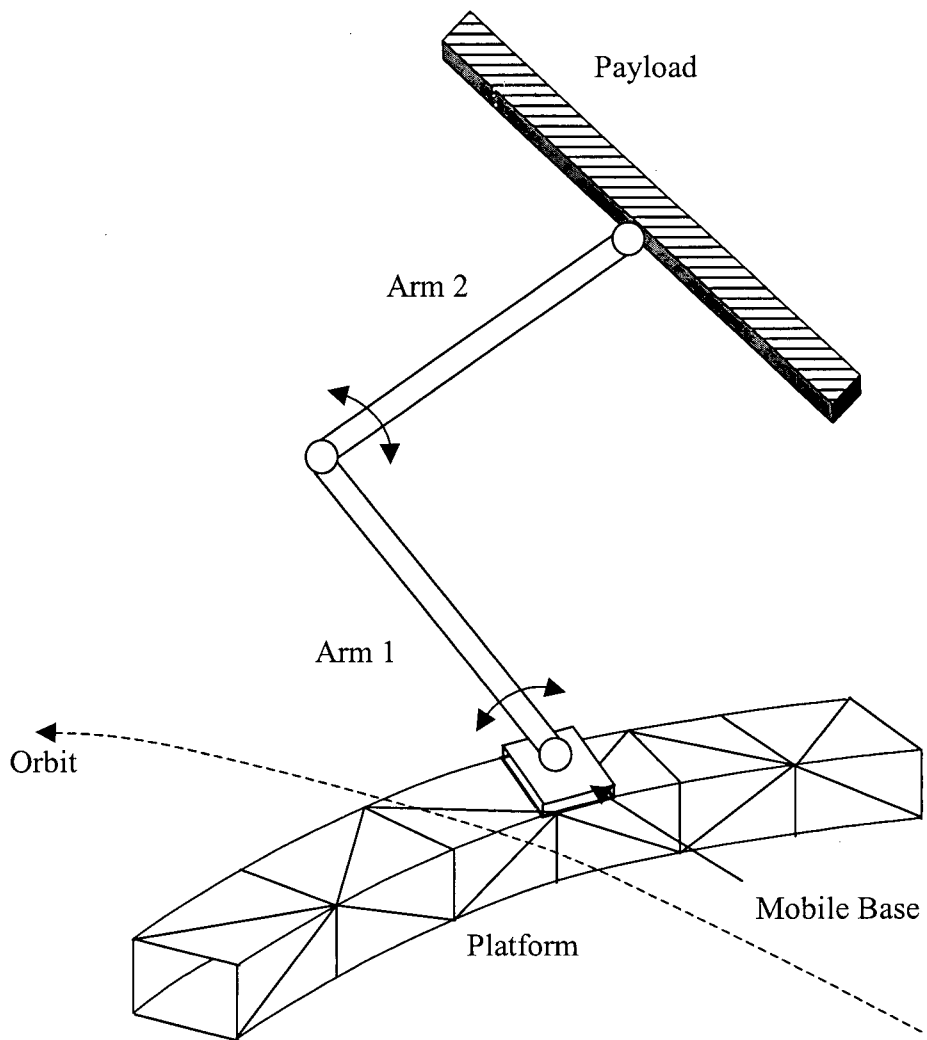


Figure 1-2 All the space-based manipulators have used, so far, revolute joints thus permitting only slewing motion of links.

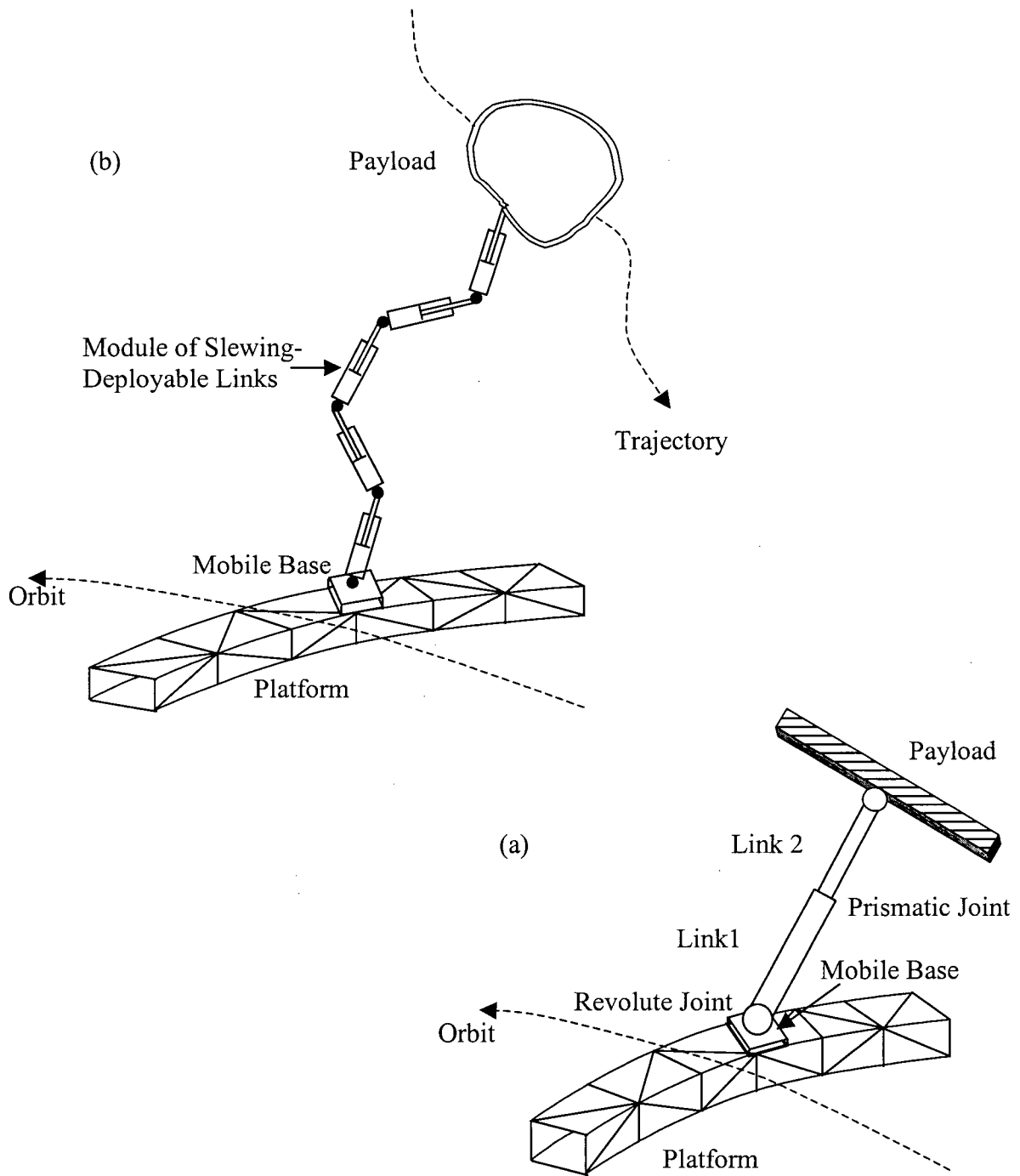


Figure 1-3 Variable geometry manipulator showing: (a) single module with a pair of slewing and deployable links; (b) several modules connected to form a snake-like geometry.

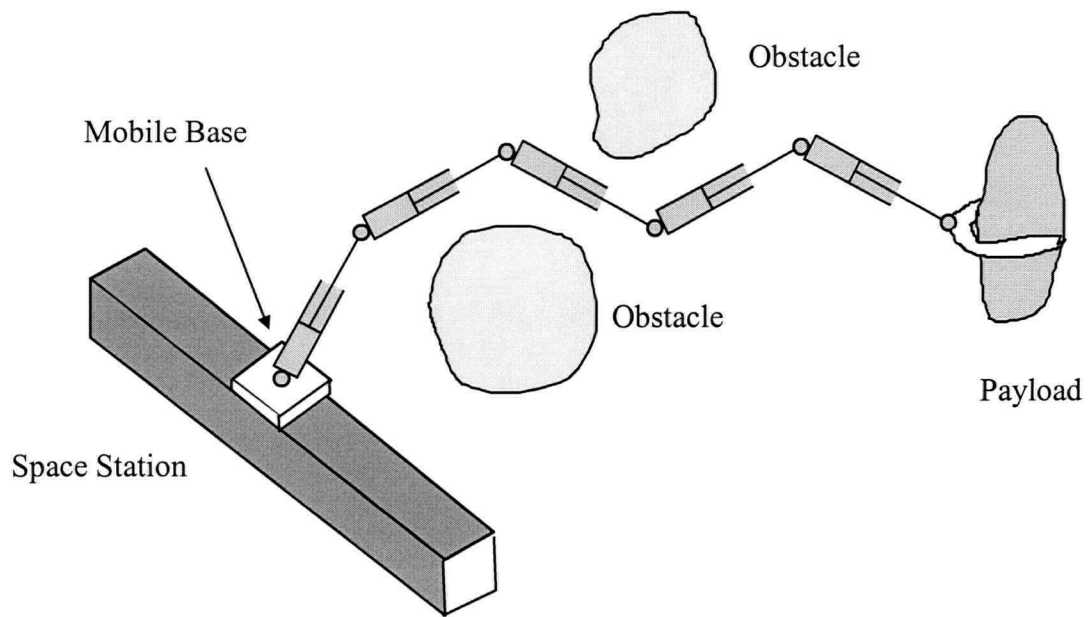


Figure 1-4 Variable geometry manipulator showing obstacle avoidance character.

- (a) Due to zero-weight condition at the system center of mass and microgravity field elsewhere, the environmental torques due to free molecular flow, Earth's magnetic field and solar radiation can become significant in the study of space manipulators [9]. The large temperature variations encountered in space may significantly affect the system dynamics and control due to thermal deformations [10,11].
- (b) As the manipulator rests on a flexible orbiting platform, their dynamics are coupled [12,13]. The manipulator maneuvers can affect attitude of the platform as well as excite it to vibrate [14]. Conversely, the librational motion of the platform would affect the manipulator's performance. Fortunately, manipulator maneuvers in space tend to be relatively slow permitting the end-effector to approach equilibrium [15].
- (c) Space manipulators tend to be large in size, lighter and highly flexible. Obviously, this will make the study of system dynamics , and its control, a formidable task.
- (d) The ratio of the payload to manipulator mass for a typical space-based system can be several orders of magnitude higher [16]. For example, in case of the Canadarm the ratio is 61.5. The corresponding ground-based manipulator used in nuclear industry (supplied by the same manufacturer) has the payload to manipulator mass ratio of 0.167 !
- (e) Obviously, space manipulators are not readily accessible for repair in case of, say, joint failure. This requires incorporation of a level of redundancy in their design [17]. Correspondingly, more degrees of freedom are involved than required for a given task.

- (f) Remote operation of a space-based manipulator would involve time delays, an important factor in control of the system. For the ROTEX teleoperation experiment it reached seven seconds [18] !

These important differences emphasize the fact that one cannot entirely rely on the vast body of literature available for ground-based manipulators. We will have to explore and understand distinctive character of the space robotic systems. Dynamics and control of a large orbiting flexible platform (like the International Space Station), supporting a mobile elastic manipulator, carrying a compliant payload represent a class of problems never encountered before. Major challenges presented by such large-scale systems are summarized in Figure 1-5. It is only recently, some of the issues mentioned here have started to receive attention. Obviously, there is an enormous task facing space dynamicists and control engineers that will keep them occupied for years to come. The points which concern us are the nonlinear, nonautonomous and coupled character of the governing equations of motion, relatively low frequencies, and development of a controller, preferably robust.

1.2.2 Dynamics and control of space-based manipulators

From the observations made earlier, it is apparent that space manipulators, as well as large flexible space structures in general, have unveiled a new and challenging field of space dynamics and control. Over the years, a large body of literature has evolved, which has been reviewed quite effectively by a number of authors including Meirovitch and Kwak [19], Roberson [20], Likins [21], as well as Modi *et al.* [22 - 26].

In the majority of studies aimed at manipulators, only revolute joints were involved, i.e. links were permitted to undergo slewing motion. On the other hand, several space

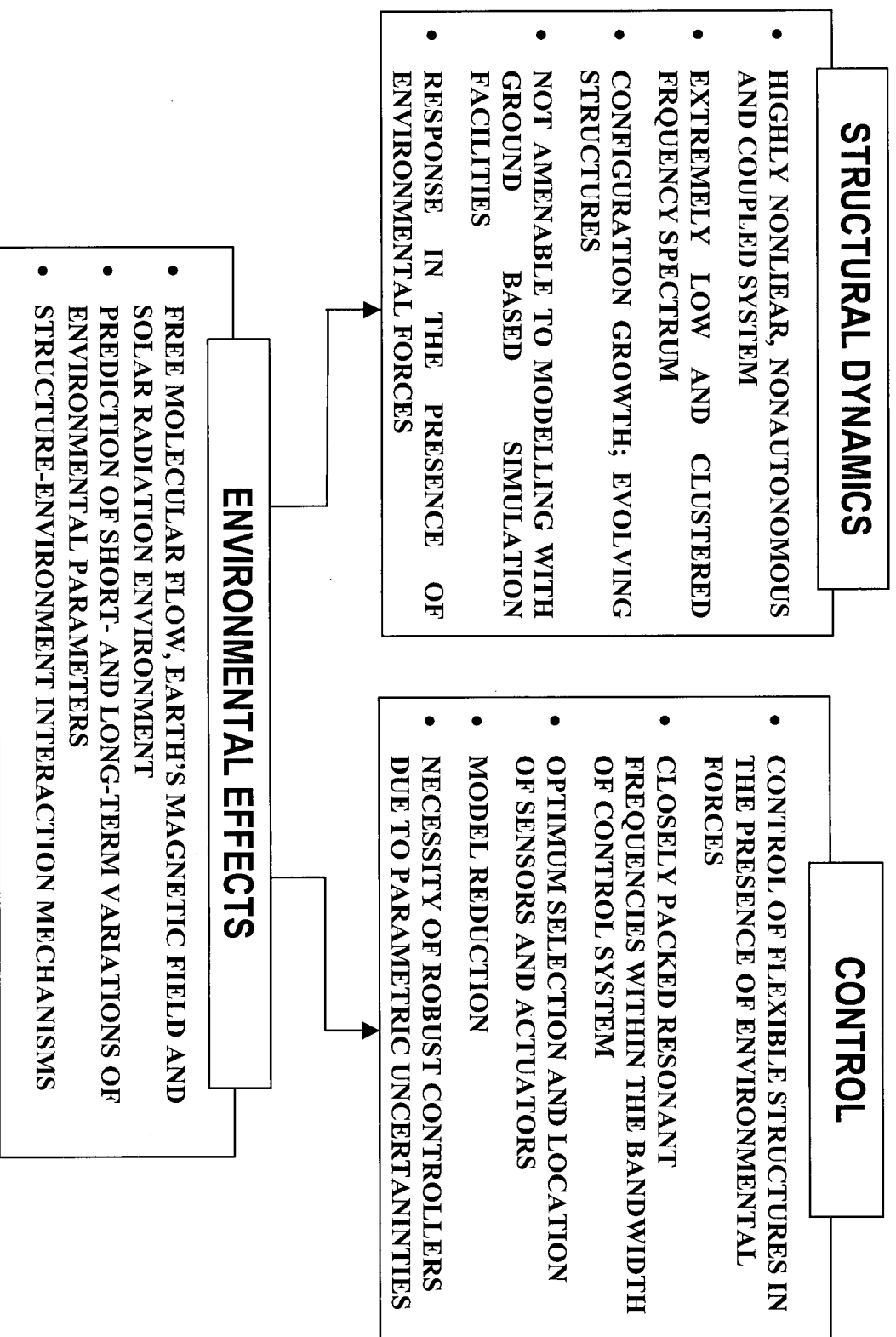


Figure 1-5

Challenges faced by studies aimed at dynamics and control of large, space-based systems.

structures feature deployment capabilities. For instance, a large solar array was deployed from the Space Shuttle cargo-bay during the Solar Array Flight Experiment (SAFE), in September 1984. Cherchas [27], as well as Sellappan and Bainum [28], studied the deployment dynamics of extensible booms from spinning spacecraft. Lips and Modi [29,30] have studied at length the dynamics of spacecraft with a rigid central body connected to deployable beam-type members. Modi and Ibrahim [31] presented a relatively general formulation for this class of problems involving a rigid body supporting deployable beam- and plate-type members. Subsequently Modi and Shen [32] extended the study to account for deployment as well as slewing of the appendages. Lips [33], Ibrahim [34], and Shen [35] have reviewed this aspect of the literature in some detail. In the above mentioned studies [29-35], although slewing and/or deployment were involved, each appendage was directly connected to the central body, i.e. a manipulator-type chain geometry of the links (appendages) was not involved. Figure 1-6 shows schematically the different models described above.

The new manipulator system, schematically shown in Figures 1-3(a) and 1-6(d), was first proposed for space application by Marom and Modi [36]. Planar dynamics and control of the one module mobile manipulator with a flexible revolute joint, located on an orbiting flexible platform, were investigated. Results showed significant coupling effects between the platform and the manipulator dynamics. Control of the system during tracking of a specified trajectory, using the computed torque technique, proved to be quite successful. Modi et al. [37] as well as Hokamoto et al. [38] extended the study to the multimodule configuration, referred to as the Mobile Deployable Manipulator (MDM) system. The model, with an arbitrary number of modules, accounted for the joint as well as link flexibility. A relatively

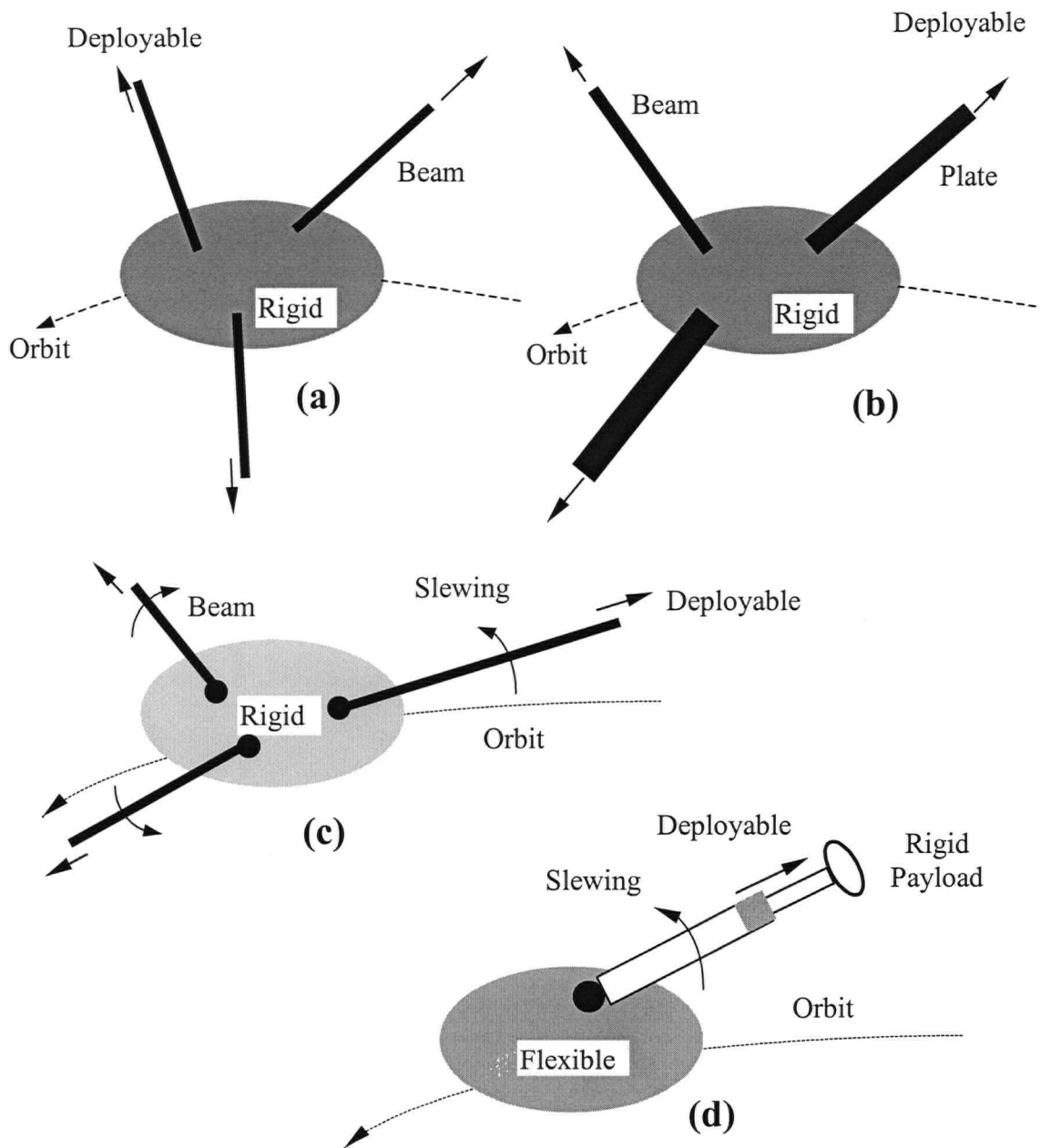


Figure 1-6 Schematic diagrams of space structure models: (a) Lips [33], rigid spacecraft with deployable beam-type members; (b) Ibrahim [34], rigid spacecraft with deployable beam- and plate-type members; (c) Shen [35], rigid spacecraft with slewing-deployable appendages; (d) Marom [36], flexible platform supporting one rigid slewing-deployable manipulator module and a rigid payload at the deployable link end. The revolute joint was flexible.

general formulation for three-dimensional dynamics of the system in orbit was the focus of the study by Modi et al., while Hokamoto et al. explored a free-flying configuration. More recently, Hokamoto et al. [40] studied control of a single unit system and demonstrated successful tracking of a straight-line trajectory at right angle to the initial orientation of the manipulator.

A comment concerning a rather comprehensive study by Caron [12] would be appropriate. He has presented an $O(N)$ formulation for studying planar dynamics and control of such formidable systems. The dynamical parametric study [42] clearly shows involved interactions between the orbital motion, flexibility, librational dynamics, and manipulator maneuvers. Furthermore, Caron [12] successfully demonstrated control of a single module (i.e. two links) manipulator, free to traverse a flexible platform, using the Feedback Linearization Technique (FLT) applied to rigid degrees of freedom, and suppression of flexible members' response through the Linear Quadratic Regulator (LQR). Recently, Chen [43] extended Caron's study and presented an order- N formulation for three-dimensional motion of a mobile manipulator traversing an orbiting flexible platform. Control of a single module manipulator, i.e. with two flexible links and an elastic revolute joint, was investigated with the Feedback Linearization Technique applied to the rigid degrees of freedom. The controlled response of the system during commanded maneuvers of the manipulator was surprisingly good. Goulet [44] studied control of a single-unit rigid manipulator with a knowledge-based hierarchical approach. The control strategy proved quite successful during pick-and-place operations as well as trajectory tracking.

Based on the literature review, following general observations can be made:

- (i) Although there is a vast body of literature dealing with modeling, dynamical performance and control of space-based manipulators, most of it is concerned with systems having revolute joints.
- (ii) Manipulators with revolute as well as prismatic joints have received relatively little attention, and that too only recently. As the concept of space-based manipulators with slewing and deployable links was developed at U.B.C., the few contributions in the field have also come from the same source. Here too, focus has been on the dynamical response of the system.
- (iii) A few reported control studies involve one-module manipulator, i.e. the system comprised of two links: One free to slew while the other is permitted to deploy. The control of multimodule manipulator does not seem to have received attention.

1.3 Scope of the Investigation

With this as background, the thesis investigates planar dynamics and control of a two-module (four links) flexible manipulator based on an elastic orbiting platform. To begin with, in Chapter 2, model used and the governing order- N equations of motion, as developed by Caron [12], are explained. A detailed dynamical response study is undertaken which assesses the influence of initial conditions, system parameters, and manipulator maneuvers. Results suggest that under critical combinations of system parameters and disturbances the response may not conform to the acceptable limit. This points to a need for active control.

Control of multimodule manipulators with slewing and deployable links logically follows the dynamical study. Two different control methodologies are used (Chapter 3):

- (a) the nonlinear Feedback Linearization Technique applied to rigid degrees of freedom with flexible generalized coordinates indirectly regulated through coupling, and
- (b) a synthesis of the FLT and LQR to achieve control of both rigid and flexible degrees of freedom.

Also, several prescribed trajectories are tracked with the FLT applied to rigid degrees of freedom.

So far the control studies were conducted using numerical simulations. In Chapter 4, a two-unit ground-based prototype manipulator, designed and constructed by Chu [8], is used to assess effectiveness of Proportional-Integral-Derivative (PID) and FLT control procedures in performing several trajectory tracking maneuvers. This brings to light, quite vividly, problems of friction and backlash often present in real-life manipulator systems.

The thesis ends with a brief review of important conclusions, significant original contributions and suggestions for future study (Chapter 5).

2. DYNAMICS OF SPACE-BASED MULTI-MODULE MANIPULATOR

2.1 Background to Formulation

It was mentioned earlier that the order- N Lagrangian formulation for the novel variable geometry manipulator was developed by Caron [12]. The distinct features of the system model used may be summarized as follows:

- (a) The manipulator with an arbitrary number of modules, each carrying a slewing and a deployable link thus involving both revolute and prismatic joints, is supported by a mobile base free to traverse a platform. The platform is in an orbit around Earth (Figure 2-1).
- (b) The supporting platform, manipulator modules and revolute joints are treated as flexible. Prismatic joints are considered as integral parts of modules.
- (c) The module is permitted to have variable mass density, flexural rigidity and cross-sectional area along its length.
- (d) The system is permitted to undergo planar librational as well as vibrational motions. The slewing maneuver at any joint is confined to the plane of the orbit.
- (e) The damping is accounted for through Rayleigh's dissipation function.
- (f) The governing equations account for gravity gradient effects, shift in center of mass as well as change in inertia due to maneuvers and flexibility.

As pointed out in Chapter 1, such a manipulator with a combination of revolute and prismatic joints is able to change its geometry, has a marked decrease in dynamical coupling, a reduction in the number of singularity conditions, and can negotiate obstacles with ease. Note, the model considered is relatively general and applicable to a large class of space- as well as ground-based manipulator systems.

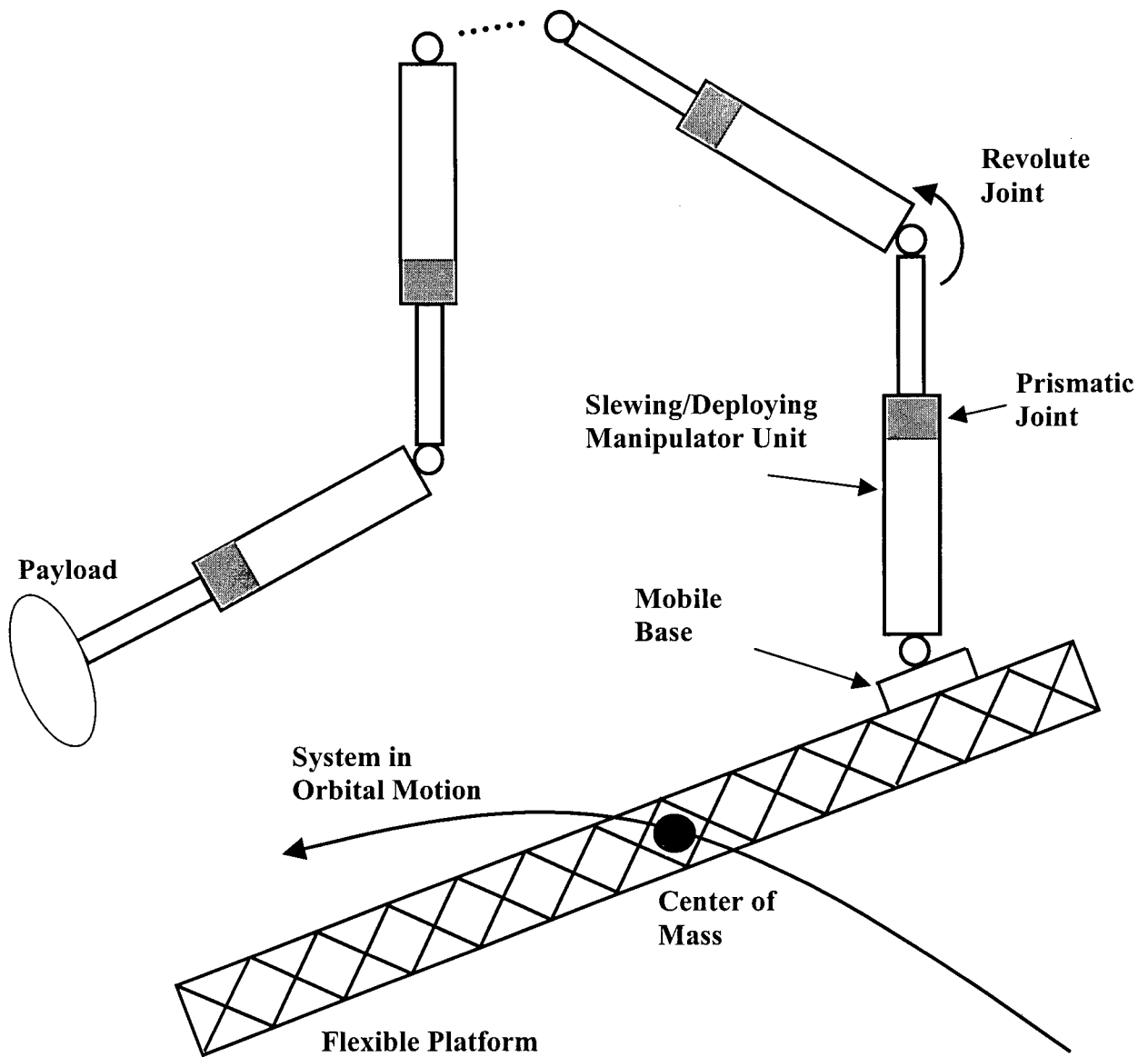


Figure 2-1 Schematic diagram of the mobile flexible variable geometry manipulator, based on an elastic space platform.

The Lagrangian approach adopted for derivation of the governing equations is particularly well suited to the flexible multibody system, with a large number of degrees of freedom, under consideration. It automatically satisfies holonomic constraints while the nonholonomic constraints can be accounted for, quite readily, using Lagrange multipliers. The form of the equations of motion conveys a clear physical meaning in terms of contributing forces. Equally important is the fact that the equations are readily amenable to stability study and well suited for controller design. Furthermore, validity of the formulation and numerical integration code can be checked with ease through the conservation of energy for nondissipative systems.

A comment concerning representation of the revolute joint's flexibility would be appropriate. The rotation γ_i of the frame F_i , attached to the module i , with respect to the frame F_{i-1} has three contributions (Figure 2-2): elastic deformation of the $i^{\text{th}} - 1$ body in the transverse direction (ξ_i); rotation of the actuator rotor (α_i), which corresponds to the controlled rotation of the revolute joint; and elastic deformation of the joint i (β_i) which could be due to, for instance, flexible coupling. Hence,

$$\gamma_i = \xi_i + \alpha_i + \beta_i. \quad (2.1)$$

2.2 Simulation Methodology

The equations governing the dynamics of the robotic systems mentioned above are highly nonlinear, nonautonomous, and coupled. They can be expressed in the general form

$$M(\mathbf{q}, t)\ddot{\mathbf{q}} + F(\dot{\mathbf{q}}, \mathbf{q}, t) = \mathbf{Q}(\dot{\mathbf{q}}, \mathbf{q}, t), \quad (2.2)$$

where $M(\mathbf{q}, t)$ is the system mass matrix; \mathbf{q} is the vector of the generalized coordinates; $F(\dot{\mathbf{q}}, \mathbf{q}, t)$ contains terms associated with centrifugal, Coriolis, gravitational, elastic, and

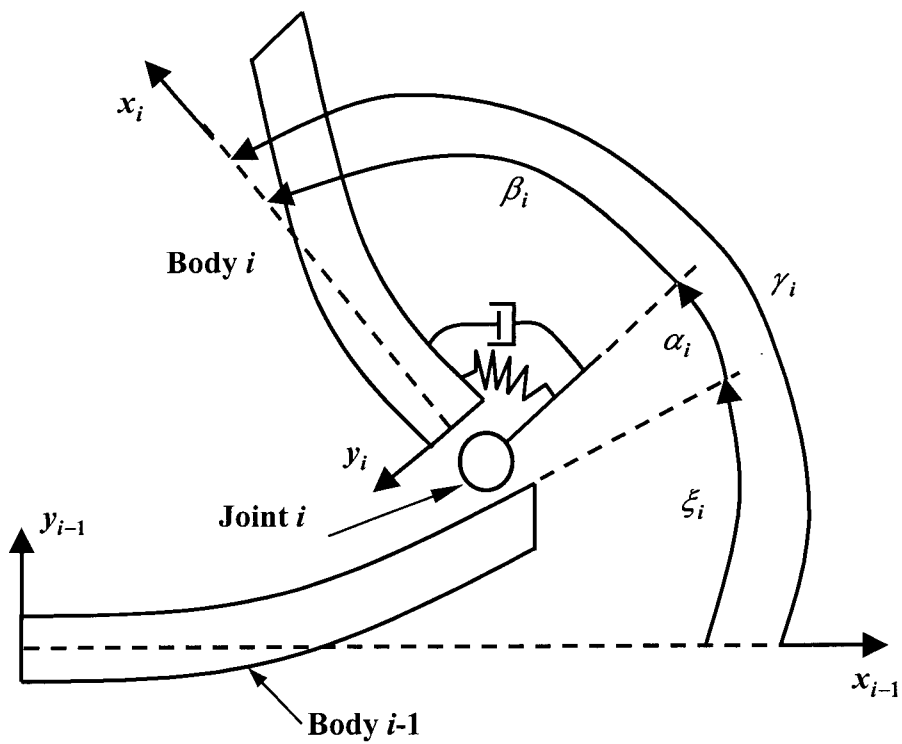


Figure 2-2 Coordinates describing flexibility of revolute joints.

internal dissipative forces; and $Q(\dot{q}, q, t)$ represents generalized forces, including the control inputs. Equation (2.2) describes the inverse dynamics (i.e. forces corresponding to a specified motion) of the system. For simulations, forward dynamics is of interest, and Eq. (2.2) must be solved for \ddot{q} ,

$$\ddot{q} = M^{-1}(Q - F). \quad (2.3)$$

The solution of these equations of motion generally requires $O(N^3)$ arithmetic operations, where N represents the number of bodies (modules) considered in the study. In other words, the number of computations required by the $O(N^3)$ algorithm will vary as the cube of the number of modules. It also depends on the number of generalized coordinates associated with each module. Clearly, the computation cost can become prohibitive for a system with a large number of modules or generalized coordinates. Hence, the development of the $O(N)$ formulation by Caron [12], where the number of arithmetic operations increases linearly with the number of bodies (or degrees of freedom) in the system, promises a significant saving in the computational cost. Equally important is a possibility of real-time implementation of a control strategy.

It is often useful to specify some of the generalized coordinates. For example, cases where the length of the units is varied in a specified manner, or where joints are locked in place at a specified angle, require the use of specified coordinates. These coordinates are prescribed through constraint relations which are introduced in the equations of motion through Lagrange multipliers.

In the present study, a sinusoidal acceleration profile is adopted for prescribed maneuvers. It assures zero velocity and acceleration at the beginning and end of the maneuver, thereby reducing the structural response of the system. The maneuver time-

history considered is as follows,

$$\mathbf{q}_s(\tau) = \frac{\Delta \mathbf{q}_s}{\Delta \tau} \left\{ \tau - \frac{\Delta \tau}{2\pi} \sin\left(\frac{2\pi}{\Delta \tau} \tau\right) \right\}, \quad (2.4)$$

where \mathbf{q}_s is the specified or constrained coordinate; $\Delta \mathbf{q}_s$ is its desired variation; τ is the time; and $\Delta \tau$ is the time required for the maneuver. The time history for \mathbf{q}_s , $\dot{\mathbf{q}}_s$, and $\ddot{\mathbf{q}}_s$ are plotted, for the case of $\Delta \mathbf{q}_s = 1$ and $\Delta \tau = 1$, in Figure 2-3.

A FORTRAN program for the dynamical simulation of the system integrates the acceleration vector $\ddot{\mathbf{q}}$ numerically using Gear's method, which is well suited for stiff systems of ordinary differential equations. To reduce computational time during simulations, a symbolic manipulation routine (MAPLE V) is used in order to obtain analytical expressions for the integrals of the shape functions. Furthermore, efficient matrix multiplication algorithms are developed to take advantage of the structure of various matrices involved.

2.3 Simulation Considerations

The system performance is governed by a large number of parameters. Some of the important variables are listed in Table 2-1.

Obviously, a systematic change of these variables would lead to a large volume of information. However, it would also demand considerable amount of time, effort and computational cost. Hence, one is forced to focus on cases that are likely to provide useful trends. These include the manipulator position; platform, link and joint flexibility; number of modes; profile and speed of maneuver; and mass of the payload. Even with these selected parameters, the task is formidable. Hence only a few typical results corresponding to a two-module manipulator, i.e. with four links, are presented for conciseness (Figure 2-4).

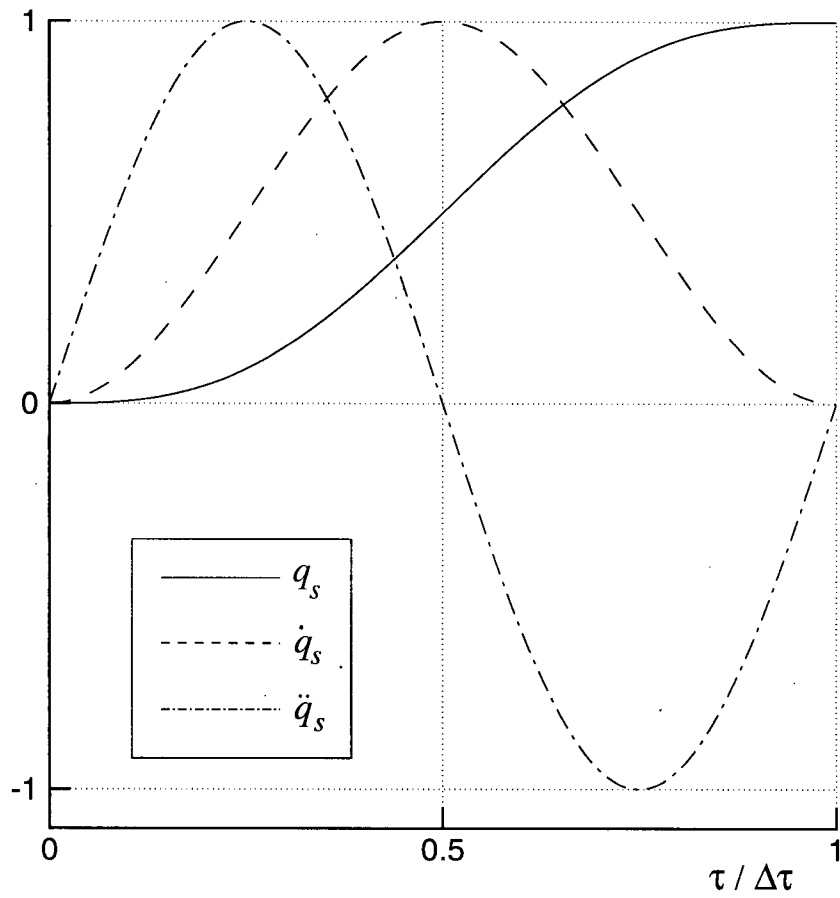


Figure 2-3 Normalized time histories of the sinusoidal maneuvering profile showing displacement, velocity, and acceleration.

Table 2-1 Important factors affecting the system performance.

Parameters	<ul style="list-style-type: none">• orbit eccentricity• mass of : platform; links; joints; payload• stiffness of : platform; links; joints• damping of : platform; links; joints• link length
Initial Conditions	<ul style="list-style-type: none">• platform attitude• manipulator location and orientation• deformation of platform, manipulator links, joints
Maneuvers	<ul style="list-style-type: none">• type : slewing; deployment; retrieval; base translation• amplitude• speed
Discretization	<ul style="list-style-type: none">• shape of admissible functions (modes)• number of admissible functions (modes)

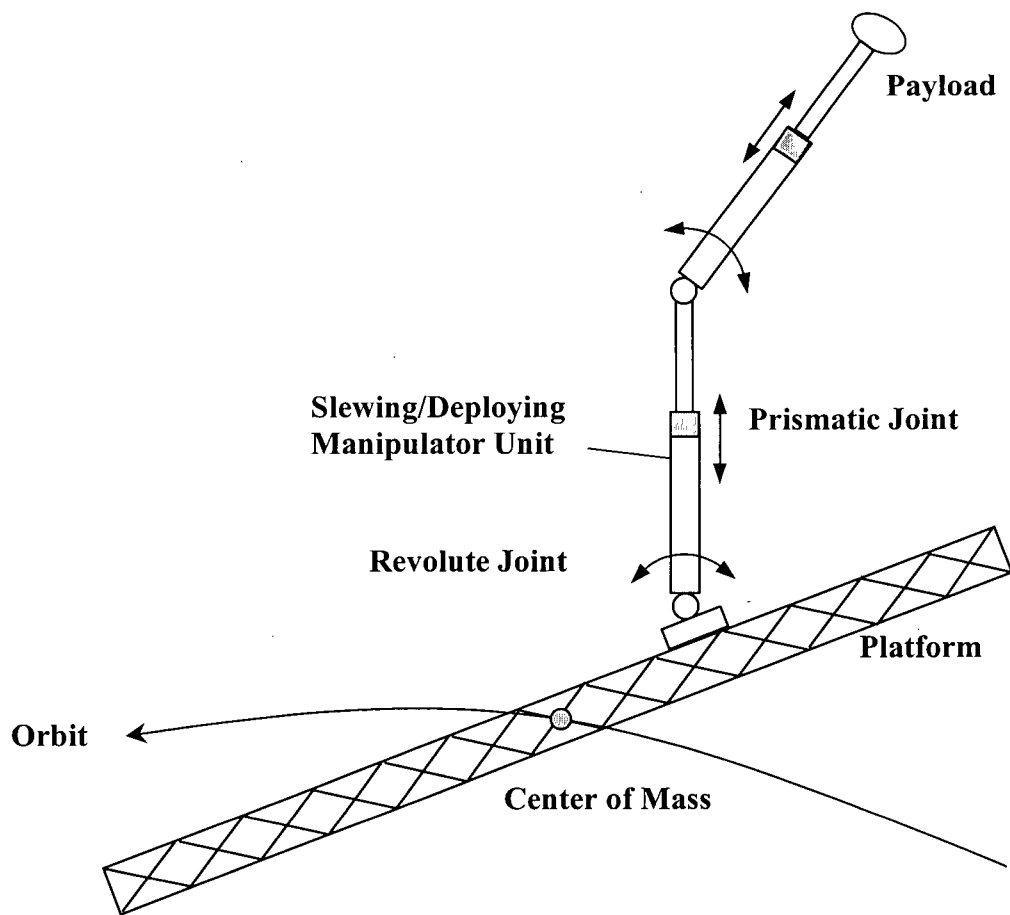


Figure 2-4 Schematic diagram of a two-module, flexible, variable geometry manipulator, based on an elastic space platform, considered for study.

Numerical values used in the analysis, unless specified otherwise, are indicated below:

Orbit:

Circular orbit at an altitude of 400 km; period = 92.5 min.

Platform:

Geometry: circular cylindrical with diameter = 3 m; axial to transverse inertia ratio of 0.005;

Mass (m_p) = 120,000 kg;

Length (l_p) = 120 m;

Flexural Rigidity (EI_p) = 5.5×10^8 Nm².

Manipulator Position (d):

$d = 0$ or 60 m.

Manipulator Module (l_1, l_2):

Initial length of the manipulator module (i.e. $l_s +$ deployed length, $7.5 + l_d$) is taken as 7.5 m, i.e. the deployable link is initially not extended. Here l_s, l_d represent lengths of slewing and deployable links, respectively.

Manipulator Links (Slewing and Deployable):

Geometry: circular cylindrical with axial to transverse inertia ratio of 0.005

Mass (m_s, m_d) = 200 kg;

Length ($l_s, l_{d,max}$) = 7.5 m;

Flexural Rigidity (EI_s, EI_d) = 5.5×10^5 Nm².

Revolute Joint:

Mass (m_j) = 20 kg;

Moment of Inertia (I_{jz}) = 10 kgm²;

Stiffness (K_j) = 10⁴ Nm/rad .

Note, the prismatic joint is treated as a part of the slewing link.

Payload:

Nominally zero. Specified in figure legend when different.

Modes:

Fundamental mode for a cantilever beam with tip mass for modules, free-free beam mode for platform.

Note, subscripts d, j, m, p, and s correspond to deployable link, revolute joint, manipulator, platform and slewing link, respectively. Initially the platform is in equilibrium either along the local vertical (stable) or aligned with the local horizontal (unstable) position. The manipulator links are aligned with the platform, i.e. they are also along the local vertical or local horizontal before the maneuver. The system is subjected to a maneuver of 90° in slew and 7.5 m deployment. Maneuver time is variable. The damping is purposely assumed to be zero in all components to obtain conservative estimate of the response, i.e. the damping coefficient for joints (C_j) as well as structural damping coefficients for manipulator links (ζ_m) and the platform (ζ_p) are considered zero. More important specified and response parameters are summarized below and indicated in Figure 2-5:

d position of the base from the center of the platform;

e_1, e_2 tip vibrations of modules one and two, respectively;

e_p platform tip vibration;

x, y body fixed coordinate system with x aligned with the undeformed axis of the platform and y normal to x in the orbital plane;

α_1, α_2 rigid body rotations, during slew maneuvers of modules one and two, respectively;

β_1, β_2 contributions due to flexibility of revoluted joints at modules one and two, respectively;

ψ_p platform pitch libration.

2.4 System Response

This section studies effect of system parameters and disturbances, in the form of initial conditions as well as manipulator maneuvers, on the resulting response. It clearly shows that under certain combinations of system's physical properties and disturbances, the response can become unacceptable suggesting a need for control.

2.4.1 Effect of manipulator location and orientation

At the outset it must be recognized that the platform, a long flexible beam, has two equilibrium positions: along the local vertical (stable) and aligned with the local horizontal (unstable). The presence of manipulator, when aligned with the platform, has virtually no effect on the equilibrium as the geometry remains effectively unchanged, as well as relatively massive (120,000 kg) character of the platform compared to the manipulator (800 kg). However, with different orientations of the modules, the geometry changes, i.e. they no longer remain in alignment with the local vertical or the local horizontal position. The system's new equilibrium orientation slightly deviates depending on the slew and deployment characters as well as location of the manipulator on the platform. For example, consider the equilibrium position corresponding to the case when the manipulator is located

at the tip ($d = 60$ m), $\alpha_1 = \alpha_2 = 90^\circ$, and the deployable links of both modules remain unextended ($l_1 = l_2 = 7.5$ m) as indicated in Figure 2-6. The deviation in the equilibrium position ($\psi_{p,e}$) from the local vertical (or local horizontal) is around 0.13° . This acts as a small disturbance and sets the platform oscillating. The local vertical orientation being stable, the platform tends to move towards and oscillate about the new equilibrium position. On the other hand, the local horizontal position being unstable, the platform moves away from it; the direction of rotation being governed by the position of the center of mass with respect to the local horizontal (Figure 2-7).

Figure 2-8 shows the effect of a two-module manipulator located at the center of the platform ($d = 0$) and at the platform tip ($d = 60$ m). Each module is taken to be 7.5 m long, i.e. the links are not deployed ($l_1 = l_2 = 7.5$ m). Both modules are locked in position with $\alpha_1 = \alpha_2 = 90^\circ$. This results in a shift in the center mass causing a pitch moment, which increases as the base supporting the manipulator moves towards the platform tip. Note, with $d = 60$ m, the peak platform deviation from the local vertical is $\approx 0.27^\circ$. This may appear small, however, depending on the mission, the permissible deviation may be as small as 0.1° . The system oscillates about the new equilibrium position of $\psi_{p,e} \approx 0.13^\circ$. The librational period of 0.6 orbit matches precisely with the established value for a long spacecraft in a circular orbit. On the other hand, with the manipulator at the center of the platform, the center of mass is slightly below the local horizontal (i.e. $-x_{cm}$). This leads to the pitch angle for equilibrium, $\psi_{p,e}$, that is positive. The amplitude of oscillation, as can be expected, is rather small ($\approx 0.01^\circ$) due to an insignificant pitching moment caused by the shift in the center of mass because of the presence of the manipulator.

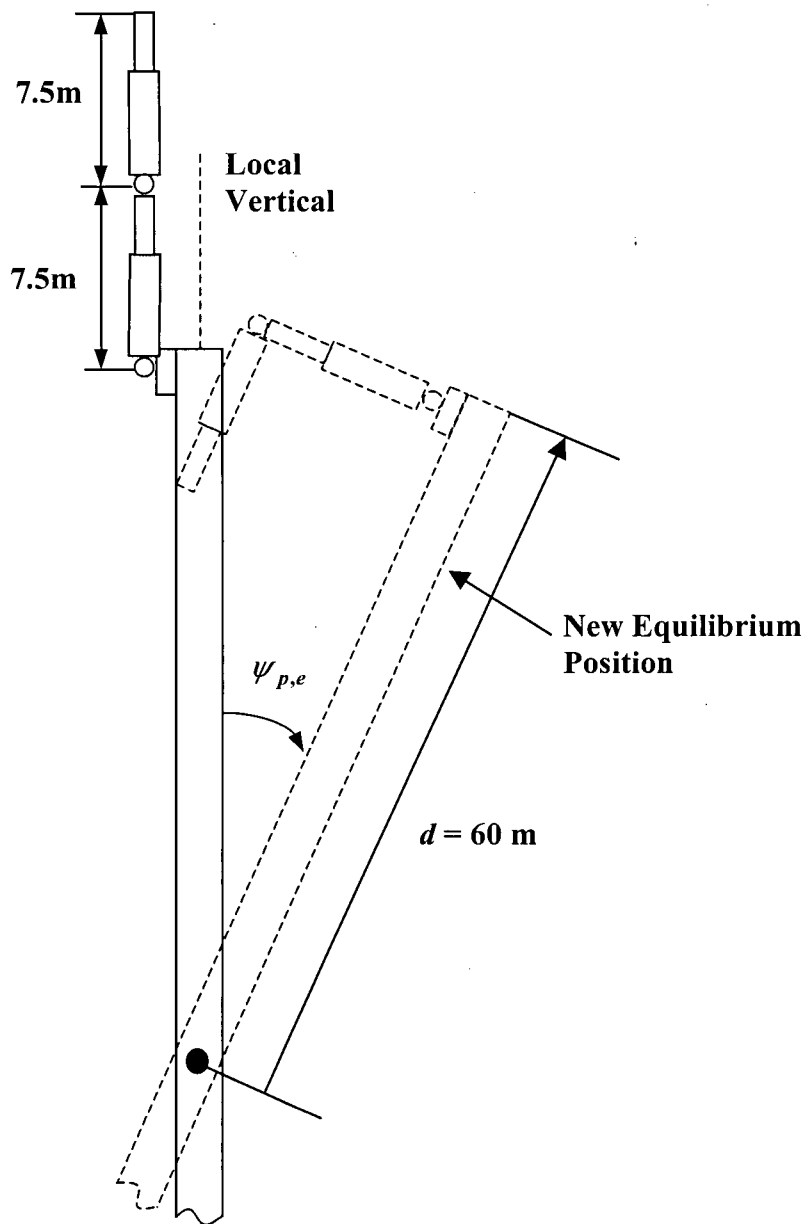


Figure 2-6 Equilibrium of the system as affected by the manipulator's geometry and location on the platform. The diagram shows a case where the links are locked in position at $\alpha_1 = \alpha_2 = 90^\circ$ and $l_1 = l_2 = 7.5\text{m}$. The equilibrium configuration deviates from the local vertical by $\approx 0.13^\circ$.

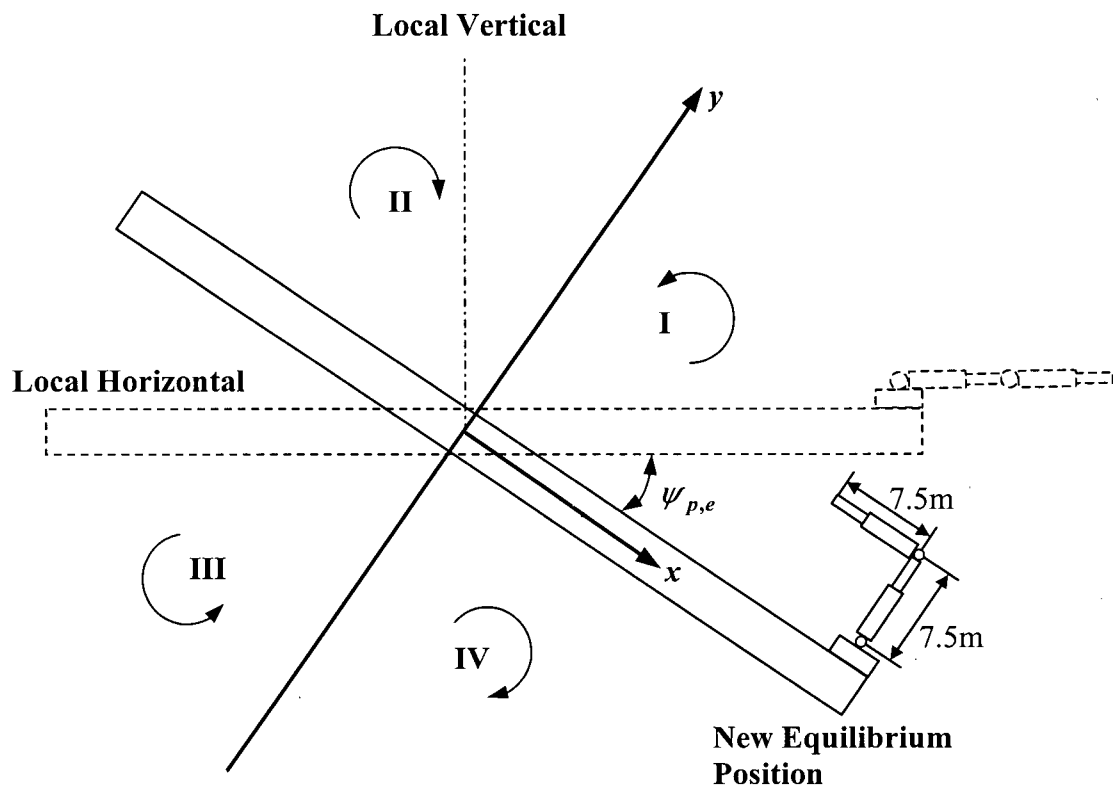


Figure 2-7 Direction of rotation of the platform, initially in the local horizontal equilibrium position, due to a change in the manipulator orientation. It is governed by the location of the center of mass in different quadrants.

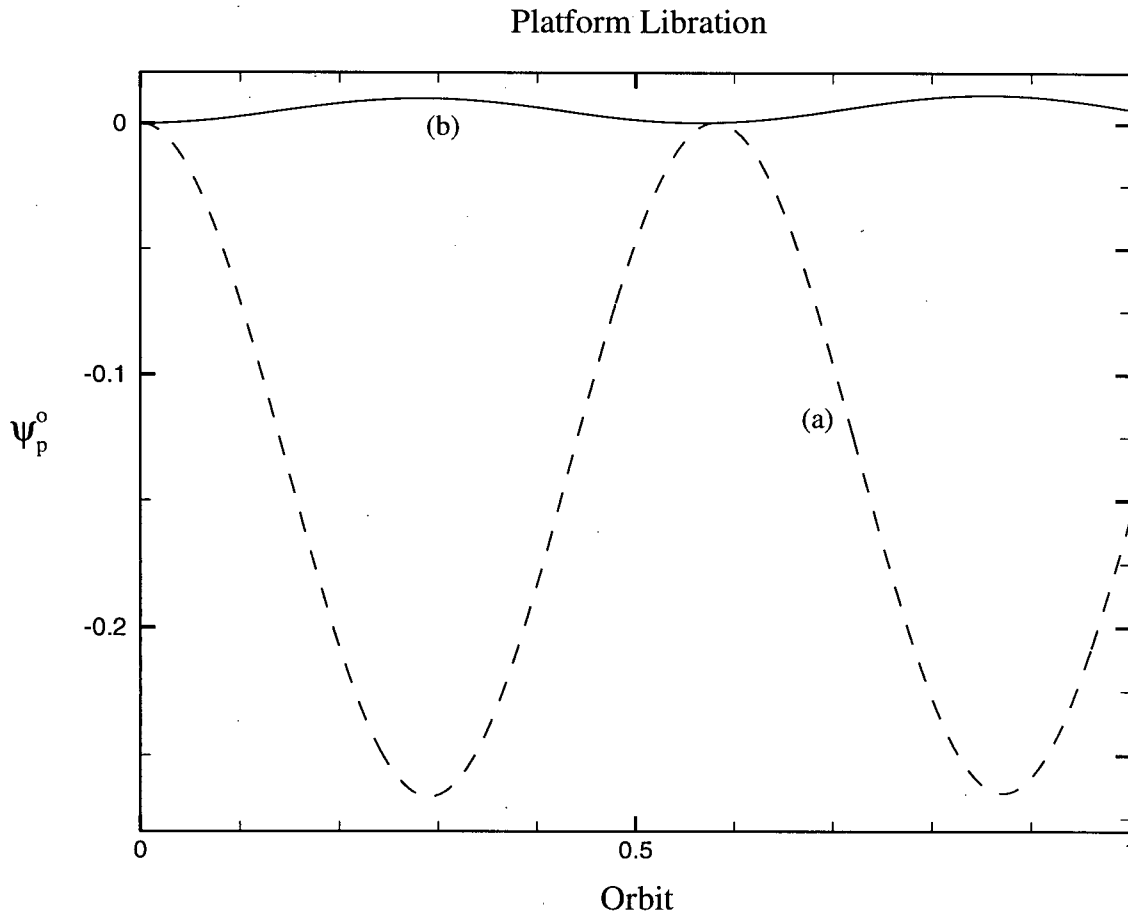
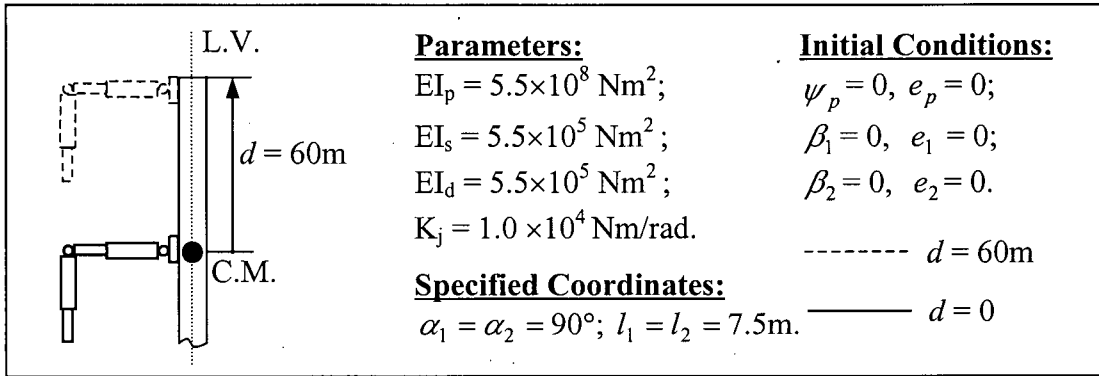


Figure 2-8 System response with a two-module manipulator located at different positions on the platform: (a) $d = 60 \text{ m}$; (b) $d = 0$.

Figure 2-9 shows the effect of initial conditions on the resulting response. The manipulator is located at the platform tip ($d = 60\text{m}$) with the same orientation as before, i.e. $l_1 = l_2 = 7.5\text{m}$ and $\alpha_1 = \alpha_2 = 90^\circ$. Three different initial positions of the platform with respect to the local vertical are considered: $\psi_p(0) = +10^\circ, -10^\circ$ and -80° . In all the three cases, the platform oscillates about the stable equilibrium position close to the local vertical ($\psi_{p,e} = -0.13^\circ$). With a small damping, the system would have returned to the equilibrium position, i.e. essentially to the local vertical orientation. Note, the amplitude of oscillations in Case (a) is slightly larger than 10° ($\approx 10.13^\circ$) as the oscillations take place about the equilibrium position, which is now at $\psi_{p,e} = -0.13^\circ$. On the other hand, the amplitude in Case (b) is slightly lower than 10° ($\approx 9.87^\circ$). Similarly in Case (c), the starting position is 79.87° away from the equilibrium location leading to the resulting amplitude of 79.87° .

A word about the pitch librational period would be appropriate. It can be obtained from the governing equation [9]

$$(1 + e \cos \theta) \psi_p'' - 2e \sin \theta (\psi_p' + 1) + 3K_i \sin \psi_p \cos \psi_p = 0, \quad (2.5)$$

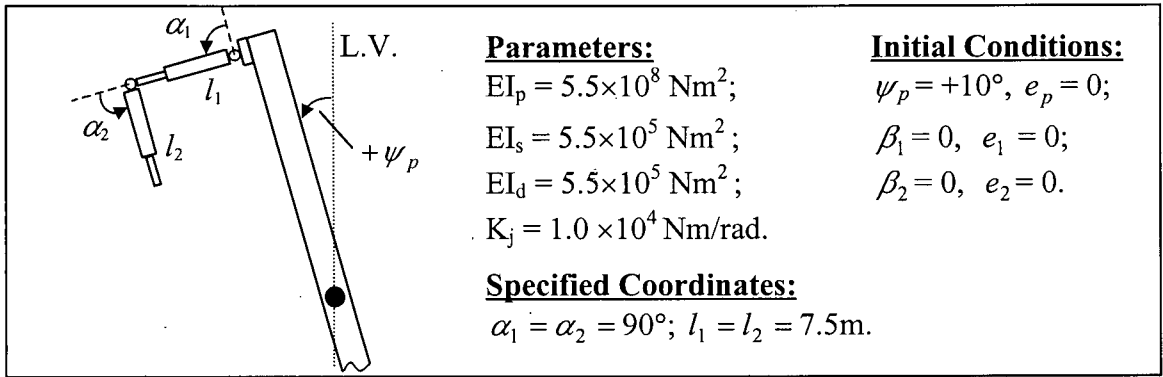
where: ψ_p = pitch librational angle;

e = orbital eccentricity;

θ = true anomaly;

K_i = spacecraft's inertia parameter, $(I_y - I_x)/I_z$;

x, y, z = body coordinate system; in equilibrium x, y in the orbital plane with x along the local vertical, y along the local horizontal and z aligned with the orbit normal.



Platform Libration

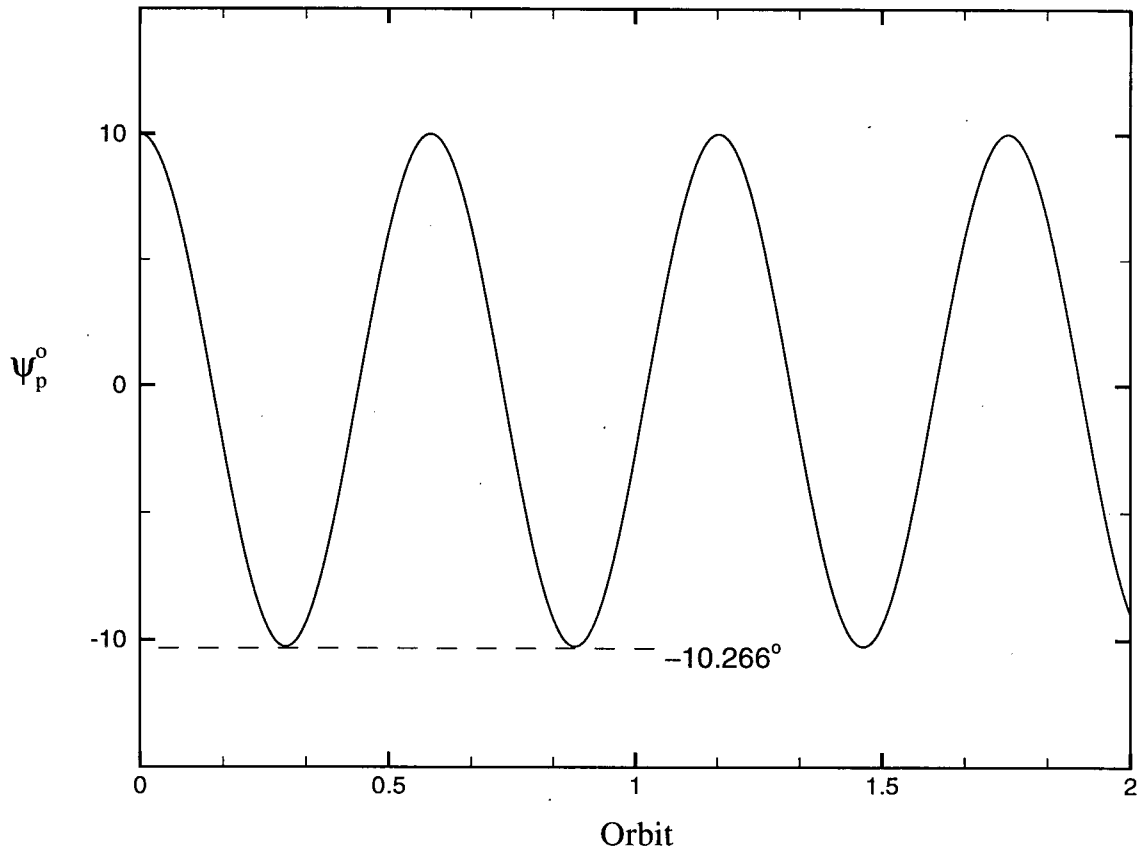


Figure 2-9 System response as affected by the initial orientation of the platform:
 (a) $\psi_p(0) = +10^\circ$.

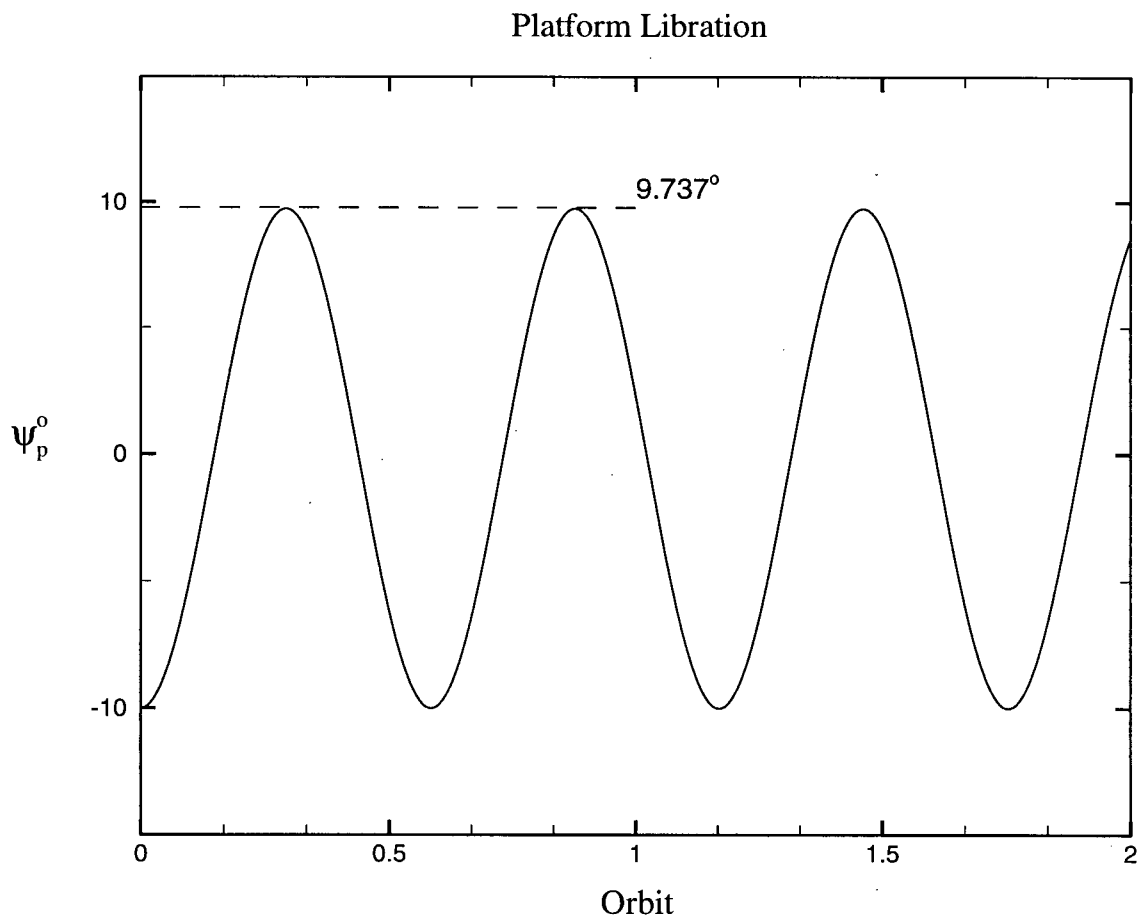
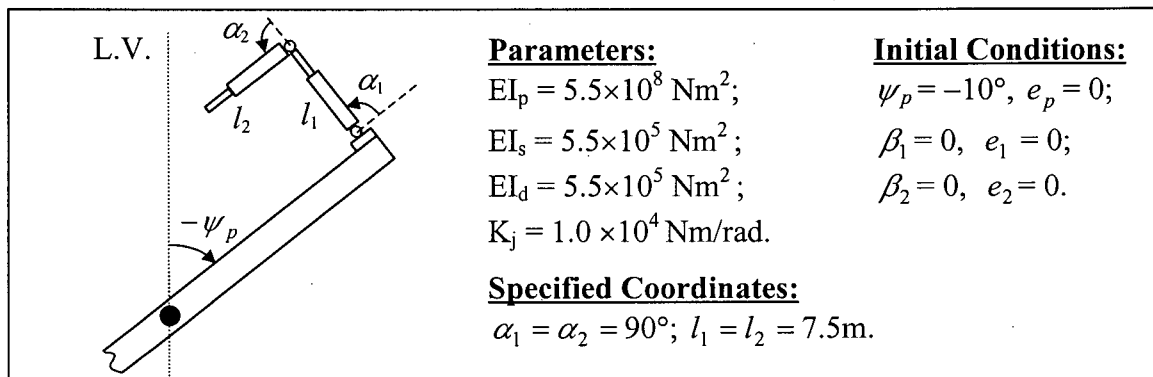
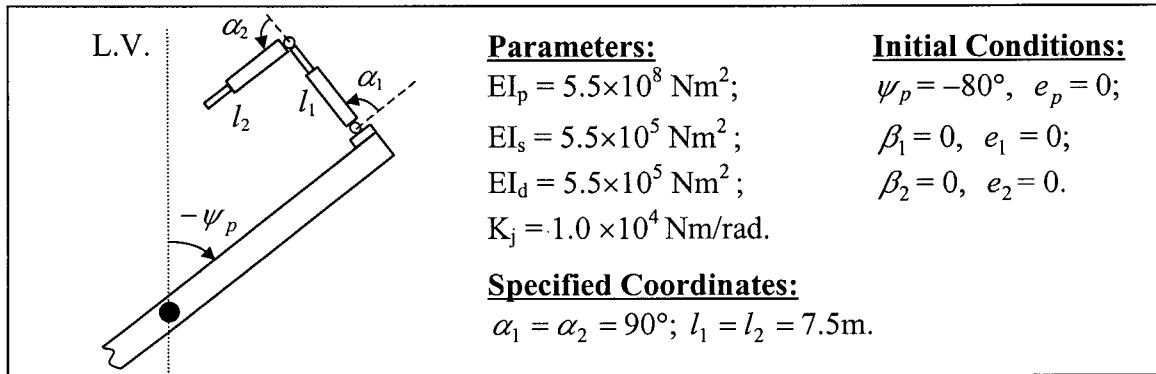


Figure 2-9 System response as affected by the initial orientation of the platform:
 (b) $\psi_p(0) = -10^\circ$.



Platform Libration

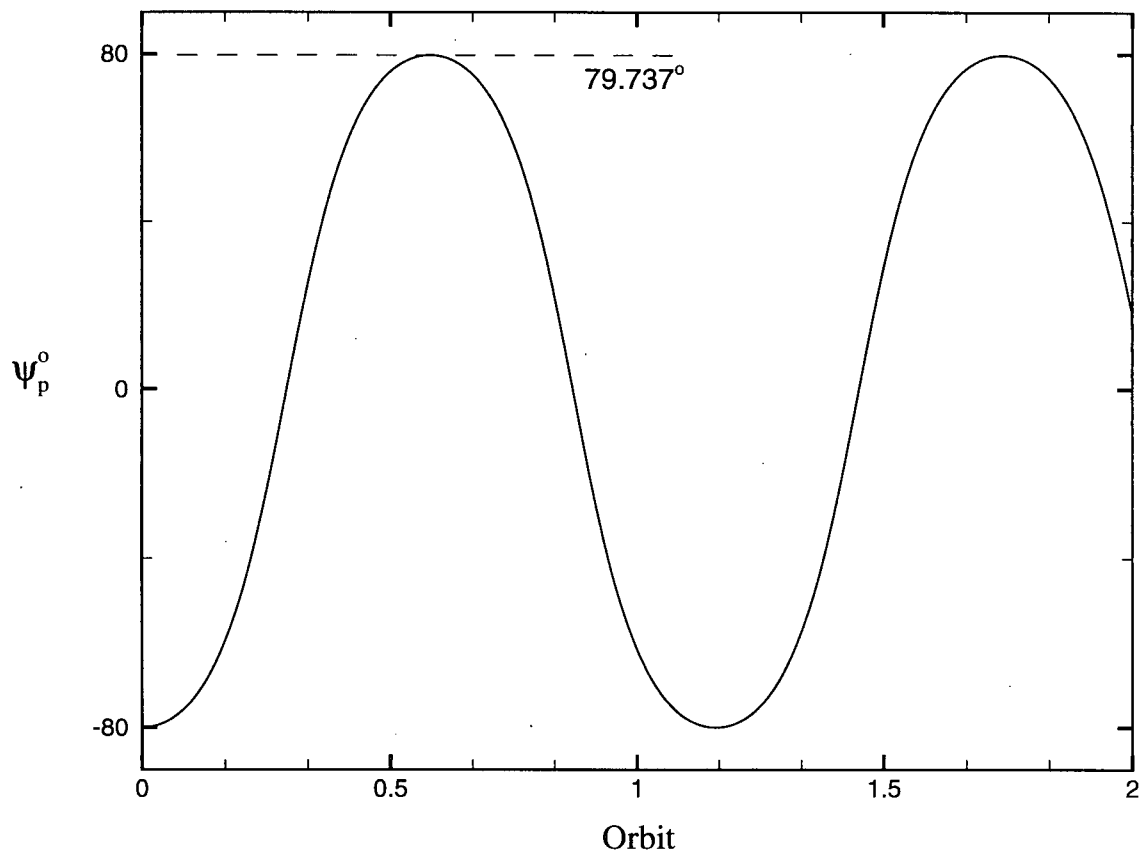


Figure 2-9 System response as affected by the initial orientation of the platform:
(c) $\psi_p(0) = -80^\circ$.

Primes denote differentiation with respect to θ . For a circular orbit, $e = 0$, i.e.

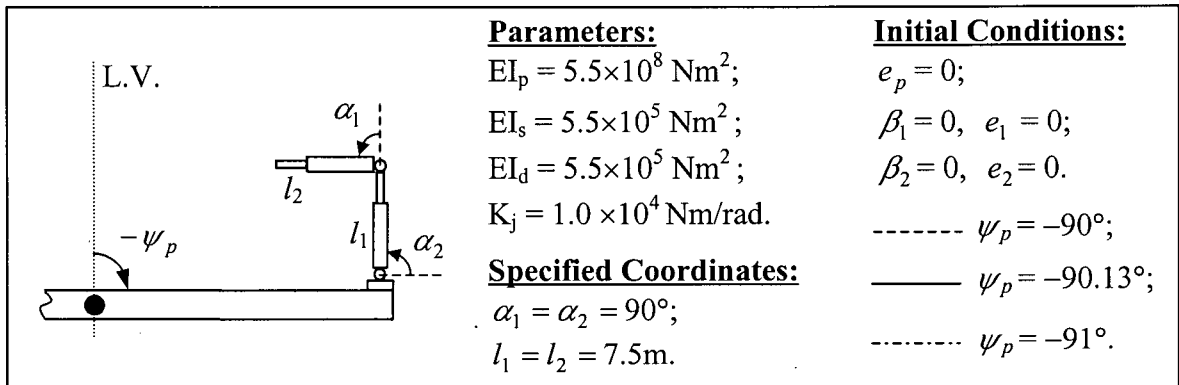
$$\psi_p'' + 3K_i \sin \psi_p \cos \psi_p = 0.$$

In the case of a long spacecraft like a 120m long uniform platform (120,000 kg) with a small two-module manipulator (800 kg), $K_i \approx 1$. Thus the librational period τ_p is given by

$$\begin{aligned} \tau_p &= \frac{2\pi}{\sqrt{3}} && \text{radian per pitch cycle,} \\ &= \frac{1}{\sqrt{3}} && \text{orbit per pitch cycle,} \\ &= 0.577 && \text{orbit per cycle.} \end{aligned}$$

Note, in Figures 2-9(a) and 2-9(b), the pitch amplitude is relatively small and the linear approximation is valid giving the pitch period of around 0.58 orbit. However, with large amplitude oscillations in Case (c), the nonlinearities significantly affect the period, which is now ≈ 1.17 orbits.

Figure 2-10(a) considers the case where the platform is initially aligned with the local horizontal, i.e. $\psi_p(0) = -90^\circ$. In absence of the manipulator, the platform would have stayed there, being an equilibrium position. However, due to presence of the manipulator ($l_1 = l_2 = 7.5\text{m}$, $\alpha_1 = \alpha_2 = 90^\circ$), the new equilibrium orientation corresponds to $\psi_{p,e} = -90.13^\circ$. This, being the unstable equilibrium position, causes the platform to swing away from it. When the platform reaches $\psi_p = 90^\circ$, the same thing happens. As seen in Figure 2-7, the center of mass is now in quadrant III causing the platform to continue rotation in the anticlockwise sense. Thus, in absence of dissipation, one has a perpetually rotating platform ! Of course, the energy input corresponds to the initial deviation of the platform from the new equilibrium position.



Platform Libration

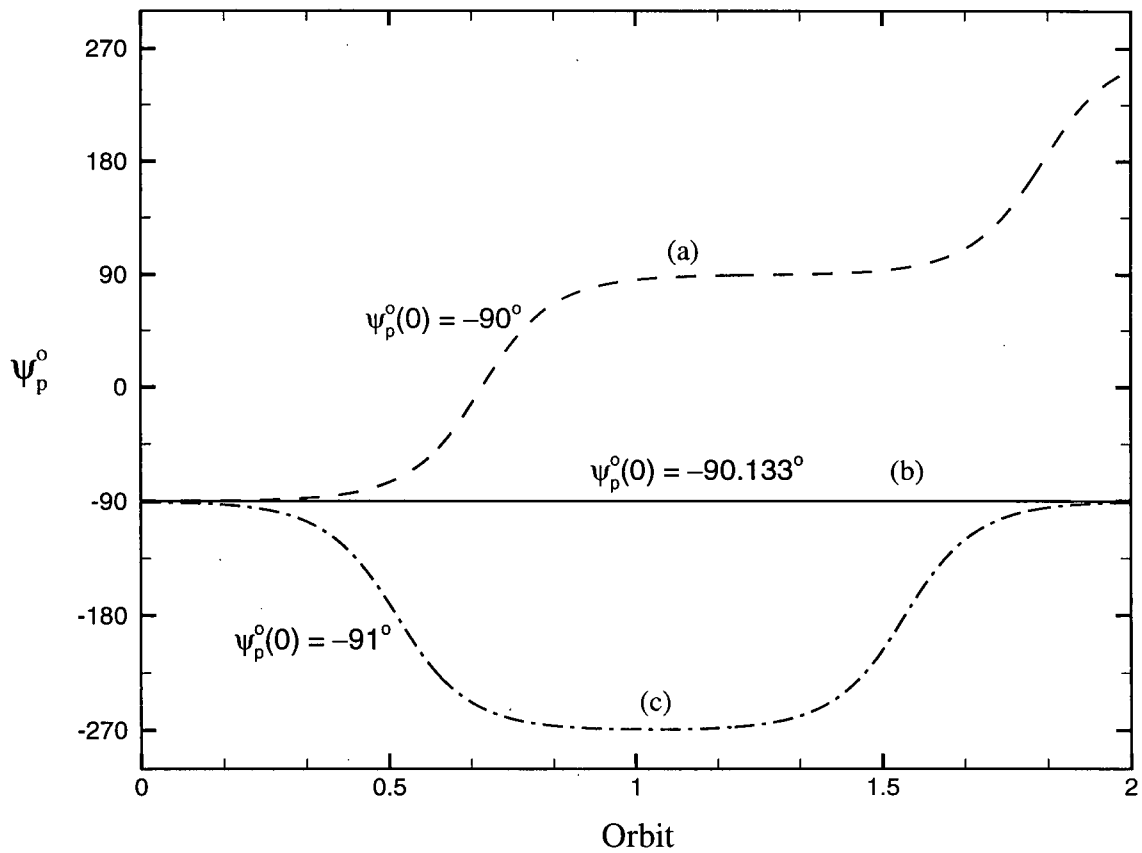


Figure 2-10 System response with the manipulator when the platform is initially at:
 (a) $\psi_p(0) = -90^\circ$, i.e. aligned with the local vertical; (b)
 $\psi_p(0) = \psi_{p.e} = -90.13^\circ$; (c) $\psi_p(0) = -91^\circ$.

Note, when the platform is initially set at its equilibrium position, $\psi_{p,e} = -90.13^\circ$, it remains there as it should (Figure 2-10b). Thus a small change in initial conditions near the unstable configuration can lead to widely different system responses. This is further emphasized in Figure 2-10(c) where the platform is initially at $\psi_p = -91^\circ$. Note, now the system center of mass is in the fourth quadrant and experiences a clockwise moment. The platform continues to swing until its velocity becomes zero at $\psi_p = +91^\circ$. The return journey in the clockwise sense starts and the platform continues to swing back and forth around the stable local vertical position. This is in sharp contrast to the results in Figure 2-10(a) and (b).

2.4.2 Response due to platform's tip excitation

With the manipulator located at the tip and joints locked in position as before ($l_1 = l_2 = 7.5\text{m}$, $\alpha_1 = \alpha_2 = 90^\circ$, $d = 60\text{m}$), the end of the platform, aligned with the local vertical, was given an initial disturbance of 0.5m (Figure 2-11). The platform vibrates at its natural frequency with a period of around 0.001 orbit ($\approx 6\text{s}$). Note, due to coupling effects, the librational motion of the platform is induced. The pitch librational response is modulated at the platform frequency. The flexibility effects of the manipulator joints and modules (links) are also apparent. The platform tip motion and the corresponding tip moment (free-free beam) excite joints of the manipulator, resting on the platform, with peak amplitudes of $\beta_1 \approx 6^\circ$ and $\beta_2 \approx 25^\circ$. The beat character of the response is attributed to the proximity of the joint 2 and platform frequencies ($\omega_{j2} \approx 0.21\text{ Hz}$, $\omega_p \approx 0.18\text{ Hz}$). The beat period approximately corresponds to 0.012 orbit ($\approx 0.015\text{ Hz}$). One can discern presence of the low

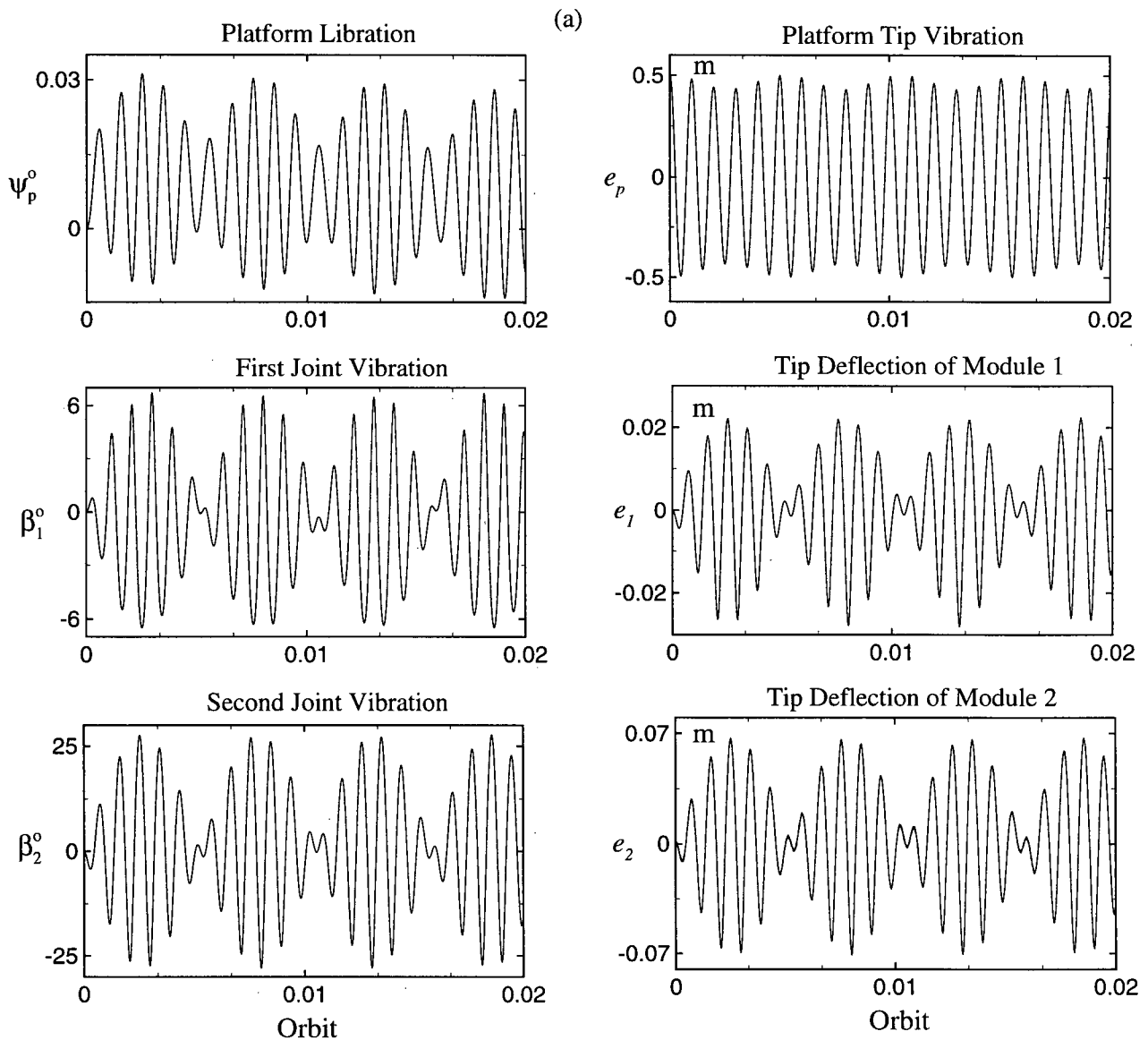
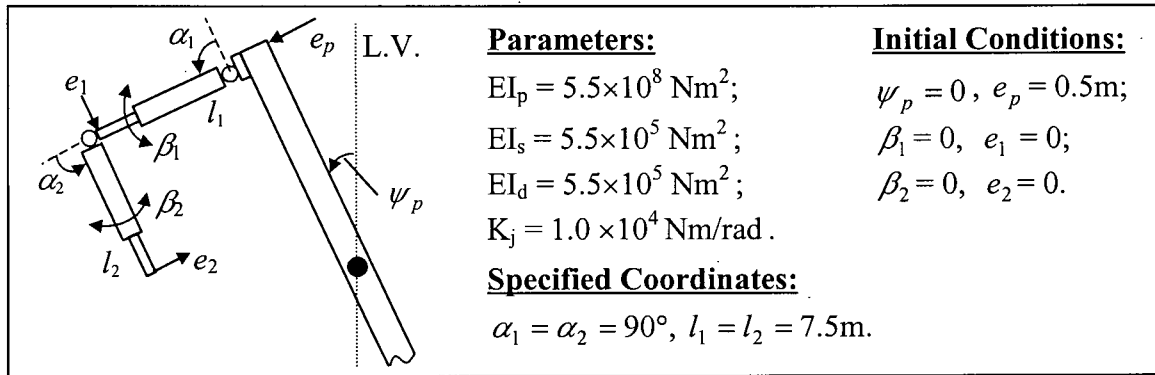
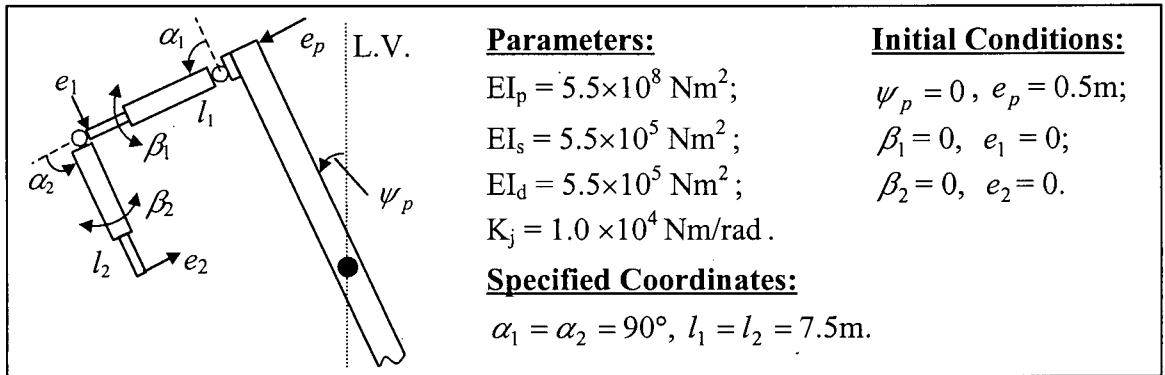


Figure 2-11 Response of the system to an initial disturbance of 0.5m tip displacement of the platform: (a) short duration behavior of rigid and flexible degrees of freedom.



Platform Libration

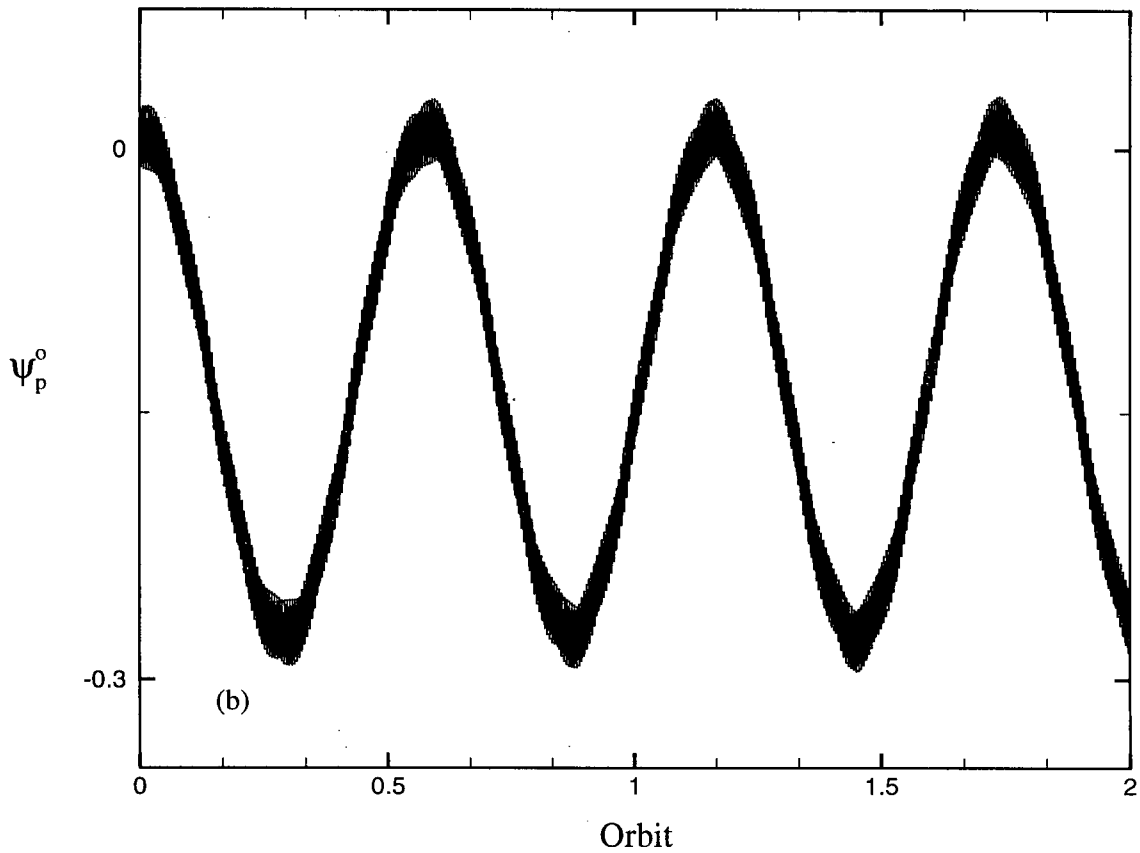


Figure 2-11 Response of the system to an initial disturbance of 0.5m tip displacement of the platform: (b) long duration evolution of the platform's pitch libration.

frequency beat induced modulations in the platform's librational (ψ_p) as well as tip (e_p) responses. The large amplitude vibration of the second revolute joint is due to near resonance condition, its frequency being close to the platform's bending frequency ($\omega_p \approx 0.18$ Hz, $\omega_{j2} \approx 0.21$ Hz) which here acts as the forcing frequency.

Long duration evolution of the librational response is presented in Figure 2-11(b). It clearly shows, as expected, a period of around 0.6 orbit. The high frequency modulations are at the platform's bending frequency (0.18 Hz). Small ridges at the periphery are due to the beat phenomenon as observed in Figure 2-11(a).

2.4.3 Response to manipulator tip displacement

It should be recognized that the system consists of elastic and rigid degrees of freedom with wide variations in their natural frequencies. Obviously, depending on the disturbance, a number of them with significant response would be excited revealing complex interactions at different frequencies. This is precisely the case with the manipulator displacement of 0.2m at the tip of module 2 (Figure 2-12). To help appreciate involved coupling effects, it was desirable to establish natural frequencies of the elastic members and dominant frequencies affecting a given response. To that end the platform, two revolute joints, and two modules were individually subjected to an initial disturbance and power spectral density functions of the response were obtained. The results are given in Appendix I. Natural frequencies of various system components thus obtained are summarized in Table 2-2.

With the manipulator tip initially deflected through 0.2m, the system is set vibrating. In absence of damping, the tip continues to oscillate (e_2) at a constant amplitude and with a

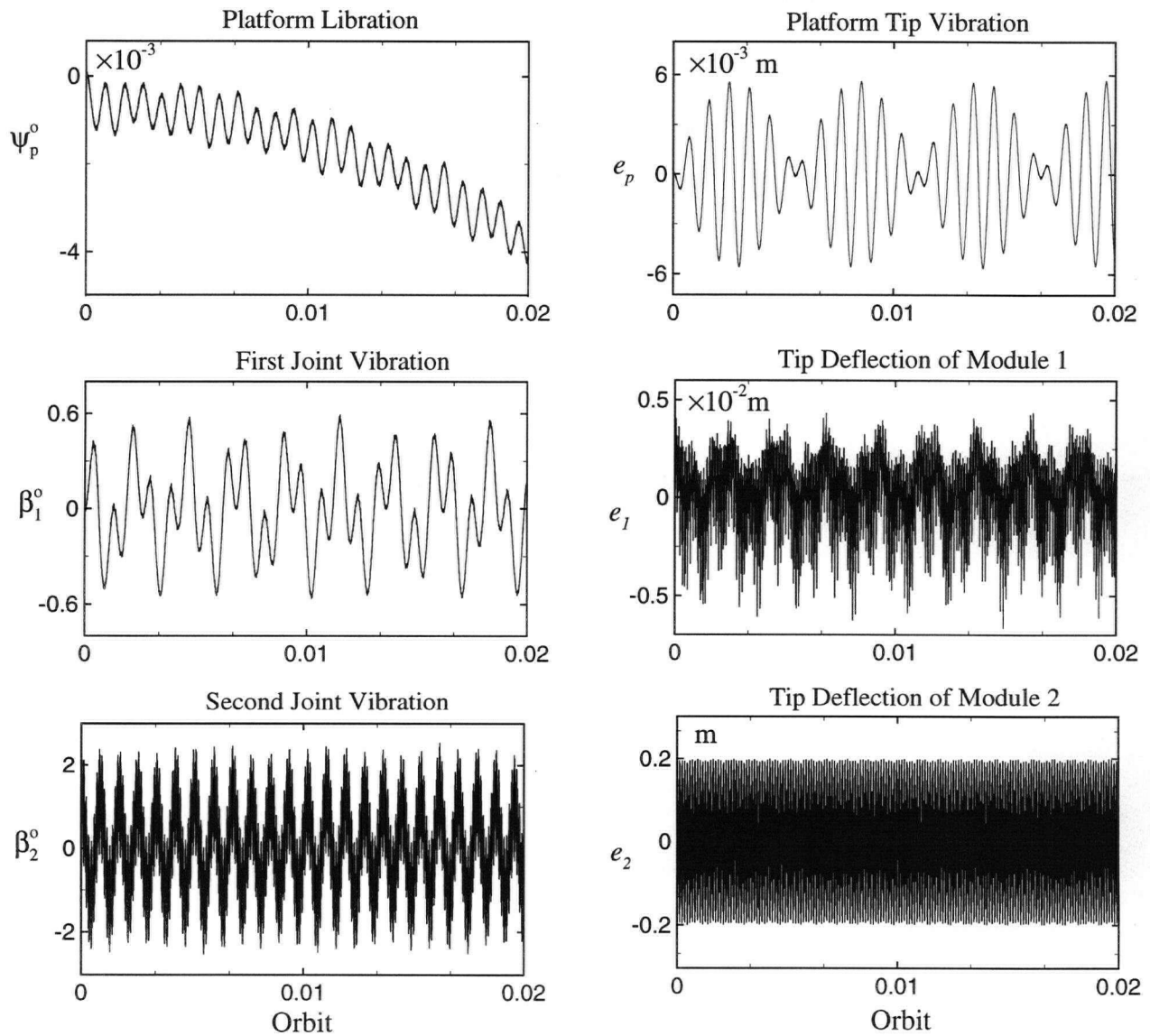
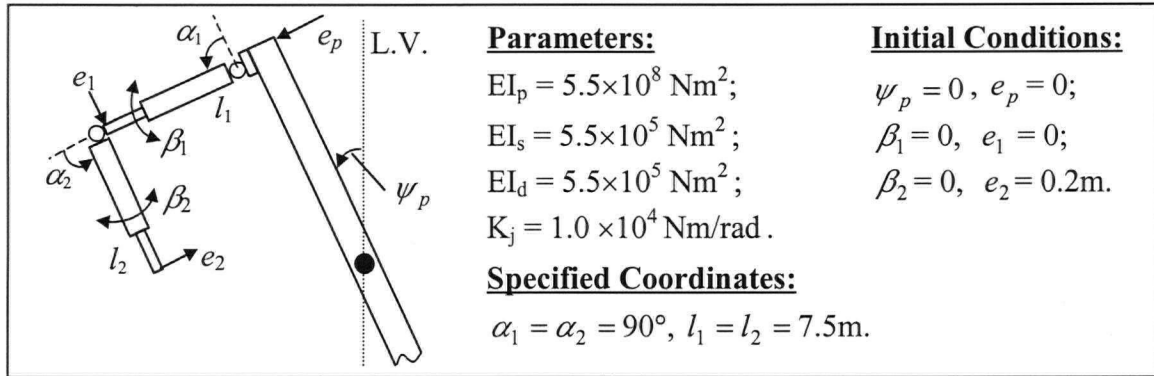


Figure 2-12 System response to the manipulator's tip displacement of 0.2 m.

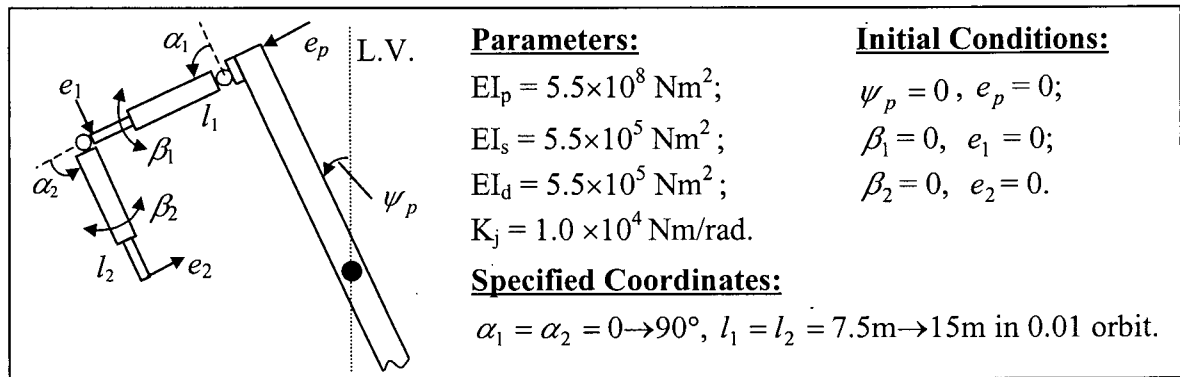
Table 2-2 Fundamental natural frequencies of the components, forming the platform-based manipulator system, in absence of payload.

Component	Frequency, Hz	Period	
		Second	Orbit
Platform, Libration	3.12×10^{-4}	3204	0.6
Platform, Bending	0.18	5.555	1.0×10^{-3}
Module 1, Bending	5.85	0.171	3.1×10^{-5}
Module 2, Bending	8.50	0.117	2.1×10^{-5}
Joint 1, Torsion	0.08	12.500	2.3×10^{-3}
Joint 2, Torsion	0.21	4.762	8.6×10^{-3}

frequency of 5.2 Hz (≈ 290 cycles in 0.01 orbit). This, in turn, excites joint 2 through coupling (β_2) which oscillates at its natural frequency of 0.21 Hz (approximately 12 oscillations in 0.01 orbit) with high frequency module 2 oscillations superposed. Joint 1 displays a rather complex response showing coupling effects of β_2 and e_2 (Figure I-2b). The platform tip shows a typical beat response, as its frequency is quite close to that of β_2 ($\omega_{j2} \approx 0.21$ Hz, $\omega_p \approx 0.18$ Hz) as mentioned earlier. The beat frequency of 0.015 Hz corresponds to a period of ≈ 66 s. The platform pitch response is modulated at the β_2 frequency with high frequency contribution from e_2 appearing at the peaks.

2.4.4 Response in presence of manipulator maneuvers

In the study so far, the manipulator joints were locked in position, i.e. there were no maneuvers involved. The next logical step is to assess the effect of the manipulator executing slewing and deployment maneuvers. The manipulator is taken to be at the tip of the platform, i.e. $d = 60$ m. It undergoes simultaneous slewing (α_1, α_2 from 0 to 90°) and deployment (l_1, l_2 from 7.5m to 15m) in 0.01 orbit. Figure 2-13(a) shows the librational response when the platform is initially aligned with the local vertical, a stable equilibrium position. The character of the response is quite similar to that observed in Figure 2-8(a). However, because of the initial disturbance, the amplitude is higher. Effect of the maneuver on the flexible degrees of freedom can be appreciated from Figure 2-13(b). Note, both the joints are set into vibration with a characteristic frequency having a period of ≈ 28 s (6 oscillations in 0.03 orbit). The module tip oscillations display the same frequency. Their amplitude due to flexibility of the links alone (e_1, e_2) are rather significant, around 10cm and



Platform Libration

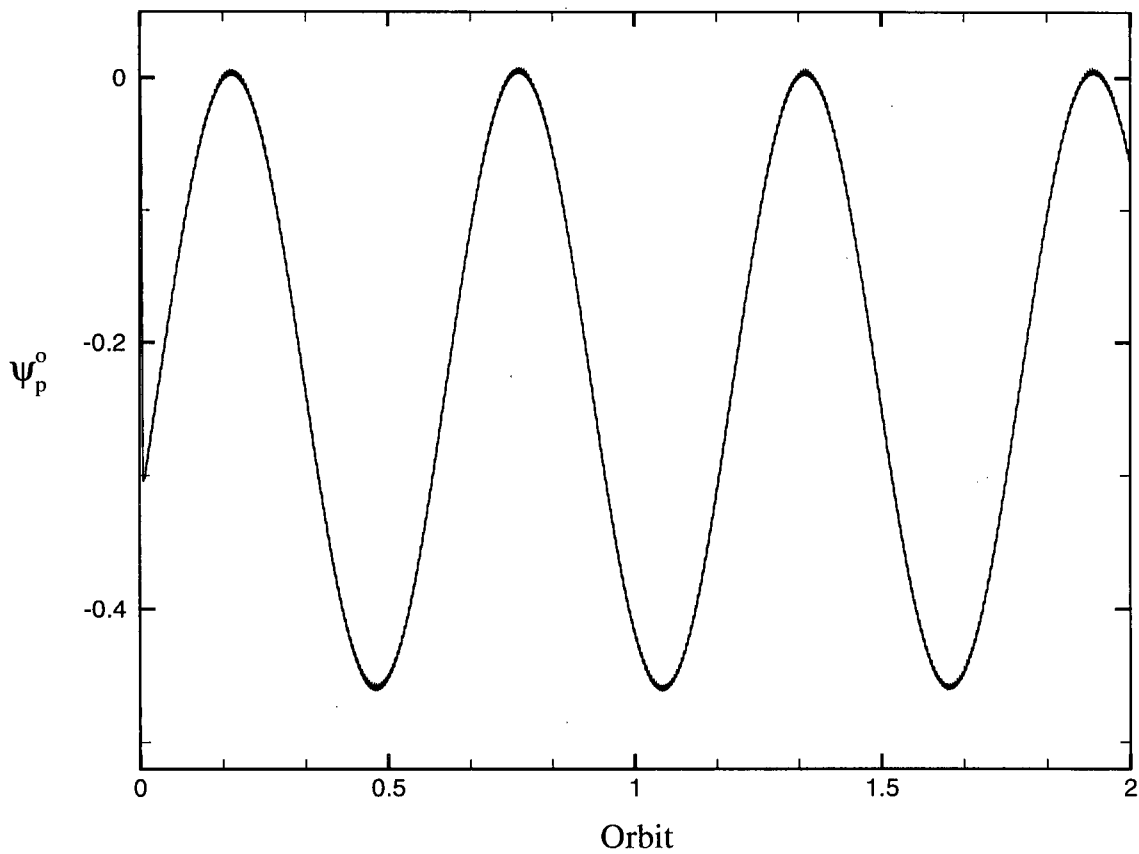


Figure 2-13 System response in presence of a manipulator maneuver with the platform initially aligned with the local vertical: (a) long duration evolution of the platform pitch libration.

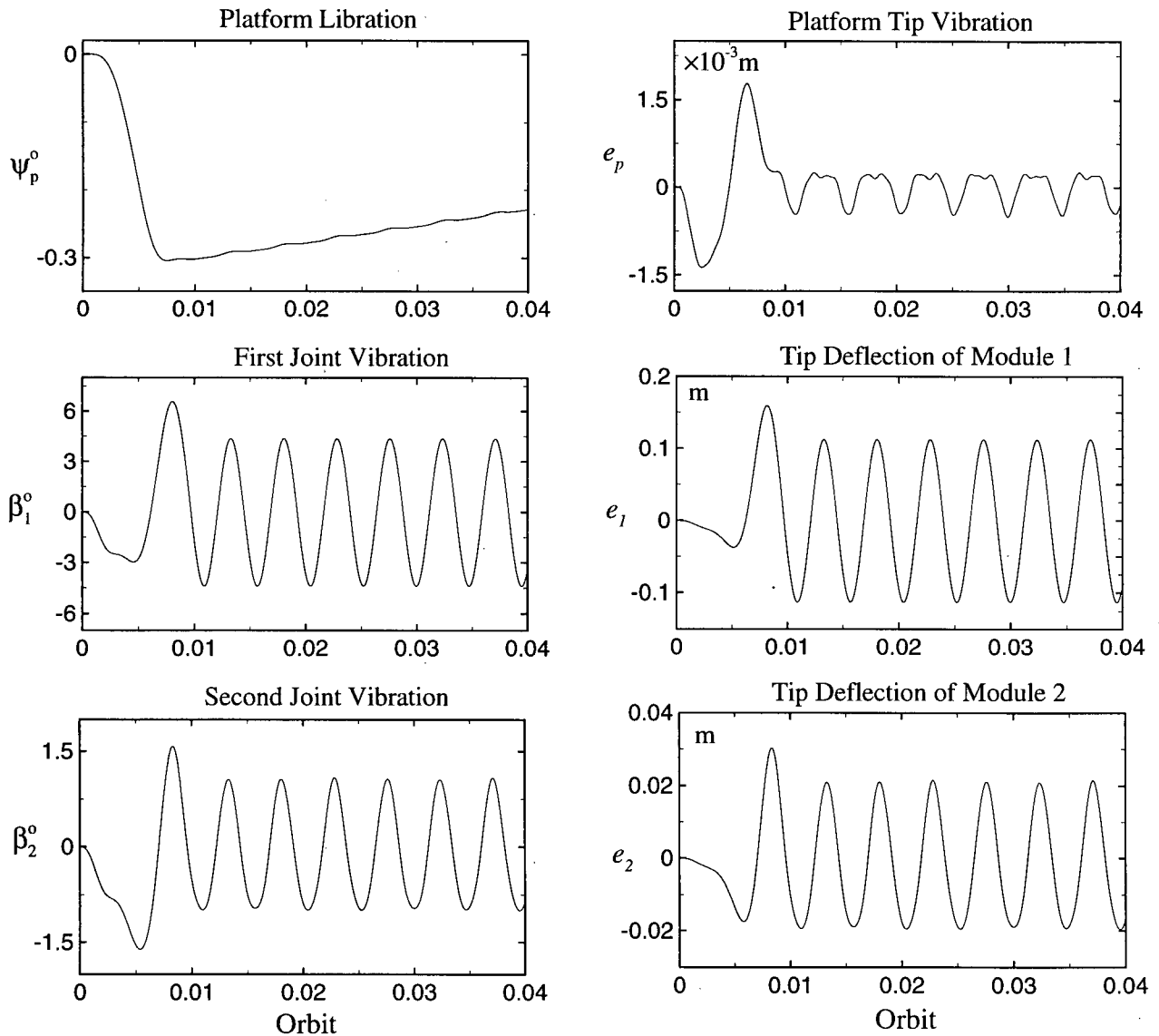
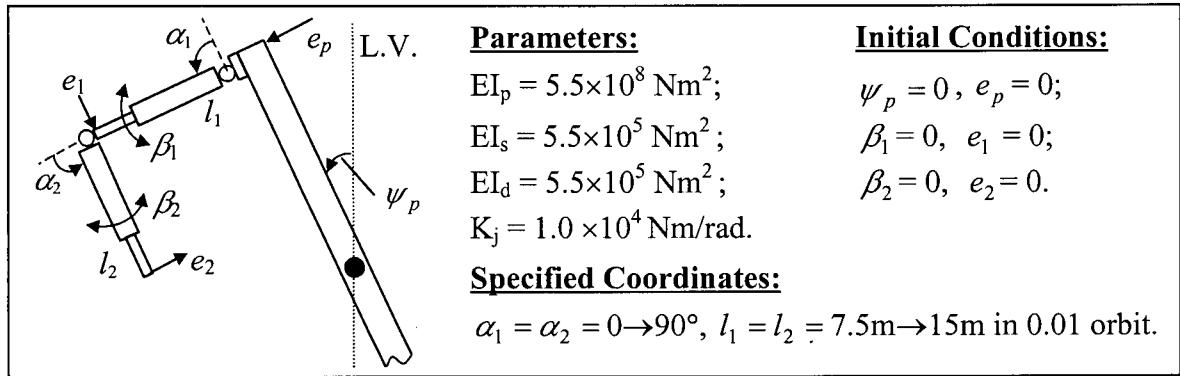


Figure 2-13 System response in presence of a manipulator maneuver with the platform initially aligned with the local vertical: (b) short duration behavior of rigid and flexible degrees of freedom.

2cm, respectively, in the steady state. Note, the flexible joint vibrations with steady state amplitudes of around 1.3° (β_2) and 4.5° (β_1) would accentuate the effect leading to a significant deviation of the manipulator tip from its desired position. This suggests a need for control.

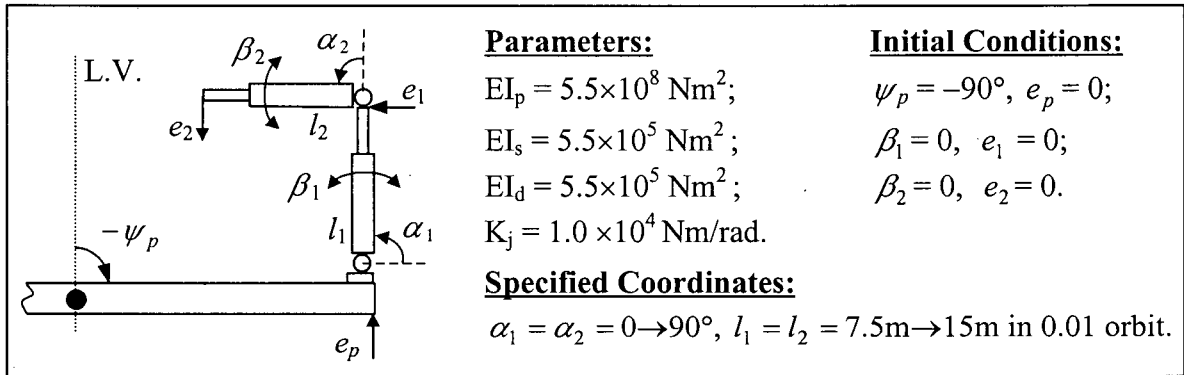
The librational response with the platform initially aligned with the local horizontal and the manipulator performing the same maneuver is presented in Figure 2-14(a). As anticipated, the system becomes unstable and the anticlockwise rotational motion, similar to that observed in Figure 2-10(a), sets in. It is interesting to observe (Figure 2-14b) that response of the flexible generalized coordinates remains essentially the same as that for the platform along the local vertical (Figure 2-13b). Hence in the subsequent study, focus is on the platform along the stable equilibrium position.

2.4.5 Effect of system parameters

Next, the attention was turned to assess the influence of several important parameters such as payload, speed of maneuvers, joint flexibility, and number of modes used in the flexibility discretization. In all the cases, the initial orientation of the platform (aligned with the local vertical) and the manipulator maneuver are purposely kept the same as before to assist in the comparison of data and isolate parameter effects.

Effect of Payload

Figure 2-15 presents the influence of payload carried by the manipulator during the execution of a prescribed maneuver of slew and deployment (α_1, α_2 from 0 to 90° and l_1, l_2 from 7.5m to 15m ; maneuvers completed in 0.03 orbit). Note, the maneuver time is



Platform Libration

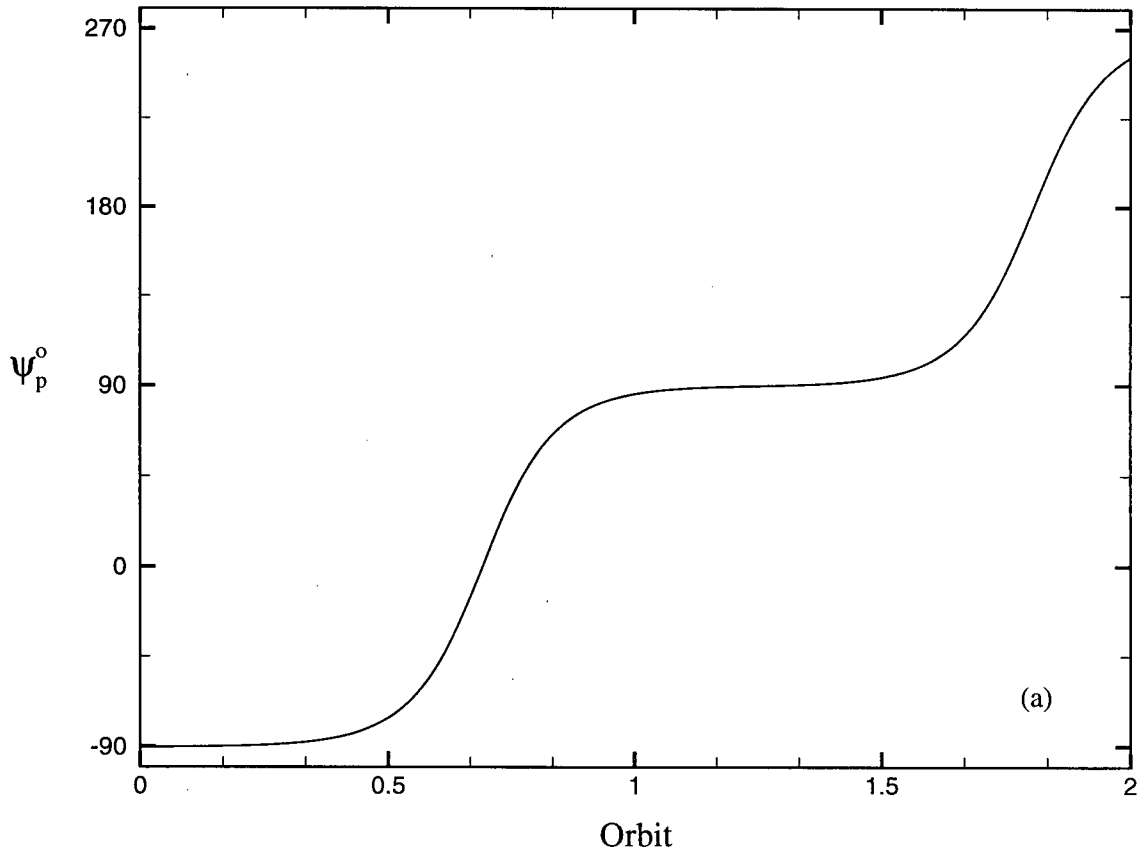


Figure 2-14 System response in presence of a manipulator maneuver with the platform initially aligned with the local horizontal: (a) long duration evolution of the platform pitch libration.

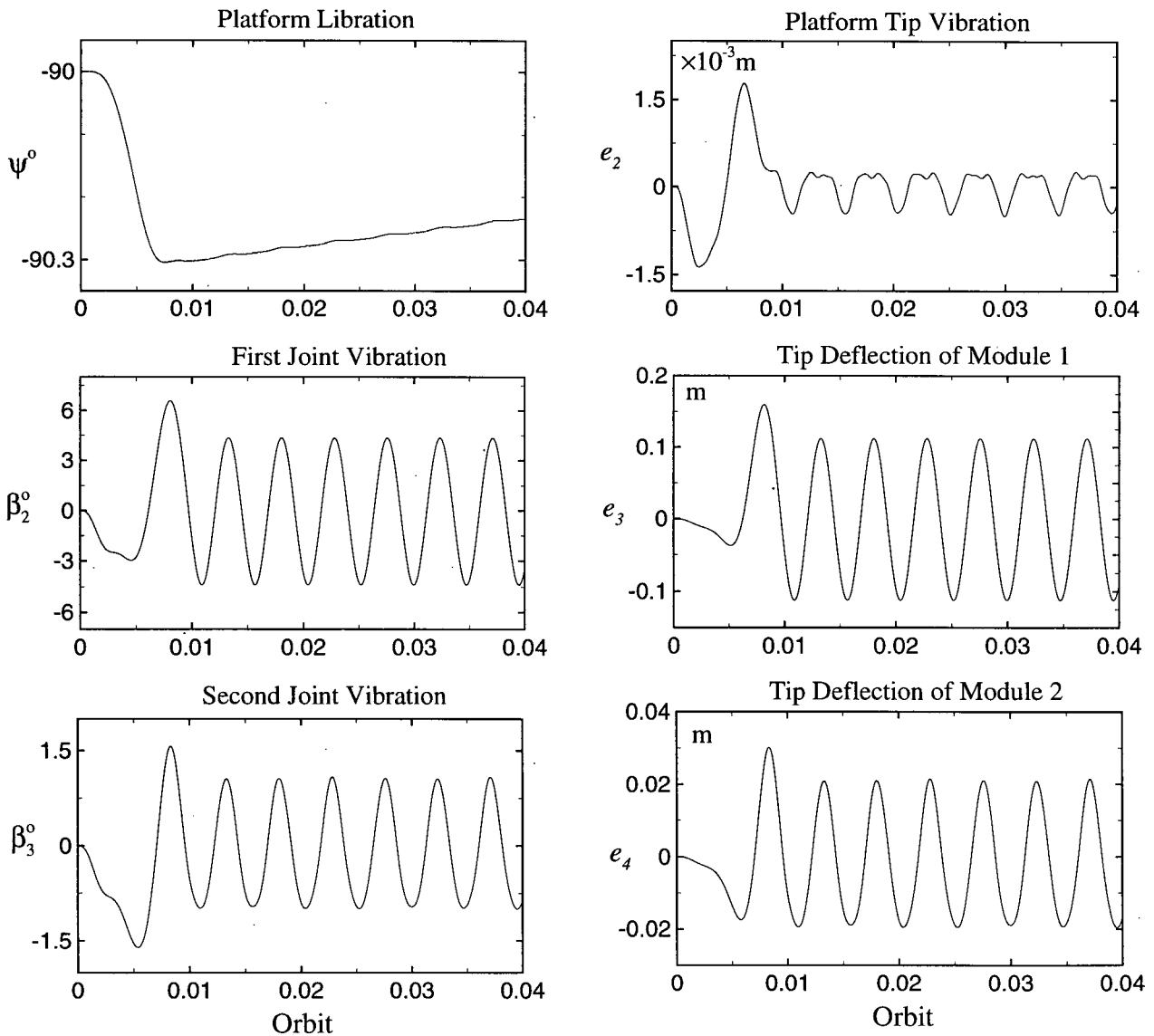
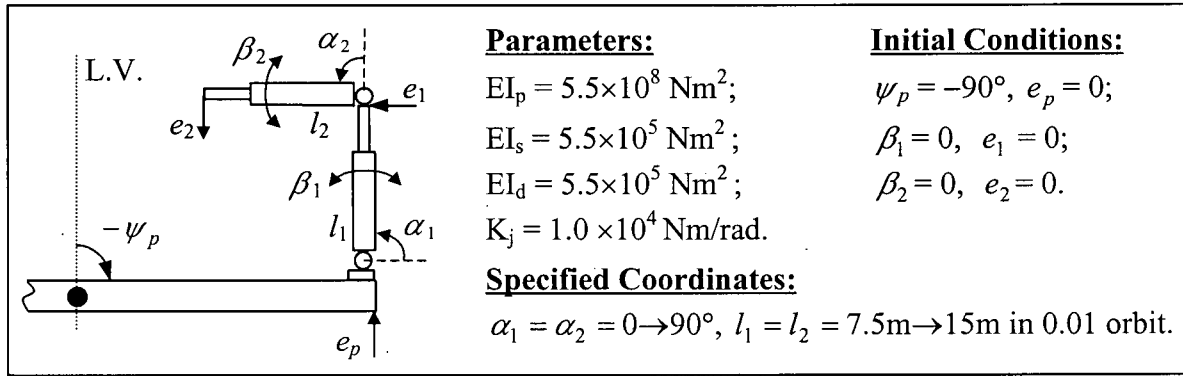


Figure 2-14 System response in presence of a manipulator maneuver with the platform initially aligned with the local horizontal: (b) short duration behavior of rigid and flexible degrees of freedom.

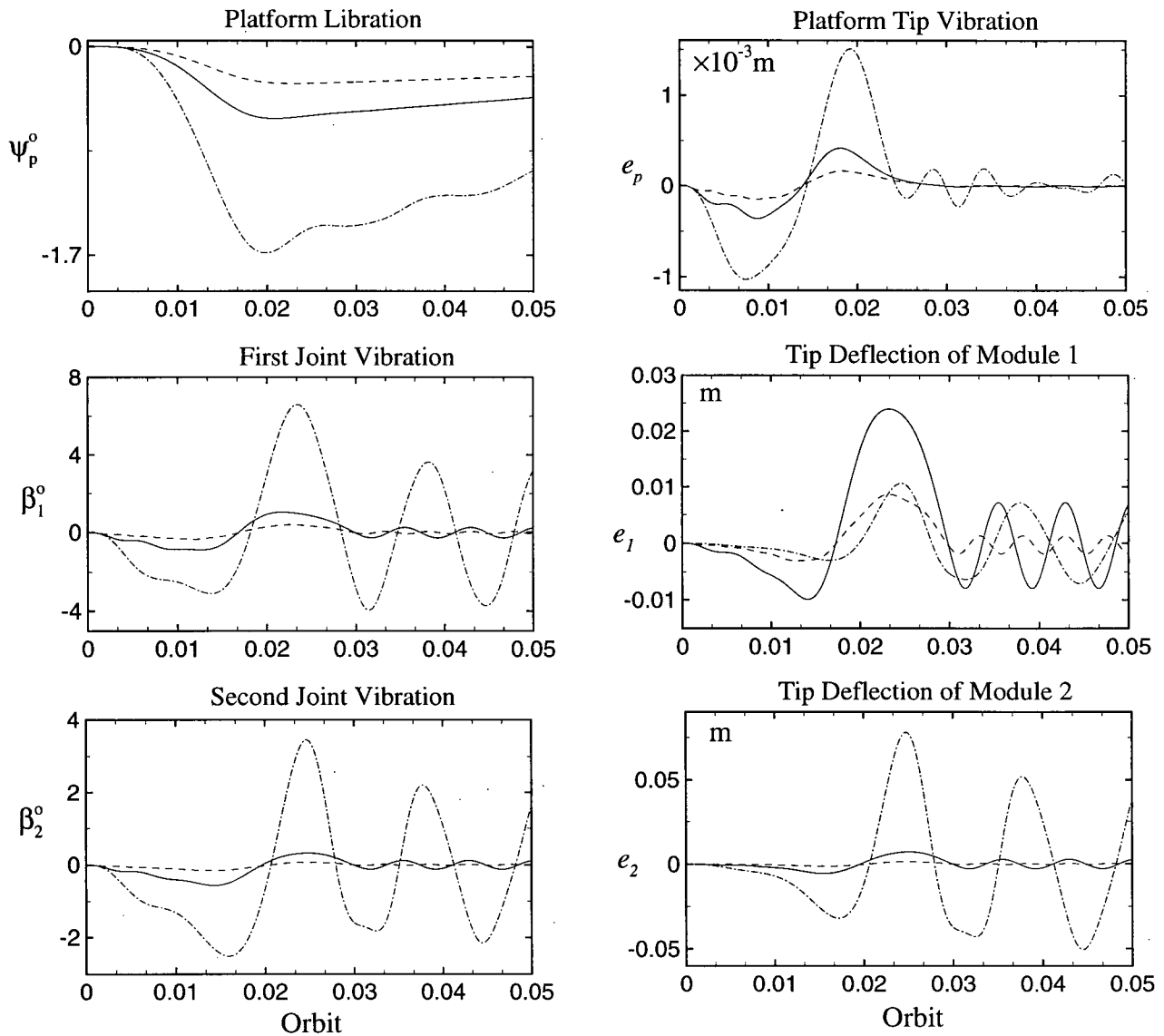
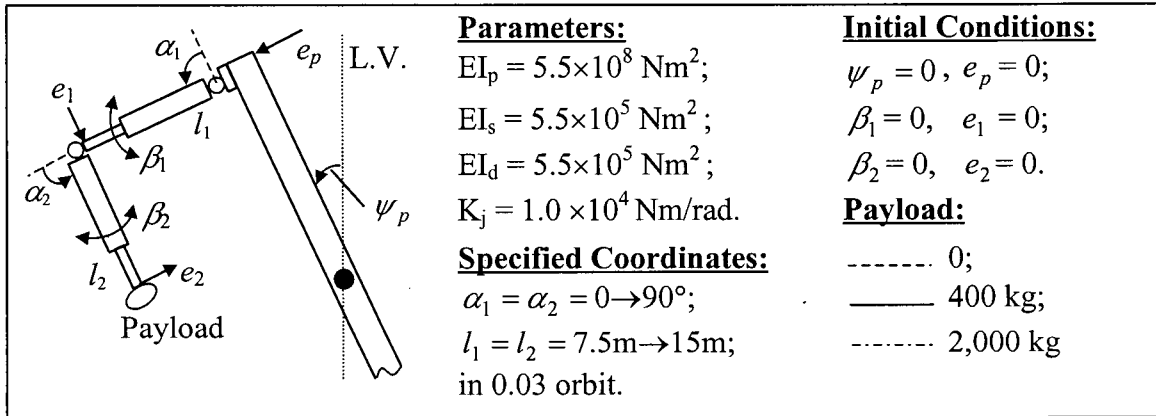


Figure 2-15 System response as affected by payload with the manipulator completing simultaneous slew and deployment maneuvers in 0.03 orbit.

purposely taken longer (0.03 orbit instead of 0.01 orbit) due to the presence of a payload. As can be expected, with an increase in the payload ratio from 0 to 5 (i.e. from 0 to 4,000 kg), the joint oscillations reach a peak value of $\approx 6^\circ$ for the first joint and around 3° for the second joint. Although the manipulator tip deflection (e_2), which is measured relative to β_2 , appears rather modest ($\approx 7.5\text{cm}$), that is somewhat misleading as pointed out before. Accounting for the two revolute joints' elastic deformations, the peak tip deviation from the desired orientation would be more than 2m along as well as normal to the platform. Obviously this would be unacceptable. Thus, one would be faced with:

- (i) limiting the load carried to a lower value;
- (ii) reduction in the speed of maneuver;
- (iii) introduction of an active control.

As maneuver in the present case is only one of the numerous ones the manipulator will be called upon to execute, and the speed of maneuver is rather modest, introduction of control is the logical solution.

Influence of Speed of Maneuver

Figure 2-16 shows the effect of speed of maneuver (in absence of payload). Three different speeds are considered: simultaneous slew and deployment maneuvers completed in 0.03 orbit (slow), 0.01 orbit (nominal rate), 0.005 orbit (fast). In general, the response results show trends as anticipated. The platform being massive (120,000 kg), the effect of maneuvering speed on the peak librational response is the same, around 0.3° . The speed affects only the local response character. Note the high frequency modulations, for the fast maneuver case, are due to flexible joint oscillations. Again, such large amplitude joint

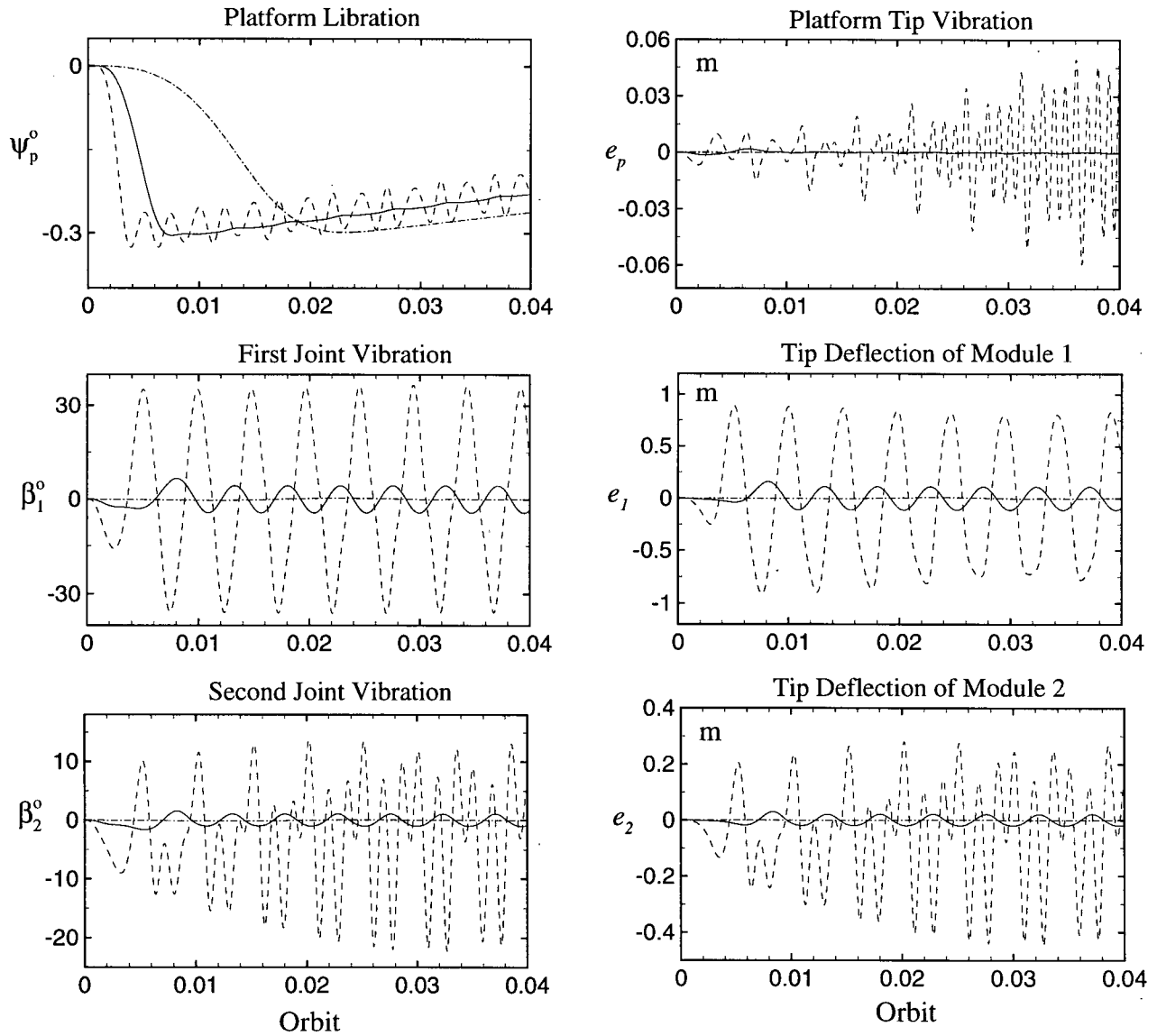
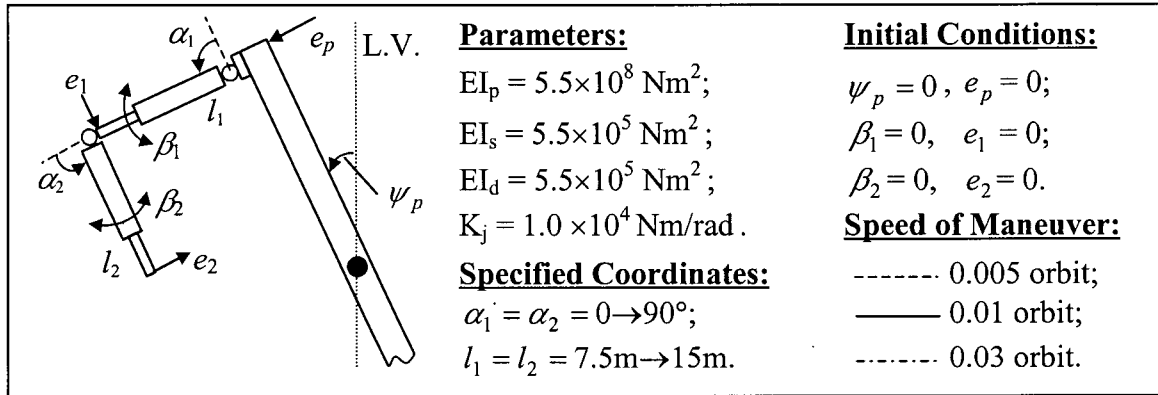


Figure 2-16 Influence of the speed of maneuver on the system response.

oscillations ($\beta_{1,\max} \approx 35^\circ, \beta_{2,\max} \approx 12^\circ$) as well as link flexibility effects (e_1, e_2) would be unacceptable. Design and operation criteria for the manipulator will have to be modified to limit the maneuvering speed, increase joints' torsional rigidity and, most importantly, include an active control strategy.

Effect of Joint Stiffness

The earlier results clearly showed the important role played by the joint response. To help arrive at an acceptable value for the joint flexibility, three different cases were considered: $K_j = 5 \times 10^3$ (low), 1×10^4 (considered nominal) and 5×10^4 (high) Nm/rad. The manipulator executes the same maneuver as before, in 0.01 orbit and without a payload. Response results are presented in Figure 2-17. The librational response remains virtually unaffected by the joint stiffness, with peak deviation of the platform from the local vertical of around 0.3° . The peak value of the platform's tip vibrations also remains essentially unaffected. As anticipated, it is the manipulator's response that is affected the most and it follows the expected trend: amplitudes of joints and module tip vibrations increase as the joints' torsional rigidity diminishes. To limit the tip deflection of a fully deployed manipulator of 30m length to, say, 3cm would require the joint deflection to be less than 0.1° ! Thus the joint rigidity should be at least 5×10^4 Nm/rad. Again this points to the need of an active control.

Effect of Number of Modes

Analysis of large scale flexible systems has often raised a question concerning representation of elastic deformations through admissible functions. Complexity of the

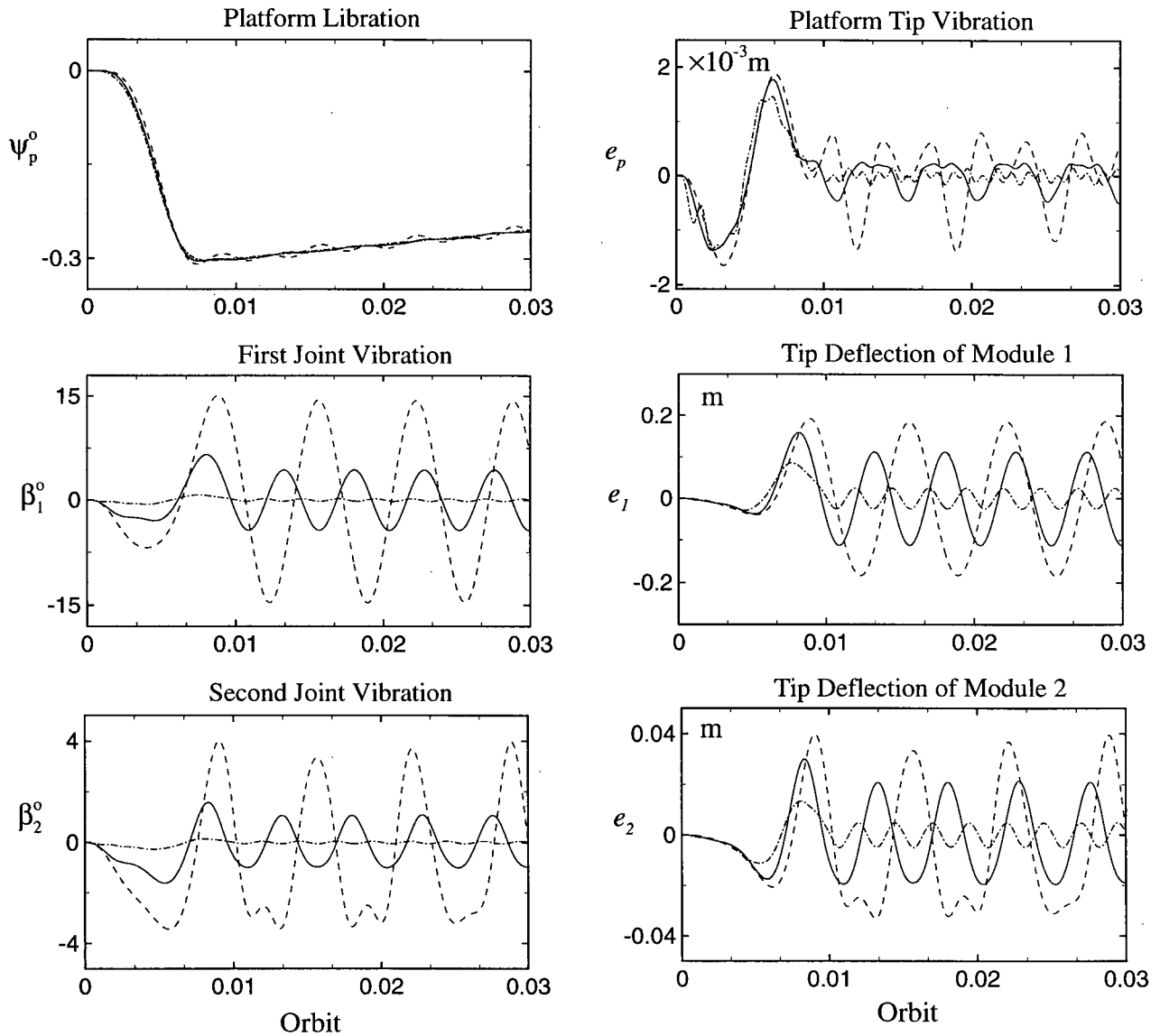
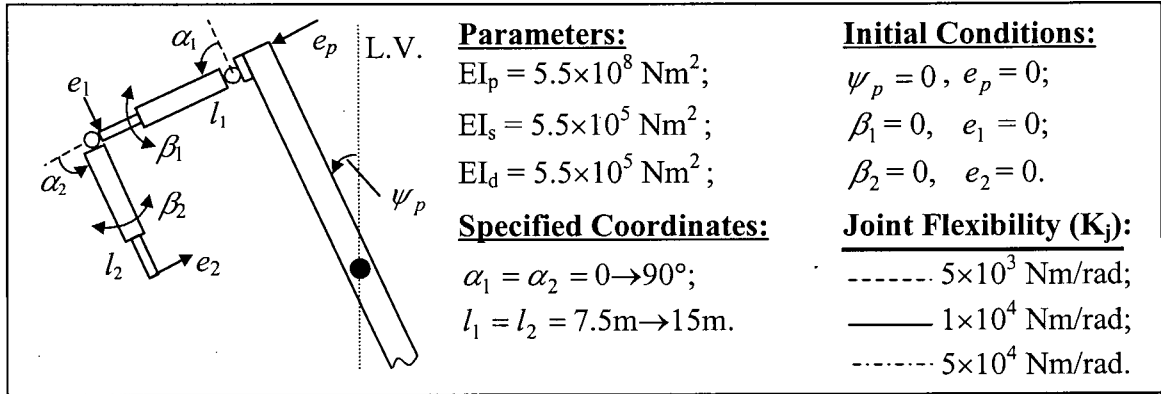


Figure 2-17 System response as affected by the joint stiffness which appears to be a rather critical parameter.

formulation as well as the computational effort involved significantly increase with the number of modes used for flexibility discretization. So the question is: how many modes are necessary to capture physics of the problem ?

To help answer the question, the system with a 800 kg payload performing the same maneuver as before, i.e. $\alpha_1 = \alpha_2 = 0 \rightarrow 90^\circ$, $l_1 = l_2 = 7.5\text{m} \rightarrow 15\text{m}$ in 0.01 orbit, was considered. Response results were obtained using one-mode as well as three-mode flexibility representation for the platform and the modules (Figure 2-18). It is apparent that, even in this demanding situation leading to large amplitude of oscillations in virtually all degrees of freedom ($\beta_1, \beta_2 > 30^\circ$! $e_1, e_2 \approx 1\text{m}$, $\psi_p \approx 1^\circ$), the fundamental mode is able to predict the system dynamics quite well.

In the investigations so far, the maneuver was purposely considered rather severe to check performance under demanding situations. In a real-life operation, the maneuver will likely proceed differently (e.g. Figure 2-19), and take place in a longer time. The illustration shows execution of a task requiring the manipulator to pick-up a payload from position 'A' (e.g. from the Space Shuttle) to a desired position 'B'. The sequence of maneuvers involving deployment (Phase I), 90° slew of module 2 (Phase II) and 90° slew of module 1 (Phase III) represents the procedure expected to be used in practice.

To assess the system performance under a realistic situation, consider a rather conservative situation of the same maneuver ($\alpha_1 = \alpha_2 = 0 \rightarrow 90^\circ$, $l_1 = l_2 = 7.5\text{m} \rightarrow 15\text{m}$) completed in 0.05 orbit, for a manipulator with $K_j = 5 \times 10^4 \text{ Nm/rad}$, and carrying a payload of 2,000 kg. Note, the maneuver rate is rather slow, the joint stiffness is quite high and the payload is somewhat moderate (a typical communication satellite weighs 3 to 5 tons). Response results are presented in Figure 2-20. It is apparent that the peak platform libration

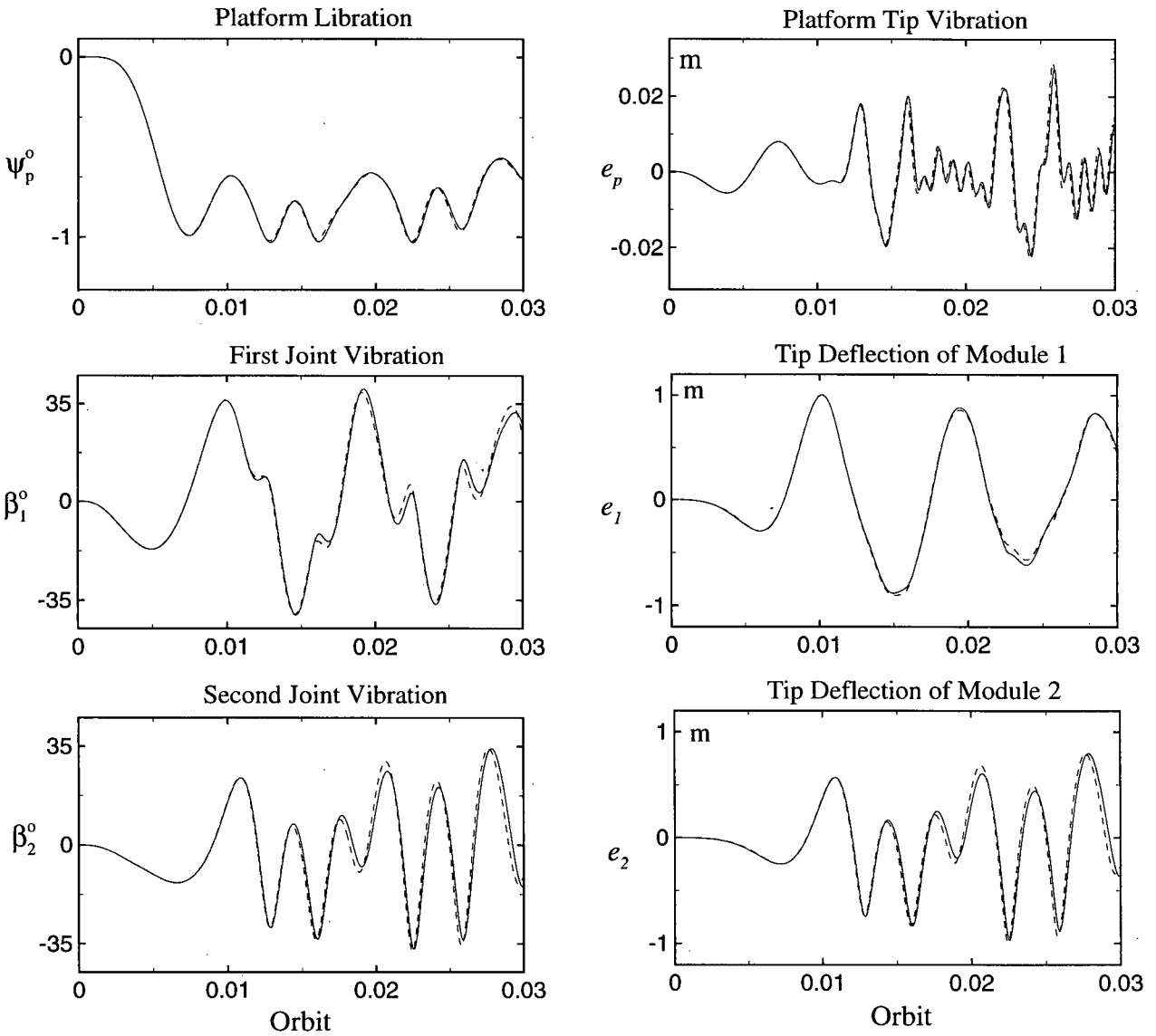
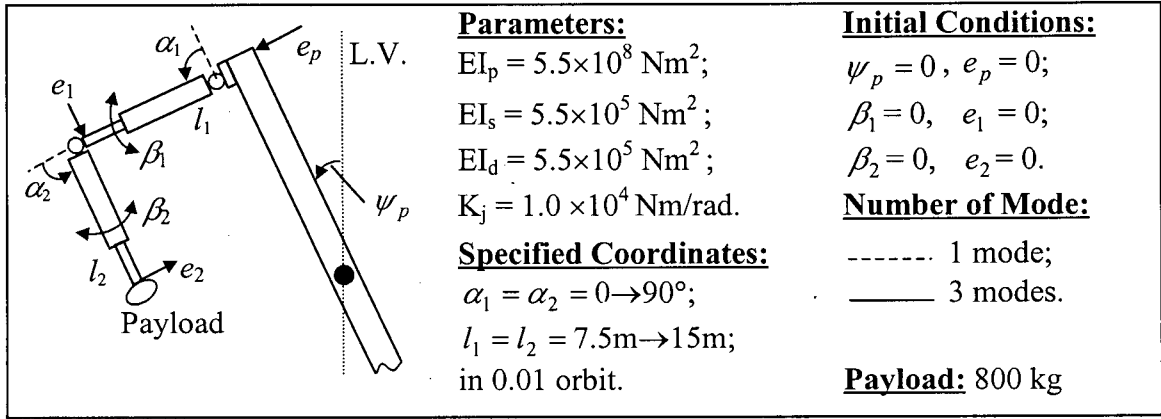


Figure 2-18 System response as affected by the number of modes used in flexibility discretization.

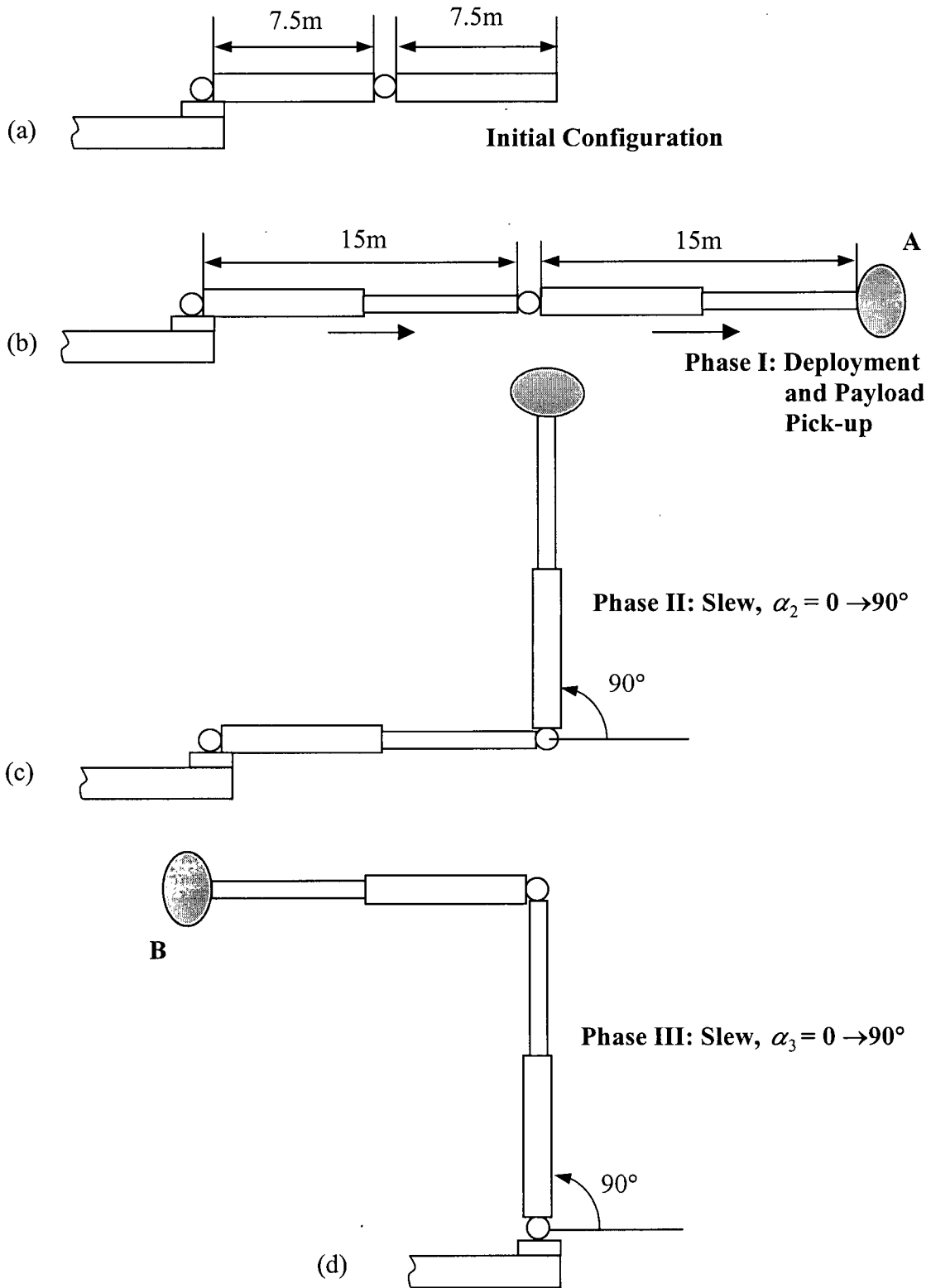


Figure 2-19 A likely procedure would involve slew and deployment separately instead of all four joints maneuvering at the same time.

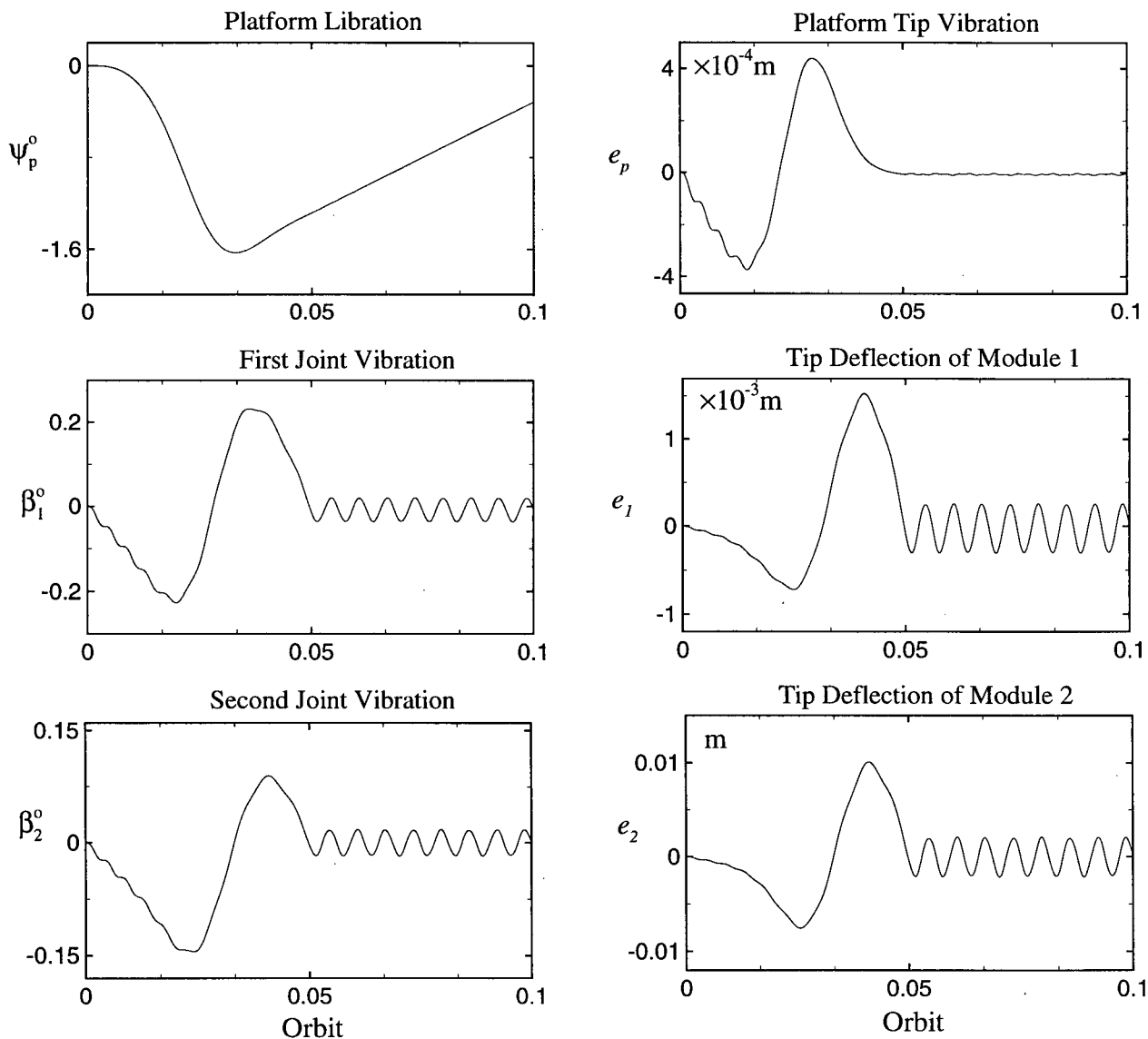
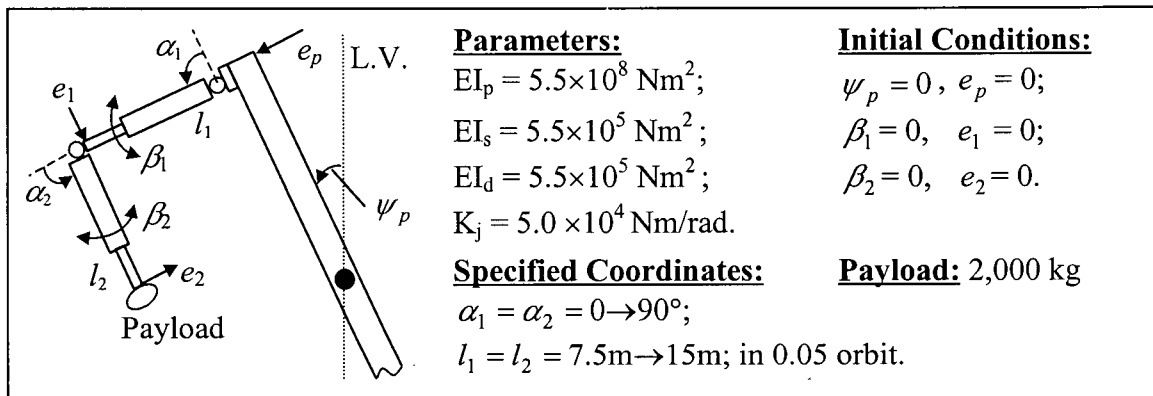


Figure 2-20 System response, even under a set of conservative values for payload (2,000 kg), joint stiffness ($5 \times 10^4 \text{ Nm/rad}$) and maneuver speed (0.05 orbit), is unacceptable. This suggests a need for control.

far exceeds the permissible range of $0.1^\circ - 1.0^\circ$. The maximum joint vibrations of $\beta_1 \approx 0.23^\circ$ and $\beta_2 \approx 0.09^\circ$ would lead to the manipulator tip deviation from the desired position by $\approx 5\text{cm}$ along the x axis and $\approx 9\text{cm}$ in the y direction. Thus a need for control is clearly indicated and this is the subject of the following chapter.

3. SYSTEM CONTROL

The previous chapter clearly established a need for control, under critical combinations of system parameters, initial conditions and maneuvers, to maintain desirable performance of the manipulator. In particular, joint stiffness, maneuver speed and payload constituted parameters having significant effect on the system dynamics. The present chapter focuses on the next logical step of control of the system with a platform-based two-unit (four links) manipulator. As before, the platform, modules and joints are treated as flexible members. To recapitulate, more frequently used symbols are summarized below and indicated in Figure 3-1:

- θ true anomaly with reference at perigee;
- C.M. center of mass;
- d position of the manipulator from C.M.;
- L.V. local vertical;
- L.H. local horizontal.

Rigid Degrees of Freedom

- ψ_p platform pitch;
- l_1, l_2 lengths of modules one and two, respectively;
- α_1, α_2 rigid components of slew maneuvers associated with modules one and two, respectively.

Flexible Degrees of Freedom

- β_1, β_2 flexible components of slew maneuvers associated with modules one and two, respectively;
- e_p platform tip deflection;

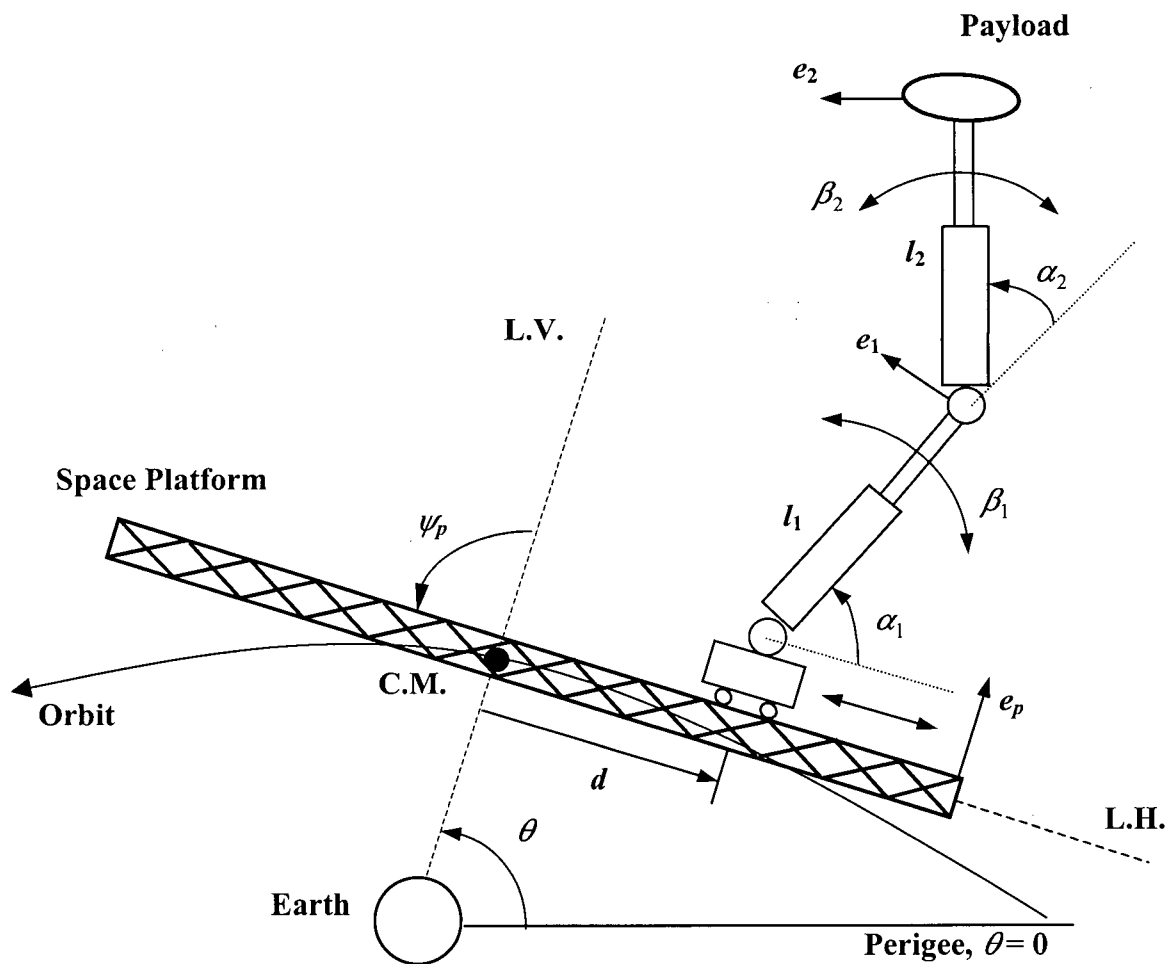


Figure 3-1 A two-module manipulator system showing frequently used symbols.

e_1, e_2 tip deflections of modules one and two, respectively.

3.1 Control Methodologies

The torques and forces responsible for slewing and deployment maneuvers are illustrated in Figure 3-2. The objective here is to control operational behavior of the system. For example, the slewing maneuvers will arise with application of torques (T_1, T_2) provided by actuators located at revolute joints of the manipulator. Similarly, forces (F_1, F_2) for the deployment and retrieval of units are provided by actuators at the prismatic joints of the manipulator. In addition to joint actuators which regulate the manipulator link dynamics, there are Control Momentum Gyros (CMGs). They are used to regulate the platform orientation as well as its vibration. CMGs located near the center of the platform contribute the torque (T_{pr}) which controls the rigid body motion of the platform, i.e. its attitude or pitch response. On the other hand, a pair of CMGs, located symmetrically about the platform's center and providing equal torques $(T_{pr}/2)$ in the opposite sense, control its elastic vibration by regulating the local slope.

The present section is concerned with the selection of control inputs which will result in the desired motion of the system. Two different control strategies are considered:

- (i) Nonlinear Feedback Linearization Technique (FLT) applied to the rigid degrees of freedom, with flexible generalized coordinates indirectly affected through coupling but not actively controlled. The FLT leads to uncoupled linearized equations of motion which are then subjected to the conventional PD control.

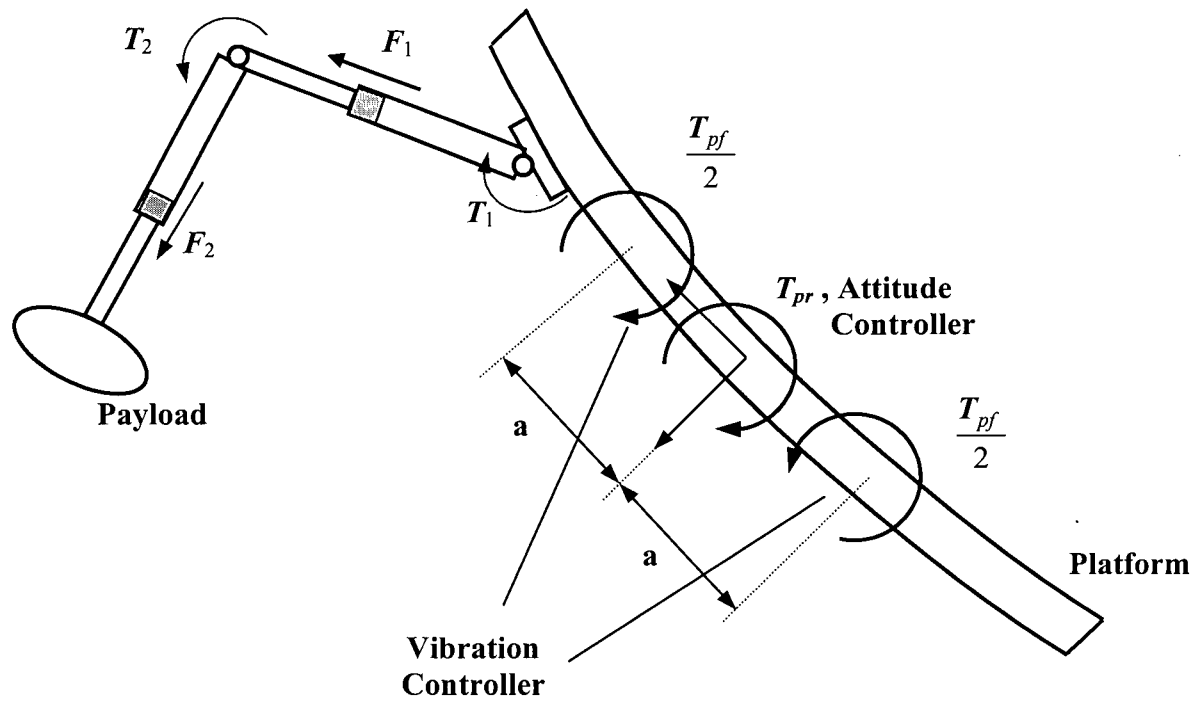


Figure 3-2 Schematic diagram of the manipulator system showing the location of the control actuators. The two torques $T_{pf}/2$, opposing each other, control the platform's vibration by regulating the local slope.

- (ii) The classical Linear Quadratic Regulator (LQR), based on a linear approximation of the flexible subsystem, is designed for active vibration suppression [45,46]. Both rigid as well as flexible degrees of freedom are now controlled through the FLT and LQR, respectively.

3.1.1 FLT control

The FLT is an approach particularly suited to a class of nonlinear systems. The procedure was pioneered by Bejczy [47]. It has been further developed and applied by many investigators resulting in a considerable body of literature [48-54]. The basic idea is to use a mathematical model and find a transformation to decouple and linearize the dynamics of the controlled system. The main advantage of the feedback linearization over point-wise linearization is that once such a transformation is determined, a global linearization is achieved independent of the operating point. In the present study, a controller based on the FLT is designed to regulate the rigid degrees of freedom, i.e. rotations of the revolute joints (α_1, α_2) , deployment of the links (l_1, l_2) , and attitude motion of the system (ψ_p) . However, the effectiveness of the controller is assessed using the original fully flexible system so that the potential effects of uncontrolled dynamics can be investigated.

Equations governing dynamics of a flexible space-based manipulator can be written as

$$M(q,t)\ddot{q} + F(\dot{q},q,t) = Q(\dot{q},q,t), \quad (3.1)$$

$$\underbrace{\begin{bmatrix} M_{rr} & \vdots & M_{rf} \\ \dots & \dots & \dots \\ M_{fr} & \vdots & M_{ff} \end{bmatrix}}_M \underbrace{\begin{Bmatrix} \ddot{q}_r \\ \dots \\ \ddot{q}_f \end{Bmatrix}}_{\ddot{q}} + \underbrace{\begin{Bmatrix} F_r \\ \dots \\ F_f \end{Bmatrix}}_F = \underbrace{\begin{Bmatrix} Q_r \\ \dots \\ Q_f \end{Bmatrix}}_Q,$$

where: $M(q,t)$ is the system mass matrix composed of rigid (M_{rr}), flexible (M_{ff}) and coupled (M_{rf} , M_{fr}) contributions; q_r , q_f are rigid and flexible generalized coordinates, respectively; $F(\dot{q},q,t)$ contains terms associated with centrifugal, Coriolis, gravitational, and elastic forces; and $Q(\dot{q},q,t)$ represents nonconservative generalized forces including the control inputs. Subscripts r and f refer to contributions associated with rigid and flexible degrees of freedom. If only the rigid degrees of freedom are controlled:

$$\begin{aligned} M_{rr}\ddot{q}_r + M_{rf}\ddot{q}_f + F_r &= Q_r; \\ M_{fr}\ddot{q}_r + M_{ff}\ddot{q}_f + F_f &= 0. \end{aligned} \quad (3.2)$$

A suitable choice for Q_r would be

$$Q_r = \hat{M} [(\ddot{q}_r)_d - u] + \hat{F}, \quad (3.3)$$

with:

$$\begin{aligned} \hat{M} &= M_{rr} - M_{rf}M_{ff}^{-1}M_{fr}; \\ \hat{F} &= F_r - M_{rf}M_{ff}^{-1}F_f. \end{aligned} \quad (3.4)$$

Here subscript ' d ' refers to the desired value of a parameter. One way to select the control signal u is the Proportional-Derivative (PD) feedback, i.e.

$$u = -K_v [(\dot{q}_r)_d - \dot{q}_r] - K_p [(q_r)_d - q_r], \quad (3.5)$$

where K_p and K_v are position and velocity gains, respectively. Let $e = (q_r)_d - q_r$, then the controlled equations of motion become:

$$\begin{aligned} 0 &= \ddot{e} + K_v \dot{e} + K_p e; \\ \ddot{q}_f &= -M_{ff}^{-1}M_{fr}[(\ddot{q}_r)_d - u] - M_{ff}^{-1}F_f. \end{aligned} \quad (3.6)$$

Now Q_r can be written as

$$Q_r = \hat{M}(\ddot{q}_r)_d + \hat{F} + \hat{M}(K_v \dot{e} + K_p e), \quad (3.7)$$

which can be visualized as a combination of two controllers: the primary ($Q_{r,p}$); and the secondary ($Q_{r,s}$);

$$Q_{r,p} = \widehat{M}(\ddot{q}_r)_d + \widehat{F}; \quad Q_{r,s} = \widehat{M}(K_v \dot{e} + K_p e). \quad (3.8)$$

The function of the primary controller is to offset nonlinear effects inherent in the rigid degrees of freedom; whereas the secondary controller ensures a robust behavior. A block diagram of the control procedure is presented in Figure 3-3.

It is undesirable for a robot to exhibit an overshoot, since this could cause impact if, for instance, a desired trajectory terminates at the surface of a workpiece. Therefore, to ensure asymptotic and critically damped behavior of the closed-loop system, a suitable candidate for the PD gains, K_p and K_v , would be diagonal matrices such that

$$K_p = \begin{bmatrix} \omega_1^2 & 0 \\ & \ddots \\ 0 & \omega_i^2 \end{bmatrix}, \quad K_v = \begin{bmatrix} 2\omega_1 & 0 \\ & \ddots \\ 0 & 2\omega_i \end{bmatrix}, \quad (3.9)$$

where ω_i is the desired natural frequency associated with the i^{th} joint or link error (Eq. 3.6).

3.1.2 FLT/LQR control

A combined FLT/LQR approach was also applied to the two-unit manipulator system (Figure 3-2). When the manipulator is in a fixed configuration (no deployment, slew, or translation), the platform attitude (ψ_p) and manipulator length (l_1, l_2) are maintained using the FLT strategy. However, the joint rotation (α_1, α_2), the platform's tip vibration (e_p), as well as the links' tip deflections (e_1, e_2) are controlled using the LQR approach. During large slew and deployment maneuvers, variables ψ_p , α_1 , α_2 , l_1 , and l_2 are regulated by the FLT controller until the manipulator reaches the vicinity of its target position. Structural vibrations are left uncontrolled. At the end of the large maneuver, the system's configuration

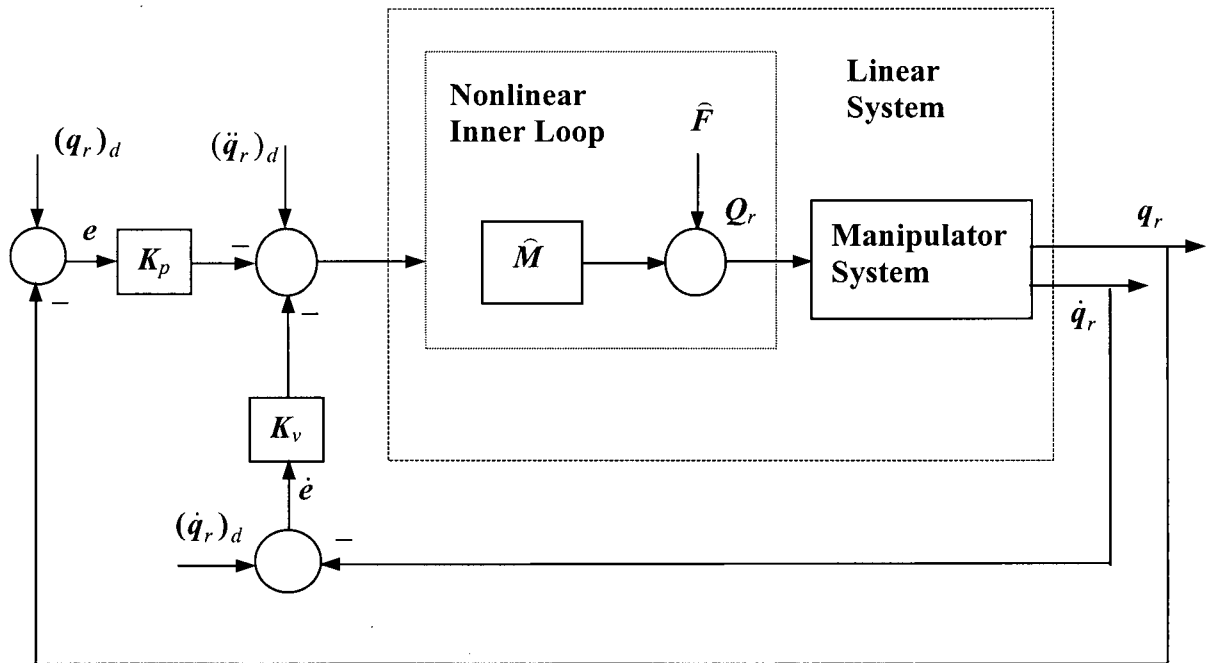


Figure 3-3 FLT-based control scheme showing inner and outer feedback loops.

remains nearly constant and nonlinear effects can be neglected. This allows the Linear Quadratic Regulator to take over the control of α_1 and α_2 to actively damp flexible generalized coordinates disturbed due to the maneuver.

The optimal LQR controller is designed based on a linearized model of the system. To begin with, the governing equations are linearized about an operation point \mathbf{q}_0 . To that end, the following substitutions are made in the left hand side of Eq. (3.1):

$$\mathbf{q} = \mathbf{q}_0 + \Delta\mathbf{q}; \quad \dot{\mathbf{q}} = \dot{\mathbf{q}}_0 + \Delta\dot{\mathbf{q}}; \quad \ddot{\mathbf{q}} = \ddot{\mathbf{q}}_0 + \Delta\ddot{\mathbf{q}}. \quad (3-10)$$

Trigonometric functions are expanded in the Taylor series, and the second and higher order terms in \mathbf{q} , $\dot{\mathbf{q}}$ and $\ddot{\mathbf{q}}$ are neglected. After some algebra, this leads to

$$\tilde{\mathbf{M}}(\mathbf{q}_0) \Delta\ddot{\mathbf{q}} + \tilde{\mathbf{K}}(\mathbf{q}_0) \Delta\mathbf{q} = \tilde{\mathbf{Q}} = \mathbf{Q}, \quad (3-11)$$

where $\tilde{\mathbf{M}}$ and $\tilde{\mathbf{K}}$ are the mass and stiffness matrices for the linearized system, respectively. Note, both $\tilde{\mathbf{M}}$ and $\tilde{\mathbf{K}}$ are evaluated at the operating point \mathbf{q}_0 and thus made time-invariant. Since the system's librational motion and the deployment length of the manipulator are controlled by the FLT, only the linearized equations governing the elastic degrees of freedom are needed. The decoupled vibrational subsystem is now described by

$$\bar{\mathbf{M}}(\mathbf{q}_0) \Delta \ddot{\mathbf{q}}_L + \bar{\mathbf{K}}(\mathbf{q}_0) \Delta \mathbf{q}_L = \mathbf{u}_L, \quad (3-12)$$

where $\Delta \mathbf{q}_L = [e_p, \Delta\alpha_1, \beta_1, e_1, \Delta\alpha_2, \beta_2, e_2]$, with $\Delta\alpha_1$ and $\Delta\alpha_2$ as the deviations of the slew angle from their desired values; $\bar{\mathbf{M}}$ and $\bar{\mathbf{K}}$ are the mass and stiffness matrices, respectively, corresponding to the elastic subsystem; and \mathbf{u}_L is the input determined from the Linear Quadratic Regulator to control e_p , $\Delta\alpha_1$, e_1 , $\Delta\alpha_2$ and e_2 . Note, the operational point is $\mathbf{q}_{L0} = [0, \alpha_{10}, 0, 0, \alpha_{20}, 0, 0]^T$. Solving for $\Delta \ddot{\mathbf{q}}_L$,

$$\Delta \ddot{\mathbf{q}}_L = -\bar{\mathbf{M}}^{-1} \bar{\mathbf{K}} \Delta \mathbf{q}_L + \bar{\mathbf{M}}^{-1} \mathbf{u}_L, \quad (3.13)$$

which can be rewritten in the state-space form as

$$\underbrace{\begin{bmatrix} \Delta \dot{\mathbf{q}}_L \\ \Delta \ddot{\mathbf{q}}_L \end{bmatrix}}_{\dot{\mathbf{x}}_L} = \underbrace{\begin{bmatrix} 0 & \mathbf{I} \\ -\bar{\mathbf{M}}^{-1} \bar{\mathbf{K}} & 0 \end{bmatrix}}_{\mathbf{A}} \underbrace{\begin{bmatrix} \Delta \mathbf{q}_L \\ \Delta \dot{\mathbf{q}}_L \end{bmatrix}}_{\mathbf{x}_L} + \underbrace{\begin{bmatrix} 0 \\ \bar{\mathbf{M}}^{-1} \end{bmatrix}}_{\mathbf{B}} \mathbf{u}_L, \quad (3.14)$$

where $\mathbf{x}_L \in \mathfrak{R}^{14 \times 1}$; $\mathbf{A} \in \mathfrak{R}^{14 \times 14}$; and $\mathbf{B} \in \mathfrak{R}^{14 \times 5}$. For simplicity, it is assumed that all states are available, thus making the system observable. Controllability of the system is assured if and only if

$$\text{rank}\{\mathbf{B}, \mathbf{A}\mathbf{B}, \mathbf{A}^2\mathbf{B}, \dots, \mathbf{A}^{13}\mathbf{B}\} = 14. \quad (3.15)$$

The control input \mathbf{u}_L can be written as

$$\mathbf{u}_L = -\mathbf{K}_{\text{LQR}} \mathbf{x}_L, \quad (3.16)$$

where \mathbf{K}_{LQR} is the optimal feedback gain matrix. It minimizes a quadratic cost function J which considers tracking errors and energy expenditure,

$$J = \int_0^T (\mathbf{x}_L^T \mathbf{Q}_{\text{LQR}} \mathbf{x}_L + \mathbf{u}_L^T \mathbf{R}_{\text{LQR}} \mathbf{u}_L) dt. \quad (3.17)$$

Here \mathbf{Q}_{LQR} and \mathbf{R}_{LQR} are symmetric weighting matrices which assign relative penalties to state errors and control effort, respectively. The matrix \mathbf{R}_{LQR} is required to be positive definite while \mathbf{Q}_{LQR} can be positive semi-definite. The optimal control input \mathbf{u}_L is given by

$$\mathbf{u}_L = -\mathbf{K}_{\text{LQR}} \mathbf{x}_L = -\mathbf{R}_{\text{LQR}}^{-1} \mathbf{B}^T \mathbf{P}_{\text{LQR}} \mathbf{x}_L, \quad (3.18)$$

where \mathbf{P}_{LQR} is the positive definite solution to the steady-state matrix Riccati equation which, for infinite time, becomes

$$\mathbf{P}_{\text{LQR}} \mathbf{A} + \mathbf{A}^T \mathbf{P}_{\text{LQR}} - \mathbf{P}_{\text{LQR}} \mathbf{B} \mathbf{R}_{\text{LQR}}^{-1} \mathbf{B}^T \mathbf{P}_{\text{LQR}} + \mathbf{Q}_{\text{LQR}} = 0. \quad (3.19)$$

The FLT/LQR control strategy is indicated in Figure 3-4. Note, q_r , represents generalized coordinates controlled by the FLT.

3.2 Simulation Results and Discussion: Commanded Maneuvers

The numerical values used in the simulation are summarized below:

<u>Orbit:</u>	circular at an altitude of 400 km; period = 92.5 min.
<u>Platform:</u>	cylindrical with axial to transverse inertia ratio of 0.005; mass = 120,000 kg; length = 120m; flexural rigidity = $5.5 \times 10^8 \text{ Nm}^2$.
<u>Manipulator Module:</u>	cylindrical with axial to transverse inertia ratio of 0.005; mass = 400 kg each; length = 7.5m each at start; flexural rigidity = $5.5 \times 10^5 \text{ Nm}^2$.
<u>Revolute Joints:</u>	mass = 20kg; moment of inertia = 10 kg m^2 ; stiffness = 1.0×10^4 Nm/rad.
<u>Payload:</u>	no payload unless specified.
<u>Damping:</u>	assumed zero for all components.
<u>Mode:</u>	fundamental.

Damping is purposely not included to obtain conservative results and test the controller under severe conditions. Furthermore, character and precise value of damping in the space environment is still a subject of considerable debate.

To assess the system control under a rather demanding situation, the platform is initially taken to be along the local horizontal ($\psi_p = -90^\circ$), an unstable equilibrium configuration. The manipulator is located at the platform tip to accentuate the maneuver effect, and is initially aligned with the platform. The system, without any payload, is commanded to undergo simultaneous slew and deployment maneuvers, in a sine-on-ramp

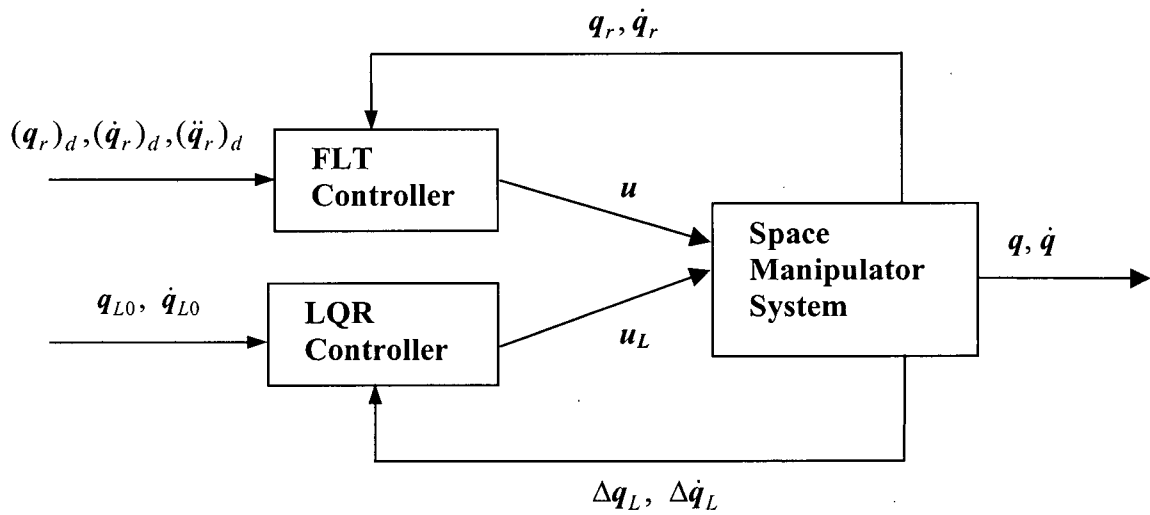


Figure 3-4 Block diagram illustrating the combined FLT/LQR approach applied to the manipulator system.

profile (Figure 2-3), completed in 0.01 orbit (55.50s), so that α_1, α_2 change from zero to 90° and l_1, l_2 from 7.5 m to 15 m.

3.2.1 FLT control

Figure 3-5 shows the FLT controlled response of the platform libration (ψ_p), its tip vibration (e_p), the first and second modules' revolutes joint rotations ($\alpha_1, \beta_1, \alpha_2, \beta_2$), as well as the modules' tip deflections (e_1, e_2). The maneuver sets the platform librating with a peak amplitude of around 0.04° which is rather small (permissible limit can vary from 0.1° to 1° depending on the mission). The platform returns to the original local horizontal orientation in less than 100 s even in presence of such a severe maneuver ! The negligible ($\approx 0.05^\circ$) limit cycle type oscillations persist due to vibrations of the flexible joints (β_1, β_2). The tip response of the massive platform, as expected, is also vanishingly small ($\approx 0.2 - 2$ mm). The steady state joint vibration (β_1, β_2) amplitudes (4° and 2° , respectively) may be considered acceptable recognizing the fact that the flexible generalized coordinates are uncontrolled, the disturbance is unusually severe and the inherent structural damping is not accounted for. Clearly, the unmodeled dynamics of the flexible generalized coordinates affects the performance of the controller. However, the controller demands remain rather modest. The five controlled variables ($\psi_p, \alpha_1, l_1, \alpha_2$, and l_2) show satisfactory response even during such a large maneuver and display small oscillations after the desired values are reached. Thus the FLT control of the rigid degrees of freedom does provide encouraging results.

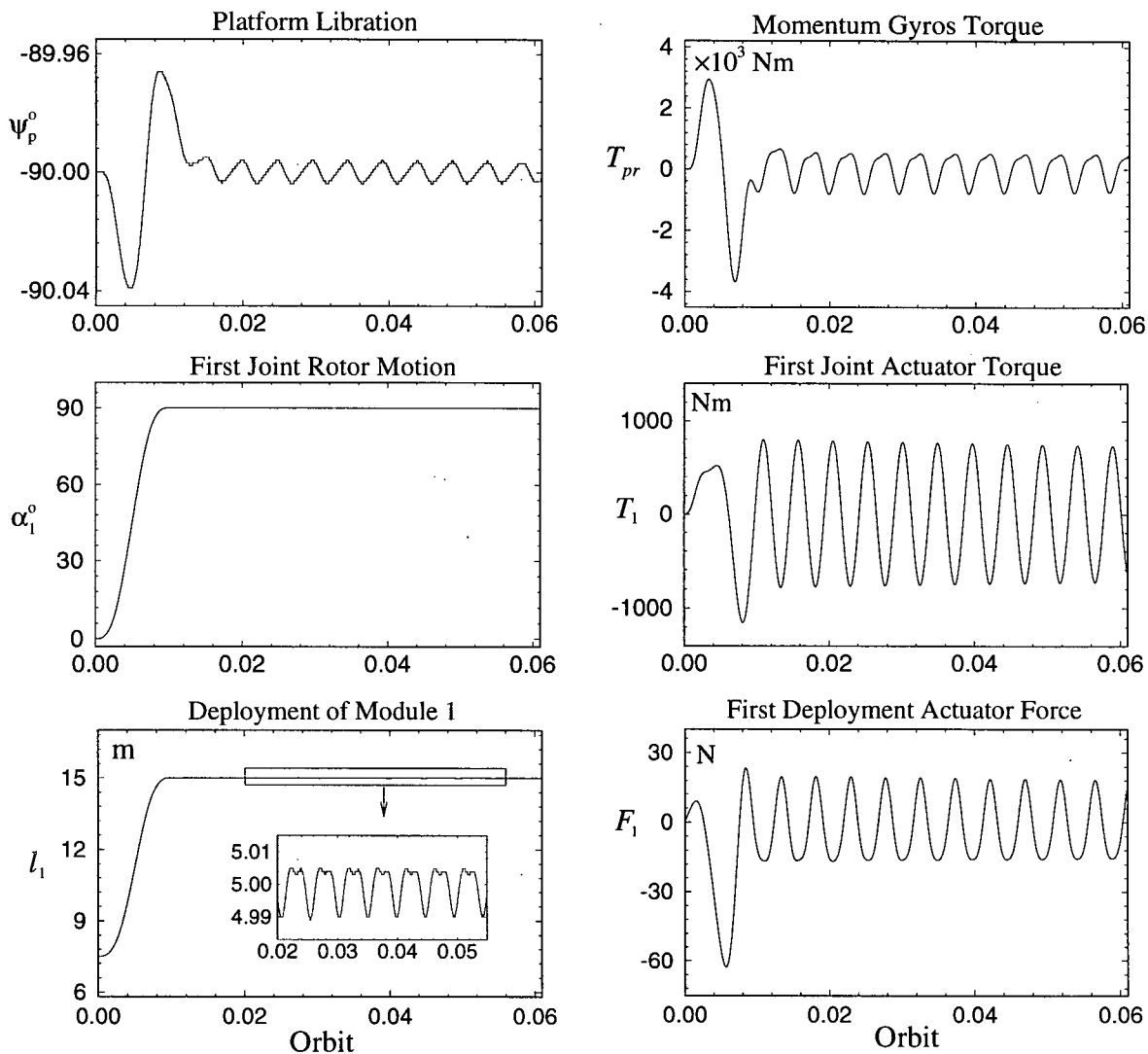
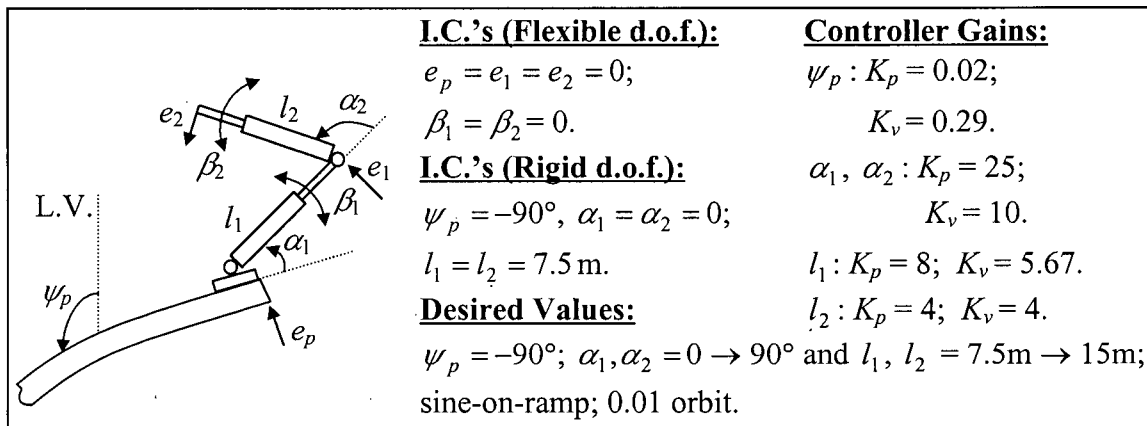


Figure 3-5 Response of the system during a simultaneous 90° slew and 7.5m deployment maneuver of the two-unit manipulator with rigid degrees of freedom controlled by the FLT: (a) rigid degrees of freedom and control inputs for module 1.

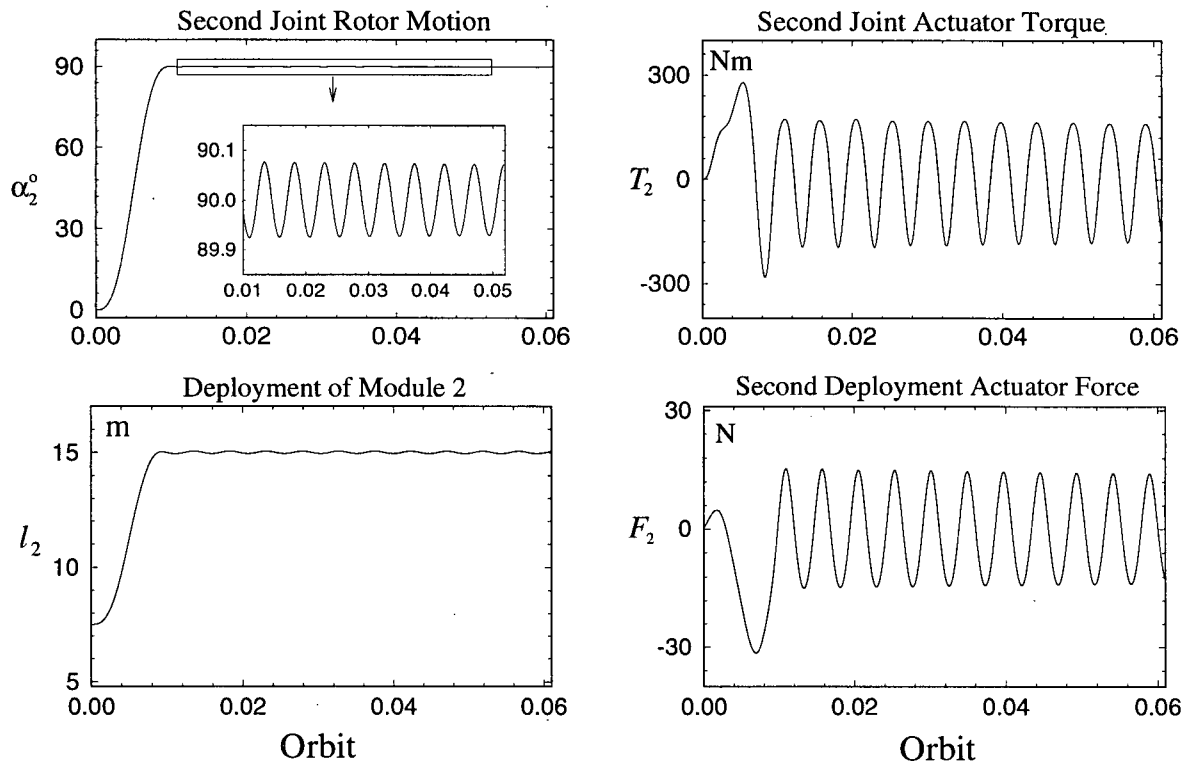
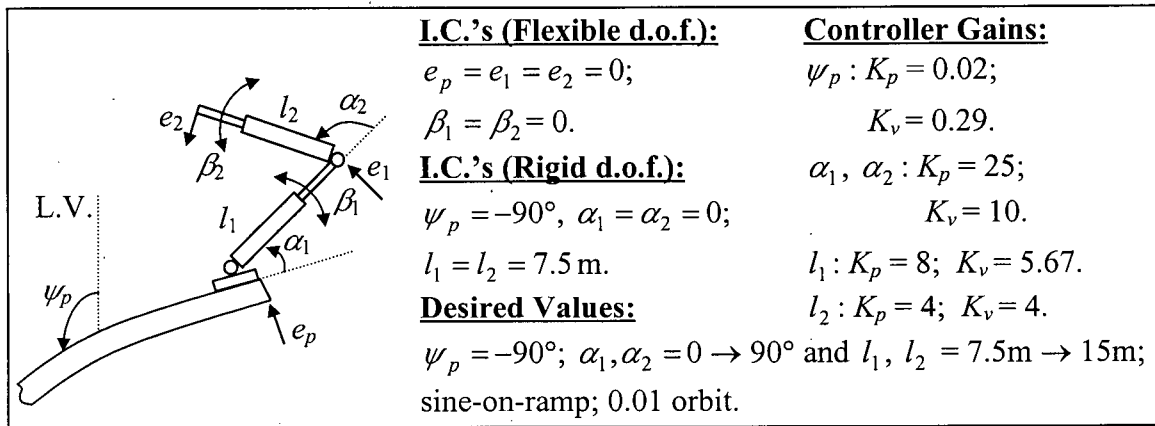


Figure 3-5 Response of the system during a simultaneous 90° slew and 7.5m deployment maneuver of the two-unit manipulator with rigid degrees of freedom controlled by the FLT: (b) rigid degrees of freedom and control inputs for module 2.

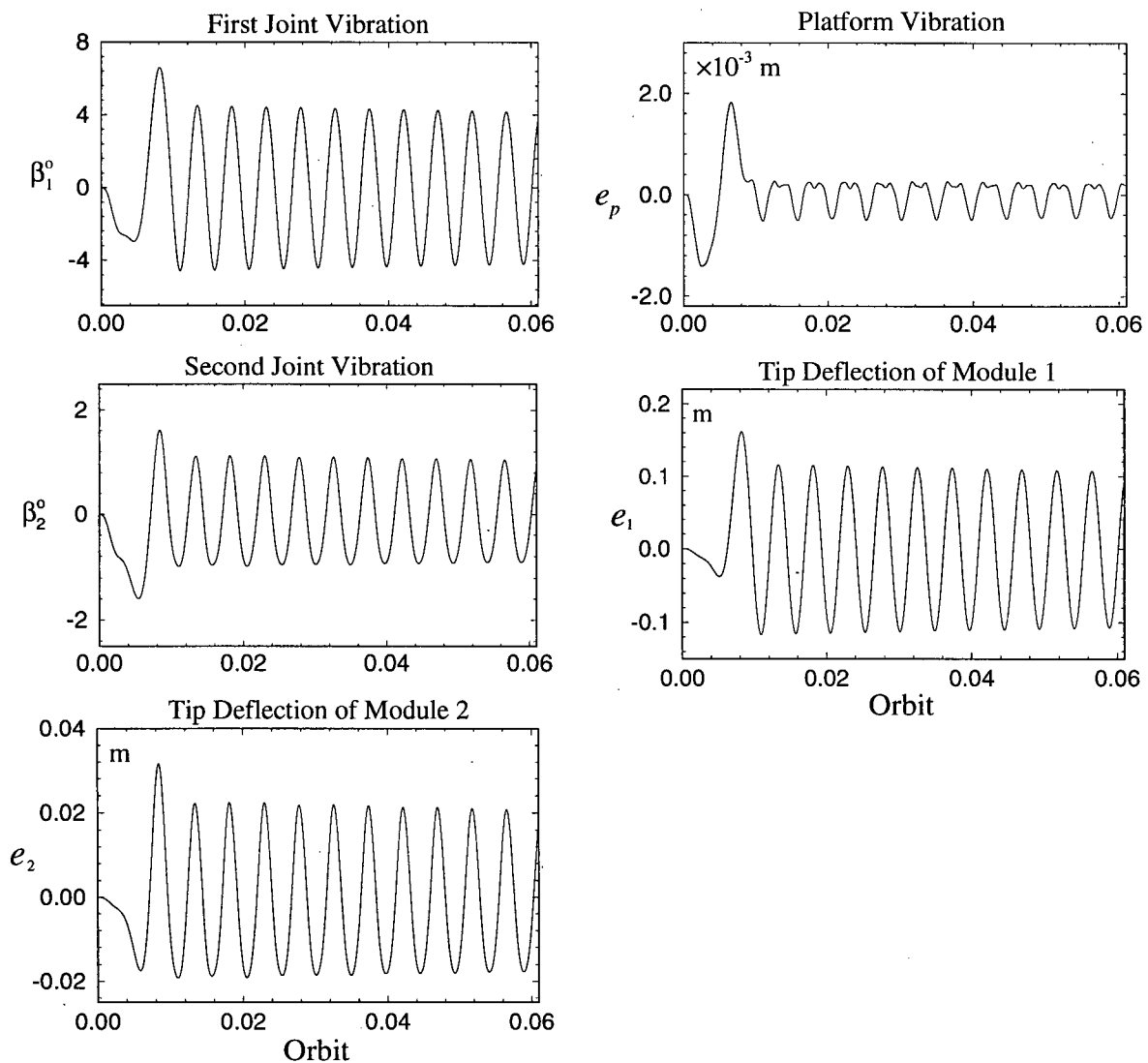
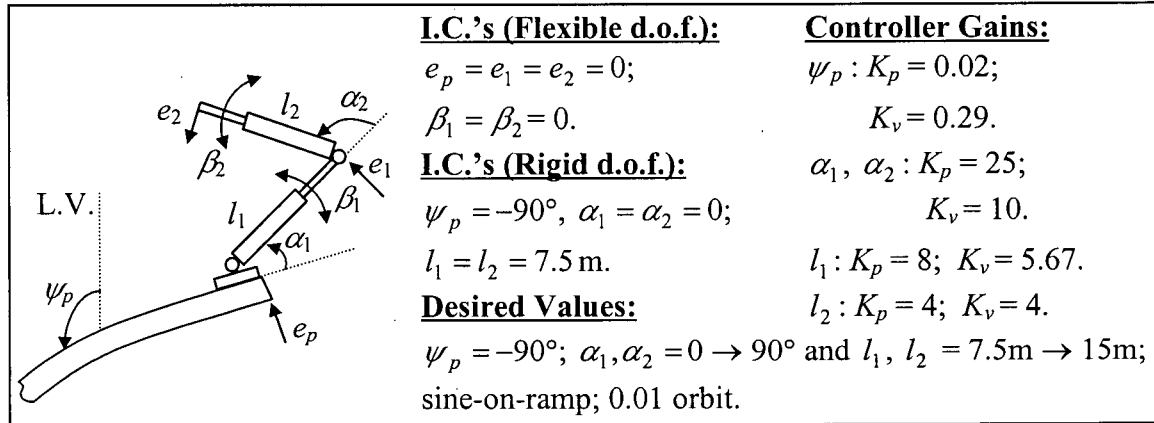


Figure 3-5 Response of the system during a simultaneous 90° slew and 7.5m deployment maneuver of the two-unit manipulator with rigid degrees of freedom controlled by the FLT: (c) flexible degrees of freedom.

3.2.2 FLT/LQR control

With the control of rigid as well as flexible degrees of freedom (FLT/LQR approach), the situation further improves remarkably (Figure 3-6), particularly in the steady state librational and vibrational responses. In this particular case, the LQR controller is only activated after 0.01 orbit, i.e. at the end of the maneuver. This means, in the first 0.01 orbit, the FLT is used to regulate the large maneuver where it satisfactorily controlled the rigid degrees of freedom. After 0.01 orbit, the system enters the steady state phase and vibrates around the reference point. At this stage, the LQR begins to control vibrations. Note, the FLT controller is still active to regulate the platform's attitude and length of the links. The LQR is quite effective in suppressing the joints and platform vibrations which, in turn, help eliminate the librational limit cycle. The joint angles and link lengths attain and remain at their commanded values. Furthermore, the control torques required, in the steady state, are virtually negligible.

Effect of payload

In the previous two cases, the payload was purposely taken to be zero to help isolate coupling effects. The next logical step was to assess the influence of a point mass payload at the manipulator's tip. Three values of the payload ratio (mass of the payload / mass of the manipulator) were considered: 1, 2 and 5; which correspond to the payloads of 400 kg, 800 kg and 2,000 kg, respectively. The initial configuration of the manipulator remains the same as described in the previous cases. The maneuver, as before, involves a simultaneous 90° slew of the revolute joints and 7.5m deployment of the links in a sine-on-ramp profile. It is

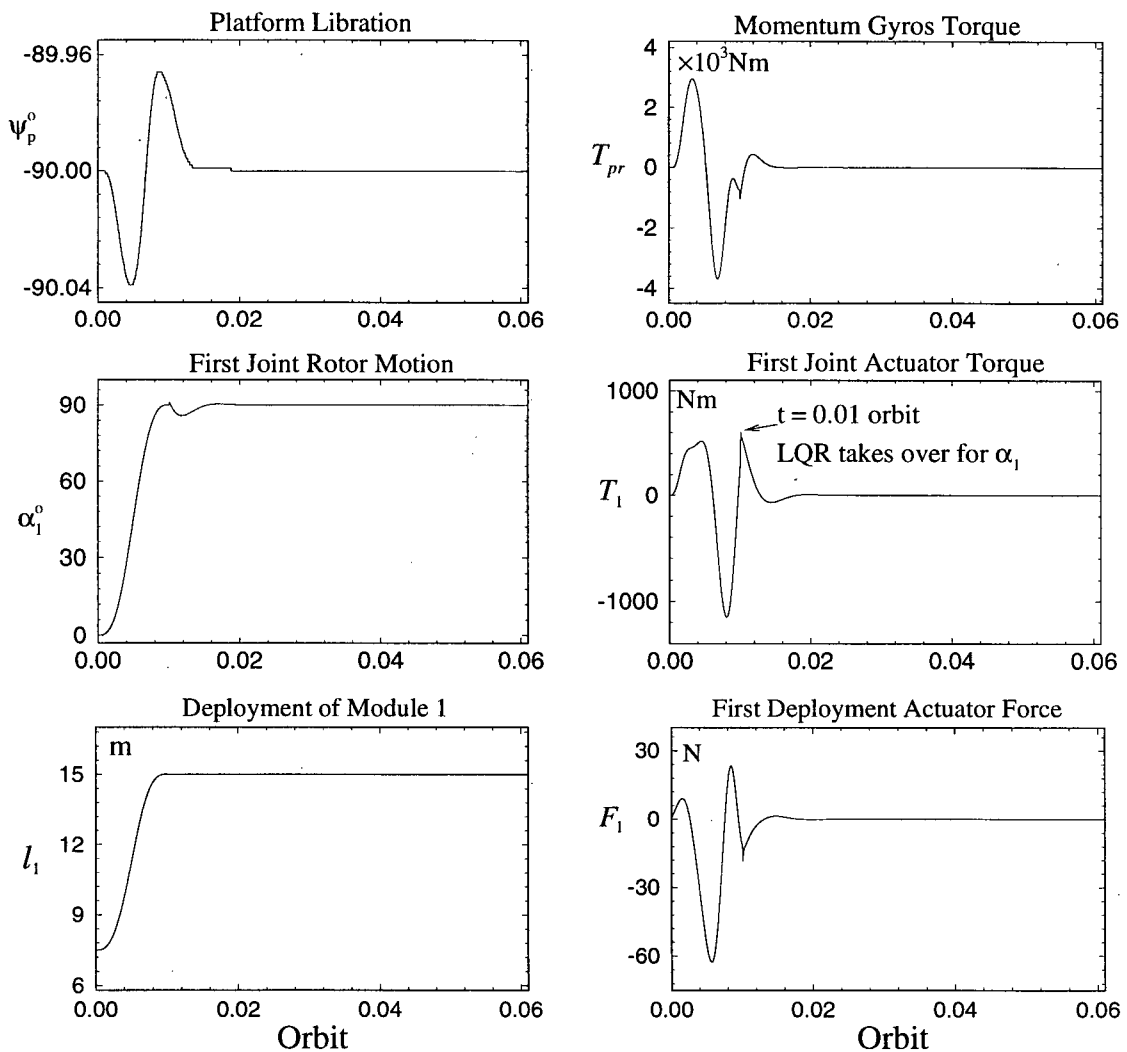
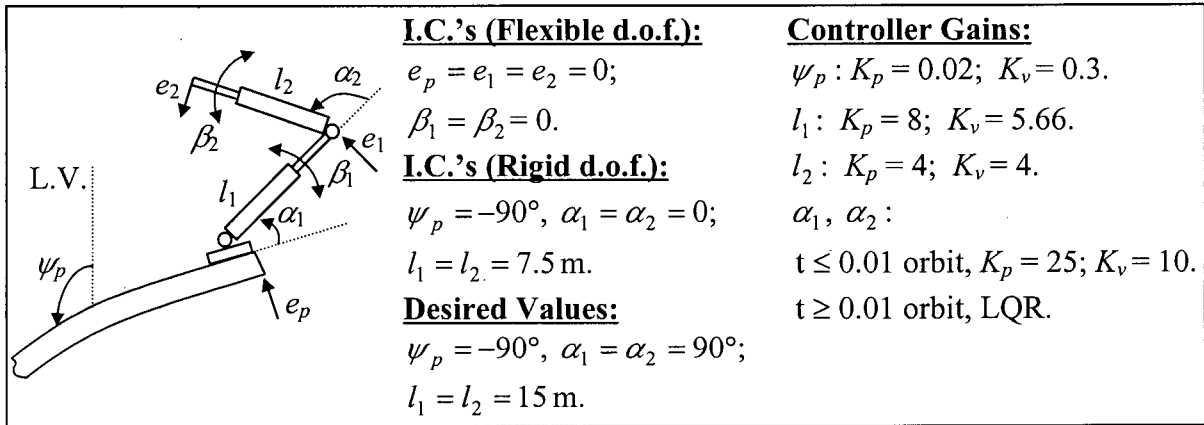


Figure 3-6 FLT/LQR controlled response of the two-unit system during a simultaneous 90° slew and a 7.5 m deployment maneuver of the manipulator units: (a) rigid degrees of freedom and control inputs for module 1.

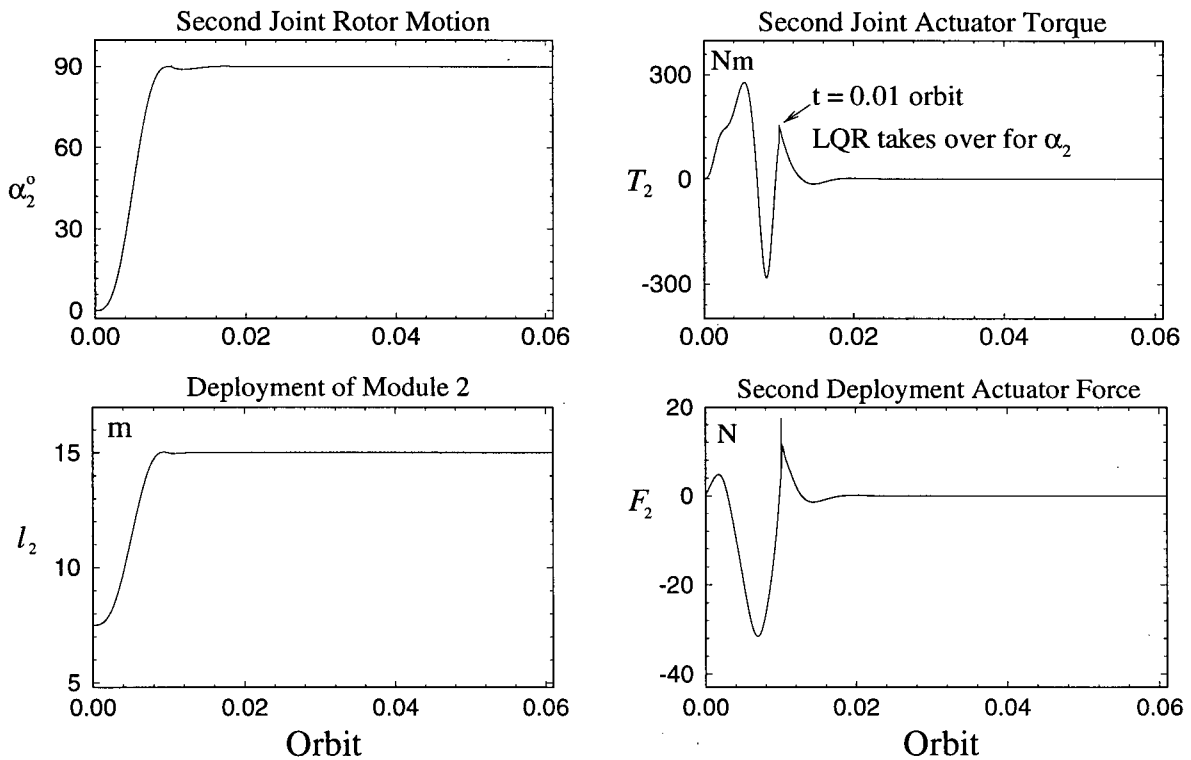
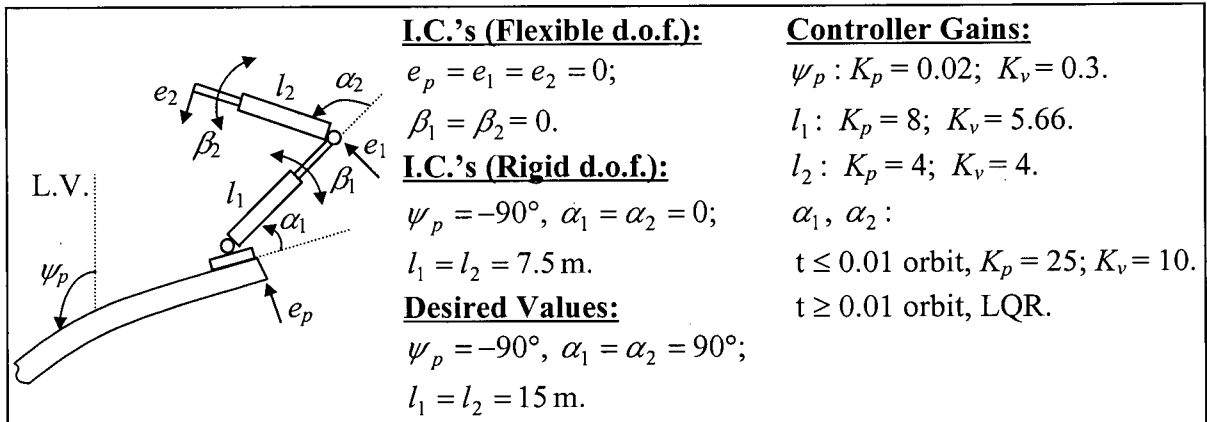


Figure 3-6 FLT/LQR controlled response of the two-unit system during a simultaneous 90° slew and a 7.5 m deployment maneuver of the manipulator units: (b) rigid degrees of freedom and control inputs for module 2.

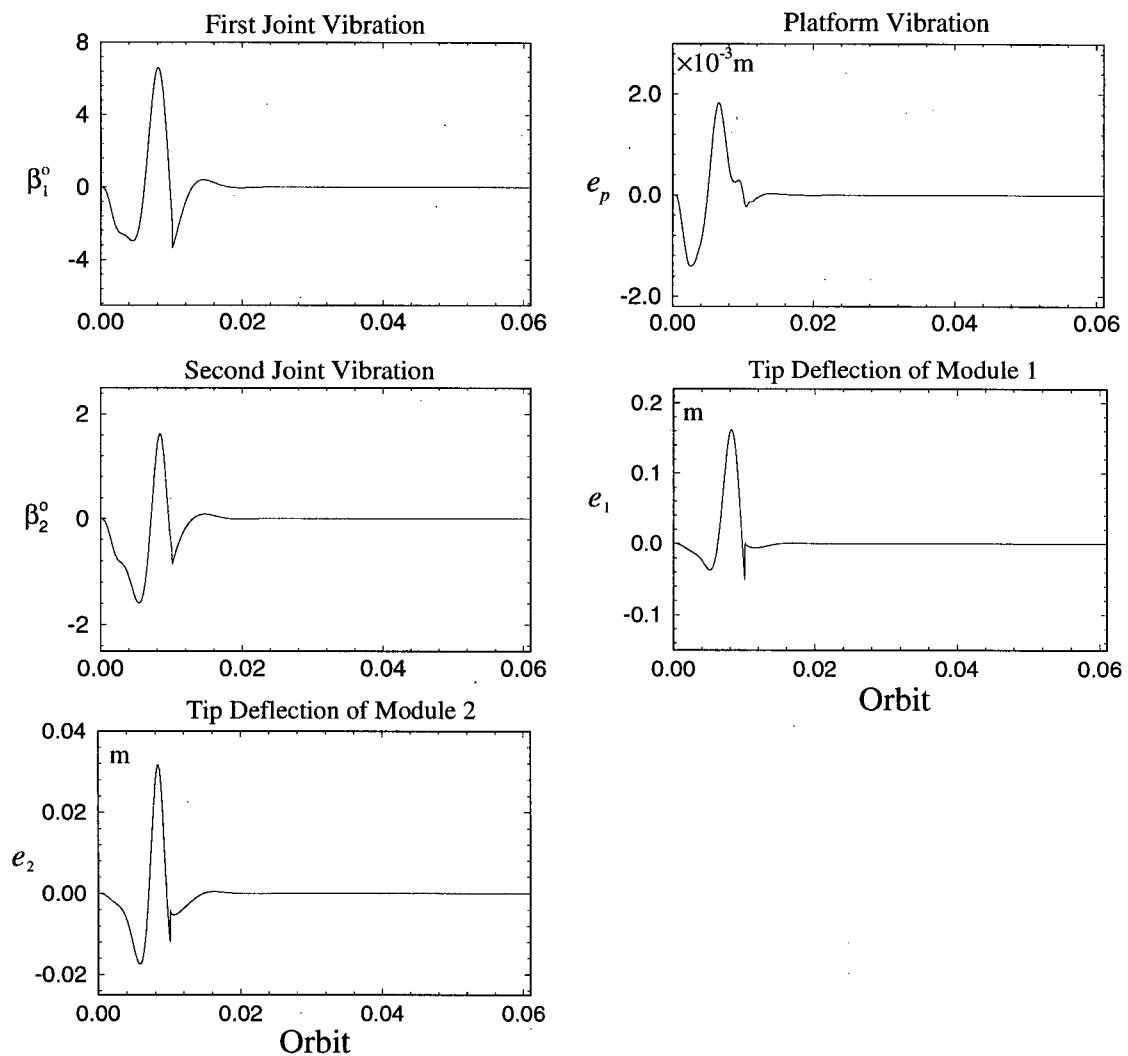
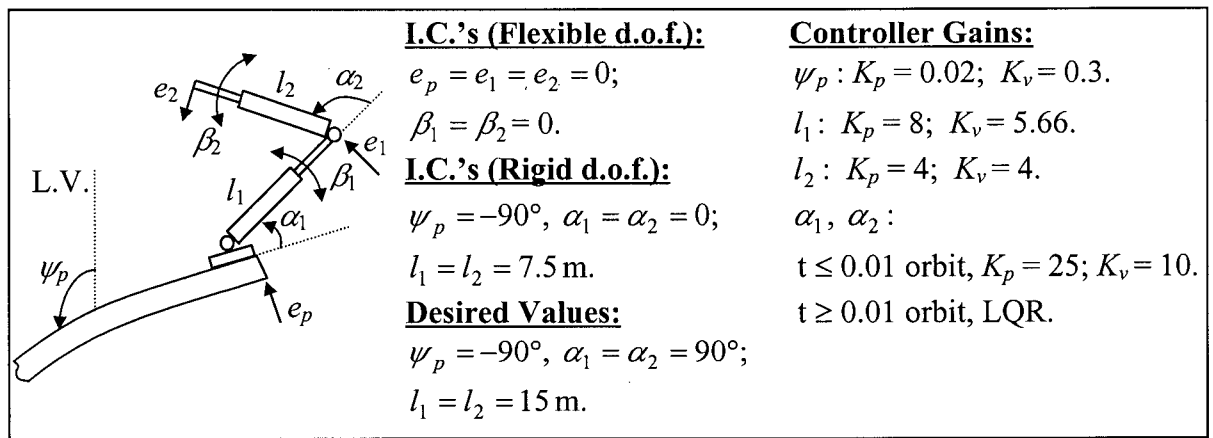


Figure 3-6 FLT/LQR controlled response of the two-unit system during a simultaneous 90° slew and a 7.5 m deployment maneuver of the manipulator units: (c) flexible degrees of freedom.

desired that the maneuver be finished in 0.03 orbit. As in the case of the uncontrolled dynamical study (Figure 2-15), a longer maneuver time is used here because of the presence of the payload.

Figure 3-7 presents results as affected by the payload. The controller gains used by the FLT are indicated in the legend. The gains were purposely kept fixed to help assess robustness of the controller. The LQR becomes effective at 0.03 orbit, i.e. when the maneuver is completed. At the outset, it is apparent that the manipulator is able to attain the commanded values of slew and deployment even in presence of payloads (Figures 3-7a, 7b). As can be anticipated, the peak control efforts increase with an increase in the payload, however the additional demands are rather modest and remain well within the permissible limits. For example, with the largest payload of 2,000 kg, the absolute peak value of the CMG demand changes from around 3000 Nm (no payload) to 4400 Nm while the force (F_2) at the prismatic joint of module two has corresponding variations from 32 N to 56 N. Note, the control effort is required for a relatively longer period of time, however, after approximately 0.08 orbit, the system settles down to the new equilibrium position, very close to the original, and the control effort required is virtually negligible. Flexible degrees of freedom are also controlled, in presence of payload, quite effectively (Figure 3-7c).

Effect of Maneuver Speed

Another important system parameter is the speed of the maneuver. The same maneuver as before was considered in absence of payload. Of course, one would like to complete the maneuver as quickly as possible without adversely affecting the performance. Three different values were considered: 0.05 orbit (fast), 0.01 orbit (nominal), and 0.03 orbit

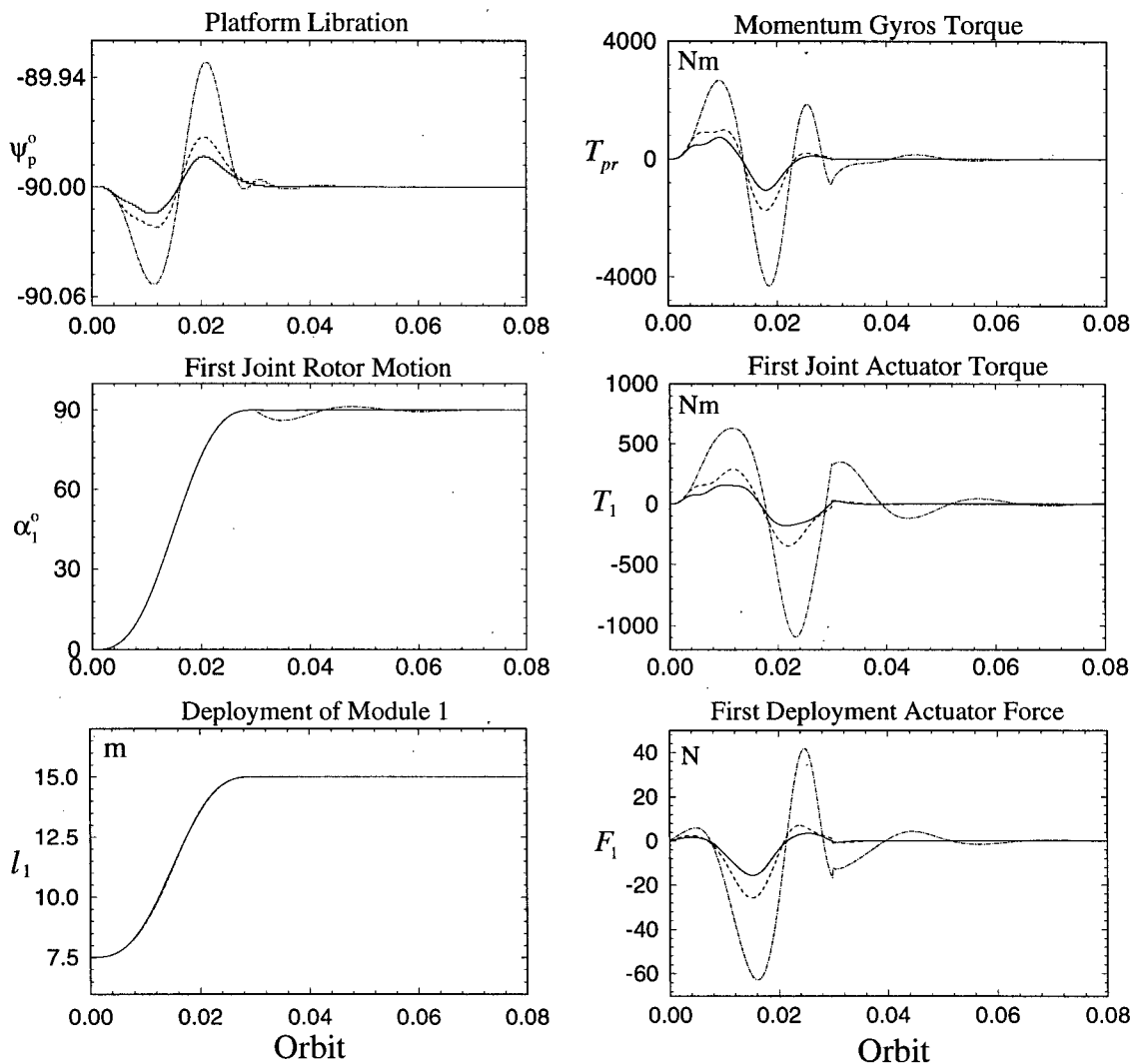
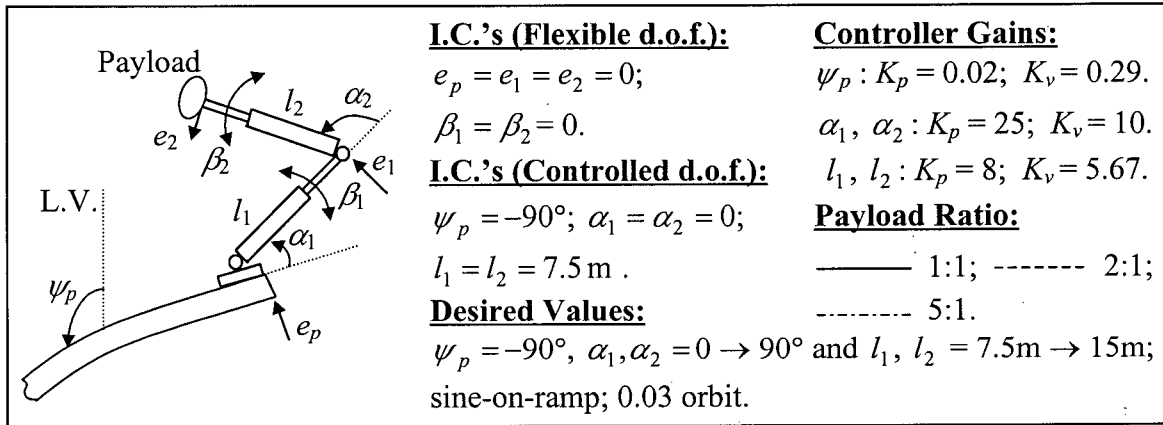


Figure 3-7 FLT/LQR controlled response of the system during a simultaneous 90° slew and 7.5 m deployment maneuver of the two-unit manipulator with different payload ratios: (a) rigid degrees of freedom and control inputs for module 1.

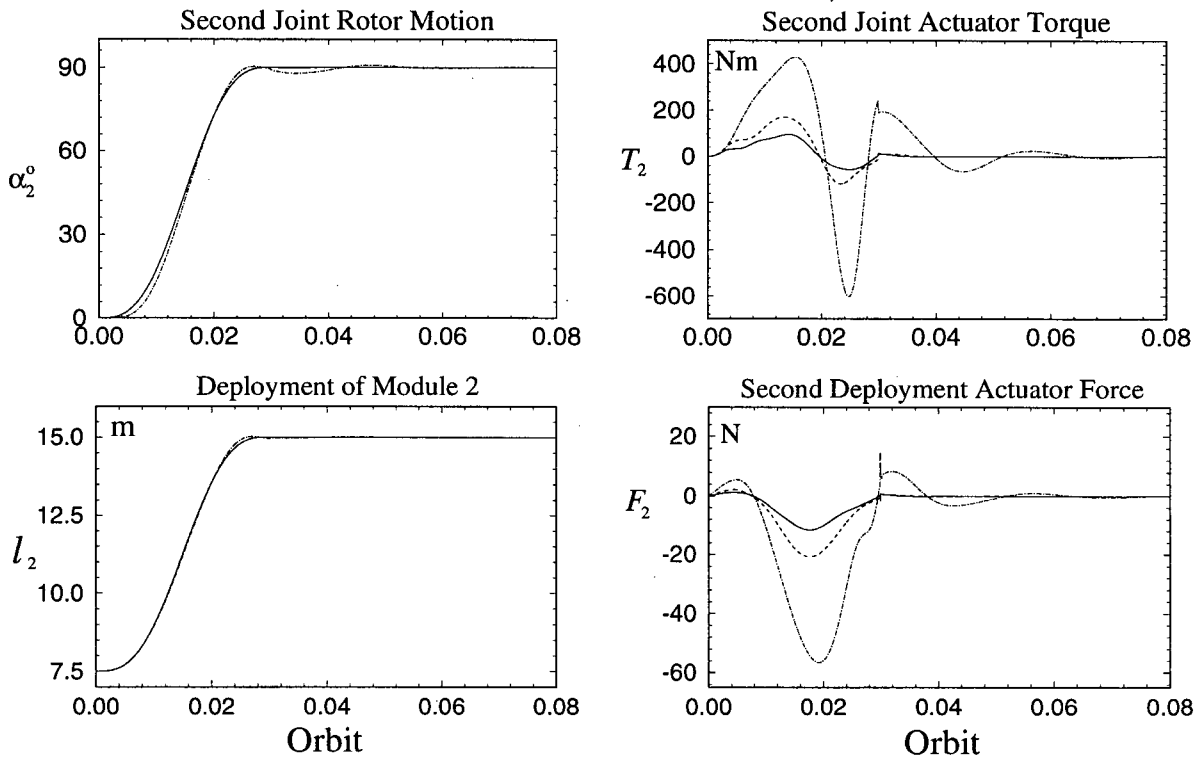
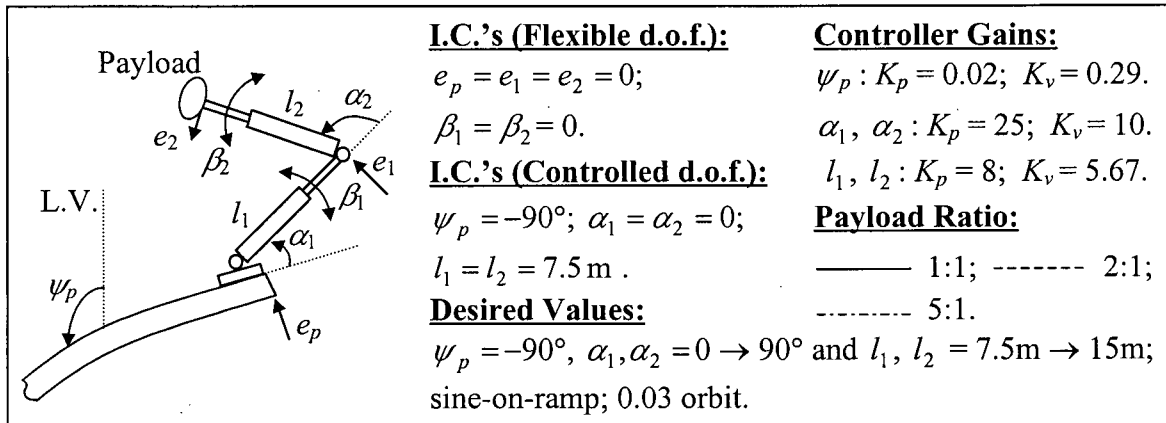


Figure 3-7 FLT/LQR controlled response of the system during a simultaneous 90° slew and 7.5 m deployment maneuver of the two-unit manipulator with different payload ratios: (b) rigid degrees of freedom and control inputs for module 2.

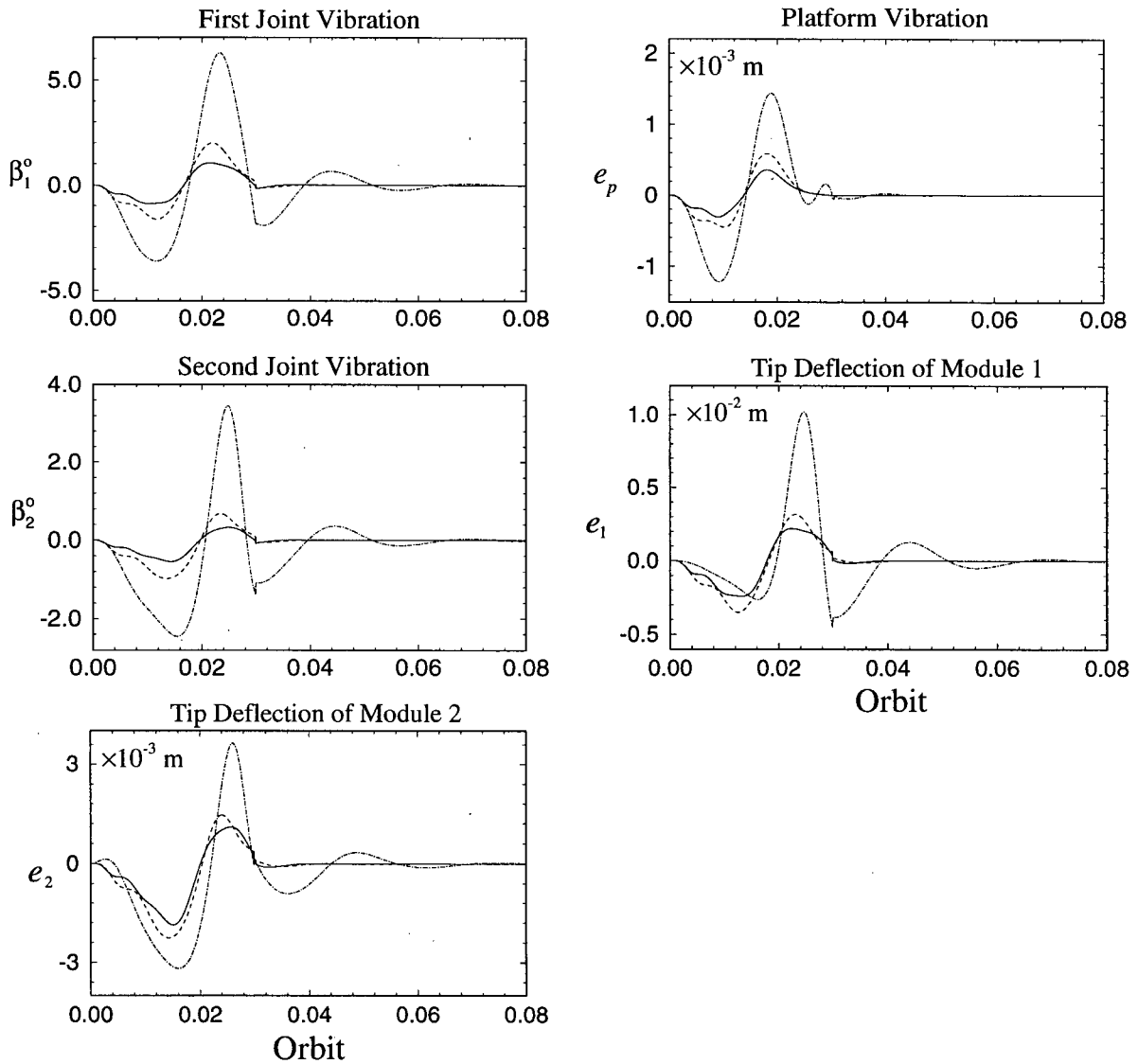
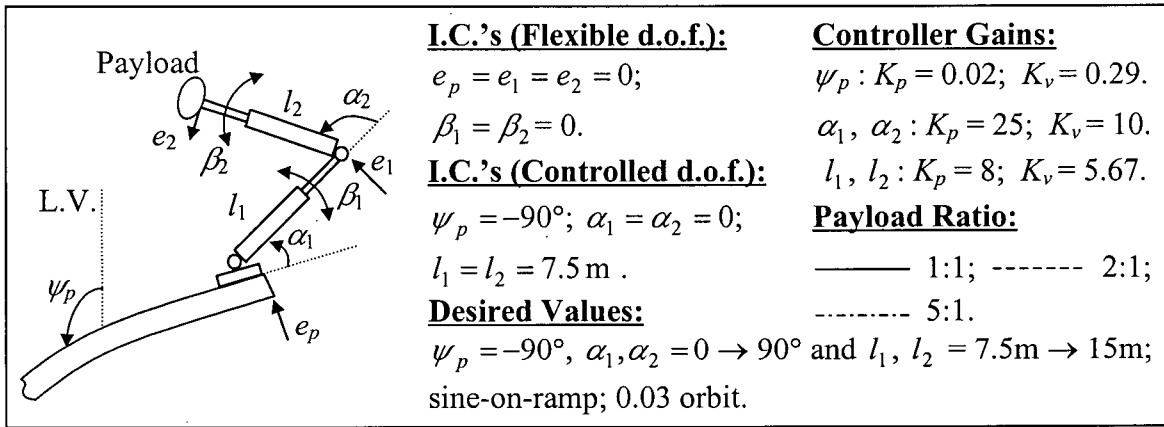


Figure 3-7 FLT/LQR controlled response of the system during a simultaneous 90° slew and 7.5 m deployment maneuver of the two-unit manipulator with different payload ratios: (c) flexible degrees of freedom.

(slow). Results are presented in Figure 3-8.

It is apparent that the manipulator attains the commanded values rather quickly after the specified period even in the case of a fast maneuver. The force and torque demands remain modest. Note, the peak platform deviation from the unstable equilibrium position is around 0.1° (Figure 3-8a) for the fast maneuver and virtually negligible for the slow case of 0.03 orbit. The peak torques and forces encountered are well within the accepted limit (Figure 3-8a,b). Even the flexible degrees of freedom are controlled rather well with the equilibrium configuration regained in less than 0.03 orbit (≈ 167 s).

Effect of Revolute Joint Stiffness

Stiffness of revolute joint also represents a significant variable. Its effect on the controlled performance while executing the same maneuver in 0.01 orbit, with no payload, was also assessed. These results are presented in Figure 3-9. Two stiffness values, one below (soft) and the other above (hard) the nominal value of 1×10^4 Nm/rad were considered. Even in the demanding situation presented by the soft spring, the system settles down to the commanded values in around 0.03 orbit (≈ 167 s). As before, the demands on control forces and torques continue to remain modest.

It is important to point out that gains during the studies aimed at assessing the influence of payload, maneuvering speed and stiffness variations are intentionally kept the same to demonstrate robust character of the FLT/LQR control. Based on the investigation reported in this chapter, it can be concluded that both the FLT by itself as well as a synthesis of the FLT and LQR, or other linear control procedure, appear quite promising. They should receive further attention in refining their implementation.

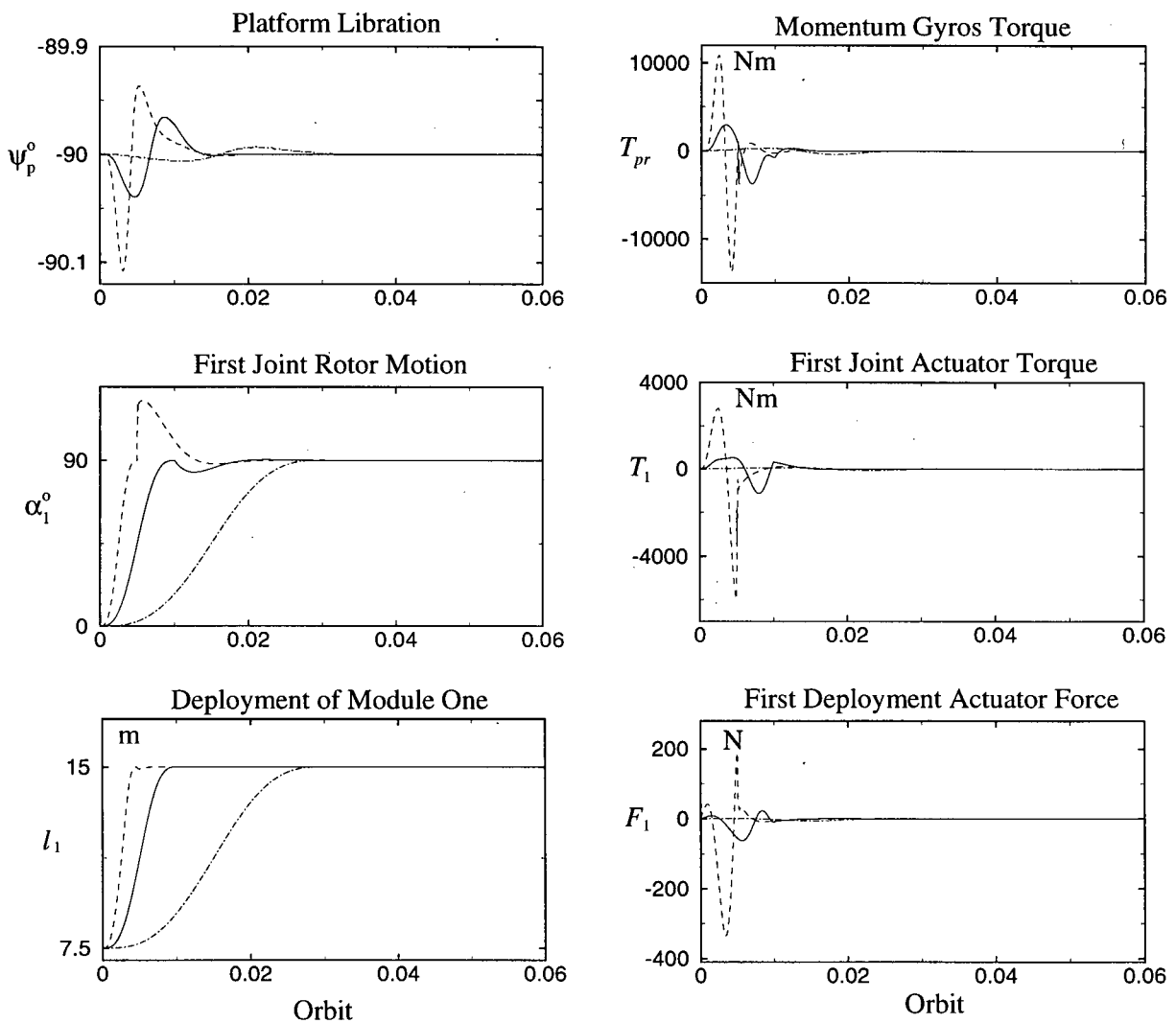
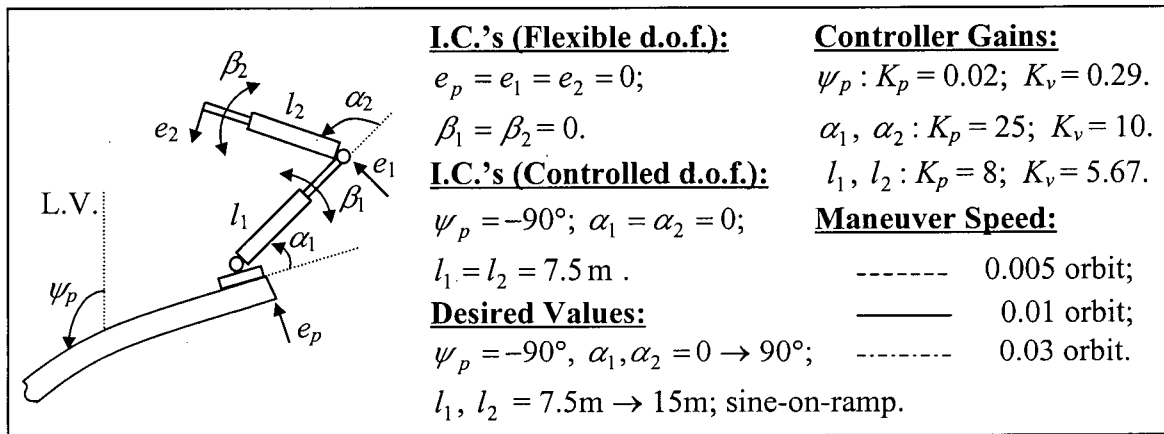


Figure 3-8 Effect of the speed of maneuver on the FLT/LQR controlled response: (a) platform and module 1.

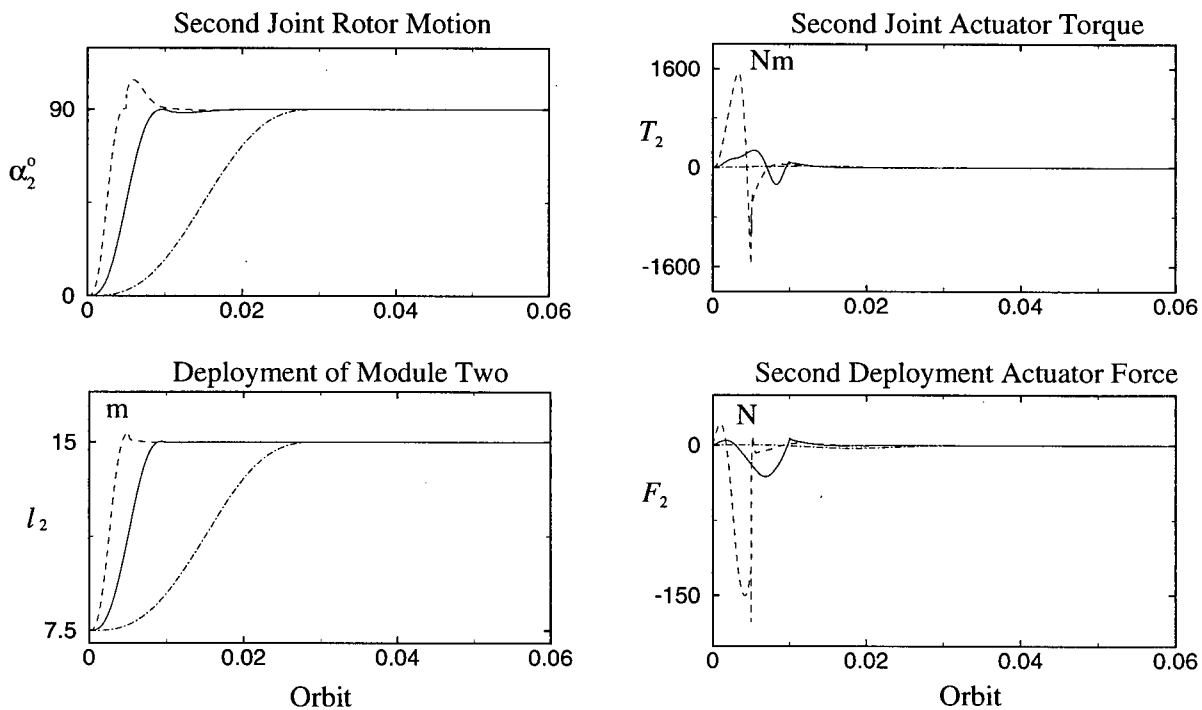
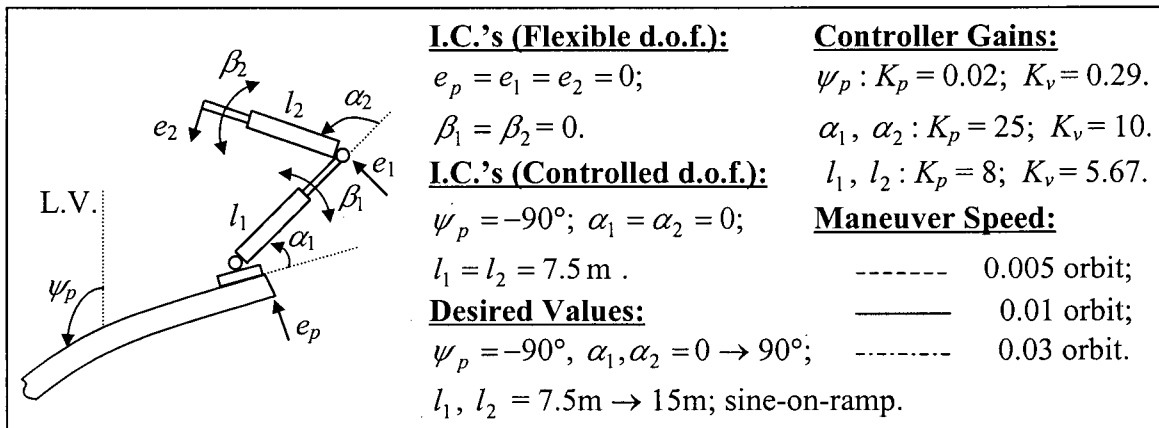


Figure 3-8 Effect of the speed of maneuver on the FLT/LQR controlled response: (b) module 2.

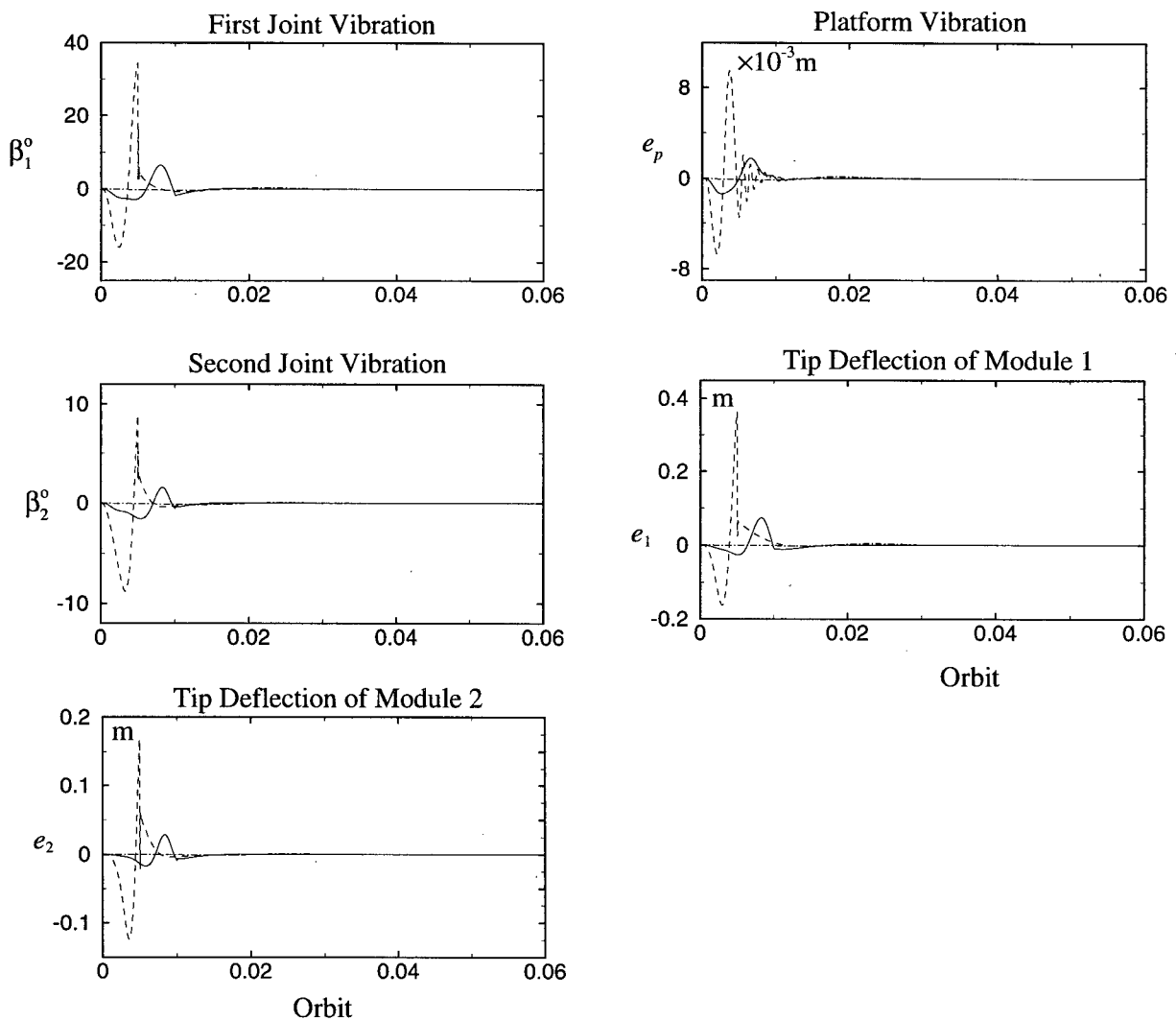
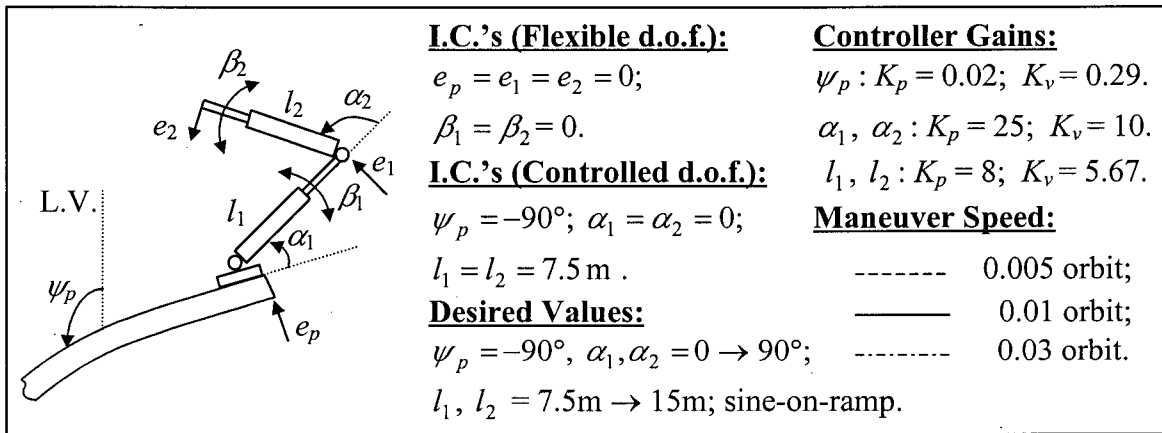


Figure 3-8 Effect of the speed of maneuver on the FLT/LQR controlled response: (c) flexible degrees of freedom.

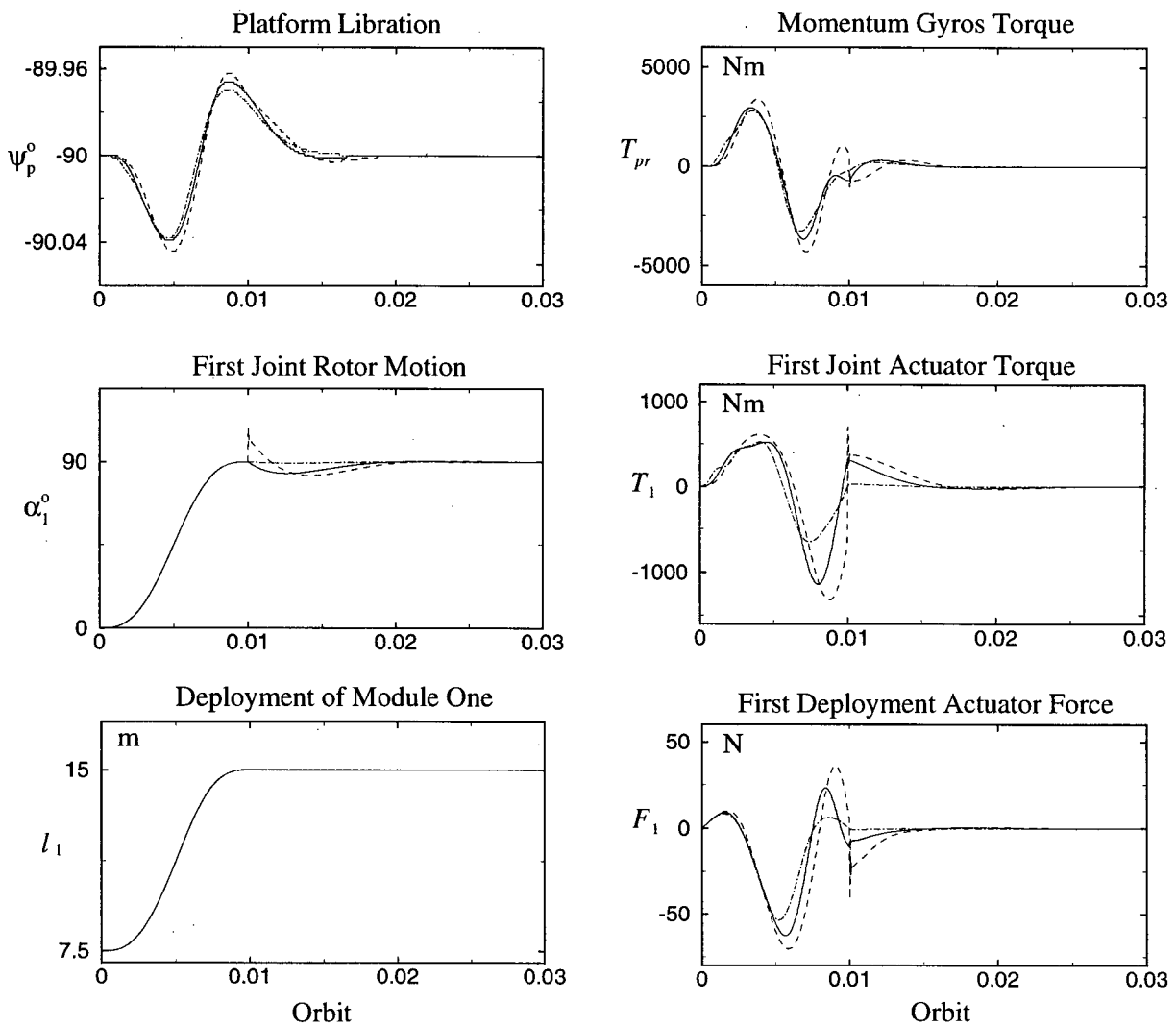
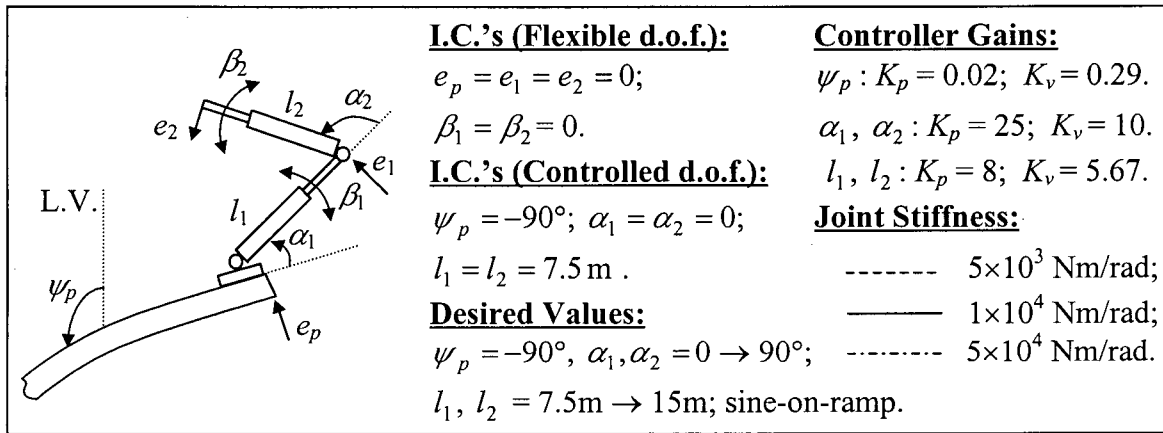


Figure 3-9 FLT/LQR controlled response as affected by the revolute joint stiffness during a manipulator maneuver: (a) platform and module 1.

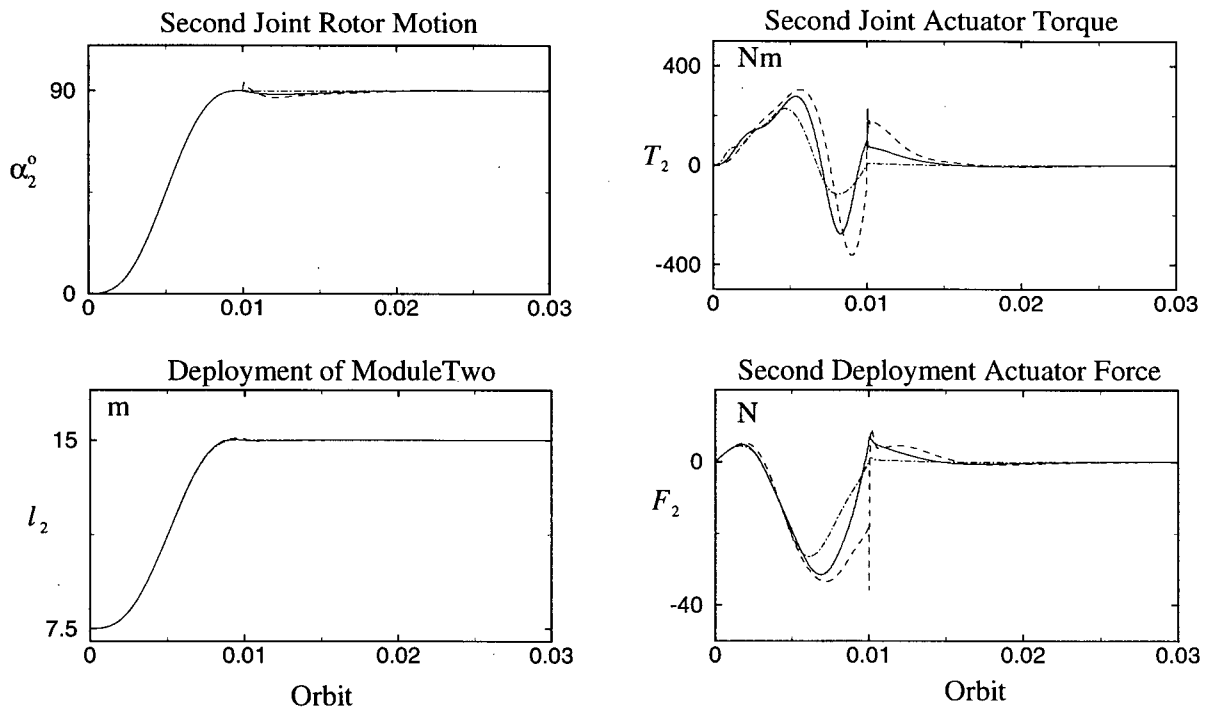
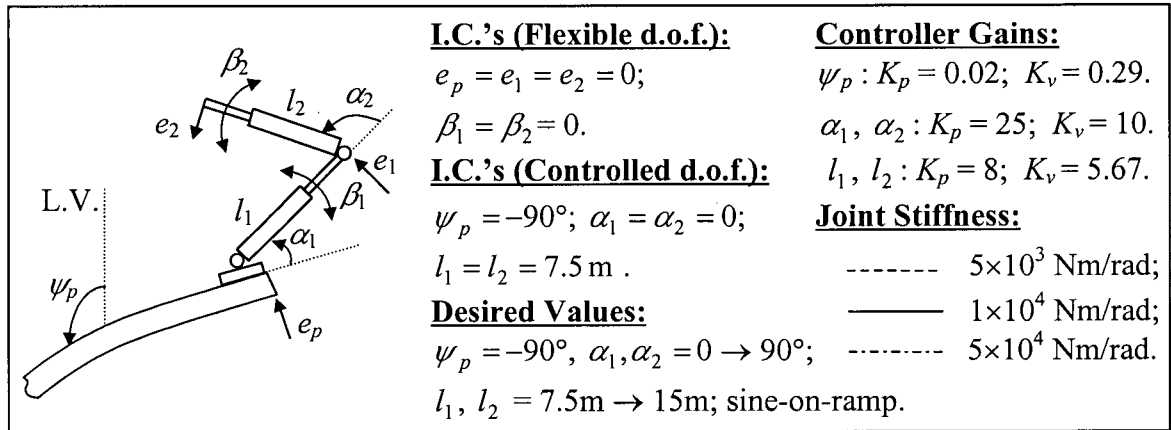


Figure 3-9 FLT/LQR controlled response as affected by the revolute joint stiffness during a manipulator maneuver: (b) module 2.

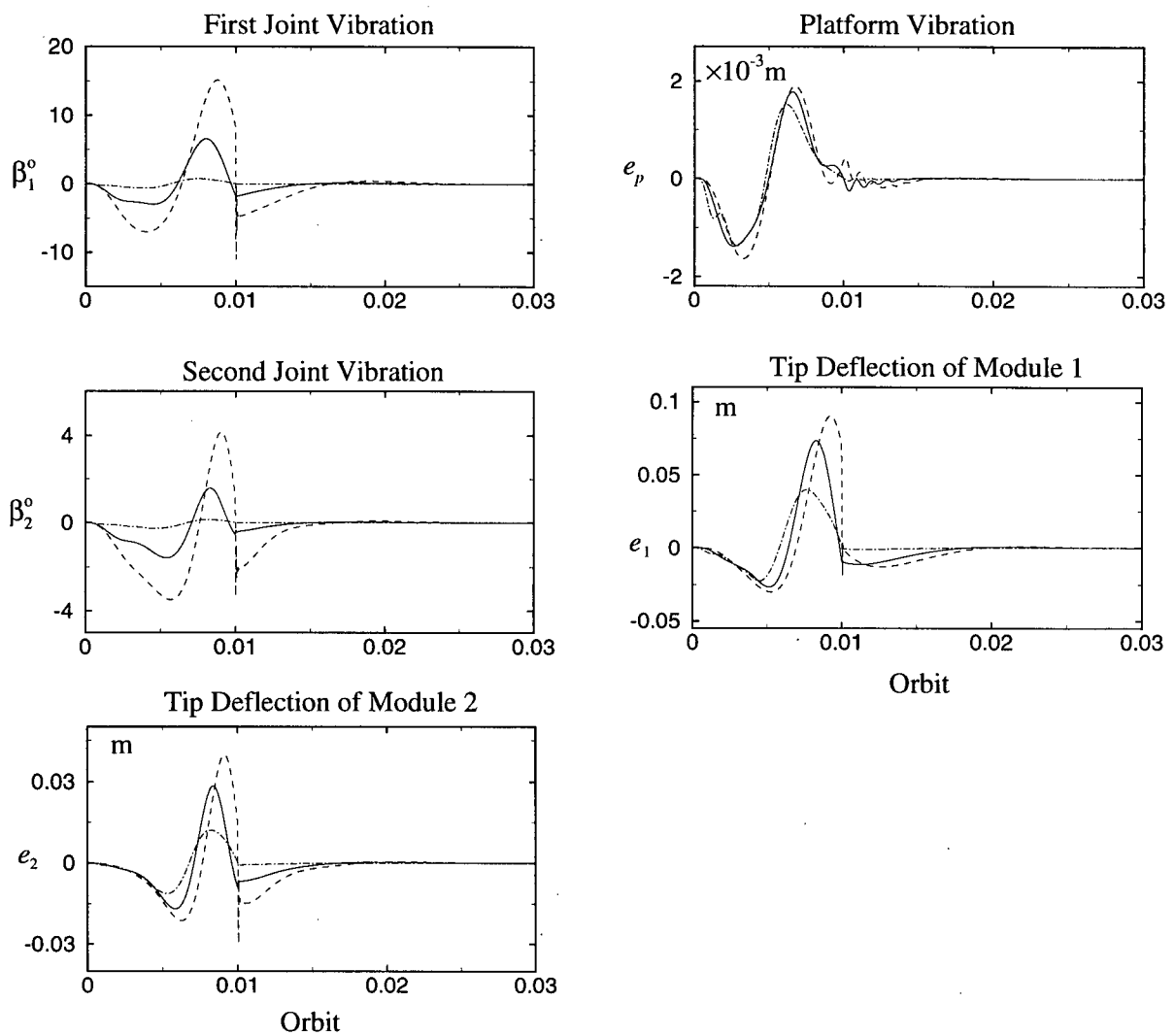
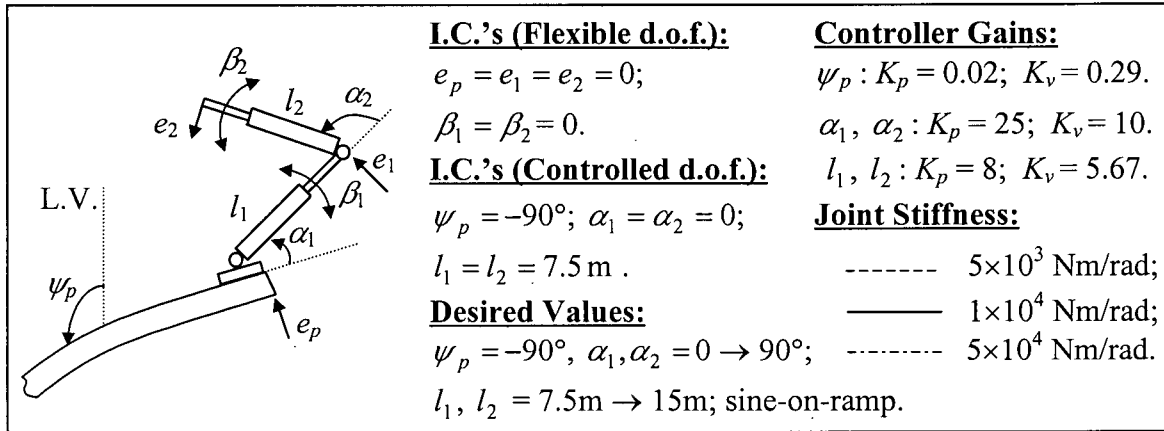


Figure 3-9 FLT/LQR controlled response as affected by the revolute joint stiffness during a manipulator maneuver: (c) flexible generalized coordinates.

3.3 Trajectory Tracking

Tracking of prescribed trajectories represents one of the important tasks a manipulator is called upon to perform. This section considers trajectories in the form of straight line and circle in the vertical x, y – plane using the FLT applied to the rigid degrees of freedom. Note, the system requires two coordinates to specify the manipulator's tip position. However, there are four actuators (T_1, F_1, T_2, F_2) in the form of two revolute (α_1, α_2) and two prismatic (l_1, l_2) joints. Thus there are two redundant coordinates. A trajectory involves both a path and the time evolution of the path. In the present study, trajectories follow sine-on-ramp profile as mentioned earlier (Figure 2-3). Three cases are considered:

- (i) Tracking of a 10 m long straight line perpendicular to the platform using revolute and prismatic joints of module two. Joints of module one are held fixed. The time allocated to complete the task is 120 s.
- (ii) Tracking of a 10 m long straight line along the platform, in 120 s, using revolute joints of modules one and two. Prismatic joints are locked in position.
- (iii) Tracking of a circle with 3 m radius in 200s using two revolute joints, i.e. prismatic joints are locked as in Case (ii) keeping the module lengths fixed.

Case (i): Straight Line Perpendicular to the Platform

The manipulator is located at the tip of the platform with modules initially aligned with the platform. The initial lengths of module one and module two are 7.5 m. The manipulator tip is commanded to move from the x, y coordinates (75m, 1.5m) to (75m, 11.5m) in 120 s. Desired time histories of α_2 and l_2 can be readily obtained from:

$$\alpha_2 = \tan^{-1}\left(\frac{y_d}{7.5}\right); \quad (3.20a)$$

$$l_2 = \sqrt{7.5^2 + y_d^2} \text{ m}; \quad (3.20b)$$

with

$$y_d = \frac{10}{120}\left(t - \frac{120}{2\pi} \sin\left(\frac{2\pi}{120}t\right)\right) \text{ m}.$$

The tracking performance and system response are presented in Figure 3-10. Initial configuration of the manipulator, its trajectory and tip errors are shown in Figure 3-10(a). Note, the peak deviation of the tip from the desired position is ≈ 4.5 mm in the x direction with a steady state oscillation amplitude, about the terminal point, of ≈ 1 mm. Thus, the maximum error in the x direction is less than 0.12% of the trajectory's length. The corresponding value in the y direction is ≈ 0.4 %. As can be expected, the maneuver has virtually no effect on the platform orientation and the peak torque required to maintain the local horizontal (unstable) position is only ≈ 80 Nm (Figure 3-10b). Demands on the revolute and prismatic joints are also rather small; only 5 Nm and 0.7 N, respectively. Response of the flexible degrees of freedom (Figure 3-10c) clearly shows that the effect of the module elasticity on the tip error (e_2) is negligible (≈ 0.26 mm maximum). The major contribution to the error arises from the joint flexibility ($\beta_{1,max} \approx 0.06^\circ$, $\beta_{2,max} \approx 0.03^\circ$).

Case (ii): Straight Line along the Platform

Here tracking of a horizontal straight line near the x -axis using the two revolute joints is considered. As before, the manipulator is initially aligned with the platform and the module lengths are held fixed at $l_1 = l_2 = 7.5$ m (Figure 3-11a). The task-time of 120 s corresponds to ≈ 0.02 orbit. The desired time history for the trajectory is given by:

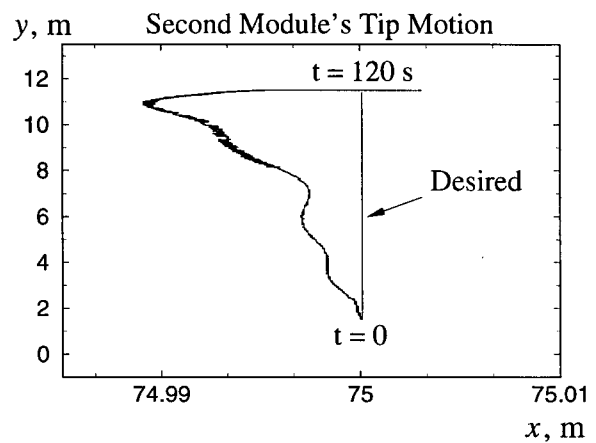
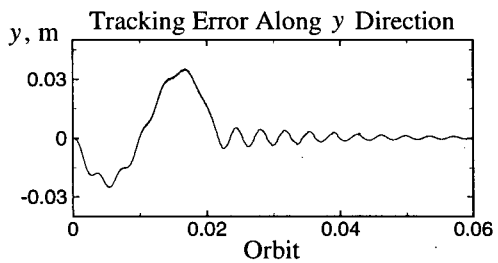
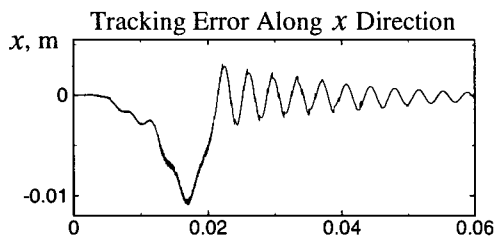
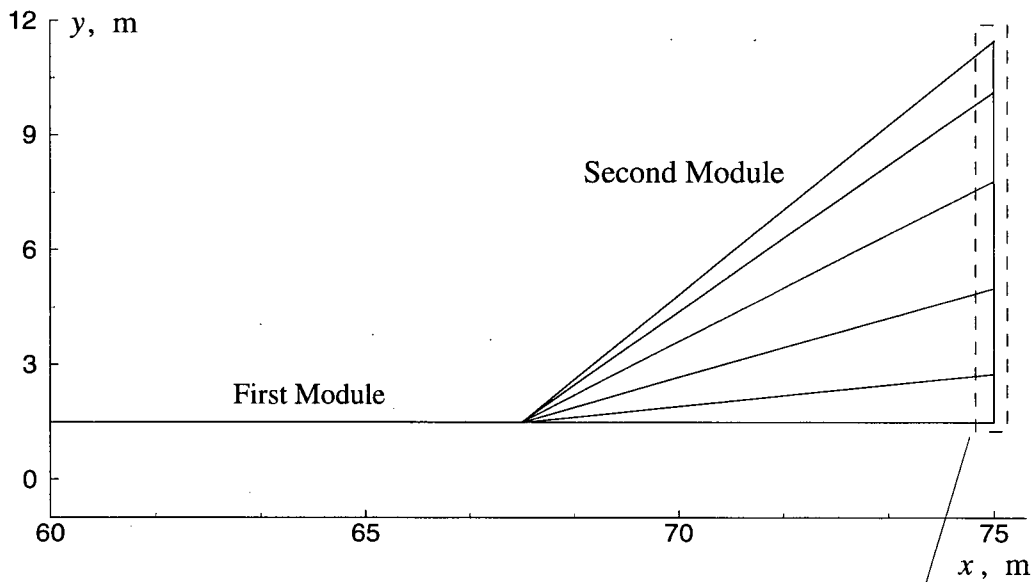
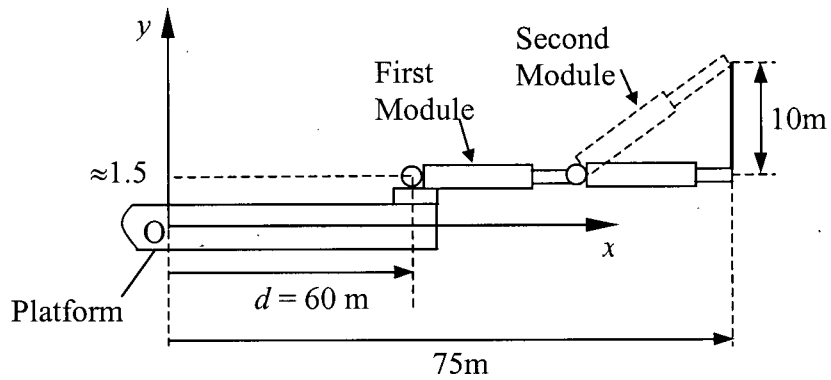


Figure 3-10 Tracking of a straight line using the second module and the FLT: (a) manipulator tip trajectory and errors.

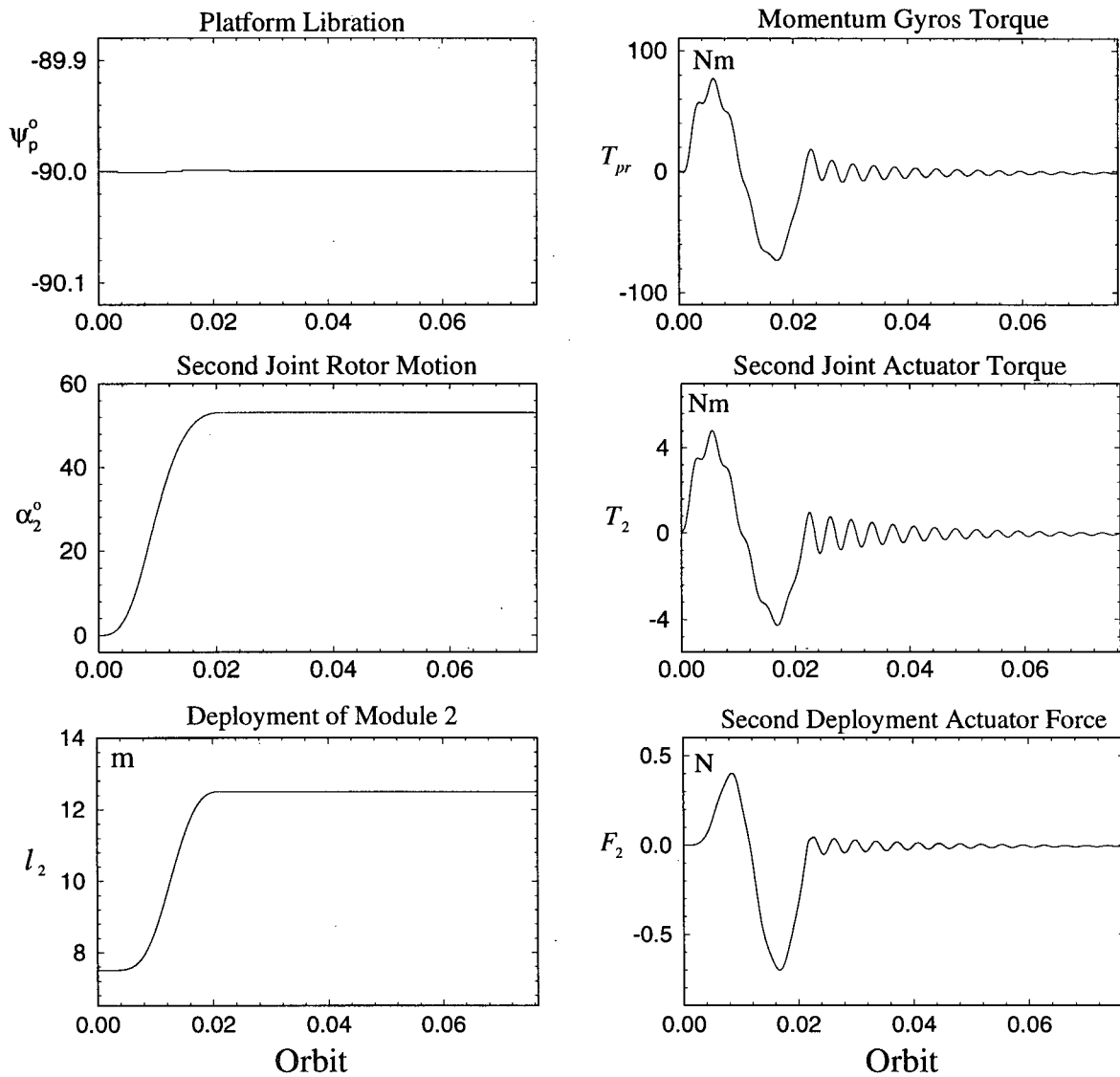
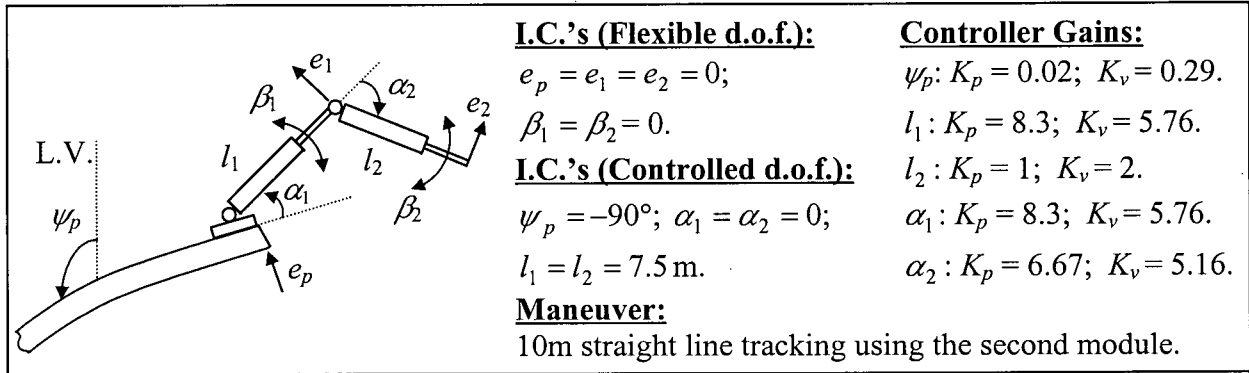


Figure 3-10 Tracking of a straight line using the second module and the FLT: (b) response of the platform and rigid degrees of freedom with control inputs.

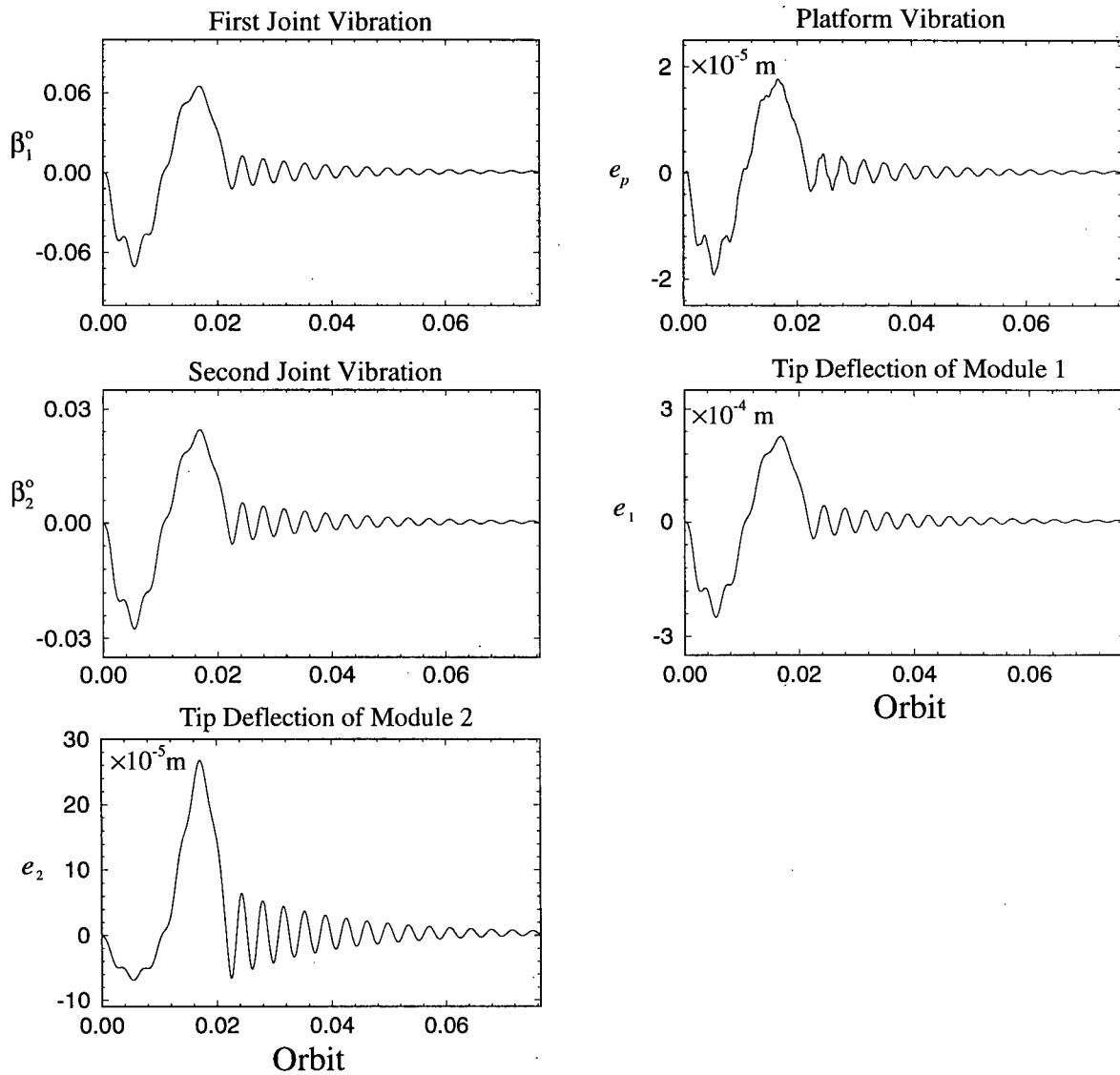
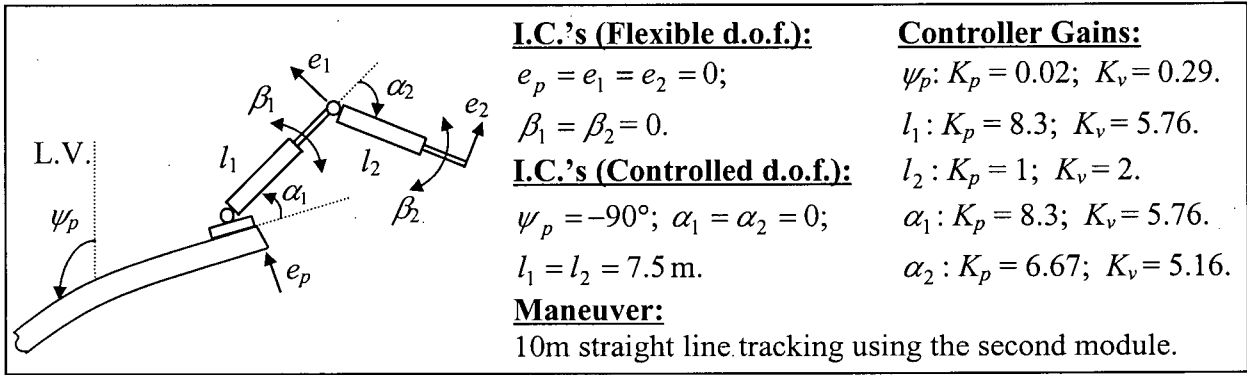


Figure 3-10 Tracking of a straight line using the second module and the FLT: (c) response of flexible degrees of freedom.

$$y_d = 1.5 \text{ m};$$

$$x_d = (10/120)(\tau - (120/2\pi)\sin[(2\pi/120)\tau]) \text{ m};$$

with the joint angles obtained using simple inverse kinematics:

$$\alpha_{1d} = \tan^{-1}\left(\frac{y_d}{x_d}\right) + \frac{1}{2} \cos^{-1}\left(\frac{l_1^2 + l_2^2 - (x_d^2 + y_d^2)}{2l_1l_2}\right) - \frac{\pi}{2}; \quad (3.21a)$$

$$\alpha_{2d} = \pi - \cos^{-1}\left(\frac{l_1^2 + l_2^2 - (x_d^2 + y_d^2)}{2l_1l_2}\right). \quad (3.21b)$$

Note, the initial manipulator configuration represents a kinematic singularity requiring $\dot{\alpha}_{1d}$, $\dot{\alpha}_{2d}$ to be ∞ . To overcome this situation, α_1 was given a small positive value (5°) at $t=0$. This also resulted in a small negative value (-10°) for α_2 . As the use of revolute joints leads to increased coupling effects, the error is anticipated to be higher. Figure 3-9(a) shows the maximum error of about 2.8 %.

Effect of the straight line tracking maneuver on the platform, though relatively higher than that in the previous case, still remains rather small (Figure 3-11b). With a peak demand of $\approx 330 \text{ Nm}$, the platform is able to maintain its equilibrium position along the local horizontal. Control demands at revolute joints also remain modest ($T_{1, \max} \approx 40 \text{ Nm}$, $T_{2, \max} \approx 10 \text{ Nm}$).

Flexible degrees of freedom exhibit trends (Figure 3-11c) which are similar to those observed before (Figure 3-10c), i.e. trajectory tracking error is primarily contributed by the flexibility of the joints. Note, the peak values of both β_1 and β_2 are now higher than before ($\beta_{1, \max} \approx 0.2^\circ$, $\beta_{2, \max} \approx 0.05^\circ$ as against $\beta_{1, \max} \approx 0.06^\circ$, $\beta_{2, \max} \approx 0.03^\circ$ for Case (i)). This reflects in a higher peak error. Contribution of modules' elasticity continues to remain small

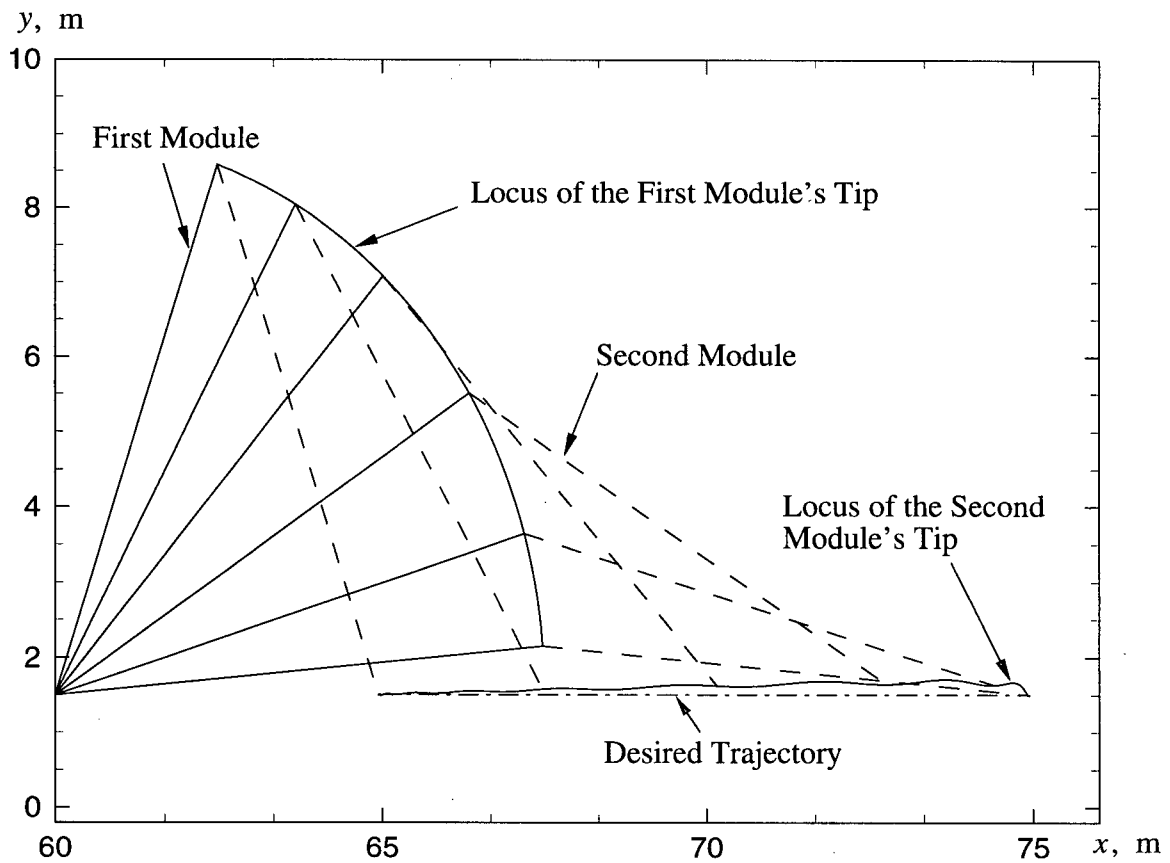
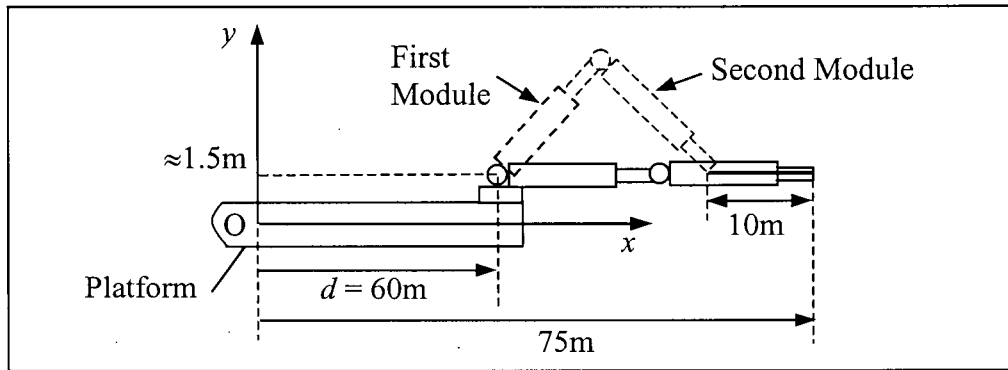


Figure 3-11 Tracking of a horizontal straight line with two revolute joints using the FLT: (a) initial configuration and the trajectory error.

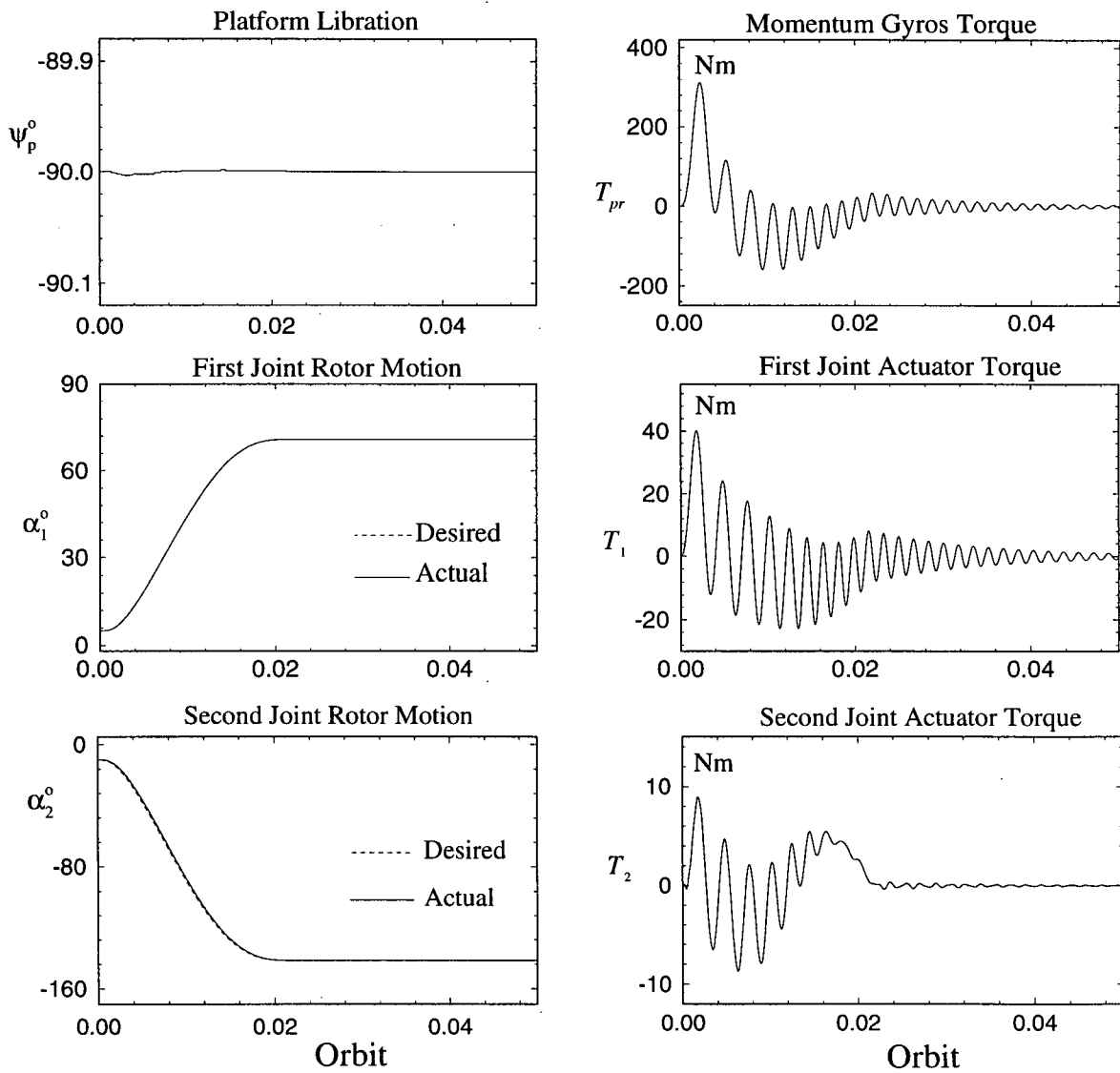
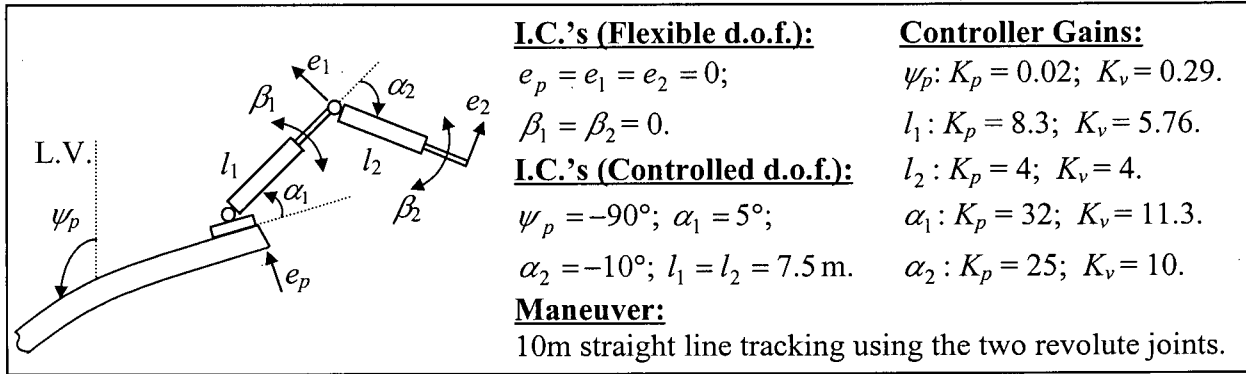


Figure 3-11 Tracking of a horizontal straight line with two revolute joints using the FLT: (b) response of rigid degrees of freedom and control inputs.

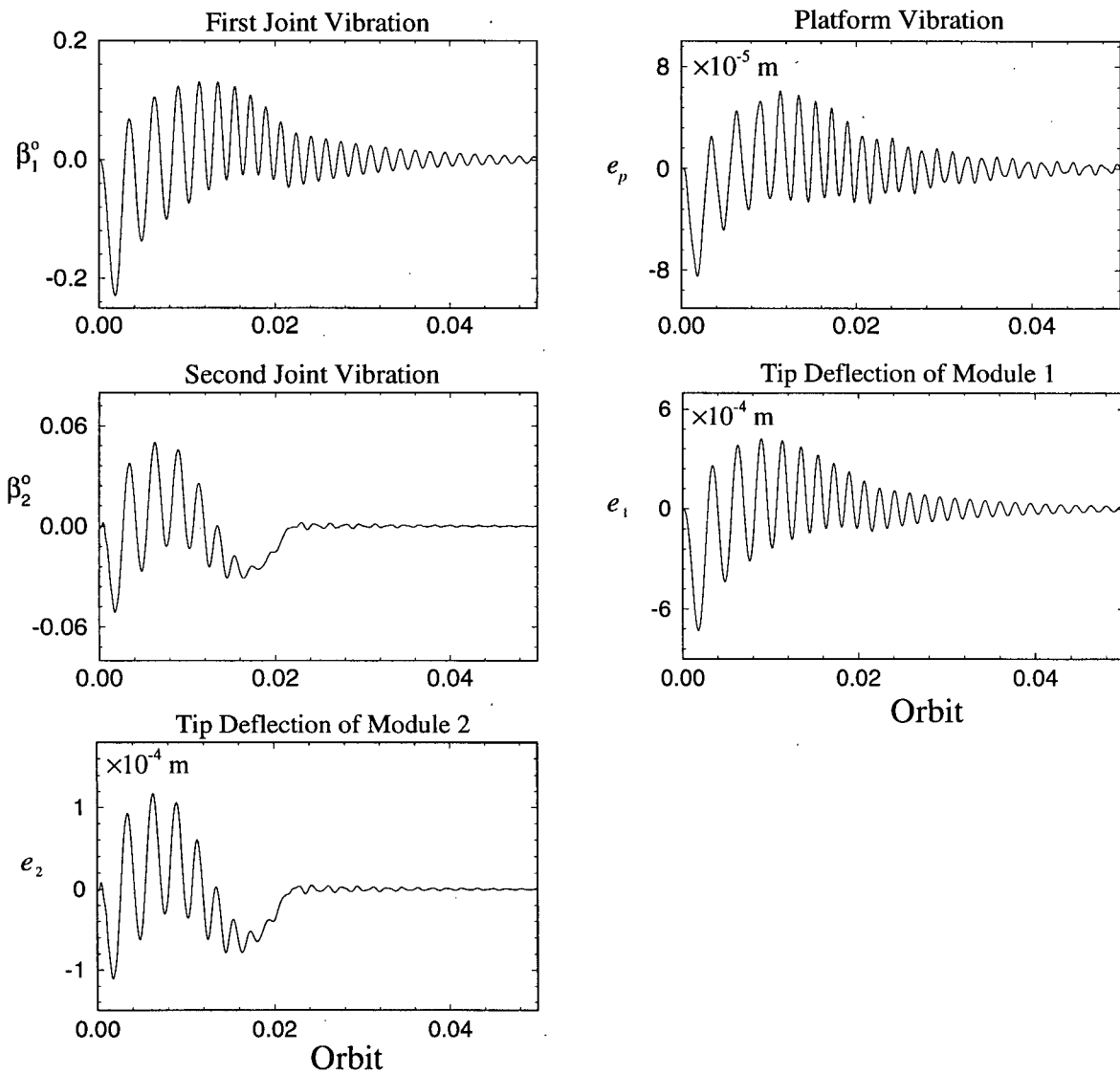
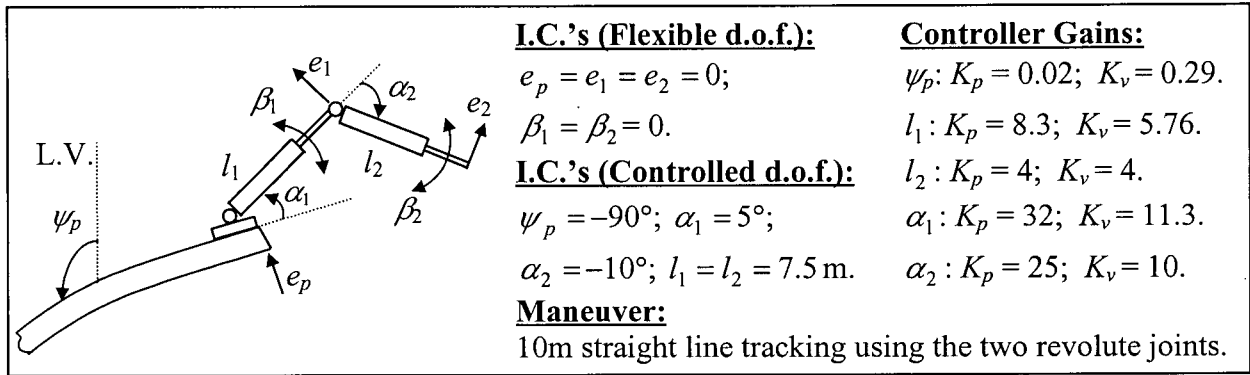


Figure 3-11 Tracking of a horizontal straight line with two revolute joints using the FLT: (c) response of flexible degrees of freedom.

(< 0.8 mm).

Case (iii): Circular Trajectory

Tracking of a circular trajectory, of radius 3 m and center located at $x = 64\text{m}$, $y = 8.5\text{m}$, using two revolute joints represents a relatively challenging task (Figure 3-12a). The module lengths are fixed at $l_1 = l_2 = 7.5\text{ m}$ and the base is located at $x = 6\text{ m}$, $y = 1.5\text{ m}$. The tracking period is 200 s. The trajectory can be represented as

$$(x - 64)^2 + (y - 8.5)^2 = 3^2, \quad (3.22)$$

or in terms of time of 200 s permitted to complete the trajectory:

$$x - 64 = 3 \cos(0.01\pi t) \text{ m}; \quad (3.23a)$$

$$y - 8.5 = 3 \sin(0.01\pi t) \text{ m}. \quad (3.23b)$$

It can be visualized as a point moving on a circle with a radius of 3 m and a period of 200s.

The point, and hence the tip of the manipulator, moves at a uniform speed of

$$V = \sqrt{\dot{x}^2 + \dot{y}^2} = 0.03\pi \text{ m/s}. \quad (3.24)$$

Figure 3-12(a) shows tracking of the circle (with reference to x' , y' coordinates) and the associated error. The period covered is the first 200 s, i.e. the time taken to complete the first circular trajectory. Note, in terms of the orbital period of 92.5 minutes, 0.01 orbit corresponds to 55.5 s. The error is rather large with a peak value of around 7 cm. However, the error diminishes significantly during the second period of 200 s to 400 s as shown in Figure 3-12(b). The maximum error is reduced to $\approx 7\text{mm}$! This can be explained quite readily by referring to the response plots in Figures 3-12(c) and 3-12(d).

At the outset it is apparent that compared to tracking of straight lines, the circle represents a large disturbance to the platform as well as the manipulator. Though within the

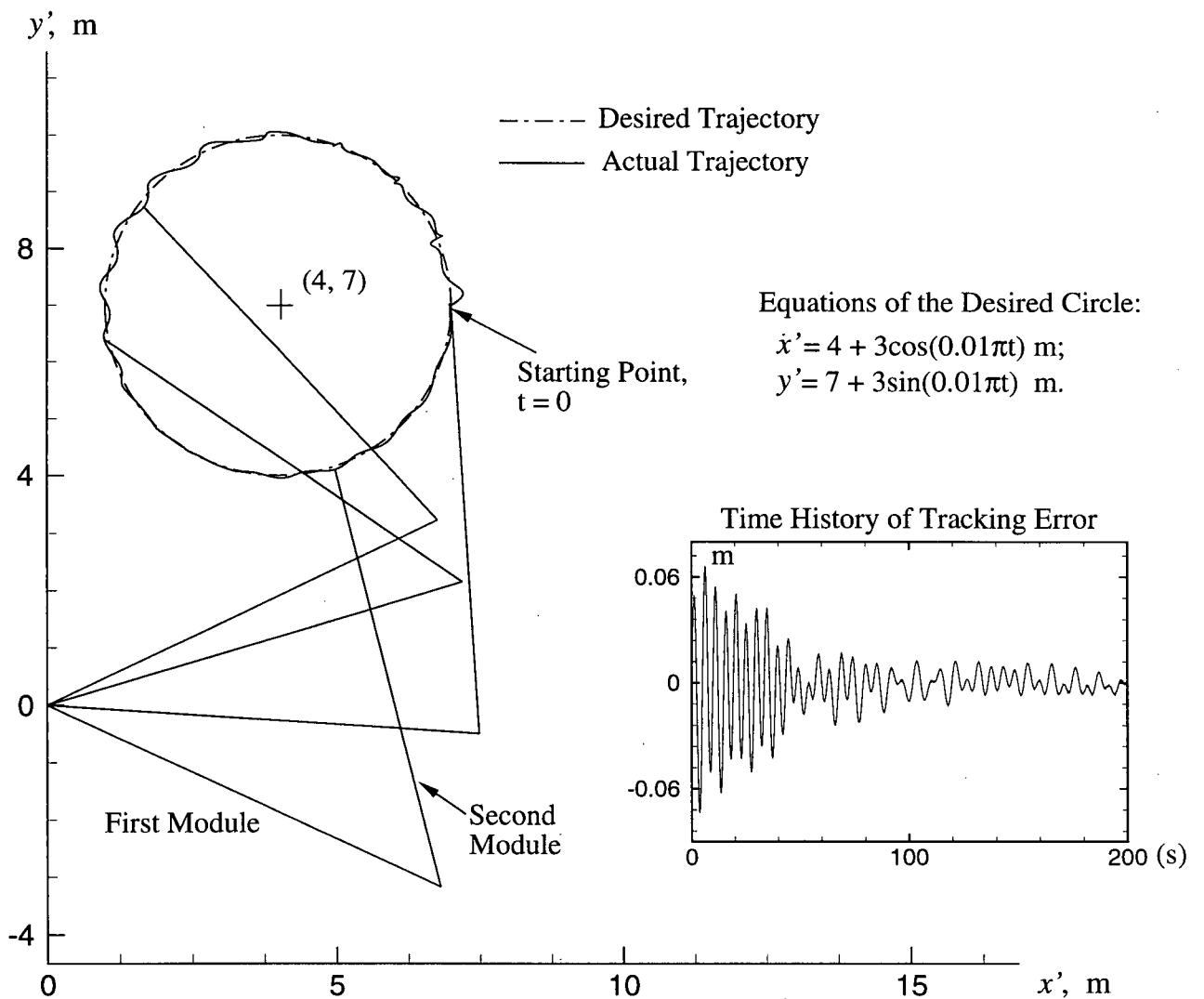
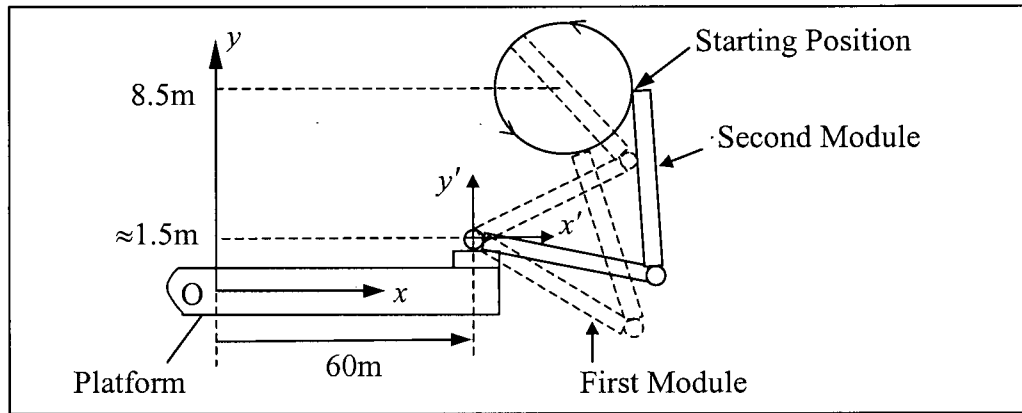


Figure 3-12 Tracking of a circle using the two revolute joints and the FLT for control: (a) manipulator tip trajectory and error during the period of 0-200 s.

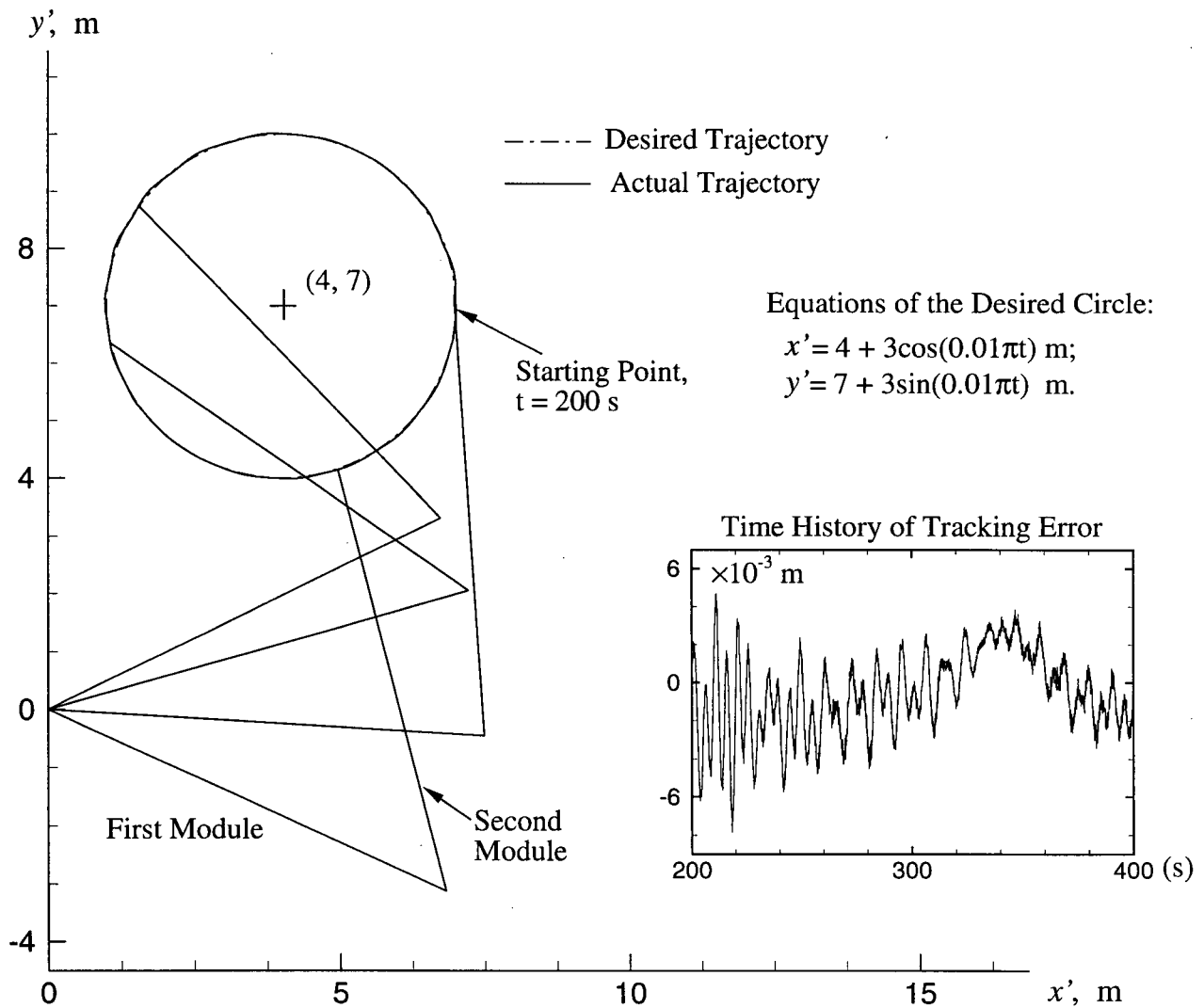
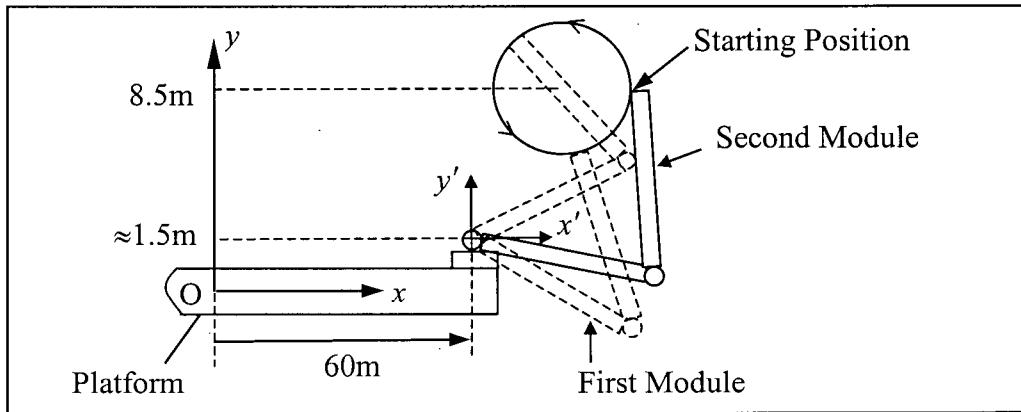


Figure 3-12 Tracking of a circle using the two revolute joints and the FLT for control: (b) manipulator tip trajectory and error during the period of 200-400 s.

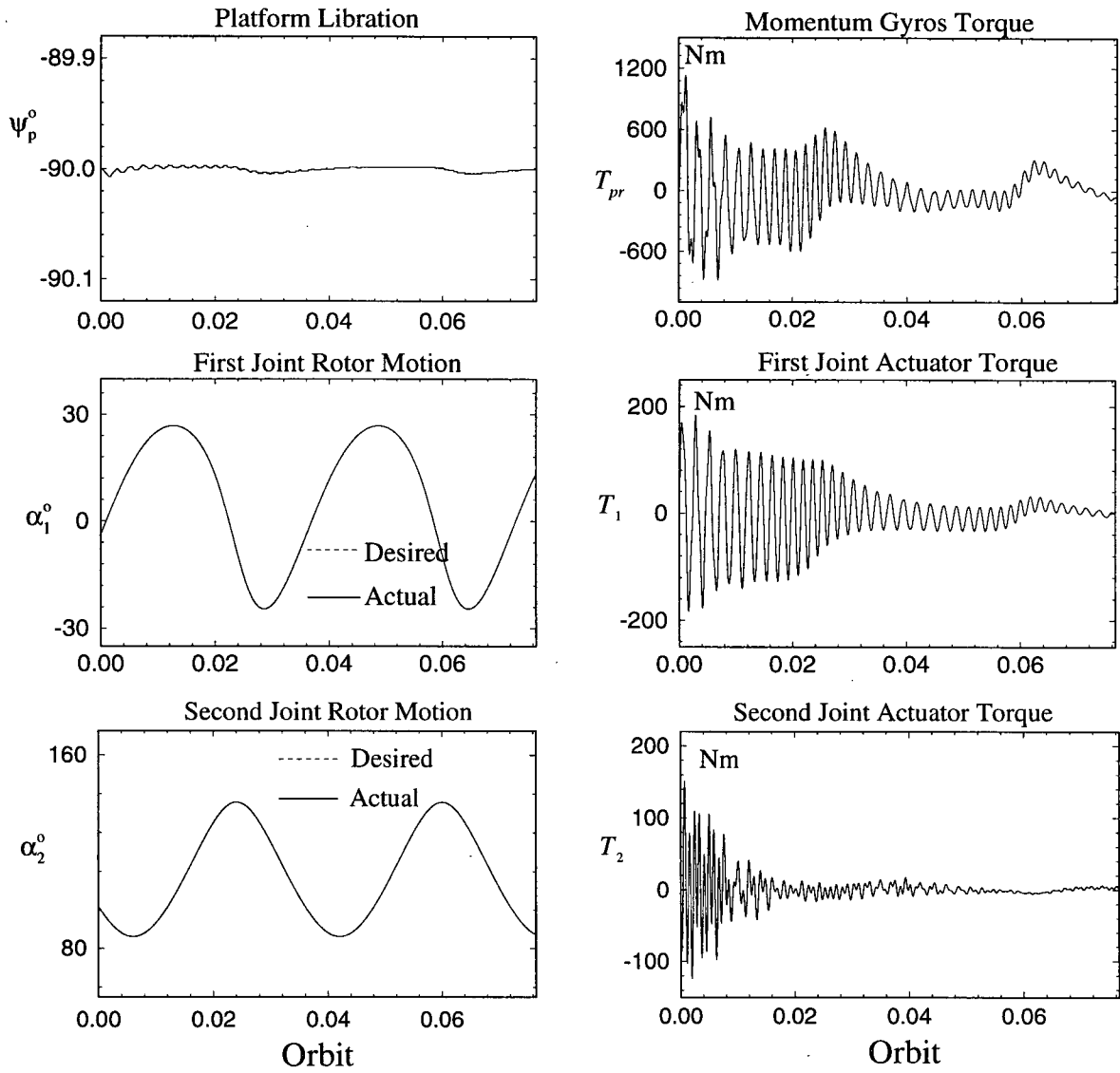
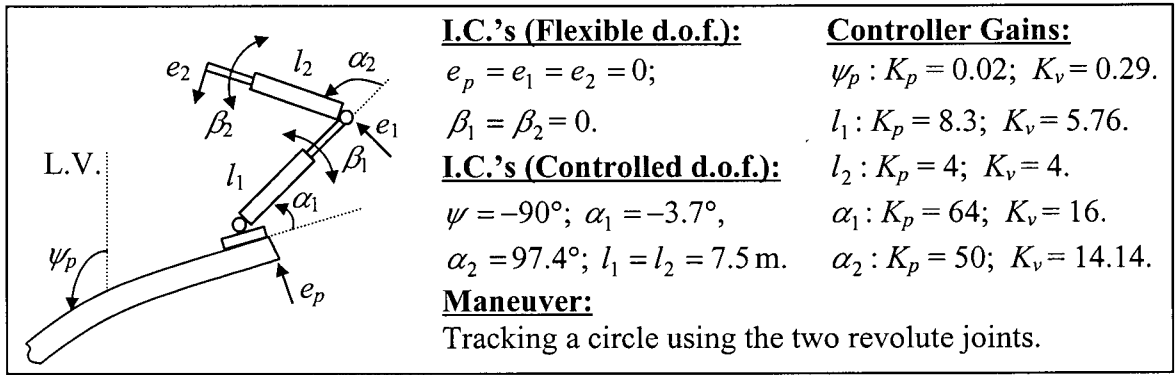


Figure 3-12 Tracking of a circle using the two revolute joints and the FLT for control: (c) response of rigid degrees of freedom and control inputs.

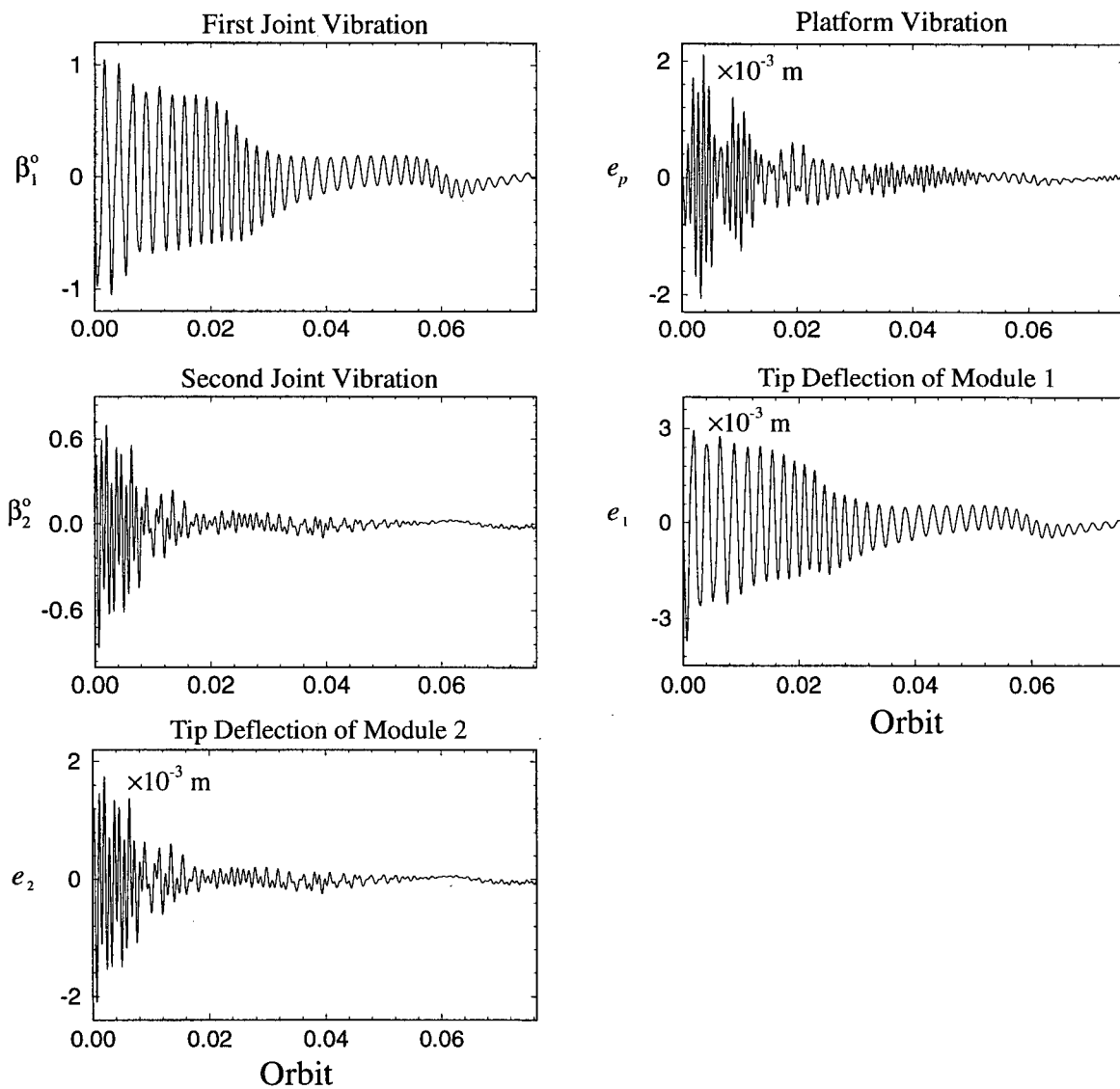
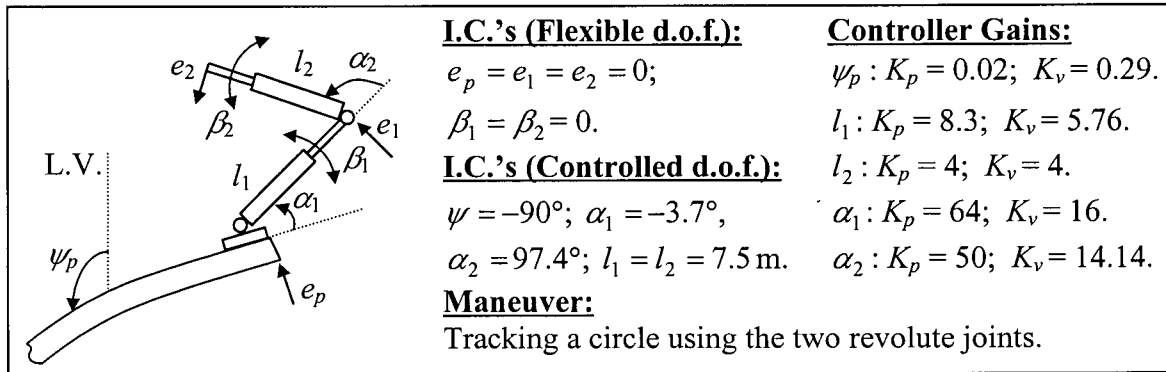


Figure 3-12 Tracking of a circle using the two revolute joints and the FLT for control: (d) response of flexible degrees of freedom.

permissible limit, the peak platform libration is $\approx 0.007^\circ$ with the CMG output of $\approx 1,100$ Nm. The revolute joints also demand higher torques with peak values reaching ≈ 200 Nm and ≈ 15 Nm for α_1 and α_2 , respectively (Figure 3-12c). The tip tracking errors are primarily contributed by joint and module flexibility effects. Both of them are relatively high during tracking of the first circle (i.e. time < 0.04 orbit) with peak values reaching:

$$\begin{aligned} e_{1,max} &\approx 2 \text{ mm}; & e_{2,max} &\approx 3 \text{ mm}; \\ \beta_{1,max} &\approx 1^\circ; & \beta_{2,max} &\approx 0.85^\circ. \end{aligned}$$

These lead to the high value of error observed during tracking of the first circle. However, during the period of 200-400 s (≈ 0.04 to 0.08 orbit) they reduce significantly resulting in better tracking performance. Results suggest that the tracking error would progressively reduce with the passage of time and should become negligible for $t > 0.06$ orbit. Note, the flexible degrees of freedom are not actively controlled by the FLT. They are regulated only indirectly through coupling. In practice, the presence of structural damping would help reduce the error. Of course, one can improve the tracking performance by actively controlling the flexibility degrees of freedom at a cost of increased demand on power and the controller complexity.

4. GROUND BASED EXPERIMENTS

Experiments in space are very costly and time consuming. They can become prohibitive and infeasible in many cases. That is one of the main reasons for the necessity of lengthy mathematical modeling and investigation through computer simulation. As an alternative to space-based experimentation, one often turns to prototypes located on Earth. Of course, for practical reasons, no ground-based setup can simulate the space environment exactly. However, a carefully designed ground-based facility can be used to advantage in assessing the performance trends. Furthermore, once the ground-based computer simulations are verified through prototype experiments, it is possible to justify, by induction, their validity in space where the forces are significantly small. In fact, since the beginning of the space-age in 1957, around 20,000 spacecraft have been launched. Every one of them was primarily designed through extensive numerical simulations, complemented by a few simplified ground-based experiments. The objective here is to evaluate real-time controlled performance of the variable geometry manipulator using the ground-based prototype facility designed by Chu [8].

4.1 System Description

Figure 4-1 shows the manipulator system that has been developed and located in the Space Dynamics and Control Laboratory of the Department of Mechanical Engineering, University of British Columbia. The prototype manipulator, employed in the experimental study, consists of a fixed base that supports two modules of the robot connected in series. Each module has two links: one able to slew, and the other free to deploy and retract. The manipulator workspace has the shape of a human heart, extending 2 m from top to bottom

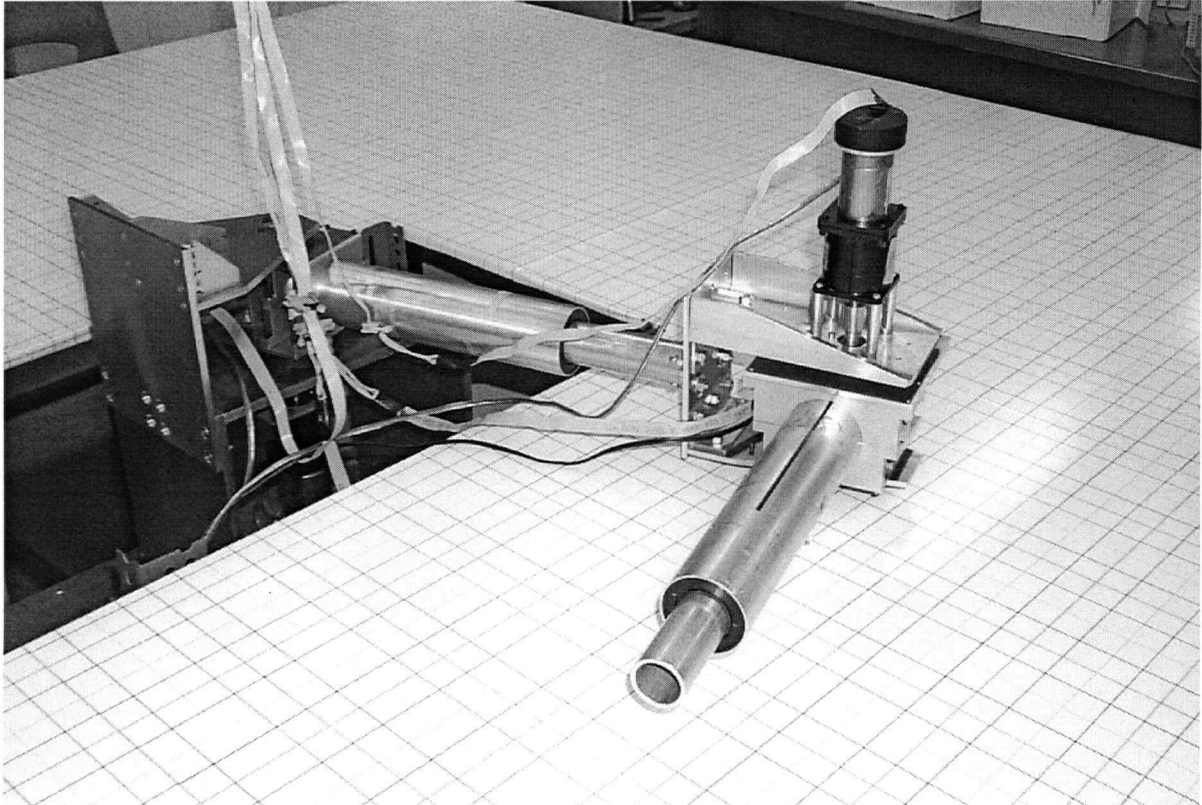


Figure 4-1 The prototype manipulator system.

and 2.5 m across. Rotational motion is made possible through the use of revolute joints actuated by DC servo-motors. The deployment and retraction are carried out with prismatic joints consisting of lead-screw and roller-nut assemblies, each of which transforms the rotational motion of a servo-motor into the translational motion of a deployable link (Figure 4-2). Actuator motors integrated with optical-encoder motion sensors are interfaced with a Pentium 200 MHz MMX PC through a three-axis multi-function input/output motion control card. The manipulator is essentially rigid.

4.1.1 Manipulator base

The fixed base supports the manipulator system. The first module is attached to the pivot plate, which is threaded to the pivot shaft. An 80 mm thrust bearing located between the pivot plate and the top plate of the base carries the weight of the manipulator. This bearing also provides the slewing freedom about the rotational axis. A second bearing is located under the top plate of the base and is held in place with a lock nut. A flexible coupling connects the pivot shaft to a gear head with a speed reduction ratio 20:1, which amplifies the torque that is delivered by the DC servo-motor. The rotational motion of the base motor is transmitted in series, through the gear box, the flexible coupling, the pivot shaft, and finally through the pivot plate holding the slew end of the first module of the manipulator system (Figure 4-3).

4.1.2 Manipulator modules

Both modules of the prototype manipulator system are identical, each having one revolute joint and one prismatic joint. The first revolute joint is located at the base, while the

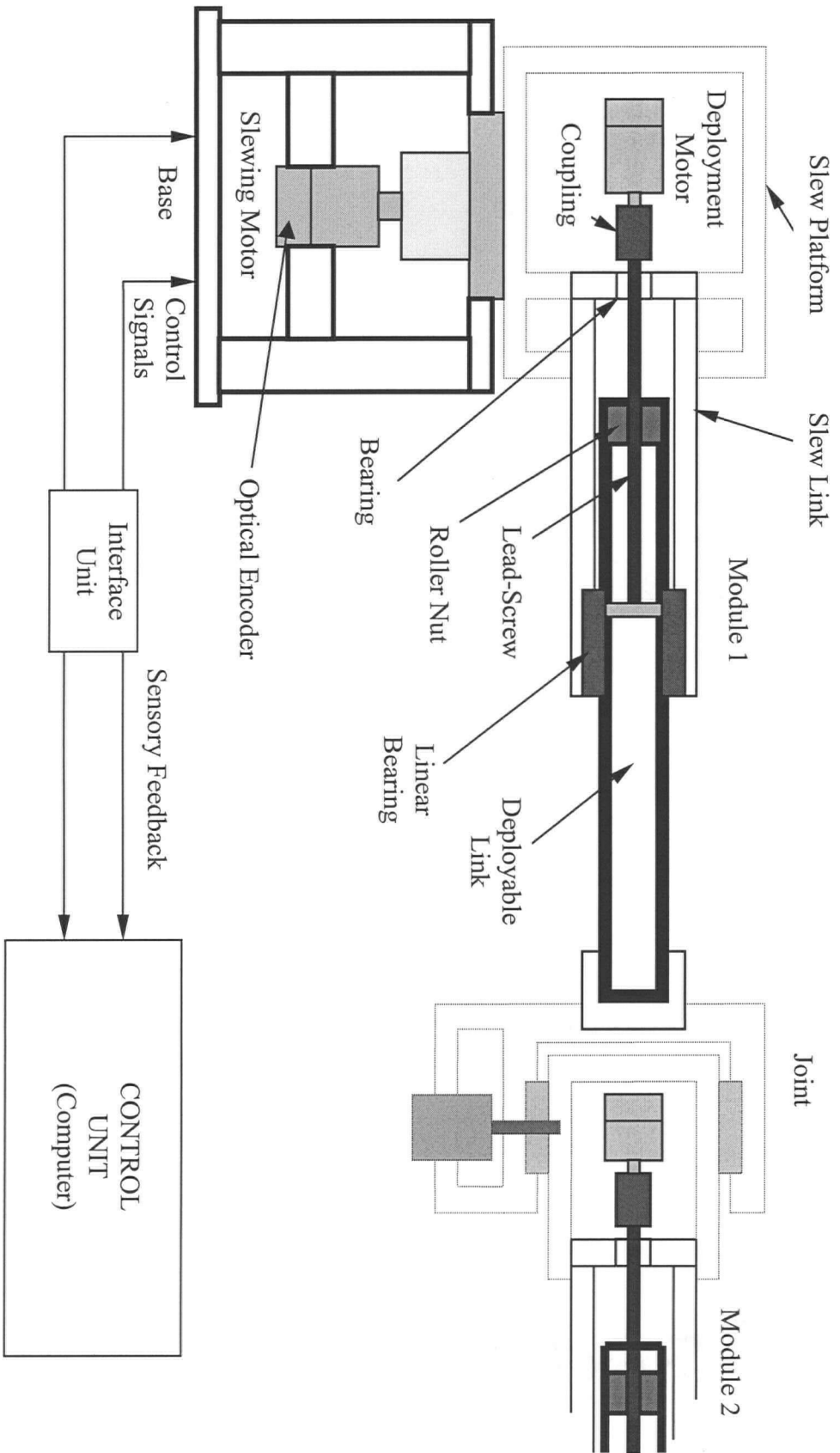


Figure 4-2 Main components of the two-module manipulator system.

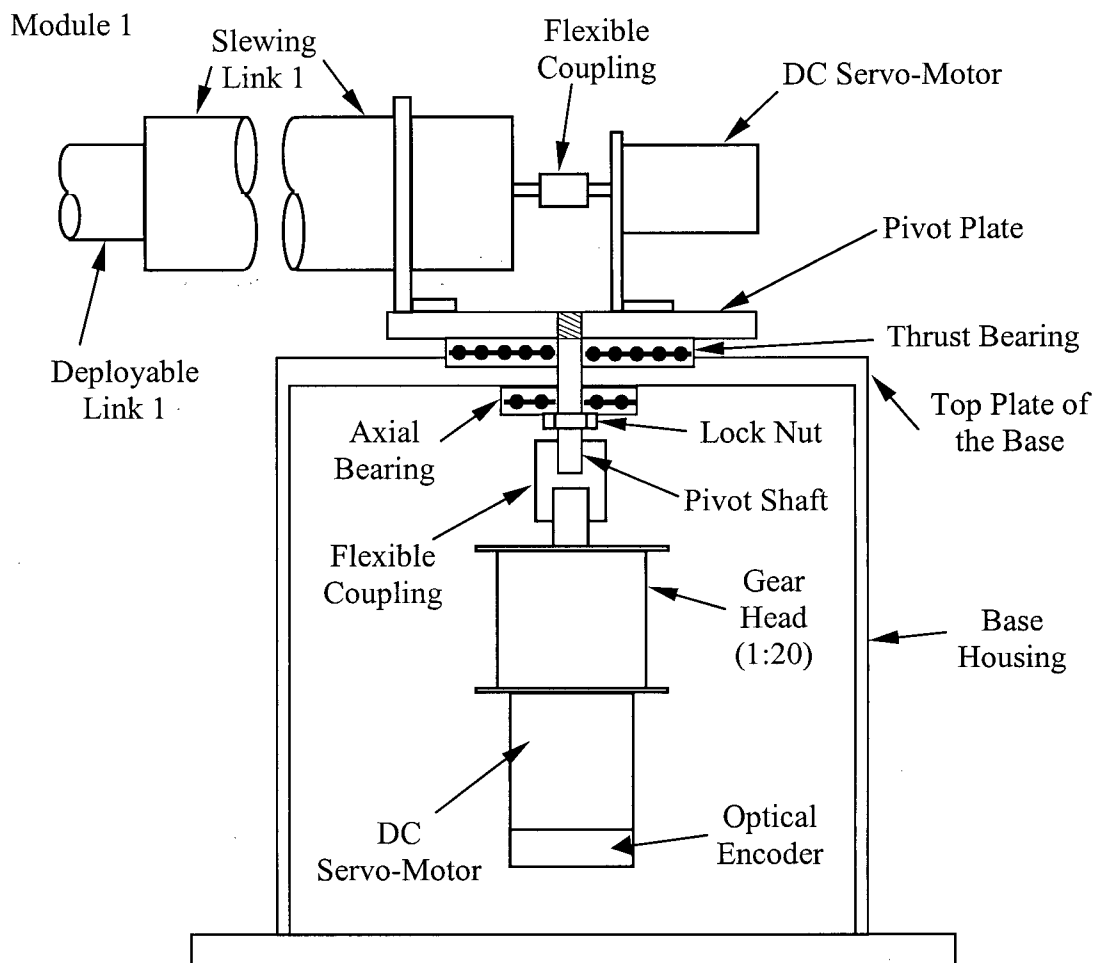


Figure 4-3 Main components of the manipulator base assembly.

second one is at the end of the first module, i.e. at the elbow joint. The deployment is realized with the transformation of the rotational motion of the motor that drives the lead screw into translational motion of a roller nut that is fixed to the deployable link (Figure 4-4). The pitch of the lead screw of the first module is 2.5 mm (i.e. the deployable link moves 2.5 mm per revolution) while it is 1 mm for the second module.

4.1.3 Elbow joint

The joint connects the deployable end of module 1 to the slewing link of module 2. The structural connection consists of two pivot plates bolted onto the deployable end of module 1. These plates support the slewing motor and the gear head. The elbow joint is supported on a flat structure within the workspace, through a spherical joint. The mechanism that provides the rotational motion, at the elbow joint, is identical to the one located at the base (Figure 4-5).

4.2 Hardware and Software Control Interface

The hardware of one closed control loop of the prototype manipulator mainly consists of an IBM compatible host computer, an MFIO 3A motion control input/output interface, a power amplifier, and DC servo-motors with built-in optical encoders (Figure 4-6). The control structure for each degree of freedom is identical.

Computer System

The computer used for control purposes is a Pentium 200 MHz MMX IBM compatible, with QNX as the operating system. Real-time application of a digital control system depends on an operating system to handle multiple events within specified time

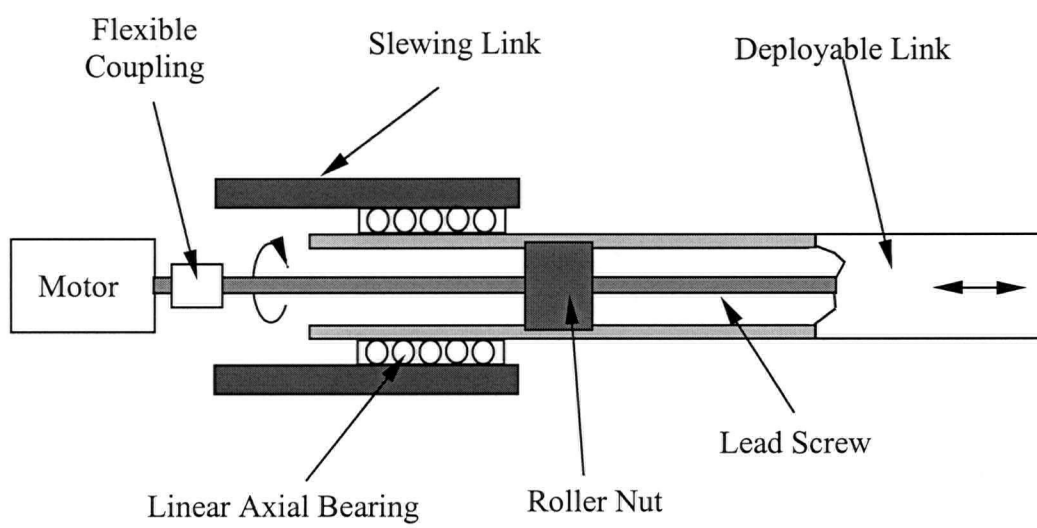


Figure 4-4 Prismatic joint mechanism which provides the deployment and retrieval capability.

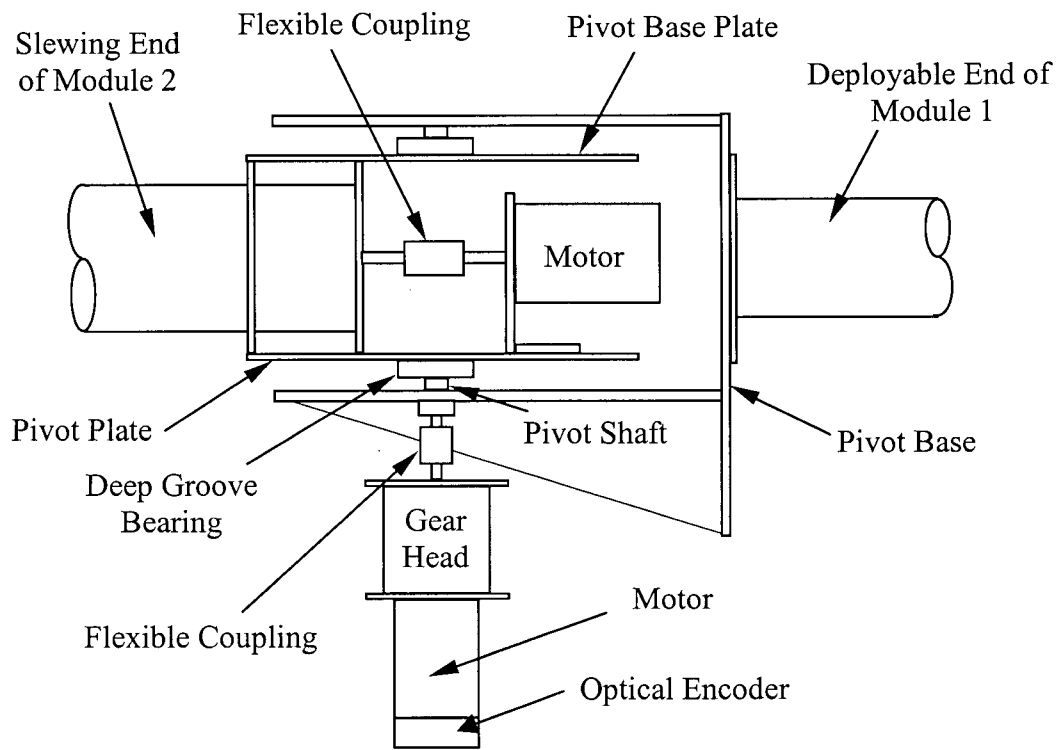


Figure 4-5 Main components of the elbow joint assembly.

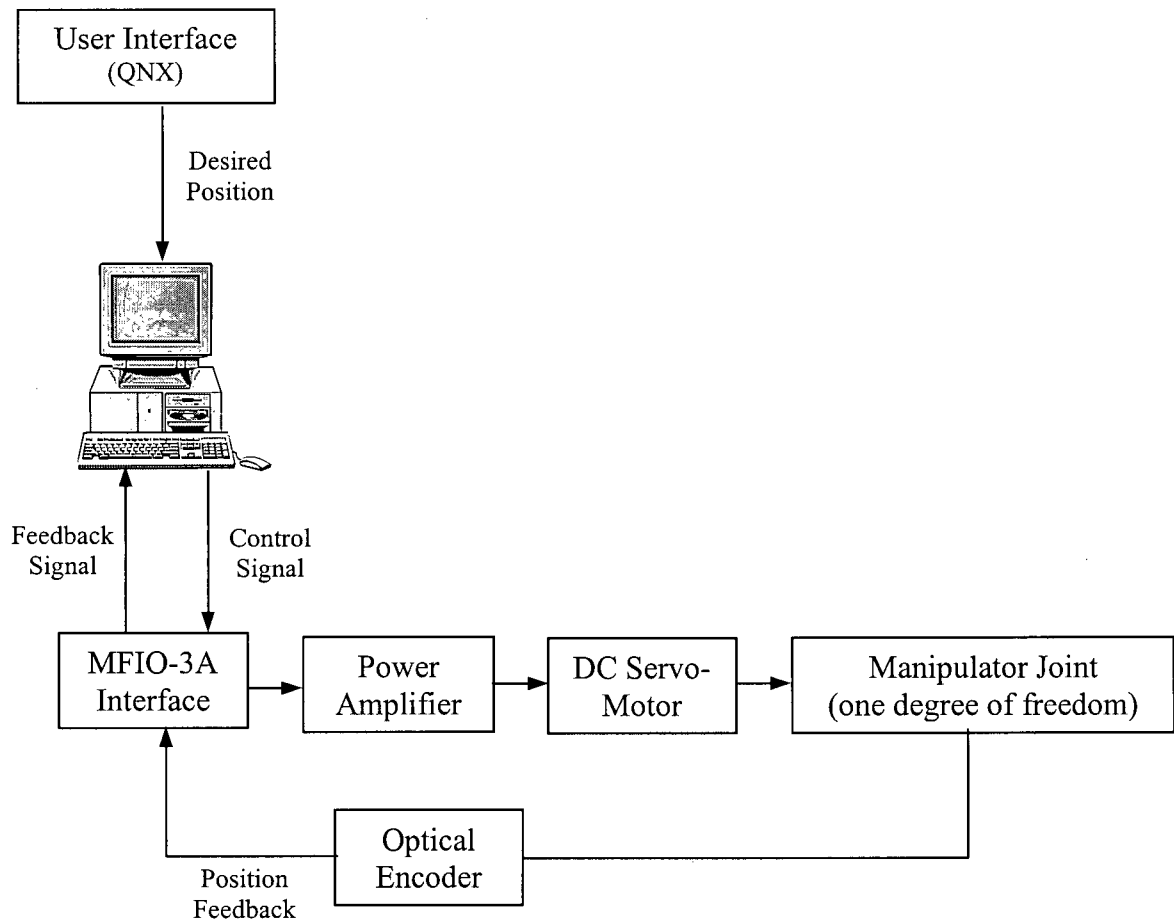


Figure 4-6 Open architecture of the manipulator control system for a single joint.

constraints. The more responsive the operating system, the more 'room' a real-time application has for maneuvering to meet its deadlines. The QNX operating system provides multitasking, priority-driven preemptive scheduling, and fast context switching.

Motion control interface card

An MFIO-3A high-speed interface card for PCs is used for multi-axis, coordinated motion control. It is a multifunction input/output (I/O) card for motion control applications using a PC. It has three-channel 16-bit digital-to-analog converter (D/A); three quadrature encoder inputs; 24 bits of programmable digital I/O, synchronized data reading and writing; a programmable interval timer; and a watchdog timer. The card has a SYNC signal, which allows for the synchronisation of data acquisition and analog output. The data from the D/A converters are latched into registers through the SYNC signal. The D/A channels have 16-bit of resolution. The encoder signals are digitally filtered for noise suppression. The programmable interval timer can generate timed intervals from 0.25 μ s to 515 seconds. The feedback controller runs as a task in the QNX operating system. The card may be programmed either by accessing the hardware at the register level in C or through the use of Precision MicroDynamics' C subroutine library. The source code is compiled with the Watcom-C compiler for QNX. The C-library provides access to the MFIO-3A hardware with routines to initialize the board; set up the Programmable Interval Timer (PIT), watchdog timer, and SYNC signal; start the PIT and watchdog timer; set up the interrupts; read and write the digital I/O; read and write the encoders; and write the digital-to-analog converters.

Linear power amplifier

Linear amplifiers are used with the joint motors of the prototype manipulator. Their function is to transform the pulse train, i.e. the ± 10 V signal from the controller, into current to drive the joint motors. The amplifier gain is set so that a 10V command generates the maximum drive current.

DC Servo-motors

Slewing motors of the manipulator are Pittman 14202 (109 oz-in peak torque) and 9413 (16 oz-in peak torque) for modules 1 and 2, respectively. A NEMA 23-20 reduction gear head of ratio 1:20 is used. The gear head reduces the speed while increasing the output torque of the motor by a factor of twenty. The deployment motors are Pittman 9414 (24 oz-in peak torque). The motors operate through the DC current supplied by the power amplifier, in response to a controller signal.

Optical encoders

The position of each motor is sensed through the use of the optical encoder attached to the motor shaft. The encoders have the offset track configuration (two tracks with their windows having an offset of $1/4$ pitch with respect to each other). An encoder disk has two identical tracks, each having 1000 windows. A third track with a lone window generates a reference pulse for every revolution [53]. The physical resolution of the encoders is 0.09° . The signal from the encoder is monitored at every sampling interval by the controller whose objective is to correct any deviation of the actual joint position from the desired one.

4.3 Digital Control of the Ground-Based Manipulator

Chu [8] has carried out extensive numerical simulation study aimed at dynamics of the ground-based manipulator model. He has also reported a PID control of the system. Objective here is the real-time implementation of the control algorithms, developed earlier, on the ground-based system.

From the governing equations of motion, it follows that the manipulator, as a control plant, is nonlinear, non-autonomous and coupled. That makes the Feedback Linearization Technique (FLT), sometime called the computed torque method [53], a reasonable choice as a control procedure for this manipulator. A typical Proportional-Integral-Derivative (PID) controller is also implemented for the purpose of comparison with the FLT.

Robot control schemes often involve a great deal of computation for the evaluation of nonlinear terms. Therefore, they are implemented as digital control laws on digital signal processors (DSPs). As obtained before for the FLT in the continuous time domain, the control input can be written as (Eq. 3.3)

$$\mathbf{Q}_r = \widehat{\mathbf{M}} [(\ddot{\mathbf{q}}_r)_d - \mathbf{u}] + \widehat{\mathbf{F}},$$

or in the general form

$$\tau(t) = \mathbf{M}(\mathbf{q})[\ddot{\mathbf{q}}_d - \mathbf{u}] + \mathbf{F}(\dot{\mathbf{q}}, \mathbf{q}). \quad (4.1)$$

The objective here is to discretize the above relation for the digital implementation.

One approach to this end is shown in Figure 4-7. $\mathbf{q}(t)$ and $\dot{\mathbf{q}}(t)$ are sampled to define

$$\begin{aligned} \mathbf{q}_k &= \mathbf{q}(kT), \\ \dot{\mathbf{q}}_k &= \dot{\mathbf{q}}(kT), \end{aligned} \quad (4.2)$$

with T as the sample period. Typically, a sample period in robotic applications can vary from about 1 to 20 ms. A zero-order hold is used to reconstruct the continuous time control input

$\tau(t)$, needed for the actuators, from the samples τ_k . The FLT digital control law amounts to selecting

$$\hat{M} = M(q(kT)), \quad \hat{F} = F(q(kT), \dot{q}(kT)), \quad (4.3)$$

and a digital PD outer loop control signal u_k where

$$u_k = -K_v \dot{e}_k - K_p e_k.$$

The robot arm digital control input can now be written as

$$\tau_k = \hat{M}(q_k)(\ddot{q}_{kd} + K_v \dot{e}_k + K_p e_k) + \hat{F}(q_k, \dot{q}_k), \quad (4.4)$$

where the tracking error is $e(t) = q_d(t) - q(t)$ with subscript 'd' representing, as before, the desired trajectory.

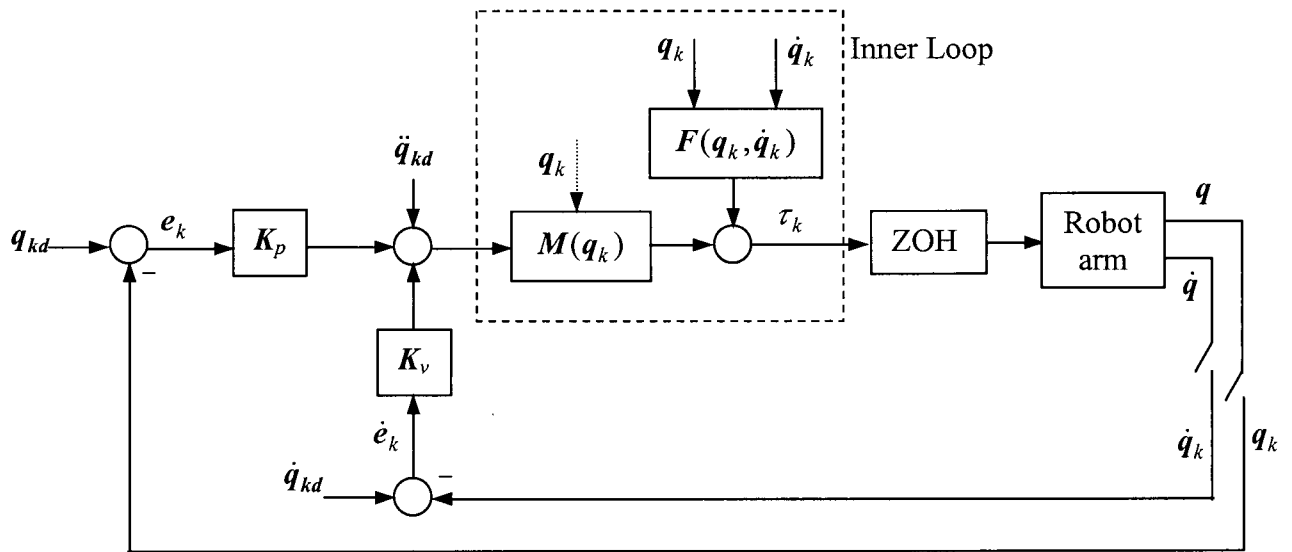


Figure 4-7 Digital robot control scheme.

Depending on the manipulator configuration, one may use different sampling rates for q_k and \dot{q}_k as against that for \hat{M} and \hat{F} , e.g. the inner nonlinear loop can be sampled more slowly than the outer linear feedback loop.

4.3.1 Discretization of the inner nonlinear loop

There is no exact way to discretize the nonlinear dynamics. Given a nonlinear state-space system

$$\dot{x} = f(x, u),$$

Euler's approximation yields

$$x_{k+1} = x_k + Tf(x_k, u_k).$$

One relies on discretizing the robot arm dynamics in such a way that energy and momentum are conserved at each sampling instant [55]. Unfortunately, this results in extremely complicated discrete dynamical equations, even for simple robot arms. Thus it is difficult to derive guaranteed digital control laws.

Here, only approximations given by Eq. (4.3), which appear in the inner nonlinear loop, are considered.

4.3.2 Joint velocity estimate from position measurements

For a continuous-time robot controller, it is assumed that both the joint position and velocity are available exactly. In fact, it is usual to measure joint position using an optical encoder, and then estimate joint velocity from these position measurements. Simply computing the joint velocity using the Euler approximation

$$\dot{q}_k = (q_k - q_{k-1})/T, \quad (4.5)$$

is virtually doomed to failure, since this high-pass filter amplifies the encoder measurement noise.

Let the joint velocity estimates be v_k . Then a filtered derivative can be used to compute v_k from q_k using

$$\mathbf{v}_k = \sigma \mathbf{v}_{k-1} + (\mathbf{q}_k - \mathbf{q}_{k-1})/T, \quad (4.6)$$

where σ is the design parameter, ideally equal to zero. Equation (4.6) corresponds to a pole at $z = 1$ with faster response, but with some filtering to reject unwanted sensor noise. It should be noted that velocity estimates are not only used in the outer linear loop for computing $\dot{\mathbf{e}}_k$, but also to evaluate the inner nonlinear term $\hat{\mathbf{F}}(\mathbf{q}_k, \dot{\mathbf{q}}_k)$ in Eq. (4.4).

4.3.3 Discretization of outer PD/PID control loop

A PID controller represents the outer feedback loop. From this continuous-time PID controller, a digital PID controller for the outer loop may be designed as explained by Lewis [56].

A continuous PID controller that only uses joint position measurements $\mathbf{q}(t)$ is given by:

$$u = -K^c(s)e;$$

$$K^c(s) = k \left[1 + \frac{1}{T_I s} + \frac{T_D s}{1 + T_D s/N} \right]; \quad (4.7)$$

where k is the proportional gain, T_I is the integration time-constant or ‘reset’ time, and T_D is the derivative time-constant. Rather than employing pure differentiation (Eq. 4.5), a ‘filtered derivative’ is used which has a pole far left in the s -plane at $s = -N/T_D$. The value for N is often in the range 3 to 10; it is usually a fixed number. Of course, the PD controller is a special case of the PID procedure.

A common approximate discretization technique for converting the continuous-time controller $K^c(s)$ to the digital controller $K(z)$ is the Bi-Linear Transform (BLT) where:

$$K(z) = K^c(s'); \quad s' = \frac{2}{T} \frac{z-1}{z+1}.$$

This corresponds to approximating integration by the trapezoidal rule. Under this mapping, stable continuous systems with poles as s are mapped into stable discrete systems with poles at

$$z = \frac{1 + sT/2}{1 - sT/2}. \quad (4.8)$$

The finite zeros also map according to this transformation. However, the zeros at infinity in the s -plane map into zeros at $z = -1$.

Using the BLT to discretize Eq. (4.7) yields

$$K(z) = k \left[1 + \frac{T}{T_{Id}} \frac{z+1}{z-1} + \frac{T_{Dd}}{T} \frac{z-1}{z-\sigma} \right], \quad (4.9)$$

with the discrete integral and derivative time constants:

$$T_{Id} = 2T_i; \quad (4.10)$$

$$T_{Dd} = \frac{NT}{1 + NT/2T_D}; \quad (4.11)$$

and the derivative-filtering pole at

$$\sigma = \frac{1 - NT/2T_D}{1 + NT/2T_D}.$$

It is easy to implement this digital outer-loop filter in terms of difference equations on a DSP. First, one writes $K(z)$ in terms of z^{-1} , which is the unit delay in the time-domain (i.e. a delay of T seconds), as

$$K(z^{-1}) = k \left[1 + \frac{T}{T_{Id}} \frac{1+z^{-1}}{1-z^{-1}} + \frac{T_{Dd}}{T} \frac{1+z^{-1}}{1-\sigma z^{-1}} \right]. \quad (4.12)$$

Now let the control input u_k be related to the tracking error as

$$u_k = K(z^{-1})e_k. \quad (4.13)$$

Then u_k may be computed from past and present values of e_k using auxiliary variables as follows:

$$v_k^I = v_{k-1}^I + (T/T_{Id})(e_k + e_{k-1}); \quad (4.14)$$

$$v_k^D = v_{k-1}^D + (T_{Dd}/T)(e_k - e_{k-1}); \quad (4.15)$$

$$u_k = -k(e_k + v_k^I + v_k^D). \quad (4.16)$$

The variables v_k^I and v_k^D represent the integral and derivative portions of the digital PID controller, respectively. These difference equations are easily implemented through an appropriate software.

4.4 Controller Implementation

4.4.1 Dynamical equations for the ground-based Manipulator

Equation governing dynamics of the ground-based prototype manipulator can be obtained quite readily by eliminating the orbital motion, gravity gradient, and the flexible degrees of freedom from the space-based formulation for the system [12]. As the FLT is a model-based controller, it is rather computationally intensive. During experiments with the prototype, the inner module (module 1) was held fixed (Figure 4-8). The corresponding governing equations are:

$$m_{d2}\ddot{l}_2 - m_{d2}\left(l_2 - \frac{l_{d2}}{2}\right)(\dot{\alpha}_2)^2 = F_2;$$

$$\underbrace{\left[I_{S2} + I_{d2} + m_{S2}\left(l_2 - \frac{l_{d2}}{2}\right)^2 \right]}_{\hat{I}} \ddot{\alpha}_2 + 2m_{d2}\left(l_2 - \frac{l_{d2}}{2}\right)\dot{l}_2\dot{\alpha}_2 = T_2, \quad (4-17)$$

where:

m_2 mass of module 2, $m_{S2} + m_{d2}$;

m_{S2}, m_{d2} mass of slewing and deployable links, respectively, of module 2;

I_{S2}, I_{d2} mass moments of inertia of slewing and deployable links, respectively, of module 2;

l_2 length of module 2;

l_{S2}, l_{d2} lengths of slewing and deployable links, respectively, module 2;

F_2, T_2 force and moment, respectively, at joint 2;

α_2 slew angles at joints 2.

Note, \hat{I} is the moment of inertia of module 2 about the swing axis.

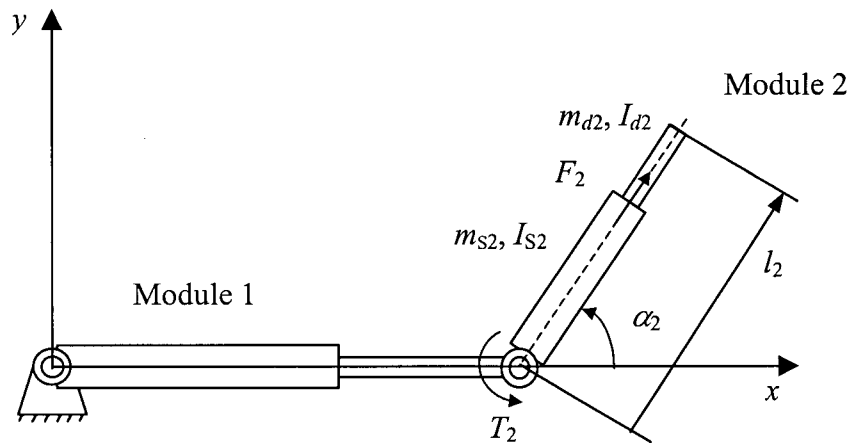


Figure 4-8 Two-module ground based manipulator system.

4.4.2 Control system parameters

The FLT has several desirable properties as pointed out before. However, in order to implement the FLT with accuracy, the system model and associated parameters must be known precisely. Design specifications of the manipulator system are:

Slewing arm length	0.3 m;
Maximum extension of the deployable arm	0.2 m;
Slewing arm sweep range	-135 to 135 deg;
Maximum rotational speed	60 deg/s;
Maximum deployment speed	0.04 m/s.

Values of the moments of inertia I_{s2} , and I_{d2} were obtained experimentally through swing (pendulum) tests as shown in Figure 4-9. A typical test involved application of a small displacement from the vertical and counting the number of cycles over a known period of time. The moment of inertia about the swing axis is given by

$$I = \frac{mgl}{\omega^2} = \frac{mglT^2}{4\pi^2}, \quad (4.18)$$

where T = period of oscillation; m = mass; and l = distance from the swing axis to the center of mass. The parameter values determined in this fashion are shown in Table 4-1. The moments of inertia were measured for the whole module with three different positions of the deployable link. For the FLT control, a single-module manipulator (module 2) was used, hence only the parameters for this module are relevant in the experiments.

The parameters for the manipulator are:

Module 1

- slewing link mass $m_{s1} = 4.3$ kg;
- slewing link length $l_{s1} = 0.3$ m;

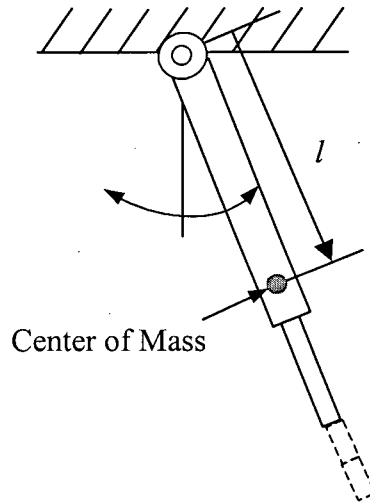


Figure 4-9 Schematic diagram of the swing test to determine the moment of inertia of a manipulator link with different lengths.

Table 4-1 Swing-test results for the ground-based robot.

	Mass (kg)	l (m)	T (s)	I (kg m ²)	Position
Module 1	4.5	0.276	1.343	0.557	fully retracted
		0.322	1.444	0.750	middle
		0.373	1.560	1.015	fully deployed
Module 2	2.4	0.106	1.021	0.066	fully retracted
		0.119	1.063	0.080	middle
		0.129	1.109	0.094	fully deployed

- deployable link mass $m_{d1} = 0.2$ kg;
- deployable link length $l_{d1} = 0.3048$ m;

Module 2

- slewing link mass $m_{s2} = 2.2$ kg;
- slewing link length $l_{s2} = 0.3$ m;
- deployable link mass $m_{d2} = 0.2$ kg;
- deployable link length $l_{d2} = 0.3048$ m;

Based on system parameters, the time constant varied in the range of 0.23 s to 0.28 s.

4.4.3 Controller design

Design of the PID controller is based on the experimental approach for the selection of gains as proposed by Ziegler and Nichols [57]. In this context a linear and time-invariant system is assumed. The parameters obtained from the Ziegler-Nichols method give an initial set of values for the PID gains. Due to the nonlinear and non-autonomous nature of the system, these parameters need to be refined and tuned for improved performance of the system.

With linear representation of the results from the swing test (Table 4-1), one has

$$\hat{I} = 4.206 \times 10^{-8} n + 0.066, \quad (4.19)$$

where n (4000 counts/mm) is the encoder reading from the actuator of the prismatic joint.

The FLT algorithm can be expressed as

$$\tau = \mathbf{M}(\ddot{\mathbf{q}}_d - \mathbf{u}) + \mathbf{F}, \quad (4.20)$$

where: $M = \begin{bmatrix} m_{d2} & 0 \\ 0 & \hat{I} \end{bmatrix}$; $F = \begin{bmatrix} -m_{d2}(l_2 - \frac{l_{d2}}{2})(\dot{\alpha}_2)^2 \\ 2m_2(l_2 - \frac{l_{d2}}{2})\dot{l}_2\dot{\alpha}_2 \end{bmatrix}$; $q = \begin{bmatrix} l_2 \\ \alpha_2 \end{bmatrix}$; $\tau = \begin{bmatrix} F_2 \\ T_2 \end{bmatrix}$; and

$u = -K_p e - K_v \dot{e}$ with $e(t) = q_d(t) - q(t)$. The FLT involves compensation for change in the mass matrix M as the system moves and also for the dynamical coupling term F . As a result, it should provide better performance compared to the fixed gain PID controller.

4.5 Trajectory Tracking

Once the controller is designed, a series of trajectories tracking tests were performed using both the FLT and PID algorithms. These tests fall into two main categories: a) straight line trajectories; b) circle tracking. The PID and FLT gains used are shown in Tables 4-2 through 4-4.

Table 4-2 Controller gains for the prismatic joint of module 2.

Module 2 (Prismatic)	K_p	K_d	K_i
PID	0.5	0.001	0.0001
FLT	0.5	0.001	—

Table 4-3 Controller gains for the revolute joint of module 2.

Module 2 (Revolute)	K_p	K_d	K_i
PID	3	0.001	0.001
FLT	0.5	0.001	—

Table 4-4 Controller gains for the revolute joint of module 1.

Module 1 (Revolute)	K_p	K_d	K_i
PID	4	0.001	0.001

These gains were used throughout the set of experiments. With the FLT, a PD controller is used in the outer loop, for the error and the derivative of the error, as mentioned before. Any other suitable controller may be used for the outer-loop after linearization, for example the Linear Quadratic Gaussian (LQG) or H_∞ procedure [58]. Important symbols involved in the trajectory tracking are defined below:

$e_{l_2}, e_{\alpha_1}, e_{\alpha_2}$ tracking errors at prismatic, revolute joint 1 and revolute joint 2, respectively;

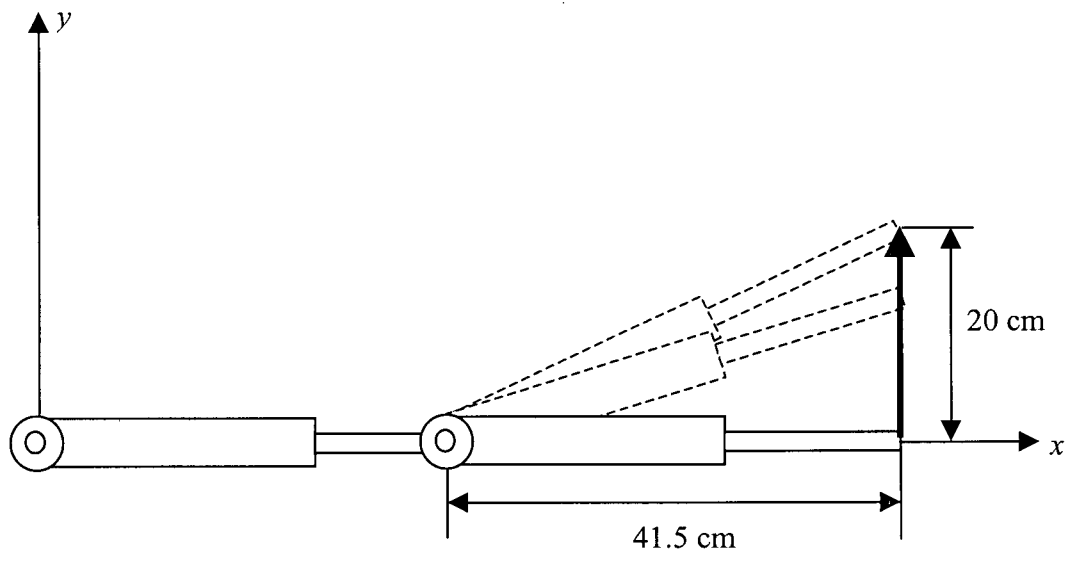
$I_{l_2}, I_{\alpha_1}, I_{\alpha_2}$ driving currents at prismatic and revolute joints, respectively;

α_1, α_2 rotation angles at revolute joints 1 and 2, respectively;

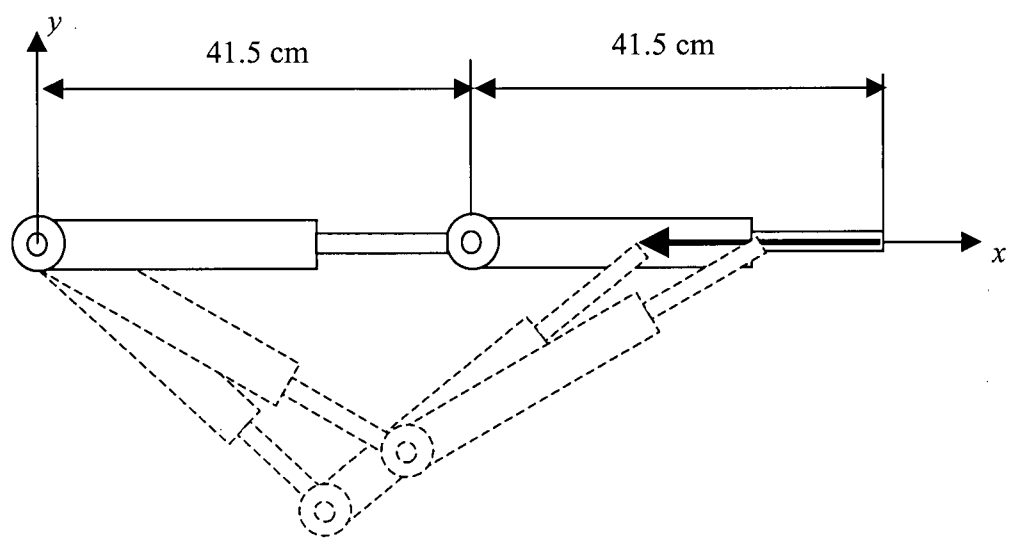
Δl_2 change in length of the deployable link of module 2.

4.5.1 Straight line trajectory

The first tracking test involves making the tip of the manipulator to follow a straight line by using one-revolute joint and one prismatic joint of the outer module (module 2) while the inner module is kept locked. The PID controller is used to perform the test. The line is located 41.5 cm from the base of module 2 and its length is 20 cm along the y direction. Figure 4-10(a) shows the location of the tracked line and the configuration of the manipulator. The specified tracking time is 4 seconds, and the tip trajectory has a prescribed sine-on-ramp profile as given in Eq. (2.4). The results of the tracking experiment are shown in Figure 4-11 (prescribed profile in dotted). It is seen that the manipulator tip follows



(a)



(b)

Figure 4-10 Schematic diagrams for straight line tracking using: (a) one revolute joint and one prismatic joint; (b) two revolute joints.

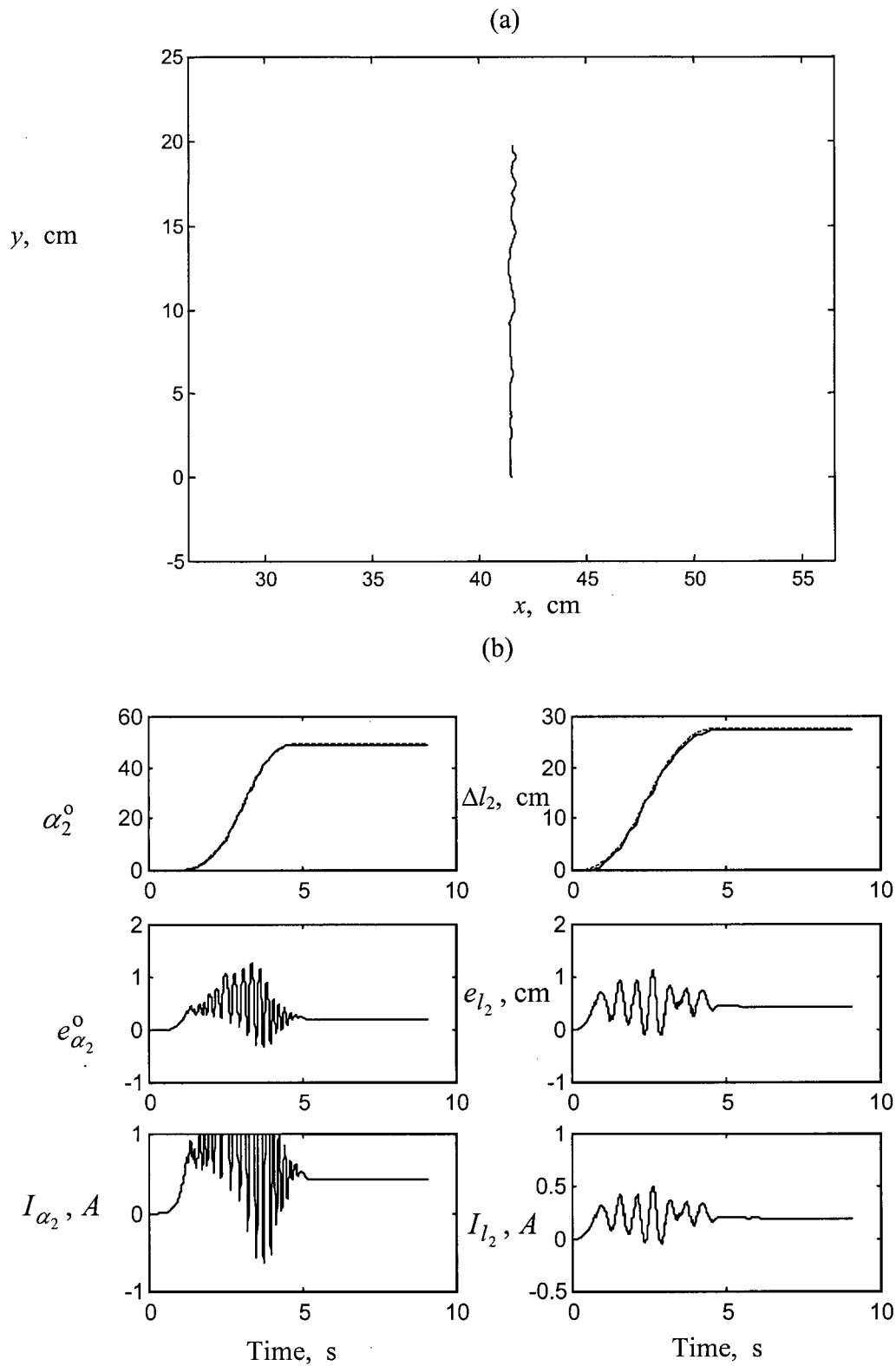


Figure 4-11 Straight line tracking using one revolute and one prismatic joint under the PID control: (a) tip trajectory; (b) joint motion and the corresponding control signals.

the straight line with reasonable accuracy. The saturation in I_{α_2} is caused by the safety limit of the current that is transmitted to the motor, which is constrained to 1 A.

Figure 4-10 (b) shows another manipulator configuration for straight-line tracking. Now a distance of 20 cm is tracked along the x direction using two revolute joints, in 8 seconds. Note, the prismatic joints are locked with each module length fixed at 41.5 cm. As pointed out in Chapter 1, a prismatic joint has the advantage that it does not possess dynamic coupling with the revolute joint of the same module, since the reaction force passes through the center of the joint. When two revolute joints are used, the reaction torque due to the rotational dynamics of the second module will try to rotate the first module in the counter-clockwise direction resulting in over-rotation of the first module. Thus the tracking error is biased in the negative direction of the y -axis, as is evident from the experimental results shown in Figure 4-12 (a). From the plot of e_{α_1} in Figure 4-12 (b), it is clear that error is in the negative side, as a result of the dynamical coupling. In a robotic system that has kinematic redundancy, it will be possible even to maneuver the first module to an appropriate position and then use only the prismatic joint for the line tracking. This will lead to virtually no error in the tracking.

Next, the FLT controller is used to carry out the same task as that shown in Figures 4-11 for the PID control. Again, the execution time is set at 4 seconds and the length of the line is 20 cm. The results are shown in Figures 4-13. By comparing the behaviors of the PID and FLT controllers, following observations can be made: (i) The FLT has an adaptive capability with respect to the variation of the mass matrix. It also has a compensation capability for dynamical coupling. Thus, the FLT produces more active control signals (high frequency I_{α_2} and I_{l_2}). (ii) The PID controller is simpler, requires less computational power, and does

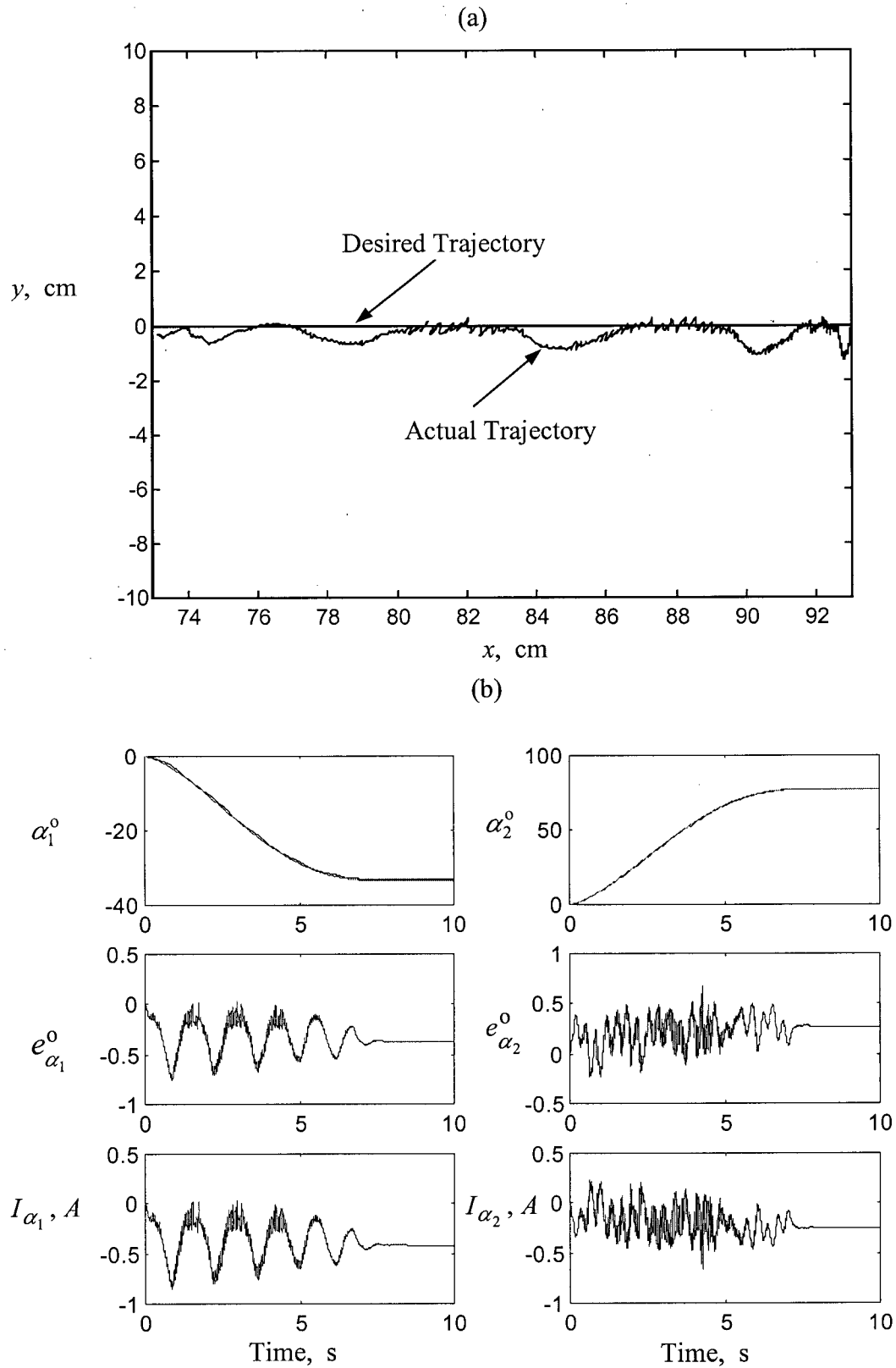


Figure 4-12 Straight line tracking using two revolute joints under the PID control: (a) tip trajectories; (b) joint motion and corresponding control signals.

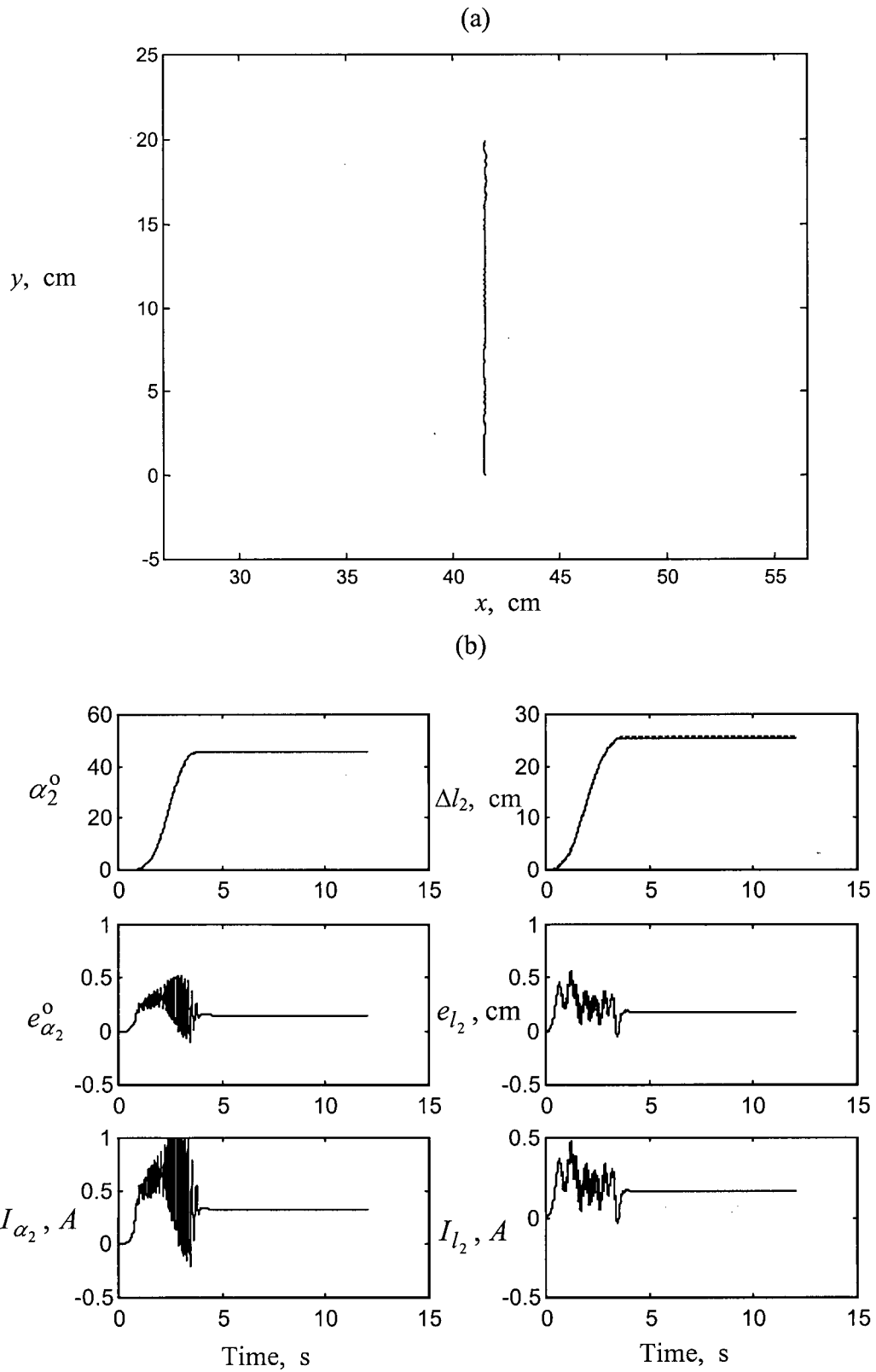


Figure 4-13 Straight line tracking using one revolute and one prismatic joint with the FLT: (a) tip trajectory; (b) joint motion and the corresponding control signals.

not depend on a model of the robot (the experimental, Ziegler-Nichols method is used here to tune the PID gains).

One is able to tune the FLT controller by incorporating a multiplicative confidence factor into the dynamical compensation term F , and gradually increasing it as more experience is gained through experimentation. This approach is used for tuning the FLT controller of the prototype robotic system.

The tip trajectories of the robot under the control of PID and FLT separately, are plotted in Figure 4-14. It is clear that at the expense of the computation cost, the FLT gives better tracking accuracy than the PID. Note that towards the end of the tracking, both controllers produce larger errors. This is due to increased dynamical coupling and the greater effort that is required for synchronizing the two joints at the end of the trajectory. Another major source of error is the unmodeled friction. It causes a steady-state error and stick-slip motion. These nonlinear effects cause vibrations and reduce the tip position accuracy.

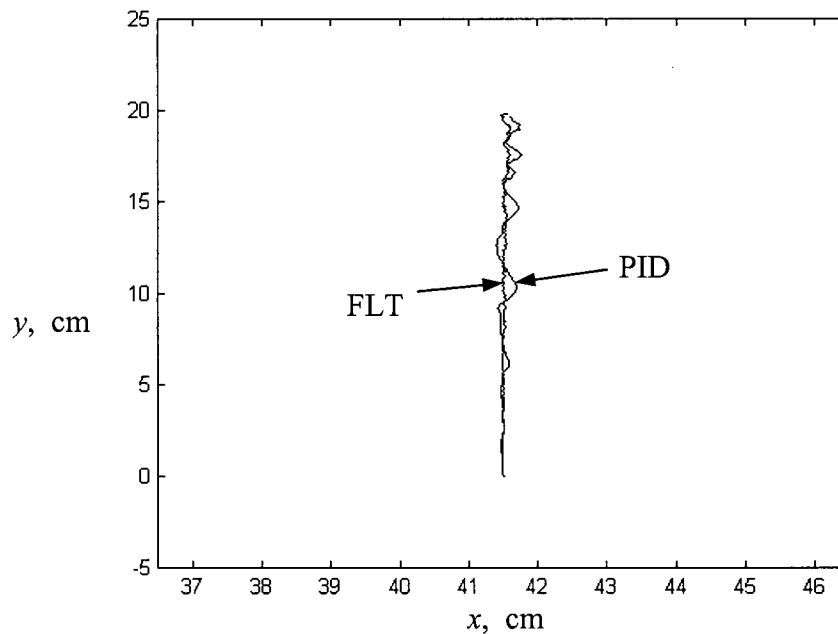


Figure 4-14 Straight line tracking using one revolute and one prismatic joint: comparison of the FLT and PID procedures.

4.5.2 Circular trajectory

In order to further investigate the system, tracking of a circular trajectory was undertaken as a typical test-case. To begin with, tracking was carried out under the PID control. Different trajectory speed profiles were employed to assess the effectiveness of the controller. The circular trajectory is defined as:

$$\begin{cases} P_x = 41.5 + r - r \cos(\omega t); \\ P_y = r \sin(\omega t); \end{cases} \quad (4.21)$$

where: P_x , P_y are tip positions in the x and y directions, respectively; r is the radius of the circle; and ω is the angular velocity of the circular motion. For instance, $\omega = 0.1\pi$ corresponds to a tip motion around the circle in 20 seconds. Figure 4-15 schematically shows the tracked circle and the corresponding manipulator configurations at three different instants during tracking. The radius r is taken to be 10 cm for all the cases. Each circle is tracked twice to check the repetitiveness of tracking.

The first experiment of tracking a circular trajectory uses $\omega = 0.1\pi$; i.e. 20 seconds a circle. The results are shown in Figure 4-16. The maximum errors occur at locations where joints change their directions of motion. Due to the Coulomb friction, the joints have nonlinear dead zones. The signal from the controller is generated based on the motion error. Once a joint stops, the error must be large enough to overcome the static friction. This, in turn, causes a larger error. When the joint starts to move, the smaller dynamic friction results in a lower error. Of course, dynamical coupling also plays a role in causing the motion error. This can be seen when the speed of the profile increases from 20 seconds a circle to 10 seconds a circle (Figures 4-17). It is clear that with the increased speed the tip trajectory is not as smooth as the one in Figure 4-16. This is mainly due to the dynamical coupling. The

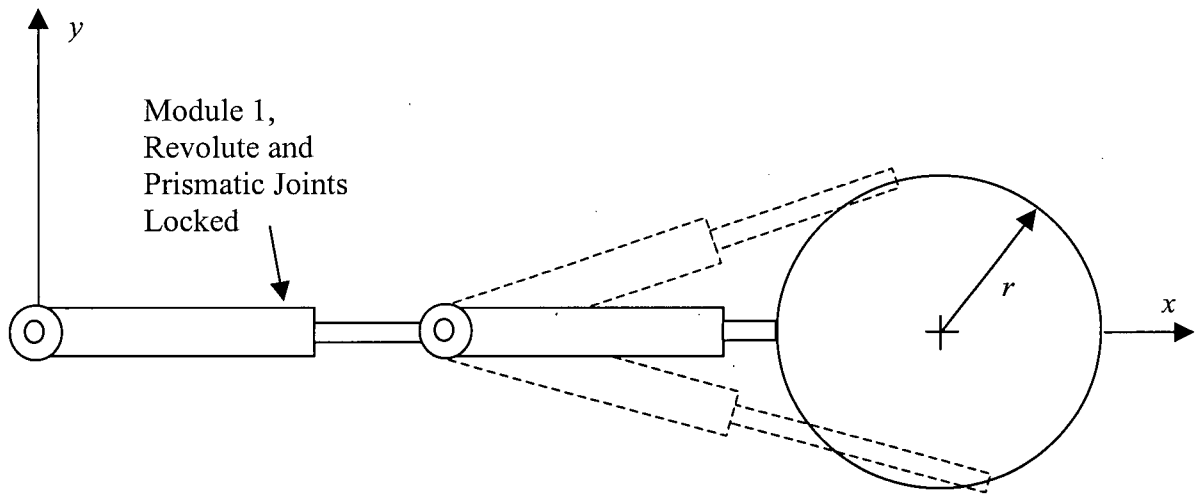


Figure 4-15 Schematic diagram showing tracking of a circular trajectory using module 2.

corresponding control effort also has increased. The repetitiveness of the trajectory worsens as well due to the same reason. When the tracking speed decreases from 20 seconds a circle to 30 seconds a circle (Figure 4-18), the repetitiveness improves but the error is slightly larger than that for the 20 seconds a circle. Here, dynamical coupling is lower, which makes the trajectory smoother and the level of repetition better. However, when the desired trajectory moves slower, the error increases gradually and the control effort needed to overcome the steady-state friction takes a longer time to accumulate. This causes the nonlinear dead-zone effect to worsen.

The FLT controller was also used in the case of 20 seconds a circle (Figures 4-19). As before, the performance of the FLT controller is better than that of the PID controller. It compensates for the dynamical coupling effect, which significantly reduces the error of the revolute joint. It is seen that, in area C, the tip error is low. In other areas (A, B, D), the

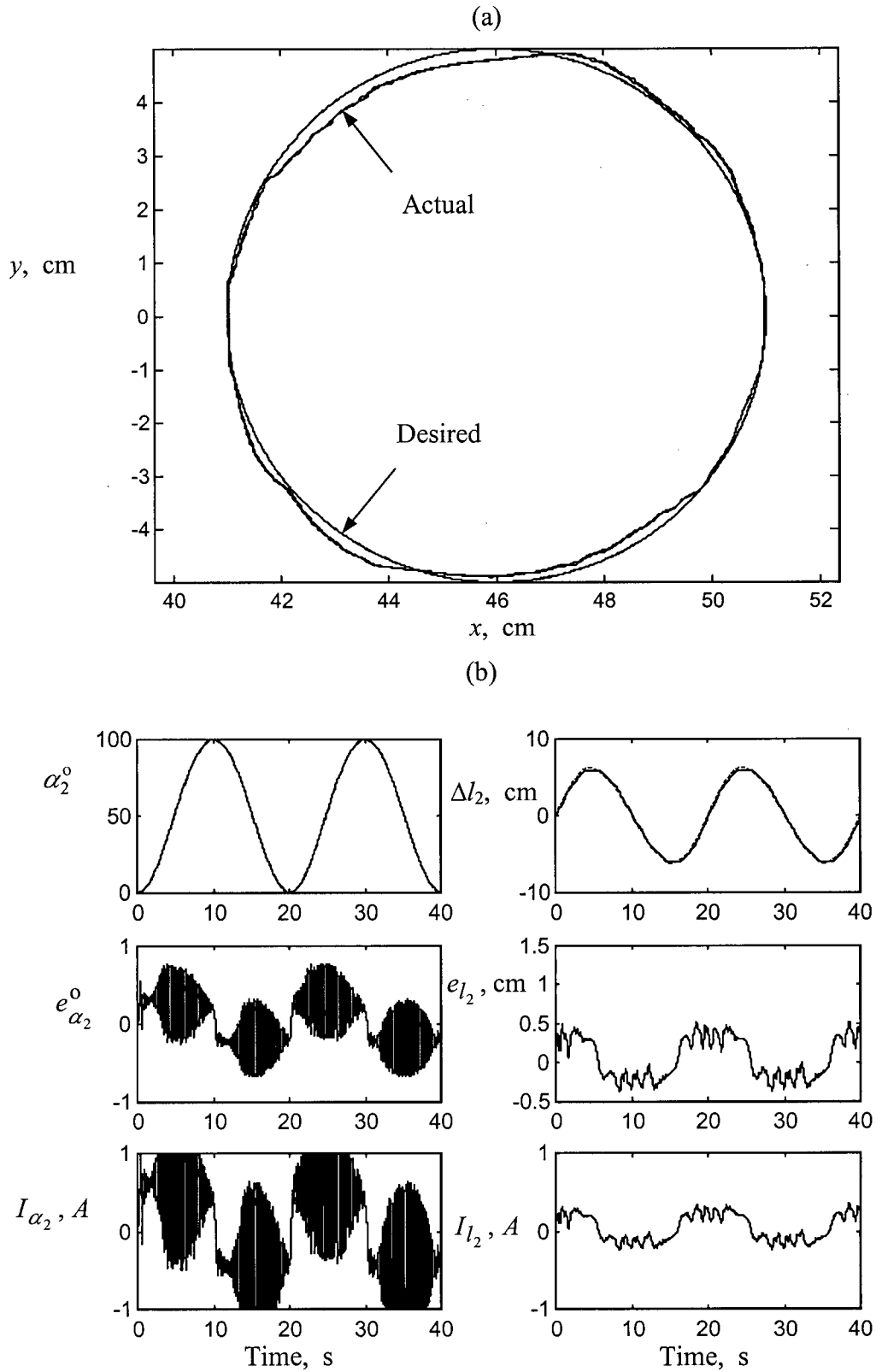


Figure 4-16 Tracking of a circle, at a speed of 0.314 rad/s, using the PID control: (a) tip trajectories; (b) joint dynamics and control signals.

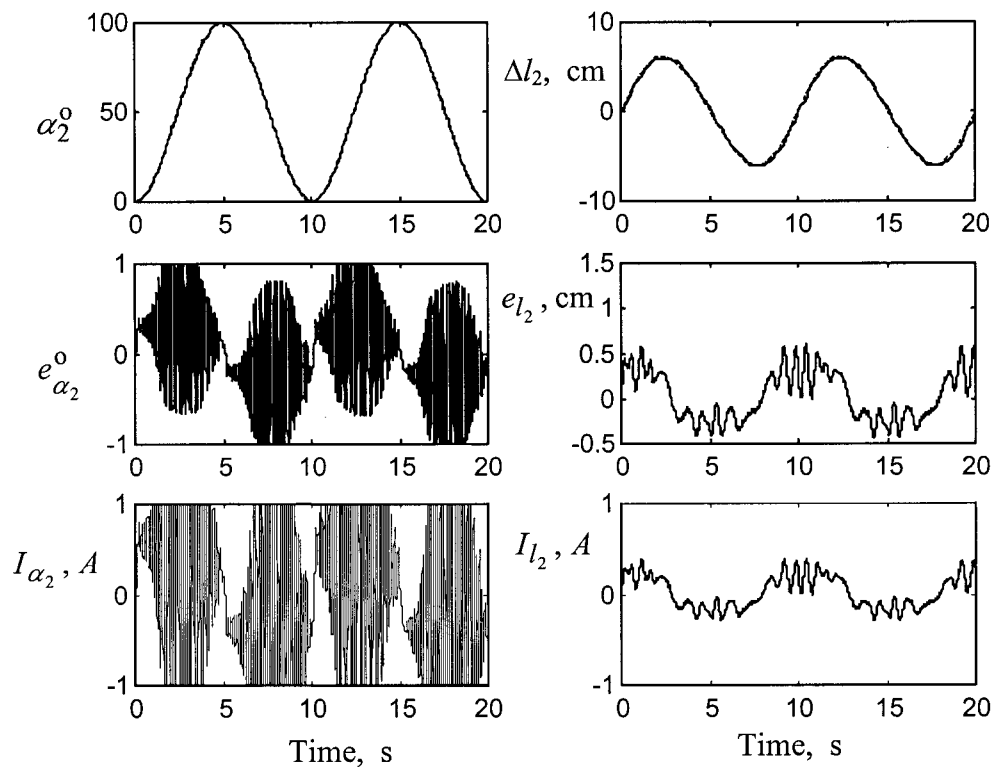
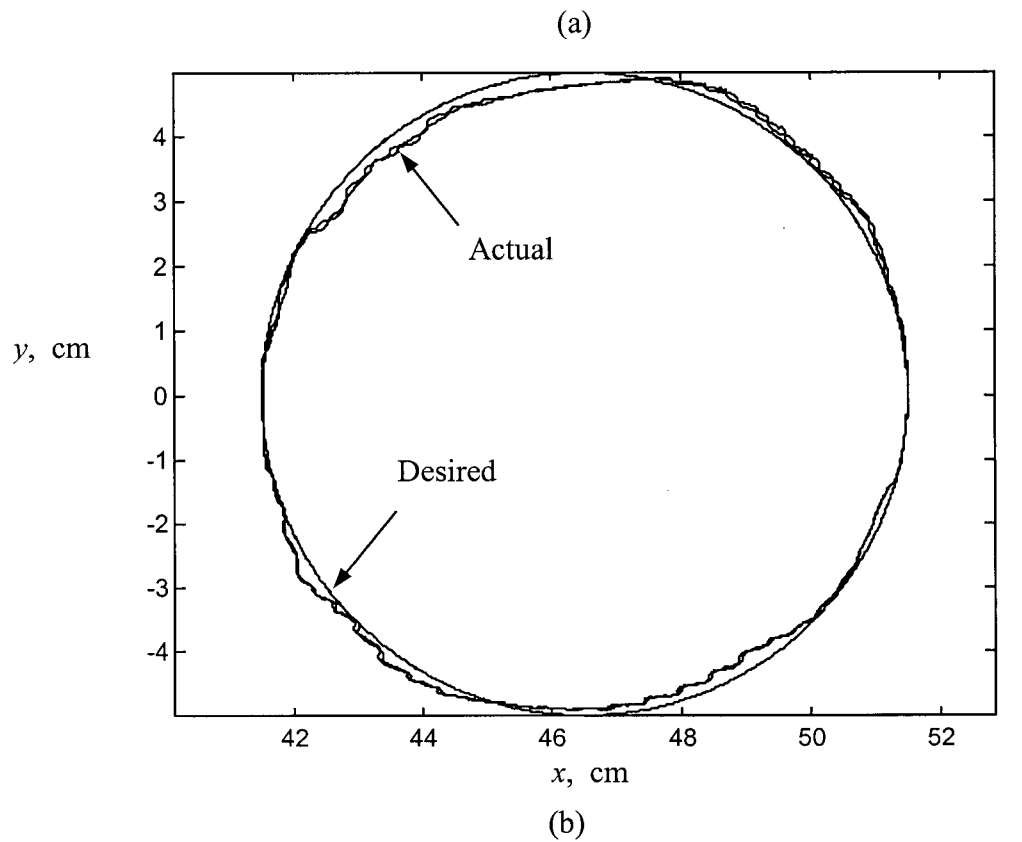


Figure 4-17 Tracking of a circle, at a speed of 0.628 rad/s, using the PID control: (a) tip trajectories; (b) joint motion and control signals.

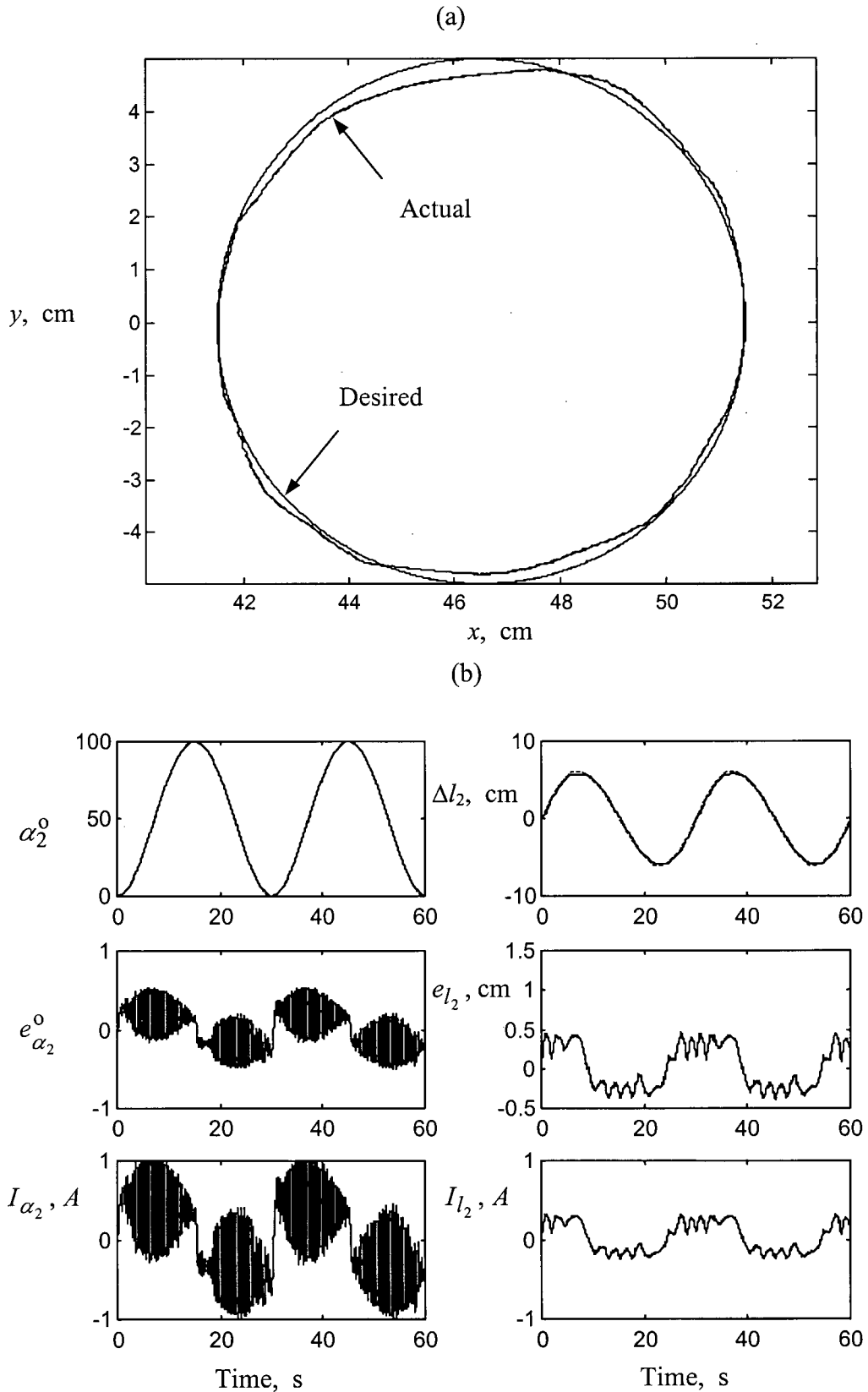


Figure 4-18 Circle tracking behavior under the PID control at a speed of 0.209 rad/s: (a) tip trajectories; (b) joint dynamics and control effort.

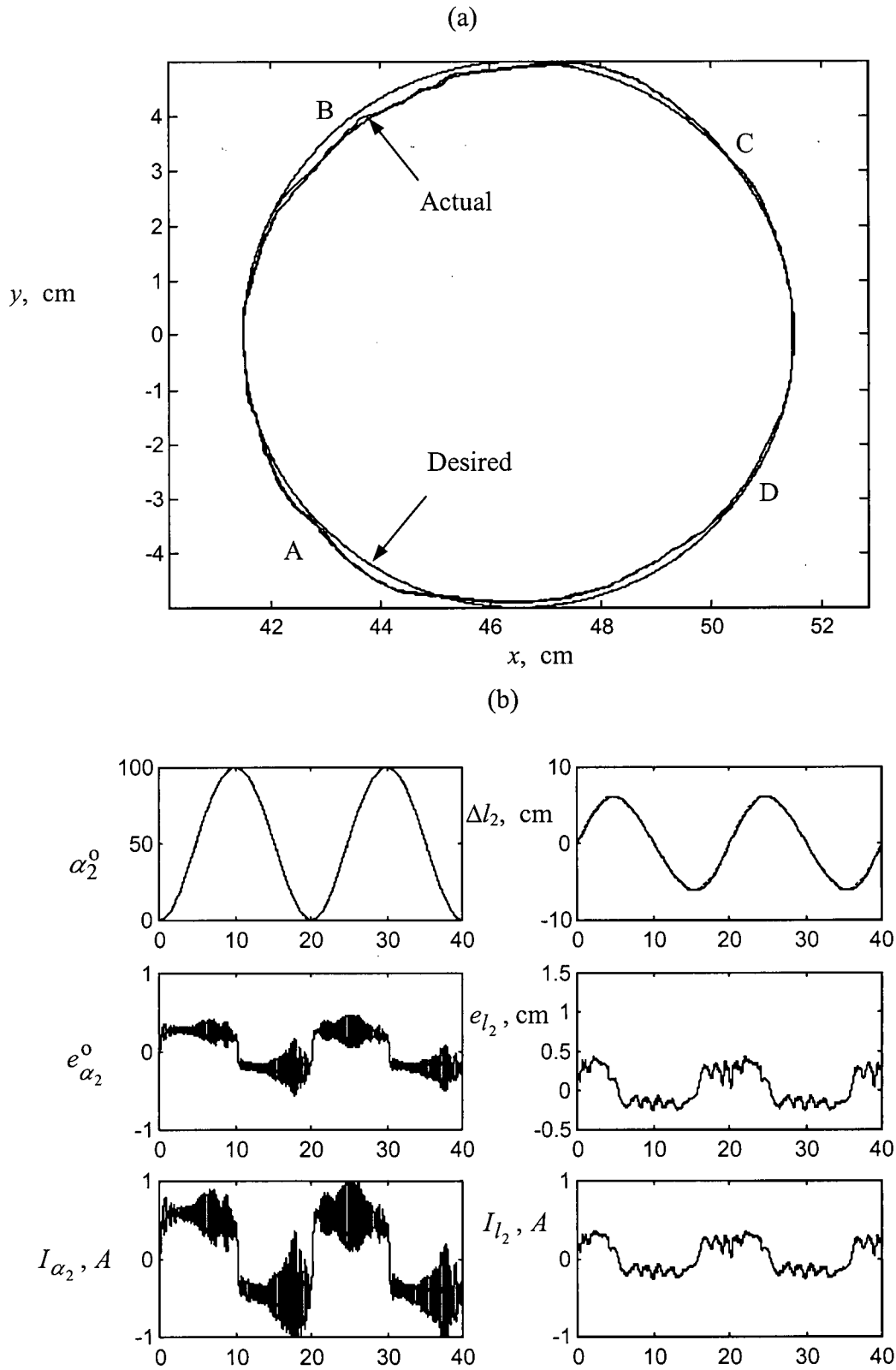


Figure 4-19 Tracking of a circle, at a speed of 0.314 rad/s, with the FLT: (a) tip trajectories; (b) joint dynamics and control effort.

dynamical compensation effort is evident. The FLT controller tries to compensate for the nonlinearity and dynamics, and consequently reduces the error and improves the repetitiveness. Again, it may be pointed out that the FLT needs a higher level of active control, and also has a higher bandwidth as expected.

The ground-based experiments verify several distinguishing characteristics of the variable-geometry manipulator system and its controllers:

- Prismatic joints have lower dynamical coupling, and are preferable for executing high precision tasks.
- Kinematic redundancy of a robot is useful in task planning to improve the tracking accuracy.
- The FLT controller is efficient, robust, and stable. It gives satisfactory performance, but at a computational cost. It is suitable for the variable-geometry manipulator system.
- The PID controller is simple and fast. It works well with most trajectory following cases. Its parameters need to be fine tuned once they are assigned by a technique such as the Ziegler-Nicholes approach.

Friction plays a significant role in causing tracking errors. It should be carefully modeled and compensated for. This is a difficult job, however, due to the highly nonlinear and time varying nature of friction. Even in presence of friction, the FLT is able to handle the control task in a robust manner. Modification of the FLT algorithm to account for friction should provide improved control performance.

5. CONCLUDING REMARKS

5.1 Contributions

The main contributions of the thesis can be summarized as follows:

- (i) A detailed dynamical study of a novel flexible space-based manipulator, involving two modules and accounting for orbital, librational as well as vibrational interactions, has not been reported before. Providing understanding of such complex interactions is indeed a contribution of importance.
- (ii) Control of this novel manipulator has received virtually no attention. The study lays a sound foundation to build on with the nonlinear Feedback Linearization Technique (FLT).
- (iii) A two-module manipulator system is linearized and a Linear Quadratic Regulator (LQR) is designed to suppress vibrations arising in the manipulator links, joints, as well as in the platform. Such synthesis of the FLT and LQR to control both rigid and flexible degrees of freedom represents a significant contribution.
- (iv) An open architecture experiment is set up for a ground-based prototype manipulator. It makes implementation of different control strategies possible.
- (v) It was indeed fortunate to have a two-module ground-based prototype manipulator designed and constructed by Chu [8]. This has made it possible to assess performance of control strategies not only through numerical simulations but also with ground-based experiments. Such correlation study for the novel robotic system is indeed rare.
- (vi) Such a comprehensive study involving numerical simulations as well as ground-based experiments represents an important step forward.

5.2 Conclusions

The project was so formulated as to emphasize the dynamics and control of a novel manipulator studied here. The objective has been to understand the system behavior at the fundamental level, through the study of representative cases, and establish trends. Based on the investigation, the following general conclusions can be made:

- (a) Significant coupling exists between the platform, link and joint vibrations, as well as system libration. The most pronounced coupling was observed between the joint and link vibrations. In general, slewing and deployment maneuvers have a significant effect on the flexible degrees of freedom response.
- (b) When the manipulator base is located near the platform's extremity, slewing and deployment maneuvers can also result in significant rigid body motion of the platform.
- (c) Excitation of the system's flexible degrees of freedom can significantly deteriorate the accuracy of the manipulator.
- (d) In general, payload, speed of maneuver and joint flexibility represent three important parameters governing the response of the system. As can be expected, heavier payload, faster speed of maneuver and reduced joint stiffness affect the manipulator tip dynamics adversely.
- (e) The system exhibits unacceptable response under critical combinations of parameters. The control strategy based on the FLT is found to be quite effective in regulating the rigid-body motion of manipulator links as well as the attitude motion of the platform. The unmodeled flexibility of the platform, joints, and manipulator links has virtually no effect on the performance of the FLT controller. It is able to regulate the elastic degrees of freedom rather well through coupling. The controller is quite robust.

- (f) Active control of flexible degrees of freedom using the LQR, together with the FLT for rigid generalized coordinates, significantly improves the situation. The controller is quite robust and continues to be effective even in presence of heavy payloads, fast maneuvers and reduced stiffness of the revolute joints. The results should prove useful in the design of this new class of promising manipulators.
- (g) The prototype manipulator with an open architecture is an effective way of evaluating performance of various control strategies.
- (h) The ground-based experiments generally validated trends indicated by the numerical simulation results. This is encouraging as the prototype system has limitations in terms of backlash, friction and, at times, less than smooth operation.

5.3 Recommendations for Future Work

Considering the diversity of research areas associated with the field of space robotics, the present thesis should be viewed as an initial step in the analysis and development of this particular class of space manipulators. There are several avenues which remain unexplored or demand more attention. Some of the more interesting and useful aspects include:

- (i) path planning and inverse kinematics with emphasis on obstacle avoidance, as well as minimization of structural vibrations and base reaction; effect of redundancy on system performance; completion of a given mission with one or more joints inoperational;
- (ii) dynamics and control of satellite capture;
- (iii) comparative study of various optimal, adaptive, intelligent and hierarchical control strategies to regulate the rigid and flexible dynamics of single and multi-module systems;

- (iv) more two-dimensional ground-based experiments to help validate numerical simulation results;
- (v) animation of simulation results for visual appreciation of the physics of the problem;
- (vi) incorporate another data acquisition board or upgrade the current one so that all four axis of the ground based manipulator can be controlled;
- (vii) introduce an 'eye-in-the-sky' camera to determine the actual location of the end-effector, and strain gauges to sense the flexibility of the links
- (viii) develop a graphical user interface for the robot system and its controller.

REFERENCES

- [1] Evans, B., "Robots in Space," *Spaceflight*, Vol. 35, No. 12, 1993, pp. 407-409.
- [2] Canadian Science and Technology, O'Brien Publishing, Ottawa, Ontario, Fall 1995, p.11.
- [3] Bassett, D.A., Wojik, Z.A., Hofer, S., and Wittenborg, J., "Mobile Servicing System Assembly, Checkout and Operations," *46th International Astronautical Congress*, Oslo, Norway, October 1995, Paper No. IAF-95-T.3.04.
- [4] Krukewich, K., Sexton, J., Cavin, K., Lee, N.E., and Cox, B., "The Systems Engineering Approach to the Integration of the Space Station Remote Manipulator System on the International Space Station (ISS)," *46th International Astronautical Congress*, Oslo, Norway, October 1995, Paper No. IAF-95-T.2.02.
- [5] Kalaycioglu, S., "Robotics Evaluation and Characterization (REACH) of the SSRMS," *46th International Astronautical Congress*, Oslo, Norway, October 1995, Paper No. IAF-95-1.2.03.
- [6] Chiun-Hogn, C., "Computer Vision System for Extravehicular Activity Helper/Retriever," *Applied Intelligence*, Vol. 5, No. 3, 1995, pp. 251-268.
- [7] Lavery, D., "Perspectives on Future Space robotics," *Aerospace America*, Vol. 32, No. 5, 1994, pp.32-37.
- [8] Chu, M.S.T., *Design, Construction and Operation of a Variable Geometry Manipulator*, M.A.Sc. Thesis, University of British Columbia, Vancouver, B.C., Canada, October, 1997.
- [9] Brereton, R. C., *A Stability Study of Gravity Oriented Satellites*, Ph.D. Thesis, The University of British Columbia, Vancouver, B.C., Canada, September 1967, pp. 1-11, 14-21.
- [10] Ambros, R.O., and Askew, R.S., "Experimental Investigation of Actuators for Space Robots," *Proceedings of the 1995 IEEE International Conference on Robotics and Automation*, Nagoya, Japan, 1995, Vol. 3, pp. 2625-2630.
- [11] "Too much Sun gives Ulysses the Wobbles," *Electronics World and Wireless World*, Vol. 97, March 1991, p. 184.
- [12] Caron, M., *Planar Dynamics and Control of Space-Based Flexible Manipulators with Slewing and Deployable Links*, M.A.Sc. Thesis, University of British Columbia, Vancouver, B.C., Canada, October 1996.
- [13] Xu, Y., and Shum, H.Y., "Dynamic Control and Coupling of a Free-Flying Space Robot System," *Journal of Robotic Systems*, Vol. 11, No. 7, 1994, pp. 573-589.

- [14] Modi, V.J., and Suleman, A., "Dynamical Study of the Proposed Space Station Type Configuration," *Acta Astronautica*, Vol. 19, No. 5, 1989, pp. 377-391.
- [15] Book, W.J., "Controlled Motion in an Elastic World," *Journal of Dynamic Systems, Measurement, and Control*, Vol.115, March 1993, pp. 252-260.
- [16] Kelly, J.H., Glade, R.L., and Depkovitch, T.M., "Addressing the Issue of System Identification for Space Manipulators," *Proceedings of SPIE - The International Society for Optical Engineering*, Vol. 1612, 1992, pp. 36-48.
- [17] Kimura, S., Mivazaki, K., and Suzuki, Y., "Application of a Decentralized Autonomous Control Mechanism for Space Robotics," *19th International Symposium on Space Technology and Science*, Yokohama, Japan, May 1994, Paper ISTS 94-c-02.
- [18] Hirzinger, G., Landzettel, K., and Fagerer, C., "Telerobotics with Large Time Delays - the ROTEX Experience," *Proceedings of the IEEE/RSJ/GI International Conference on Intelligent Robots and Systems*, Munich, Germany, 1994, Published by the IEEE, Piscataway, U.S.A., Vol. 1, pp. 571-578.
- [19] Meirovitch, L., and Kwak, M.K., "On the Maneuvering and Control of Space Structures," *Proceedings of the First International Conference on the Dynamics of Flexible Structures in Space*, Cranfield, U. K., May 1990, Editors: C.L. Kirk, and J.L. Junkins, pp. 3-17.
- [20] Roberson, R.E., "Two Decades of Spacecraft Attitude Control," *Journal of Guidance and Control*, Vol. 2, No.1, 1979, pp.3-8.
- [21] Linkins, P.W., "Spacecraft Attitude Dynamics and Control - A Personal Perspective on Early Developments," *Journal of Guidance, Control, and Dynamics*, Vol. 9, No. 2, 1986, pp. 129-134.
- [22] Modi, V.J., "Attitude Dynamics of Satellites with Flexible Appendages - A Brief Review," *Journal of Spacecraft and Rockets*, Vol. 11, 1974, pp. 743-751.
- [23] Modi, V.J., and Shrivastava, S.K., "Satellite Attitude Dynamics and Control in the Presence of Environmental Torques - A Brief Survey," *Journal of Guidance, Control, and Dynamics*, Vol. 6, No. 6, 1983, pp. 461-471.
- [24] Modi, V.J., "Spacecraft Attitude Dynamics: Evolution and Current Challenges," *Invited Address to the NATO/AGARD Symposium on the Space Vehicle Flight Mechanics*, Luxembourg, November 1989; also *Proceedings of the Symposium, AGARD-CP-489*, pp. 15-1 to 15-26; also *Acta Astronautica* Vol. 21, No. 10, 1990, pp. 698-718.
- [25] Modi, V.J., "Man, the Unknown: Fleeting Impression of an Uncertain Mind," *Acta Astronautica*, Vol. 41, No.2, 1997, pp. 63-90

- [26] Nagata, T., Modi, V.J., and Matsuo, H., "An Approach to Dynamics and Control of Flexible Systems," *A Collection of Technical Papers, AIAA/AAS Astrodynamics Conference*, Scottsdale, Arizona, U.S.A, August 1994, Paper No. AIAA-94-3756CP, pp. 366-375.
- [27] Cherchas, D.B., "Dynamics of Spin-Stabilized Satellites During Extension of Long Flexible Booms," *Journal of Spacecraft and Rockets*, Vol. 8, No. 7, 1971, pp. 802-804.
- [28] Sellappan, R., and Bainum, P.M., "Dynamics of Spin-Stabilized Spacecraft During Deployment of Telescopic Appendages," *Journal of Spacecraft and Rockets*, Vol. 13, No. 10, pp. 605-610.
- [29] Lips, K.W., and Modi, V.J., "Flexible Appendages Deployment Dynamics as Applied to Satellite Attitude Motion", *Acta Astronautica*, Vol. 5, 1978, pp. 787-815.
- [30] Lips, K.W., and Modi, V.J., "Three-Dimensional Response Characteristics for a Spacecraft with Deploying Flexible Appendages", *Journal of Spacecraft and Rockets*, Vol. 4, 1981, pp. 650-656.
- [31] Modi, V.J., and Ibrahim, A.M., "A General Formulation for Librational Dynamics of Spacecraft with Deploying Appendages", *Journal of Guidance, Control, and Dynamics*, Vol. 7, 1984, pp. 563-569.
- [32] Modi, V.J., and Shen, Q., "On the Dynamics of Spacecraft with Flexible, Deployable and Slewing Appendages", *Advances in the Astronautical Sciences*, Editors: A.K. Misra et al., Univelt Incorporated Publisher for the American Astronautical Society, San Diego, U.S.A., Vol. 85, Part I, pp. 877-896.
- [33] Lips, K.W., *Dynamics of a Large Class of Satellites with Deploying Flexible Appendages*, Ph.D. Thesis, University of British Columbia, Vancouver, B.C., Canada, 1980.
- [34] Ibrahim, A.M., *Mathematical Modelling of Flexible Multibody Dynamics with Application to Orbiting Systems*, Ph.D. Thesis, University of British Columbia, Vancouver, B.C., Canada, 1988.
- [35] Shen, Q., *On the Dynamics of Spacecraft with Flexible, Deployable and Slewing Appendages*, Ph.D. Thesis, Simon Fraser University, Burnaby, B.C., Canada, 1993.
- [36] Marom, I., and Modi, V.J., "On the Dynamics and Control of the Manipulator with a Deployable Arm", *AAS/AIAA Astrodynamics Specialist Conference*, Victoria, B.C., Canada, August 1993, Paper No. AAS-93-670; also *Advances in the Astronautical Sciences*, Editors: A.K. Misra et al., Univelt Incorporated Publisher for the American Astronautical Society, San Diego, U.S.A., Vol. 85, Part III, pp. 2211-2229.
- [37] Modi, V.J., Chen, Y., Misra, A.K., de Silva, C.W., and Marom, I., "Nonlinear Dynamics and Control of a Class of Variable Geometry Mobile Manipulators",

Proceedings of the Fifth International Conference on Adaptive Structures, Sendai, Japan, December 1994, Editor: J. Tani et al., Technomic Publishing Co. Inc., Lancaster, PA, U.S.A., pp. 140-149.

- [38] Hokamoto, S., Modi, V.J., and Misra, A.K., "Dynamics and Control of Mobile Flexible Manipulators with Slewing and Deployable Links", AAS/AIAA Astrodynamics Specialist Conference, Halifax, Nova Scotia, Canada, August 1995, Paper No. AAS-95-322; also *Advances in the Astronautical Sciences*, AAS Publications office, San Diego, California, U.S.A., Editors: K. Terry Alfriend et al., Vol. 90, pp. 339-357.
- [39] Hokamoto, S., and Modi, V.J., "Nonlinear Dynamics and Control of a Flexible Space-Based Robot with Slewing-Deployable Links", *Proceedings of the International Symposium on Microsystems, Intelligent Materials and Robots*, Sendai, Japan, September 1995, Editors: J. Tani and M. Esashi, pp. 536-539.
- [40] Hokamoto, S., and Modi, V.J., "Formulation and Dynamics of Flexible Space Robots with Deployable Links", *Transactions of the Japan Society for Mechanical Engineers*, Vol. 62, No. 596, 1996, pp. 1495-1502.
- [41] Hokamoto, S., Kuwahara, M., Modi, V.J., and Misra, A.K., "Control of a Flexible Space-Based Robot with Slewing-Deployable Links", *Proceedings of the AIAA/AAS Astrodynamics Conference*, San Diego, California, U.S.A., July 1996, AIAA Publisher, Paper No. AIAA-96-3626-CP, pp. 506-513.
- [42] Caron, M., Modi, V.J., Pradhan, S., de Silva, C.W., and Misra, A.K., "Planar Dynamics of Flexible Manipulators with N Slewing Deployable Links", *Proceedings of the AIAA/AAS Astrodynamics Conference*, San Diego, California, U.S.A., July 1996, AIAA Publisher, Paper No. AIAA-96-3625-CP, pp. 491-505.
- [43] Chen, Y., *On the Dynamics and Control of Manipulators with Slewing and Deployable Links*, Ph.D. Thesis, University of British Columbia, Vancouver, B.C., Canada, July 1999.
- [44] Goulet, J.F., *Intelligent Hierarchical Control of a Deployable Manipulator*, M.A.Sc. Thesis, University of British Columbia, Vancouver, B.C., Canada, June 1999.
- [45] Ogata, K., *Modern Control Engineering*, Prentice-Hall, Upper Saddle River, N.J., U.S.A., 1997, pp. 915-935.
- [46] De Silva, C.W., *Vibration Fundamentals and Practice*, CRC Press, Boca Raton, Florida, U.S.A., 1999, pp. 798-816.
- [47] Bejczy, A.K., *Robot Arm Dynamics and Control*, JPL TM 33-669, California Institute of Technology, Pasadena, California, U.S.A., 1974.

- [48] Singh, S.N., and Schy, A.A., "Invertibility and Robust Nonlinear Control of Robotic Systems", *Proceedings of the 23rd Conference on Decision and Control*, Las Vegas, Nevada, U.S.A., December 1984, pp. 1058-1063.
- [49] Spong, M.W., and Vidyasagar, M., "Robust Linear Compensator Design for Nonlinear Robotic Control", *Proceedings of the IEEE Conference on Robotics and Automation*, St. Louis, Missouri, U.S.A., March 1985, pp. 954-959.
- [50] Spong, M.W., and Vidyasagar, M., "Robust Nonlinear Control of Robotic Manipulator", *Proceedings of the 24th Conference on Decision and Control*, Fort Lauderdale, Florida, U.S.A., December 1985, pp. 1767-1772.
- [51] Spong, M.W., "Modeling and Control of Elastic Joint Robots", *Journal of Dynamics Systems, Measurement and Control*, Vol. 109, 1987, pp. 310-319.
- [52] Modi, V.J., Karray, F., and Ng, A.C., "On the Nonlinear Slewing Dynamics and Control of the Space Station Based Mobile Servicing System", *Nonlinear Dynamics*, Vol. 7, 1995, pp. 105-125.
- [53] De Silva, C.W., *Control Sensors and Actuators*, Prentice-Hall, Englewood Cliffs, N.J., U.S.A., 1989, pp. 196-199, pp. 218-244.
- [54] De Silva, C.W., and Mcfarlane, A.G.J., *Knowledge-Based Control with Application to Robots*, Springer-Verlag, Berlin, Germany, 1989, pp. 87-98.
- [55] Neuman, C.P., and Tourassis, V.D., "Discrete Dynamic Robot Models", *IEEE Trans. System Man and Cybernetics*, Vol. SMC-15, No. 2, March/April, 1985, pp. 193-204.
- [56] Lewis, F.L., *Applied Optimal Control and Estimation*, Prentice-Hall, Englewood Cliffs, N.J., U.S.A., 1992.
- [57] Kranklin, G.F., Powell, J.D., and Emami-Naeini, A., *Feedback control of Dynamics Systems*, Addison-Wesley Publishing Company, Inc., Massachusetts, U.S.A., 1986, pp. 103-106.
- [58] De Silva, C.W., *Intelligent Control: Fuzzy Logic Applications*, CRC Press, Boca Raton, Florida, U.S.A., pp. 15-19.

APPENDIX I : SPECTRAL DENSITY ANALYSIS OF DYNAMICAL RESPONSE

To help establish the natural frequencies of various system components and coupling effects, Power Spectral Density (PSD) distribution of the system dynamical response was carried out. Of interest are the platform's rigid body librational frequency as well as natural frequencies of the elastic degrees of freedom. To that end, an initial disturbance was given to the system, in the desired degree of freedom, and the corresponding response plots were obtained ($\psi_p, e_p, \beta_1, e_1, \beta_2, e_2$). The individual response plot was subjected to the power spectral density analysis to arrive at the characteristic frequency as well as coupling contributions from other degrees of freedom (Figures I-1 to I-4). The symbols used to designate various characteristic frequencies are as follows:

- ω_ψ frequency of platform librational motion;
- ω_p platform's bending natural frequency;
- ω_{j1} first joint's natural frequency;
- ω_{m1} first module's bending natural frequency;
- ω_{j2} second joint's natural frequency;
- ω_{m2} second module's bending natural frequency.

Note, the librational frequency of the platform pitch motion as well as its fundamental natural frequency in bending were obtained in Chapter 2 (Figure 2-11) as $\omega_\psi \approx 3 \times 10^{-4}$ Hz and $\omega_p \approx 0.18$ Hz. Information in Figures I-1 to I-4 was used to prepare Table 2-2 presented on page 42.

First Module Revolute Joint

The revolute joint of the first module was given an initial disturbance of 5° ($\beta_1(0) = 5^\circ$) and the system response was recorded (Figure I-1a). The PSD analyses of the responses associated with various flexible components are presented in Figure I-1(b). The revolute joint's natural frequency was found to be $\omega_{j1} \approx 0.08$ Hz. Major peaks representing contributions from other flexible components are also indicated to help assess coupling effects.

First Module Tip Deflection

Tip of the first module was given an initial deflection of 0.2 m ($e_j(0) = 0.2$ m). The system response and PSD plots are shown in Figures I-2(a) and I-2(b), respectively. The natural frequency of the first module's tip oscillations is found to be $\omega_{m1} \approx 5.85$ Hz. It is apparent from Figures I-1(b) and I-2(b) that there is a strong coupling between the tip and the joint vibrations of the first module. Note, dynamics of the first module excites revolute joint of the second module (β_2) at its characteristic frequency ($\omega_{j2} = 0.21$ Hz). Of course, tip of the module two should also vibrate at its natural frequency (ω_{m2}), however its PSD measure, being relatively small, is not apparent. Therefore, it was determined through an independent module two tip excitation.

Second Module Tip Deflection

Here the tip was subjected to an initial displacement of 0.2 m (Figure I-3). As apparent from Figure I-3(b), $\omega_{m2} \approx 8.5$ Hz. Coupling contributions can also be discerned,

particularly from its own joint (ω_{j_2}) as well as from module one ($\omega_{m_1}, \omega_{j_1}$).

Second Module Joint Deflection

With a 5° initial deflection for the second joint ($\beta_2(0) = 5^\circ$), Figure I-4 gives the system response and corresponding spectral plots. It is found that the natural frequency of the second joint (ω_{j_2}) is about 0.21 Hz. The bending of module two is also excited at $\omega_{m_2} \approx 8.5$ Hz (Figure I-4a, e_2) modulating the β_2 low frequency contributions. Note also the energy transfer to module one as suggested by the spectral peaks corresponding to ω_{m_1} and ω_{j_1} .

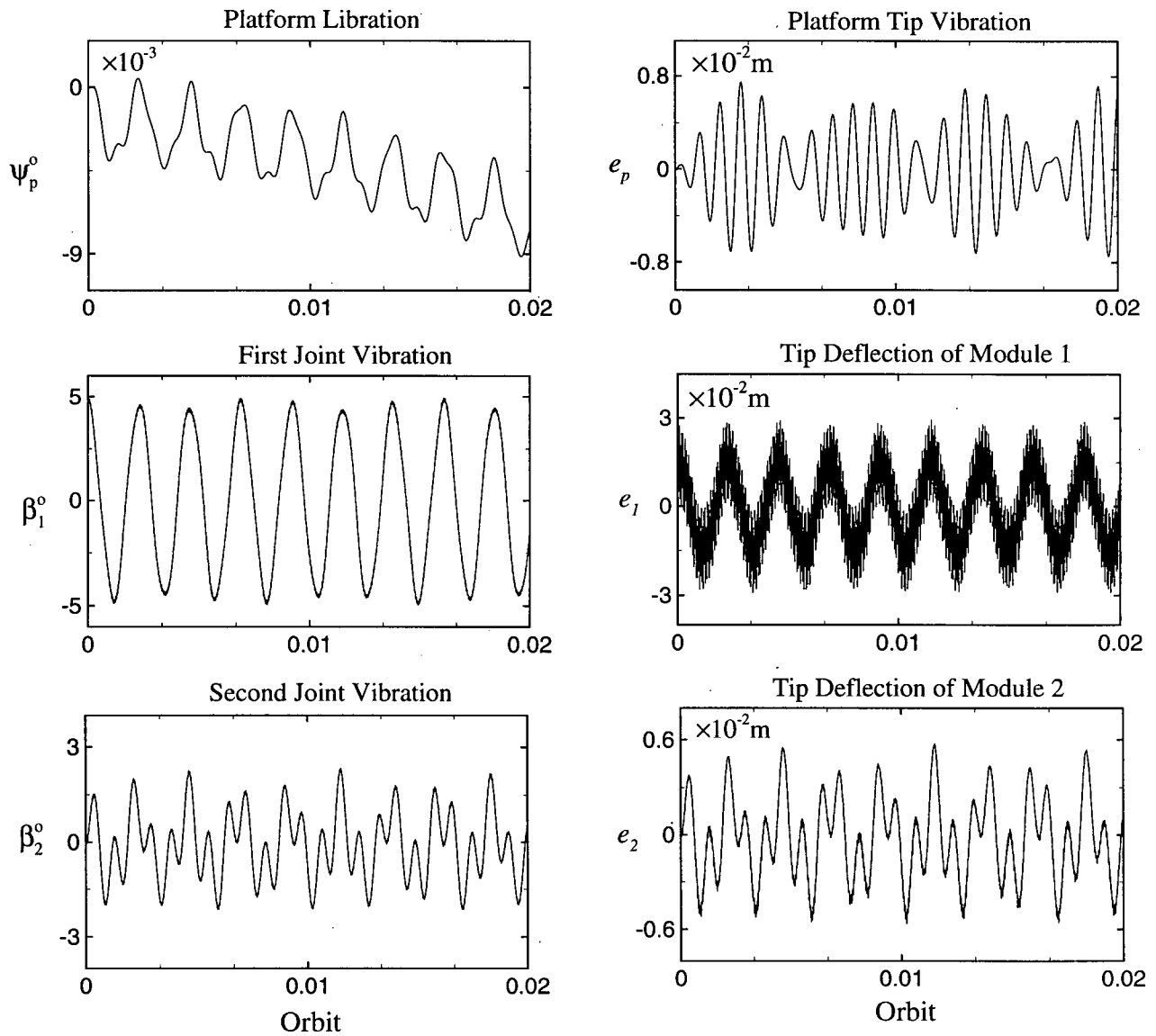
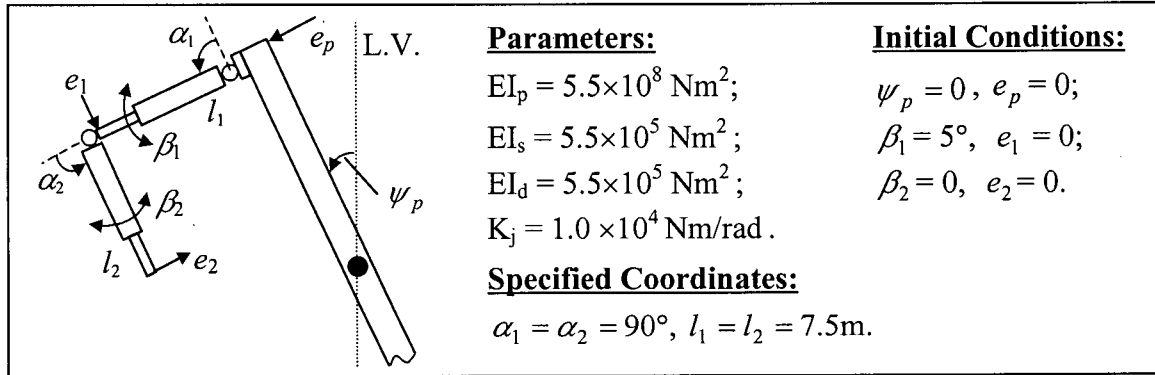


Figure I-1 Initial deflection of 5° applied to the revolute joint of module 1: (a) system response.

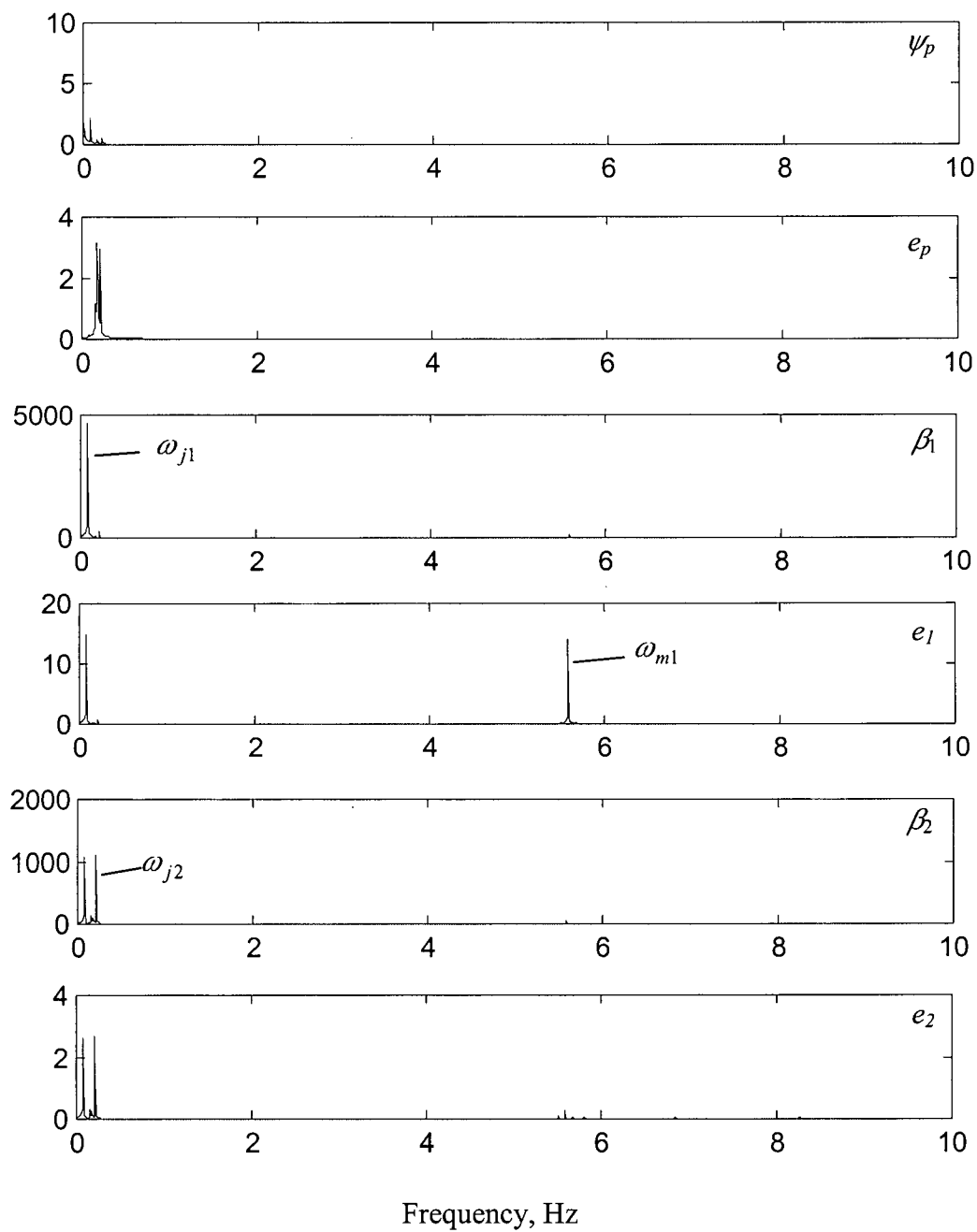


Figure I-1 Initial deflection of 5° applied to the revolute joint of module 1:
 (b) power spectral density distribution.

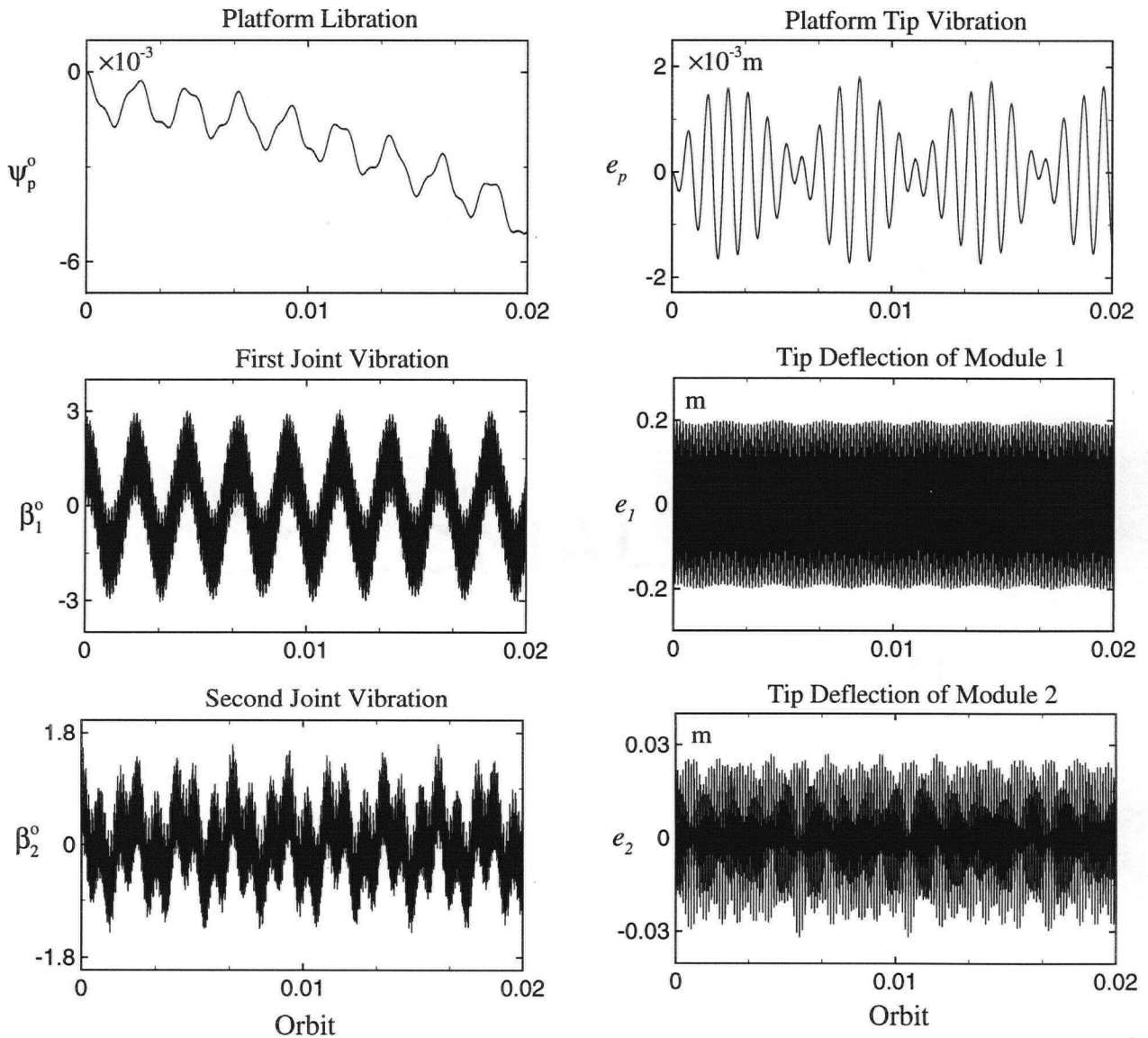
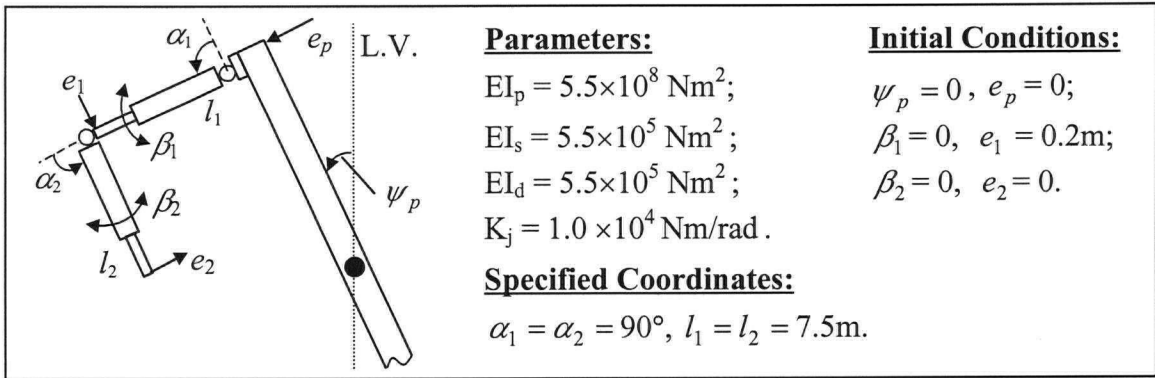


Figure I-2 Module 1 tip deflection of 0.2m: (a) system response.

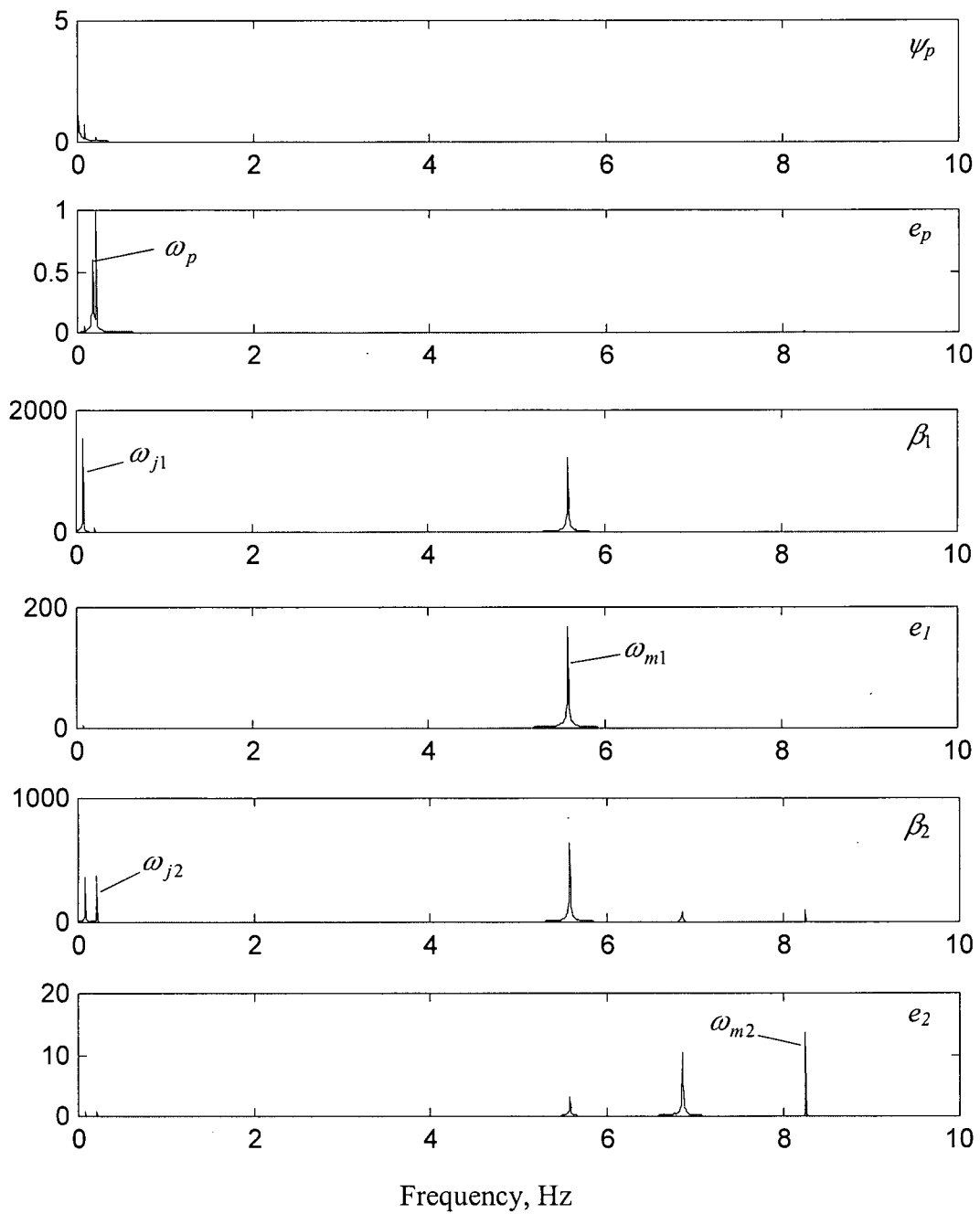


Figure I-2 Module 1 tip deflection of 0.2m: (b) power spectral density distribution.

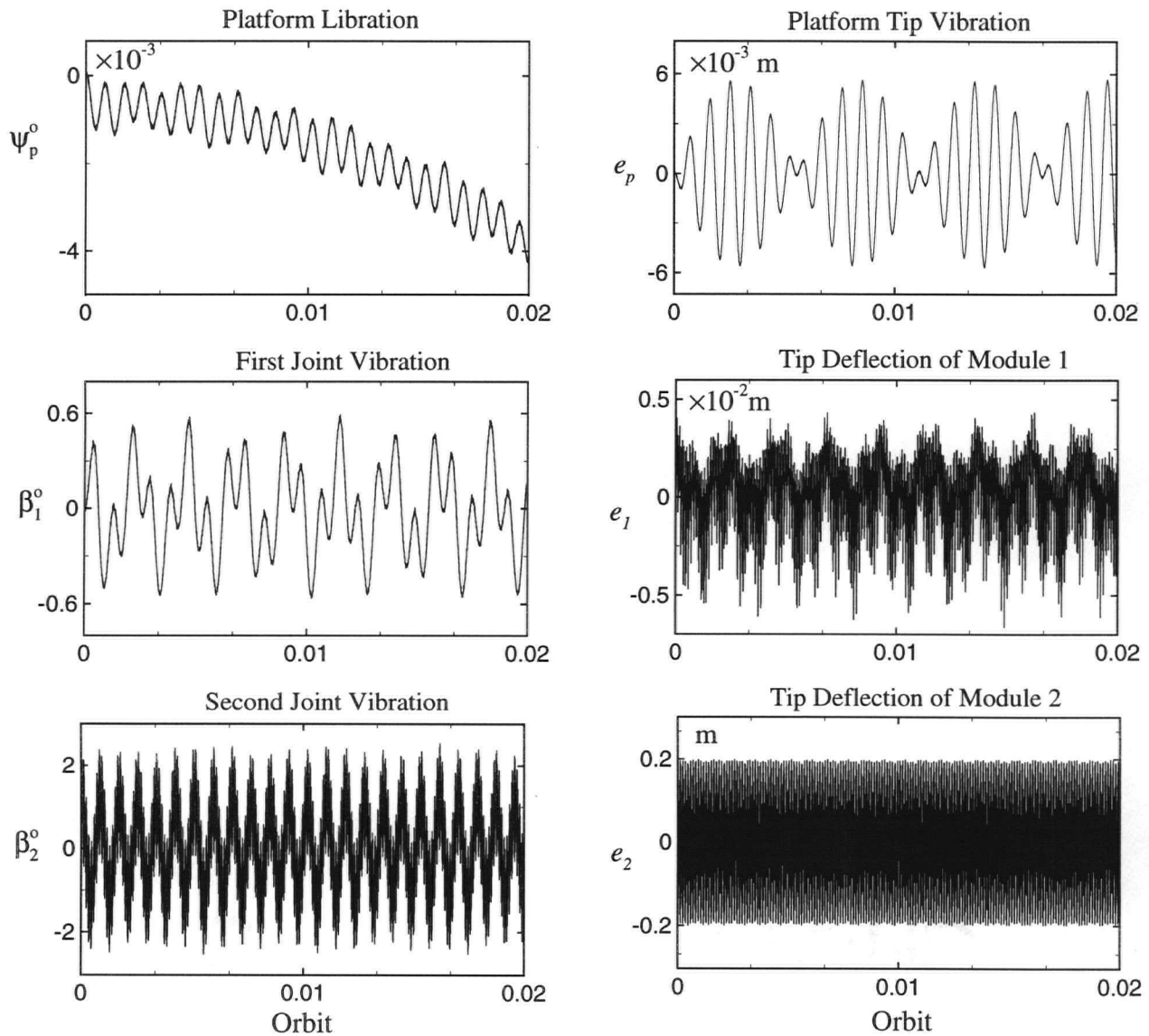
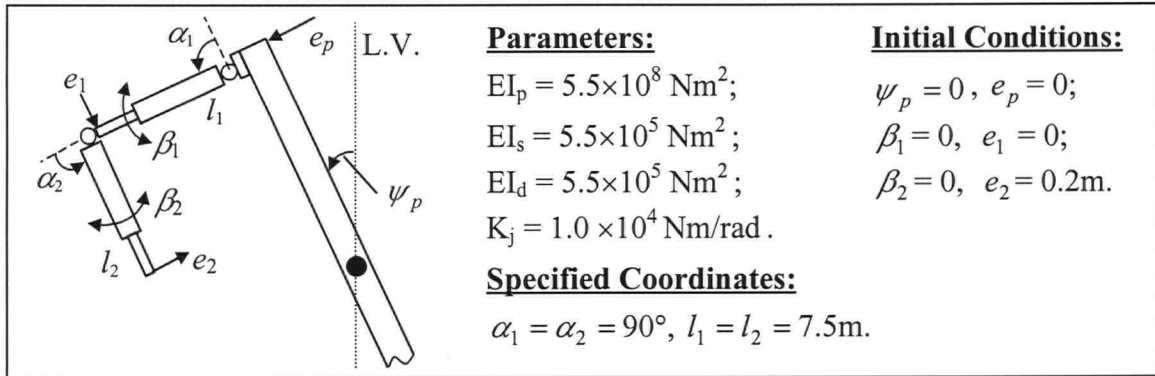


Figure I-3 Module 2 tip deflection of 0.2m: (a) system response.

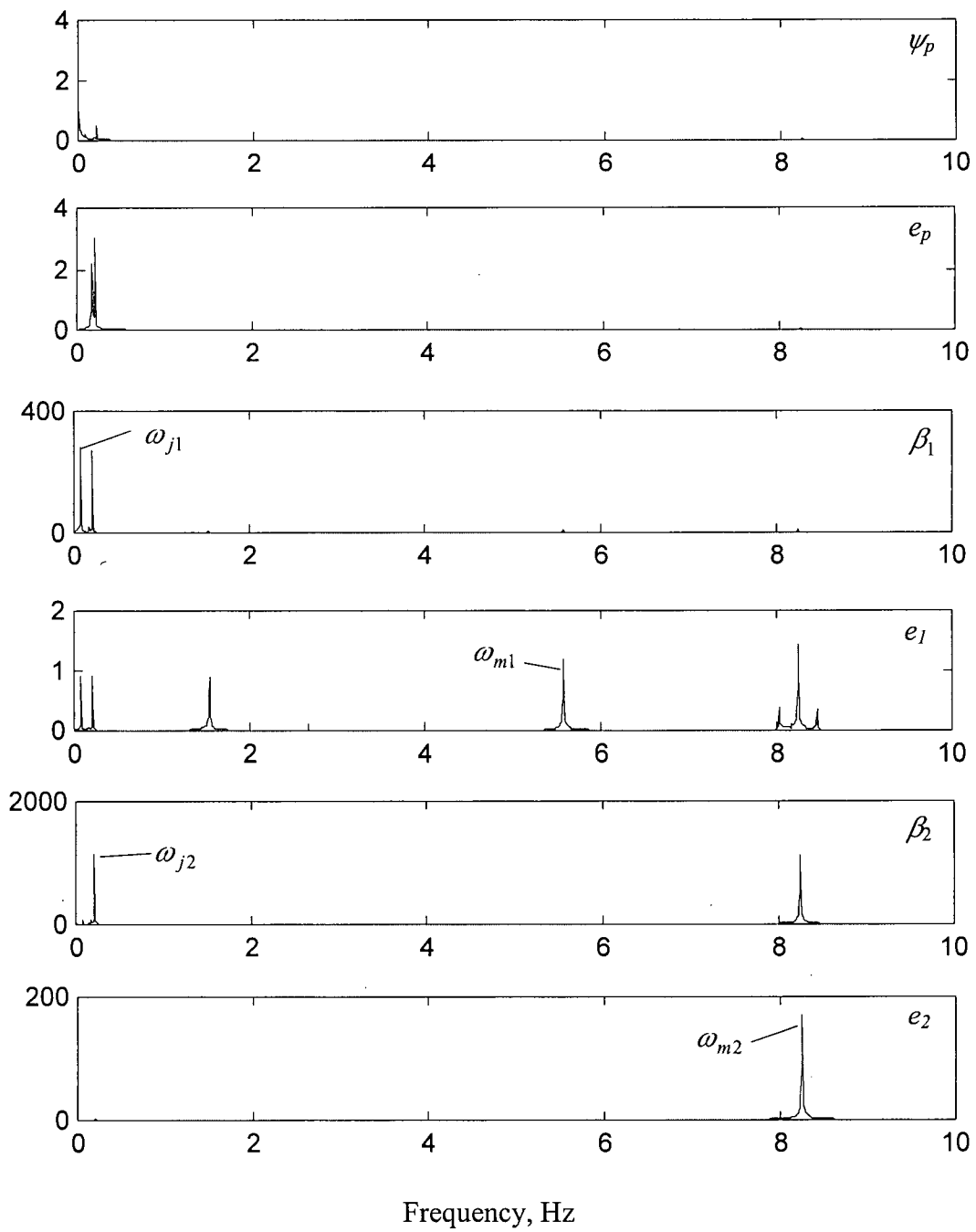


Figure I-3 Module 2 tip deflection of 0.2m: (b) power spectral density distribution.

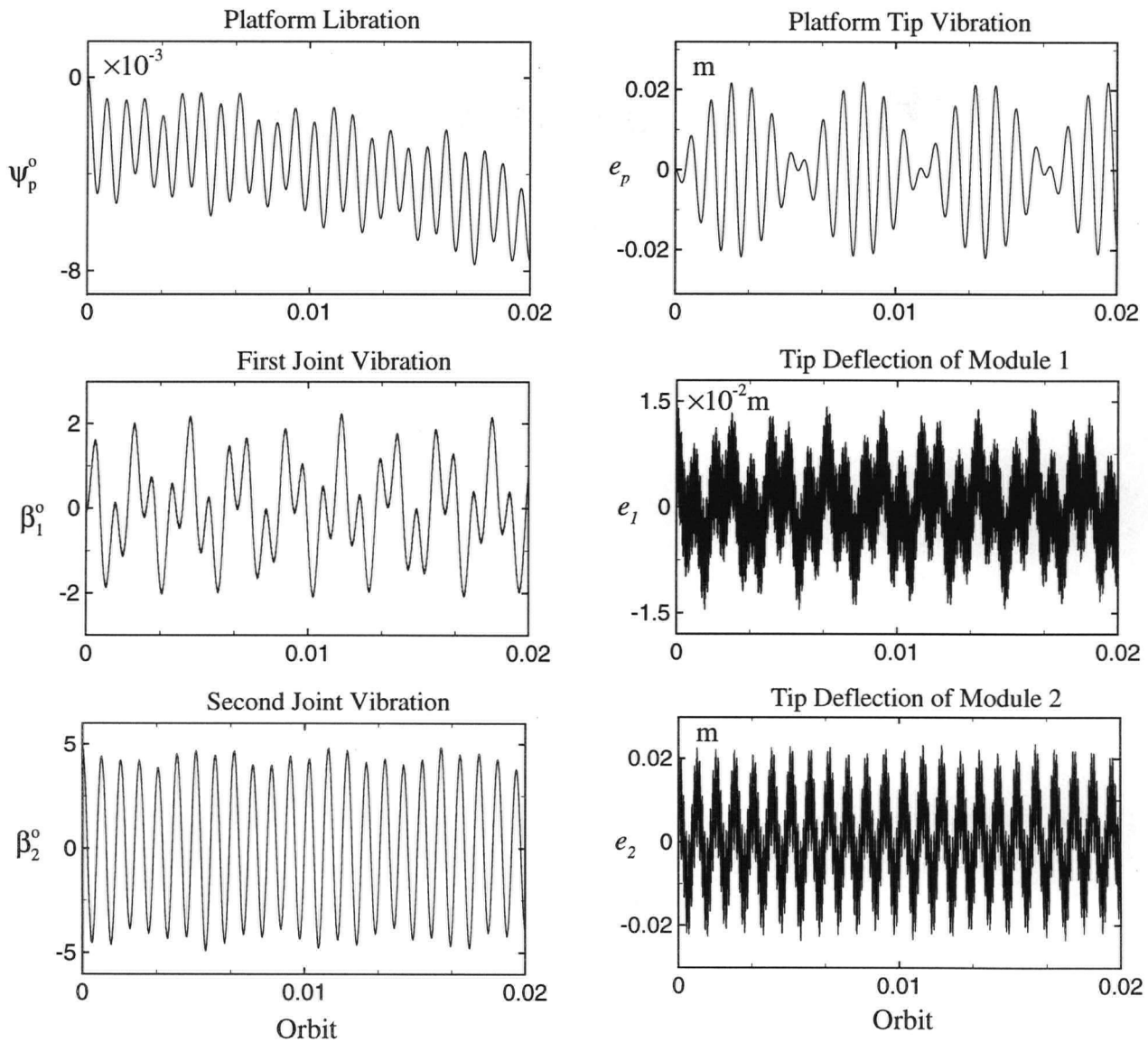
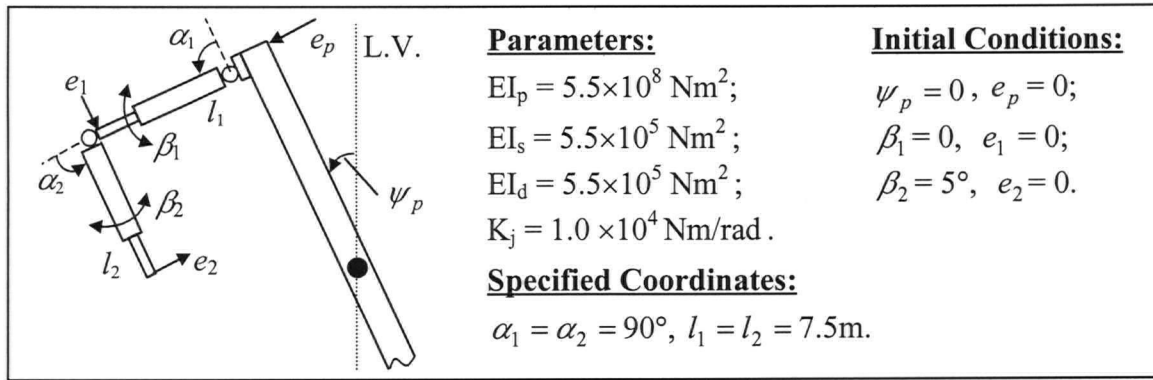


Figure I-4 Module two joint deflection of 5° : (a) system response.

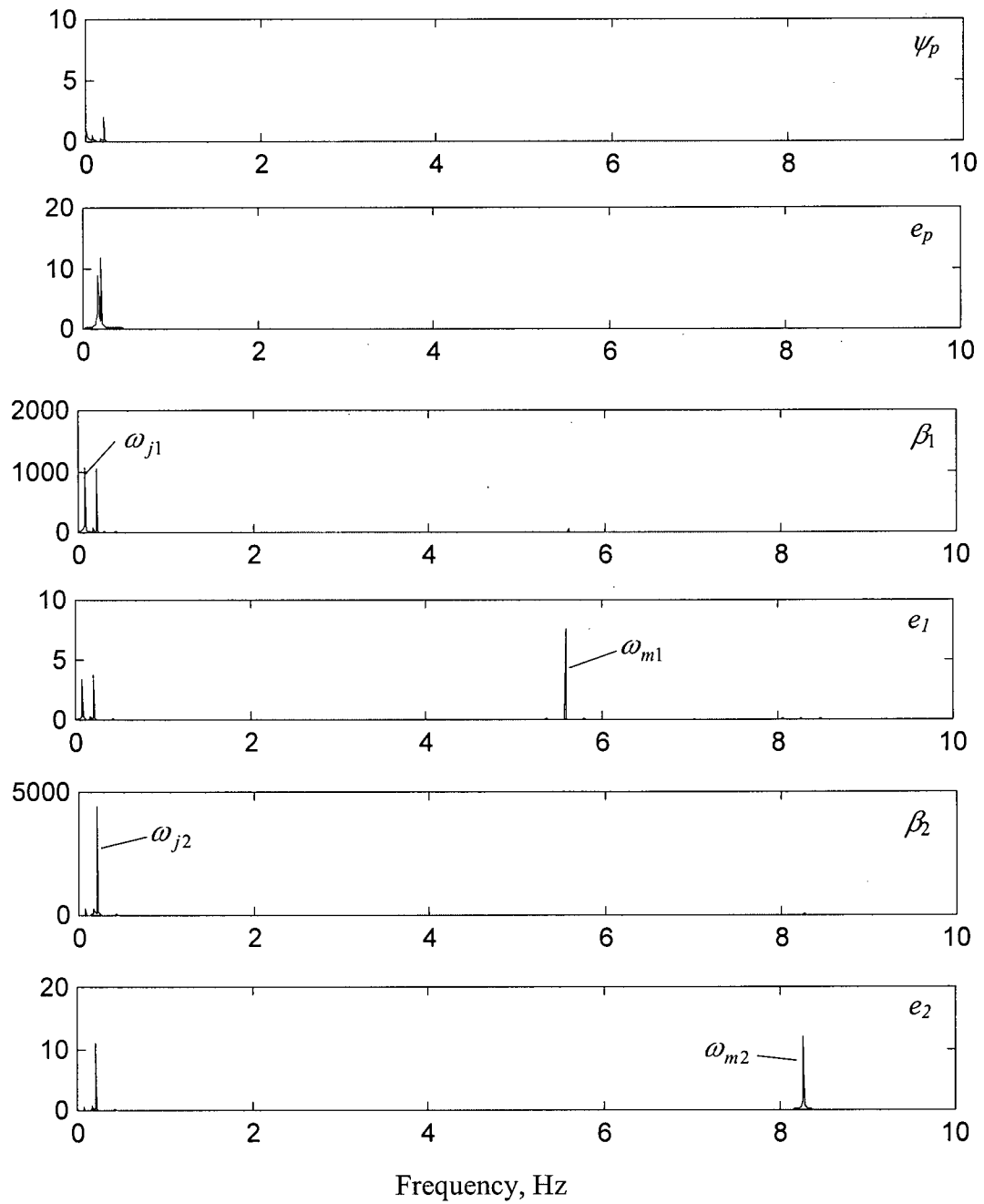


Figure I-4 Module two joint deflection of 5°: (b) power spectral density distribution with frequency.